

**Turbulence Effects on Combustion
in Spark Ignition Engines**

by

John Hynes
B.Sc Mech. Eng.

*A Thesis submitted to the University of Leeds
in fulfilment of the requirements for the
Degree of Doctor of Philosophy*

Department of Mechanical Engineering
The University of Leeds

July 1986

Abstract

Described in this thesis are the results of an experimental and theoretical study of the effects of turbulence on combustion in single and dual chamber spark ignition engines. The techniques adopted in the experimental study included the use of high speed cine photography, and the collection of simultaneous cylinder pressure records using an on-line computer.

The experimental results confirmed the potential of the dual chamber design for increasing burning rate, and for controlling the level of turbulence within an engine cylinder. High speed photographs were filmed through a perspex window in the engine cylinder head. These showed that flame propagation was much faster when the engine was fitted with a divided chamber cylinder head than when equipped with a disc shaped single chamber head. The acceleration of combustion rate has been shown to be a function of flow velocity through the interconnecting orifice during the compression stroke. At very high flow velocities the nozzle became choked, and engine performance was impaired.

In the theoretical work, a computer model for the thermodynamic cycle of an engine was developed. The use in this model of empirical laws to describe combustion rate was shown to be inadequate; this was primarily because of uncertainty in the length of the combustion period, which one needs to specify when using this method. When burning velocity data (derived from work by colleagues using a turbulent combustion bomb) were incorporated into the model, good qualitative results were possible. The use of an empirical law to describe the effect of turbulence on the burning velocity of a developing flame was, however, shown to be inaccurate.

The turbulent flame front in an engine is a thick reaction zone containing pockets of unburnt charge. Analysis of data for flame projected area (derived from high speed photographs) and simultaneous cylinder pressure data, revealed that a considerable quantity of unburnt charge was present behind the visible flame front. There was some evidence that a greater proportion of unburnt charge was present behind the flame when the mixture was lean than when it was stoichiometric. Modelling of this effect by assuming that mass, once entrained, would burn at an exponential rate, was shown to produce reasonable results.

Acknowledgments

I would like to thank my supervisor, Dr. Chris Sheppard, for his invaluable help and guidance throughout this project. His helpful suggestions, and his ability to provide an optimistic outlook have provided great encouragement. I would also like to thank Professor D. Bradley and Mr. M. Lawes for their helpful advice during this research programme.

Thanks are also due to the technicians in the Thermodynamics laboratory, particularly to Mr. A. Lawson and Mr. B. Leach, for their assistance in design and commissioning of the experimental rig. I am also grateful to Mr. S. Burrige for his assistance in operating the high speed camera.

Many thanks to Mr. L. Williams, from the Electronic Engineering Department at Leeds, for his design of an electronic ignition control system. Further thanks to Mr. S. Cail and Mr. D. Auty for building and commissioning of the ignition system. I am also very grateful to Mr. S. Allen and Mr. C. Clarke for their help in linking the experimental rig to the on-line computer.

No words are adequate to express my sincere gratitude to Jenny for her encouragement, patience and valuable assistance which she has willingly offered me throughout the preparation of this thesis.

Finally, the financial support of the Science and Engineering Research Council is gratefully acknowledged.

Nomenclature

A_b	total surface area of cylinder walls in contact with burnt charge
A_f	surface area of flame front
A_u	total surface area in contact with unburnt charge
A_{hb}	surface area of cylinder head in contact with burnt charge
A_{pb}	surface area of piston crown in contact with burnt charge
A_{wb}	surface area of cylinder walls (liner) in contact with burnt charge
A_{ht}	total surface area of cylinder head
A_{pt}	total surface area of piston crown
A_{wt}	total surface area of cylinder walls
A_o	Orifice cross-sectional area (mm^2)
B	diameter of cylinder bore (cm)
C_D	coefficient of discharge
C_p	Specific heat capacity at constant pressure (cal/gmole-K)
C_v	Specific heat capacity at constant volume (cal/gmole-K)
d_o	orifice diameter (also called <i>OD</i>) (mm)
h	instantaneous clearance height between piston crown and cylinder head
h_{in}	enthalpy of intake charge (cal)
h_f	enthalpy of residual fraction (cal)
H	Enthalpy (cal/gmole)
$H(T_b)$	Enthalpy at a base temperature (298.15K) (cal/gmole)
K_1	forward reaction constant
K_{-1}	backward reaction constant
K_i	constant of proportionality used to determine turbulence intensity in the pre-chamber of a dual chamber engine.
l/r	ratio of connecting rod length to crank shaft throw
L	integral length scale
\dot{m}	mass rate of flow (g/sec)
m_t	mass transferred (g)
Nu	Nusselt number
n	number of moles
P	cylinder pressure (atm)
P_h	pressure in high pressure chamber (atm)
P_l	pressure in low pressure chamber (atm)
P_{in}	manifold pressure
Q	quantity of heat transferred (cal)
\dot{Q}	rate of heat transfer
\dot{q}	rate of heat transfer per unit area

R	Universal gas constant (cc-atm/gmole-K) or (cal/gmole-K)
R_L	Reynolds number based on the integral length scale
R_λ	Reynolds number based on the Taylor microscale
r	flame radius (cm)
S	Entropy (cal/gmole-K)
$S(T_b)$	Entropy at a base temperature (298.15K) (cal/gmole-K)
S_e	expansion velocity of charge due to combustion
S_p	mean piston speed (cm/sec)
T	Temperature (Kelvin or Centigrade)
t	time (seconds)
u'	r.m.s. turbulent velocity (cm/sec)
u_f	flame speed (cm/sec)
u_g	unburnt gas velocity ahead of a flame (cm/sec)
u_l	laminar burning velocity (cm/sec)
u_t	turbulent burning velocity (cm/sec)
U	Internal energy (cal/gmole)
V	Volume (cc)
V_c	cylinder clearance volume at TDC (cc)
V_s	cylinder swept volume (cc)
V_t	total instantaneous cylinder volume
W	Work done

Greek

γ	index of compression
δ	flame thickness
$\frac{\epsilon}{\kappa}$	potential parameter (Kelvin)
$\Omega^{(2,2)*}$	reduced collision integral
σ	collision integral (Angstroms)
τ_b	characteristic time to burn an eddy (sec)
τ_c	chemical lifetime (sec)
λ	Taylor microscale
μ	dynamic viscosity (g/cm-sec)
ν	kinematic viscosity (cm ² /sec)
κ	thermal conductivity
ρ	density (g/cc)
ϕ	Equivalence ratio (also called PHI)
η_{th}	thermal efficiency
θ	crank angle (degrees)
θ_i	spark advance (also called SPA) (degrees)

ΔH_f	Enthalpy of formation (cal/gmole)
$\Delta\theta$	crank angle increment (degrees)
$\Delta\theta_b$	combustion duration (also called CDR) (degrees)
Δt	time increment (seconds)
ΔV_i	volume entrained in an increment (cc)

Abbreviations

ATDC	After Top Dead Centre
BDC	Bottom Dead Centre
BTDC	Before Bottom Dead Centre
CDR	Combustion Duration (also called $\Delta\theta_b$) (degrees)
COSR	cosine rate (empirical mass fraction burnt expression)
CR	Compression Ratio
fps	frames per second
IMEP	Indicated Mean Effective Pressure (atm)
ISFC	Indicated Specific Fuel Consumption (gm/lkWh)
LCV	Lower Calorific Value (KJ/Kg)
LINR	linear rate (empirical mass fraction burnt expression)
MF	Mole Fraction
MW	Molecular weight
OD	Orifice Diameter (also called d_o) (mm)
PHI	Equivalence Ratio (also called ϕ)
RF	Residual Fraction
RMW	Relative Molecular Weight
RPM	Engine speed (revolutions per minute)
SPA	Spark Advance (also called θ_i) (degrees)
VR	Volume Ratio
WB31	Weibe function (empirical mass fraction burnt expression, with $A=3$ and $M=1$)

Subscripts

av	average
b	burnt
dev	fully developed
e	entrained
egr	exhaust gas recirculation
g	gas
ig	at ignition
in	at intake
l	laminar
m	main chamber

mot	motoring
p	pre-chamber
r	reactants
rf	residual fraction
t	turbulent
u	unburnt
w	wall

TABLE OF CONTENTS

Abstract	ii
Acknowledgements	iii
Nomenclature	iv
Chapter 1 Introduction	1
1.1 INTRODUCTION	3
1.2 IGNITION	3
1.3 FLAME PROPAGATION	4
1.4 DIVIDED CHAMBER ENGINES	5
1.5 MATHEMATICAL MODELS	6
1.6 PRESENT WORK	6
Chapter 2 Review of Divided Chamber Engines	8
2.1 INTRODUCTION	10
2.2 PRE-CHAMBER CONFIGURATION	10
2.3 VOLUME RATIO	11
2.4 ORIFICE CONFIGURATION	12
2.5 DEGREE OF STRATIFICATION	13
2.6 CONCLUSIONS	16
Chapter 3 Equipment and Instrumentation	17
3.1 INTRODUCTION	19
3.2 YAMAHA ENGINE	19
3.2.1 Cylinder Head Design	20
3.2.2 Piston Modifications	23
3.2.3 Lubrication	23
3.2.4 Fuel System	24
3.3 INSTRUMENTATION	25
3.3.1 Crank Angle Position	25
3.3.2 Ignition System	26
3.3.3 Pressure Measurement	27
3.3.4 On Line Data Acquisition	27
3.3.5 Engine Speed Measurement	29
3.4 PHOTOGRAPHIC EQUIPMENT	29
3.5 TEST PROCEDURES	30

Chapter 4 Experimental Results	48
4.1 INTRODUCTION	50
4.2 RUSTON ENGINE	50
4.2.1 Pressure Records at 800 rpm	50
4.2.2 Flame Propagation	51
4.2.3 Effect of Gas Flow Velocity Through the Orifice	51
4.3 YAMAHA ENGINE - SINGLE CHAMBER	52
4.3.1 Film Analysis	53
4.3.2 Effect of Equivalence Ratio	53
4.3.3 Effect of Spark Plug Location	55
4.3.4 Effect of Engine Speed	55
4.3.5 Effect of Compression Ratio	56
4.3.6 Comparison of Results With Those of the Ruston Engine	57
4.4 YAMAHA ENGINE - DIVIDED CHAMBER	58
4.5 CONCLUSIONS	60
Chapter 5 Single Chamber Computer Model	90
5.1 INTRODUCTION	92
5.2 WORKING FLUID AND ITS PROPERTIES	93
5.3 COMPRESSION PROCESS	93
5.4 HEAT TRANSFER	95
5.5 COMBUSTION PROCESS	97
5.5.1 Instantaneous	97
5.5.2 Rate Controlled - Empirical	97
5.6 EXPANSION	100
5.7 CALCULATION OF NO AND CO CONCENTRATIONS.	101
5.8 EXHAUST PROCESS.	103
5.8.1 Exhaust Blowdown	103
5.8.2 Exhaust Stroke	104
5.9 INTAKE PROCESS	104
5.10 PERFORMANCE CALCULATIONS	105
5.11 RESULTS AND DISCUSSION	106
5.11.1 Effect of Progressive Combustion	106
5.11.2 Effect of Heat Transfer	106
5.11.3 Effect of Nature of Empirical Rate Expression	106
5.11.4 Effect of Ignition Advance	107
5.11.5 Effect of Combustion Duration	107
5.11.6 Effect of Engine Speed	108
5.11.7 Some Comparisons With Experimental Results	108
5.12 CONCLUSIONS	109

Chapter 6 Single Chamber Model - Burning Velocity Method	126
6.1 INTRODUCTION	128
6.2 DETERMINATION OF TURBULENCE PARAMETERS	129
6.2.1 Integral Length Scale (L)	129
6.2.2 Turbulence Intensity (u')	130
6.2.3 Taylor Microscale (λ)	130
6.2.4 Eddy Lifetime	130
6.3 DETERMINATION OF BURNING VELOCITIES AND FLAME STRUCTURE	131
6.3.1 Laminar Burning Velocity	131
6.3.2 Turbulent Burning Velocity	131
6.3.3 Developing Flame	133
6.3.4 Flame Thickness (δ)	133
6.3.5 Chemical Lifetime	134
6.4 MODELLING OF THE COMBUSTION PROCESS	135
6.4.1 Ignition	135
6.4.2 Rate of Entrainment	135
6.4.3 Rate of Burning	136
6.5 RESULTS AND DISCUSSION	137
6.5.1 Some Comparisons With Experimental Results (Ruston Engine).	139
6.5.2 Comparison With Experimental Results (Yamaha Engine)	140
6.5.3 Effect of EGR	140
6.6 CONCLUDING REMARKS	141
Chapter 7 Divided Chamber Computer Model	155
7.1 INTRODUCTION	157
7.2 COMPRESSION AND EXPANSION	158
7.3 COMBUSTION	160
7.3.1 Instantaneous	160
7.3.2 Burning Velocity Method	160
7.3.2.1 Pre-Chamber Combustion	161
7.3.2.2 Combustion in Both Chambers	162
7.3.2.3 Main Chamber Combustion	162
7.4 EXHAUST PROCESS	163
7.5 INTAKE PROCESS	163
7.6 PERFORMANCE	163
7.7 RESULTS AND DISCUSSION	164
7.8 CONCLUSIONS	166

Chapter 8 Further Experimental Data Analysis	174
8.1 INTRODUCTION	176
8.2 CALCULATION PROCEDURE	176
8.3 RESULTS	177
8.4 CONCLUDING REMARKS	179
Chapter 9 Summary and Conclusions	184
References	188
Appendix A Engine and Fuel Details	205
A.1 Engine Details	206
A.2 Fuel Details	207
Appendix B Calculation of Mixture Properties	208
B.1 Properties of individual species	209
B.2 Properties of mixtures	211
Appendix C Calculation of Enflamed Volumes	212
C.1 Central Ignition - Single Chamber	213
C.2 Side Ignition and Main chamber	214
C.3 Spherical Pre-chamber	219
C.4 Cylindrical Pre-chamber	219
Appendix D Calculation of Wall Surface Areas	220
D.1 Central Ignition - Single Chamber	221
D.2 Side Ignition	222
D.3 Spherical Pre-chamber	224
D.4 Cylindrical Pre-chamber	224

CHAPTER 1

Introduction

CONTENTS

1.1	INTRODUCTION	3
1.2	IGNITION	3
1.3	FLAME PROPAGATION	4
1.4	DIVIDED CHAMBER ENGINES	5
1.5	MATHEMATICAL MODELS	6
1.6	PRESENT WORK	6

1.1. INTRODUCTION

The spark ignition engine is a popular source of power for transport vehicles, due to its high power to weight ratio and compact design. Until the early seventies, manufacturers strived to produce higher power outputs; fuel economy was considered secondary. In recent years, however, the depletion of natural fuel resources has forced changes in engine design criteria. This need for an efficient use of fuel has been accompanied by pressure, often enforced by legislation, to reduce toxic emissions.

It is well known that the thermal efficiency of spark ignition engines can be improved by increasing compression ratio, and burning leaner mixtures (see, for example, Blackmore and Thomas, 1979); the latter, however, is accompanied by a reduction in power output. Flame propagation is slower with a leaner mixture; this can lead to increased hydrocarbon emissions due to incomplete combustion. Higher compression ratios can help solve this problem as the charge is heated to a greater extent, and therefore burns faster. However, higher compression ratios can lead to knock (spontaneous ignition of the end-gas due to the high temperatures), particularly at richer mixtures where the charge is more reactive. Knock is undesirable as it reduces the power output and may also result in damage to the engine because of higher local heat transfer rates (Lee and Schaefer, 1983).

To operate effectively with lean mixtures it is necessary to enhance the ignition system, as lean mixtures are difficult to ignite. The flame propagation rate must also be increased to compensate for lower burning velocity; flame propagation must be finished before the exhaust valve opens, for complete combustion. Increase in flame propagation rate may also help inhibit knock reactions; the flame has more chance to entrain all the charge in the chamber before end gas reactions can occur.

1.2. IGNITION

Lean mixtures are less reactive than the stoichiometric and slightly rich mixtures traditionally used in spark ignition engines. Hence they require greater ignition advance, to compensate for the slower burning. With advanced ignition the mixture temperature at the time of ignition is lower. An improved ignition source is therefore required when operating lean. Maly et al (1983a) stressed the need for a large ignition kernel with a high expansion velocity; this requires considerable energy. The effect of increased turbulence, introduced to accelerate the burning rate of lean mixtures, is also important - as this is accompanied by a narrowing of the flammability limits and an increase in minimum ignition energy (Akindele et al, 1982). Cole and Swords (1980) showed that a strong correlation exists between the horizontal component of the mean velocity, in the neighbourhood of the spark at ignition, and the peak cylinder pressure. Arranging the spark plug so that the ground electrode is

upstream of the centre electrode (if the flow direction is predictable) can also produce considerable improvement in flame initiation (Anderson and Asik, 1983).

A number of enhanced ignition systems have been described in the literature. Nakamura et al (1983) used a platinum tipped plug with an enlarged spark gap; this improved the lean misfire limit and decreased torque fluctuation. The increased spark gap reduced the quenching effect of the electrode, but required more voltage for breakdown. Multiple electrode spark plugs have also been shown to be effective (Durbin and Tsai 1983).

Plasma ignition systems have been used by a number of workers (Edwards et al, 1983; Boston et al, 1985); these give very much improved ignition. The lean misfire limit with these igniters is controlled by flame propagation and not ignition.

Ignition problems may also be solved by employing the stratified charge concept. In such engines it is arranged (usually by fuel injection) that the spark plug is surrounded by a rich (easily ignited) mixture at ignition. A number of these systems have been adopted commercially:

- (1) Ricardo (Norris-Jones and Russell, 1982) used a system in which the fuel is injected in a single spray onto the wall of a bowl in the piston. A swirling air motion in this bowl produces a rich mixture in the periphery of the chamber as the fuel evaporates. The spark plug is located in this region.
- (2) Ford (Bishop and Simko, 1968) injected the fuel in a conical spray well before ignition. The injector was located in the centre of a chamber which had swirl, this produced a mixture cloud which rotated as a solid body without drifting away from the spark plug.
- (3) Texaco (Mitchell and Alperstein, 1973) injected into swirling air, just prior to ignition, with the spark plug just downstream of the injector.
- (4) Honda (Date et al, 1974) used the divided chamber concept; this will be discussed in more detail later.

1.3. FLAME PROPAGATION

The simplest way to decrease the time taken by the flame to completely entrain the charge is to decrease the distance the flame has to travel. This can be achieved by either:

- (a) Using more than one spark plug; this increases the complexity of the engine design.
- (b) Decreasing the bore to stroke ratio for a given engine size; this is limited by design constraints. A lower bore to stroke ratio gives higher piston speeds and therefore greater stresses on the engine components.

- (c) Locating the spark plug centrally and designing the cylinder head in a compact manner to minimise flame travel (eg May, 1979; Sutton, 1983).

With a given chamber geometry, the time for the flame to completely entrain the charge can be reduced by increasing the flame speed. The effect that turbulence has on flame speed has been noted by many workers, and was studied in spark ignition engines by Bouchard et al (1937); turbulence can enhance the flame propagation rate. The turbulence may be increased in a number of ways:

- (1) Squish; defined as the inward radial movement of the cylinder charge caused by piston motion and chamber geometry.
- (2) Swirl; this is charge rotation and may not always lead to increased turbulence. It can produce a stable layered flow and prevent mixing occurring.
- (3) Induction generated turbulence, a function of the design of the induction tract and port (eg Hugelman and Ong, 1982).
- (4) Four valve chambers; these promote a swirl type motion perpendicular to the cylinder axis (barrel roll) which is broken up into turbulence as the piston ascends.
- (5) The divided chamber concept

1.4. DIVIDED CHAMBER ENGINES

The divided chamber engine was first developed by Ricardo (1922). Such engines have an auxiliary combustion chamber (pre-chamber), coupled by an interconnecting orifice to the usual combustion space (main chamber) contained in the cylinder between the piston crown and cylinder head. Ignition occurs in the pre-chamber and then the flame grows and enters the main chamber as a powerful torch. This provides a healthy ignition source for the main chamber charge as it has a very large surface area. Cycle to cycle variation is reduced as a result of the more consistent flame propagation associated with more consistent turbulence generation. Cyclic variation still exists however, as the ignition process is susceptible to fluctuations in air/fuel ratio (Petrovic 1982), and ignition timing (and flame propagation will still be affected by fluctuations in turbulence, albeit to a lesser extent). The geometry of the system is well suited for stratified charge operation. In such a system the pre-chamber charge is enriched and therefore ignites easily, while the main chamber charge can be very lean as the ignition source is more powerful than a conventional spark. When operated homogeneous, NO emissions from divided chamber engines are generally low, due to the relatively low temperatures associated with the high heat losses of this engine type. When operated stratified, the pre-chamber has a rich mixture; with such a mixture NO formation is slow, even at high temperature, because of low oxygen availability. Subsequent combustion in the lean main chamber occurs at a low temperature, also unfavourable for nitric oxide

formation. A review of experimental work conducted on divided chamber engines is presented in Chapter 2.

1.5. MATHEMATICAL MODELS

The development of spark ignition engines involves a great deal of optimization work in order to meet the emissions and fuel economy requirements. The mathematical model provides an important means of reducing the size of the experimental studies necessary; experimental work requires sophisticated equipment and considerable expense, and therefore any means of avoiding it will help to reduce overall cost and development time. The increase in available computing power in recent years has greatly increased the capabilities of mathematical models. However, due to the complexity of the combustion process, a great deal of progress is still necessary before a full theoretical simulation of turbulent combustion is possible.

Mathematical models of spark ignition engines consist of a set of equations governing the thermodynamic and fluid mechanics behaviour of the working fluid within the cylinder. These equations can be solved numerically on a computer. Engine models can be classified into two types:

- (1) Thermodynamic models - these involve the thermodynamic analysis of the charge in the cylinder during the cycle.
- (2) Multi-dimensional models - these involve the finite difference solution of (the time dependent) simultaneous equations for conservation of mass and energy, together with the turbulent forms of the Navier stokes equations.

These types of models are reviewed by Desoky (1981) and Al-Mamar (1983). In the work reported here, all modelling can be classified in the first category. Multi-dimensional models are considered to be beyond the scope of this work.

1.6. PRESENT WORK

The effect that turbulence has on combustion rate is important in lean burn engines. The divided chamber engine provides a useful means of studying the effect of turbulence on combustion in an engine environment; the pre-chamber size and interconnecting orifice size control the mass flow rate between chambers, and hence the turbulence intensity in each chamber. This thesis is concerned with a study of the effect of turbulence, using both single and divided chamber engines. Since the work conducted previously at Leeds [by Desoky (1981) and Al-Mamar (1983)] it has been necessary to replace the test engine, design and build improved experimental measurement and data acquisition equipment, and modify experimental techniques. These modifications are described in Chapter 3. Experimental

results for a range of engine conditions are presented and discussed in Chapter 4.

The computer models initially developed by Desoky and Al-Mamar, for both single and divided chamber engines, have been improved considerably; they have been modified to allow a progressive combustion process. The rate of combustion may be empirical or related to turbulent burning velocity, making use of burning velocity measurements reported in the literature. This work is described in Chapters 5, 6 and 7.

In chapter 8 the modelling and experimental work are combined. Experimental pressure and flame area data are used in conjunction with the model in order to calculate mass entrainment and burning rates, and entrainment velocities.

The thesis is concluded in Chapter 9 with suggestions for future work.

CHAPTER 2

Review of Divided Chamber Engines

CONTENTS

2.1	INTRODUCTION	10
2.2	PRE-CHAMBER CONFIGURATION	10
2.3	VOLUME RATIO	11
2.4	ORIFICE CONFIGURATION	12
2.5	DEGREE OF STRATIFICATION	13
2.6	CONCLUSIONS	16

2.1. INTRODUCTION

Since Ricardo's pioneering work (1922), studies of the potential of the divided chamber engine have been many and diverse. Turkish (1974) produced an excellent review for the type of divided chamber engine that has an intake valve into the pre-chamber (in addition to the usual valves into the main chamber). This extra valve is used to improve scavenging of the pre-chamber and (in stratified engines) to supply the rich pre-chamber mixture. The pre-chamber valve necessarily involves the complexity of an additional valve mechanism (reviewed by Turkish 1975).

Many workers have compared the performance of single and divided chamber engines. Purins (1974) showed that engine response to change in mixture strength and ignition timing was similar for the two engine types; however the (stratified) divided chamber engine was capable of operating at leaner mixtures - giving lower NO emissions, at the expense of HC emissions and poorer fuel economy. Wimmer and Lee (1973) noted improvements in CO and NO emissions without sacrifice of fuel economy, but again they recorded higher hydrocarbon emissions in the stratified charge divided engine. The ability of divided chamber engines to run on a wide range of fuels was highlighted by Overington and Haslett (1976); they used a Ricardo Comet indirect injection diesel engine which had been modified to incorporate a spark plug into the pre-chamber and to have a lower compression ratio.

The flow processes occurring during combustion were investigated by Oppenheim et al (1976), using a single compression-expansion machine which had full optical access. Schlieren photographs of the combustion process showed increased turbulence levels with torch ignition. As a consequence of this the combustion process was considerably faster. The strength of the torch jet not only affected combustion rate (by increasing the initial rate of entrainment by the flame), it also affected emissions and fuel economy (by controlling the mixing of burnt and unburnt regions). There are many variables in the divided chamber engine which can affect the strength of the torch process; these are discussed individually below.

2.2. PRE-CHAMBER CONFIGURATION

In the case of stratified divided chamber engines the choice of pre-chamber shape is often dictated by the method of fuel supply to the pre-chamber. If the fuel supply to the pre-chamber is carburetted, then an additional inlet valve is required (into the pre-chamber). For this arrangement a cylindrical geometry has generally been preferred, although Davis et al (1974) used an inlet valve in a spherical chamber. If pre-chamber fuel supply is by fuel injection, then the choice of pre-chamber shape is less restricted. Brandstetter and Decker

(1975) investigated a number of geometries, preferring fuel injection into a spherical pre-chamber.

In a comparison of injection and additional valve systems, Varde (1976) demonstrated better fuel economy at low load with an additional valve. Better pre-chamber scavenging resulted in lower concentrations of exhaust residuals at the time of ignition. However Brandstetter (1976) claimed that fuel injection was preferable at lean mixtures, giving reduced fuel consumption and NO emission levels. Wyczalek et al (1975a) adopted a basically cylindrical geometry with fuel injection, while Bullock et al (1980) chose a cylindrical geometry with an additional valve. In a review of stratified charge engines, Haslett et al (1976) found that (unthrottled) fuel economy was generally better with fuel injection than with carburation.

The position of the spark plug within the pre-chamber has also been shown to have an important effect on performance (Varde and Lubin 1974, Brandstetter 1980); the optimum location varies with cylinder geometry, mixture preparation method and orifice design.

2.3. VOLUME RATIO

The volume ratio, defined as the ratio of pre-chamber volume to total clearance volume, has a pronounced effect on combustion rate and emissions. It controls the total mass flowing through the connecting orifice; this affects the velocity of flow through the orifice during compression and hence the level of turbulence generated. This also (in the case of stratified engines) affects the rate of mixing in the pre-chamber. Similarly affected is the speed of the torch of combustion products entering the main chamber following pre-chamber ignition. Increased turbulence, created by increased orifice flow velocities, enhances flame propagation in each chamber. Volume ratios adopted for engine tests reported in the literature vary from 2-3% (Gussak 1983) to 70% (Hull and Sorenson 1978).

Newhall and El Messiri (1970a,1970b) used a divided chamber engine with a very large pre-chamber (65% volume ratio) to demonstrate reduced octane requirements and lower NO emissions for a divided chamber engine, vis à vis those of a conventional single chamber. These authors suggested that NO formation reactions could be suppressed by the rapid reduction in combustion temperature following mixing and quenching with cool air in the secondary chamber; at the same time the extra oxygen availability in the secondary chamber could assist oxidation of carbon monoxide and hydrocarbons at a temperature below that required for significant NO formation.

The effect of varying volume ratio in the range 3-60% was studied by Gruden (1975,1976). Poor fuel consumption and increased emissions were noted for pre-chambers of size in excess of 20% of total clearance volume. Weaving and Corkhill (1976) reported

that a large pre-chamber (30%) gave a better lean limit, while fuel economy improved as the size was reduced to 10%.

Al-Mamar (1983) studied the effect of varying volume ratio (in the range 7-25%) and showed that the power output of his engine was independent of pre-chamber size, provided that the ignition timing was optimal for each condition. He noted that less ignition advance was required with his larger pre-chamber sizes, because of faster burn rates associated with the higher orifice flow velocities that occur with increased volume ratio.

2.4. ORIFICE CONFIGURATION

Orifice size, shape and orientation also affect combustion rate, principally by altering the flow velocity through the orifice and the way in which the flame spreads.

Adams (1979) studied the effect of changing nozzle orientation. Using a homogeneous charge engine, he showed that the power output was maximised when the nozzle was directed diametrically across the combustion chamber. As the distance from the nozzle to the cylinder wall increased, the volume entrained by the torch also increased - leading to an enhanced combustion rate.

The effect of using a number of orifices of varying shape was investigated by Yagi et al (1979). They altered the angle of taper (diverging from pre to main chamber) for a single orifice (nozzle) from 0 to 14.5 degrees and noted a minimum in HC emissions with a 10 degree taper; no effect on NO emissions was observed. When multiple orifices were used, it was possible for unburnt charge from the periphery of the main chamber to recirculate through the passages into the pre-chamber and back to the main chamber. As a consequence of this the combustion process was sustained for a longer period of time, reducing peak temperature and pressure; NO emissions were therefore reduced slightly. A significant reduction in HC emissions was also observed. The authors postulated that this improvement was associated with the re-circulation and consequent combustion of a quantity of charge which might otherwise have been quenched in the wall region of the main chamber. Weaving and Corkhill (1976), however, showed fuel economy to be worse with multiple orifices.

Kerimov and Mektiev (1978) produced a novel pre-chamber design which employed two orifices in the pre-chamber. Fuel injection was directed into a pre-chamber having a volume equal to 3% of the clearance volume. The pre-chamber was unscavenged and the jet was directed through it to one of the nozzles which was arranged to be co-axial; this achieved stratification in the flow direction. As the pre-chamber was so small the jet scavenged the pre-chamber of burnt gases. Fresh air was sucked into the pre-chamber through the second orifice as a result of the vacuum caused by the fuel jet. This provided a

rich clean mixture in the chamber. At the time of ignition the piston covered one of the nozzles so the combustion process was similar to that of a more normal divided chamber engine. Successful scavenging of the pre-chamber was therefore claimed without the need for an additional valve.

Single round, oval and rectangular shaped orifices have been used by Dimick et al (1979); they also studied the use of multiple orifices. No one design showed any benefit over a single round orifice; the size however did have a large effect. Smaller orifices gave lower NO emissions and faster combustion rates. Photographs of the combustion process showed that the flame front travelled across the chamber 3 to 4 times faster than its normal speed in a single chamber engine. With large interconnecting orifice diameters they noted flame propagation rates very similar to that of a single chamber engine, since the jet action was very weak under these conditions.

Gruden (1975) also noticed lower NO emissions with a small orifice. Emissions of HC and fuel consumption were also lower with reducing orifice size, however these effects were accompanied by a reduction in engine power. This could be compensated by an increase in compression ratio as the maximum 'knock free' compression ratio proved higher than that of a conventional single chamber engine.

Cyclic variation in engine performance has been shown to reduce as the orifice diameter is made smaller (Wall and Heywood, 1978). This was considered to be a consequence of a more consistent turbulence level being generated by the jet created by the orifice flow - especially at high orifice flow rates. In a study of cyclic variation in a single chamber engine, Nakagawa et al (1982) demonstrated a reduction in cyclic variation as the combustion duration was reduced (this was achieved by using multiple spark plugs). This effect could in part explain the observations of Wall and Heywood; a reduction in orifice size would be accompanied by an increase in combustion rate due to the higher jet velocity.

An explanation for the lower NO emissions associated with small orifices was put forward by Konishi et al (1979). They suggested that the jet flow produces large scale mixing of the burned gas behind the flame front, and that this in turn leads to: (a) decreased temperature gradient and (b) lower mean gas temperature as a consequence of higher heat losses (resultant from higher gas velocities). Both these effects would inhibit NO formation.

2.5. DEGREE OF STRATIFICATION

A number of workers have reported successful lean running of divided chamber engines with homogeneous mixtures (e.g. Adams 1979, Wyczalek et al 1975b, Desoky 1981). However most workers have taken advantage of the relative ease in which engines of such a geometry can be operated stratified.

Experimental work conducted in a divided chamber constant volume bomb by Kataoka et al (1984) demonstrated the decrease in combustion duration, i.e. increase in flame speed, that could be obtained by stratifying the charge. When operating stratified the combustion duration proved virtually independent of the overall mixture strength.

Photographs of the combustion process (Sinnamon and Cole 1979) have shown that the intensity of the torch, or jet of combustion products issuing from the pre-chamber into the main chamber, increases as the pre-chamber was enriched at an overall equivalence ratio of 0.8. Increase in pre-chamber equivalence ratio above stoichiometric had little effect on jet penetration. Pressure records showed a shorter burn duration when the engine was operated stratified; it was considered that the initial combustion rate was faster as a consequence of a stronger torch effect. The film also showed that the jet plume broke up into smaller pockets of rich charge, randomly dispersed throughout the cylinder. This incomplete mixing lead to higher CO emissions when highly stratified. Higher CO emissions with very high degrees of stratification were also demonstrated by Pischinger et al (1976). Pischinger and Klocker (1974) showed a decrease in engine power and efficiency when stratified; again incomplete mixing could be responsible for this.

Slow and incomplete mixing of the jet plume at high degrees of stratification was thought to be the cause of the very high CO emissions and poor fuel economy found by Kreiger and Davis (1976). They had a small (7%) pre-chamber and large (16mm) orifice so the jet was very weak. Their recorded NO and HC emission levels were, however, very low. They suggested that the pre-chamber was the main source of CO emissions, and that the jet plume was the main region of NO formation. Poor mixing would therefore inhibit NO formation, due to the low oxygen availability in the hot rich pockets of charge. Sorenson and Pan (1979) developed a one dimensional model of divided chamber combustion. When they allowed a region of intermediate equivalence ratio to exist in the main chamber close to the nozzle, the model predicted that NO emissions would double; this appears to verify that the majority of NO formation is in the jet plume where the equivalence ratio is only slightly lean. In the divided chamber of Watfa et al (1974), NO emissions were very low. They reasoned that one chamber was too rich for NO formation, while the other was too lean. A decrease in the overall equivalence ratio with this engine led to increased NO emissions, as the enriched pre-chamber came within the range of equivalence ratios most suited for NO formation.

Sakai et al (1976) used a sodium line reversal method to measure the gas temperature in a stratified charge divided chamber engine. They observed higher temperatures in the pre-chamber and the torch than in a conventional engine; this was a consequence of the richer mixtures in those regions. They reasoned that as combustion continued in the leaner

main chamber regions, the temperature fell and so inhibited NO formation. These workers injected carbon dioxide into the pre-chamber and air into the main chamber, they then took samples at given crank angles using a high speed sampling valve. They showed a rich region to be present around the torch and in the pre-chamber at the time of ignition.

The divided chamber concept has successfully been used in a production engine by Honda (Date et al 1974); using an additional valve 1950cc four cylinder engine they managed to meet the 1975 emission standards, set by Japan and the United States, without sacrificing fuel economy or driveability. The engine was run stratified with an optimised volume ratio of 7.3%. The rich pre-chamber mixture and lean main chamber mixture gave low peak temperatures, so inhibiting NO formation, while the slow main chamber combustion (resultant from a lean mixture) ensured that the average temperature was high enough to facilitate CO and HC oxidation. Extensive work has also been conducted by British Leyland on additional valve stratified charge engines, e.g. Weaving and Corkhill (1976), Weaving (1982). They found that when the engine was tuned for optimum economy, the pre-chamber supply air/fuel ratio was 15:1. The actual air/fuel ratio in each chamber was not only a function of carburettor air/fuel ratios and flowrates, but also of ignition timing. This was because the flow between chambers (a function of piston position) reduced the degree of stratification. The pre-chamber air/fuel ratio at ignition was calculated to be in the range 16-20:1. Further stratification led to higher NO, as the charge in the pre-chamber burned at a mixture strength nearer to that giving peak NO formation rate. The extra ignition advance required for the richer pre-chamber mixtures also led to greater emissions of NO because of increased residence time.

Gussak and Turkish (1976) used a very small pre-chamber (2-3% VR) in their engine studies. They claimed that following ignition chemically active free radicals were produced; it was reasoned that these would enhance combustion in the weak main chamber by providing a large number of ignition sites. In further work, faster combustion rates (compared with single chamber operation), lower octane requirement and inhibition of knock reactions were demonstrated (Gussak et al, 1979; Gussak, 1983). The radicals were claimed to initiate combustion at temperatures 300-800°C lower than in a 'normal' flame, with the result of considerably reduced NO emissions. However, Gussak et al claimed that oxidation of CO and HC presented no problem - since the bulk of the charge was lean (oxygen availability was high).

2.6. CONCLUSIONS

The following conclusions are drawn:-

- (1) Divided chamber engines have potential for operation with very lean mixtures, with higher compression ratios and lower octane rated fuels than conventional single chamber engines.
- (2) Main chamber cylinder temperatures are lower than those of conventional engines as a result of increased heat transfer losses and leaner mixtures.
- (3) Emissions of NO are generally lower in divided chamber engines because of the generally lower temperatures within them. When operating stratified, NO formation is inhibited in the hotter richer regions as a result of low oxygen availability.
- (4) Emissions of HC are generally higher in divided chamber engines than in single chambers, as the cylinder wall surface area is larger; hence quench volumes are larger.
- (5) Emissions of CO are high when the degree of stratification is high; this is thought to be due to incomplete mixing of the rich and lean regions.
- (6) Pre-chamber volumes larger than 20% of the total clearance volume appear to give poor fuel consumption and emissions.
- (7) Orifice shape appears to have little effect; orientation, however, is important.
- (8) Less cyclic variation and lower emissions are experienced with smaller orifice size. This as a consequence of the better mixing and higher heat losses under these conditions.
- (9) Faster combustion is possible with stratified charge operation; this however requires a fuel injector or an extra carburettor and a mechanism to operate an additional valve (into the pre-chamber).

These engine types may yet prove to offer the best prospect for satisfying increasingly stringent emissions legislation in an era of deteriorating quality of gasoline fuels. However, considerably more experimental and theoretical modelling work may be needed before a full understanding of the combustion process occurring within them is developed. This is required to optimise the many variables associated with such engines, in order to realise their full potential for meeting the range of emissions and fuel economy criteria set in various world markets.

CHAPTER 3

Equipment and Instrumentation

CONTENTS

3.1	INTRODUCTION	19
3.2	YAMAHA ENGINE	19
3.2.1	Cylinder Head Design	20
3.2.2	Piston Modifications	23
3.2.3	Lubrication	23
3.2.4	Fuel System	24
3.3	INSTRUMENTATION	25
3.3.1	Crank Angle Position	25
3.3.2	Ignition System	26
3.3.3	Pressure Measurement	27
3.3.4	On Line Data Acquisition	27
3.3.5	Engine Speed Measurement	29
3.4	PHOTOGRAPHIC EQUIPMENT	29
3.5	TEST PROCEDURES	30

3.1. INTRODUCTION

Described in this chapter are the equipment and instrumentation used in the experimental work, together with a discussion of some of the problems encountered.

The study involved the use of high speed photography with simultaneous sampling of cylinder pressure using an on-line computer. Both conventional and schlieren photographic techniques were employed; the schlieren photography in the pre-chamber only, where through optical access was available. In future it may prove possible to use schlieren techniques in the main chamber by providing a mirrored piston crown. This has been done successfully in a diesel engine by Shiozaki et al (1980). Alternatively it may be possible to use a quartz piston with a mirror mounted beneath it giving through optical access in the main chamber (Hamamoto et al, 1976).

Initially work was conducted on a Ruston air cooled, single cylinder side valve engine, used previously by Desoky (1981) and Al-Mamar (1983). A detailed description of this engine and its instrumentation can be found in the above references and so is omitted here. However, details which have been changed are described together with reasons for each change. Later work was performed on a Yamaha 400cc single cylinder two stroke engine, used previously for an MSc project (Panicker, 1982). A discussion of the reasons for changing engines is given below.

3.2. YAMAHA ENGINE

When analysing films of combustion in the Ruston engine it proved difficult to take into account the effect of fuel burned in the valve chamber. Desoky (1981) and Al-Mamar (1983) used a special metal gasket in an attempt to cut off the valve chamber at TDC, to minimise its effect on the combustion event (Fig. 3.1). Nevertheless as the engine's piston moved downward and uncovered the valve chamber, the remaining unburnt mixture in the main chamber was pushed into the valve chamber and was burned there, together with mixture trapped in this space at TDC. The above workers traced flame progress from their films of combustion and measured inflamed areas - these were used to estimate the percentage volume and mass fraction burned at any instant. This procedure took no account of fuel burning in the valve chamber; its complex shape made estimation of inflamed volume difficult, this led to inaccuracies in the calculations.

Also, if the compression ratio of the engine were to be increased, for an irreducible minimum valve chamber volume, the size of the main chamber would have to be reduced. This would result in the valve chamber becoming a much larger proportion of the total clearance volume - exacerbating the problem outlined in the previous paragraph.

An overhead valve engine could not be used to overcome this problem as filming of combustion would be very difficult, involving the use of a transparent piston with a mirror beneath it and an associated loss of field of view. The only alternative therefore was to use a two stroke engine, as such an engine has no valves to interfere with optical access; the charge entering and leaving by ports in the cylinder walls.

However, a disadvantage encountered with the 2-stroke Yamaha engine adopted was that, although of almost the same nominal capacity, it had a clearance volume of only approximately half that of the Ruston used previously (Appendix A). This is because in a 2-stroke engine compression only starts when the exhaust port is covered. At this point the piston is approximately half way up the barrel instead of close to BDC, as it would be at valve closure in a 4-stroke engine. As a result there was much less room available in which to fit the orifice connecting the two chambers in the case of the Yamaha. This was further aggravated by having the orifice parallel to the piston crown instead of at an angle (as in the Ruston). The reason for this will be explained later.

The work currently reported was concerned with extending the single and divided chamber work of Al-Mamar. In particular results were needed to compare flame propagation rates and pressure histories with predictions from the computer models described in Chapters 5, 6 and 7. In order to conduct these experiments a number of major modifications to the engine and data acquisition techniques were required.

3.2.1. Cylinder Head Design

The purpose of the experiments was to examine the effect of varying turbulence levels on ignition and flame propagation. This was accomplished by altering the size of the pre-chamber and the orifice connecting the two chambers; an increase in pre-chamber size or decrease in orifice size increased the flow velocity between chambers and hence produced an increase in turbulence. Optical access was required to both chambers. Although the perspex cylinder heads had lasted reasonably well on the Ruston engine, they were difficult and time consuming to manufacture. They were made from a solid block of perspex; they could be used for only a relatively short running period as they would burn if used for a long run.

It was considered that quartz would prove a superior material, as it would permit longer runs without burning. However since quartz is difficult and very costly to machine it had to be used in simple shapes. This meant the pre-chamber could no longer be spherical, so a cylindrical geometry was chosen. Although this had disadvantages from a modelling point of view, it was considered that it would improve the prospects for successful adoption of laser doppler anemometry. A spherical chamber would have caused problems associated with differing path lengths for the two beams through the quartz, and the refraction of the

beams at exit from a curved surface. The pre-chamber size could be altered using steel inserts (Fig. 3.2(a)), the aspect ratio of the chamber was chosen to be 1 (i.e. its diameter equal to its height) in order to keep the geometry as similar to that of the Ruston as possible. In the original design the orifice size was controlled by inserts (Fig. 3.2(b)); this design was later modified.

In the Ruston engine the orifice connecting the two chambers was at an angle of approximately 30 degrees. Adoption of this angle for the Yamaha would have caused problems in modelling the flow in the pre-chamber, as the flow would not be symmetrical (Fig. 3.3(a)). To avoid this problem the pre-chamber could have been angled so that flow was symmetrical (Fig. 3.3(b)); however this would have made conventional photography difficult, involving the use of a prism. An alternative considered was to rotate the pre-chamber through 90 degrees (Fig. 3.3 (c)). This would have made it easier to use schlieren and LDA techniques without mirrors, but this would again have made conventional photography difficult.

The alternative chosen (Fig. 3.3(d)) was to have the orifice in line with the axis of both chambers, so making modelling and conventional photography easier. However since the pre-chamber is much deeper than the main chamber at TDC, the cylinder head needed to be deeper and the barrel modified so that the head would fit on. This arrangement also necessitated a mirror for LDA and schlieren photography.

The cylinder head design is shown sketched in Figs. 3.4 & 3.5. Windows were provided above and below the pre-chamber, giving through optical access; this arrangement simplified schlieren photography. It was also preferred as it would allow the adoption of the forward scattering technique in later LDA work; this needs less laser power than the alternative back scattering method.

The size of the clearance volume in the main chamber was made adjustable so that the total clearance volume could be kept constant when either the pre-chamber volume or the compression ratio was varied. The adjustment was effected by placing copper shims between the main chamber window and the step in the head, and between this step and the barrel. As mentioned previously, the clearance volume was much smaller than that of the Ruston. In order to help make results more comparable with earlier work conducted on the Ruston engine, the orifice sizes were scaled down to reproduce the orifice flow velocities obtained with the Ruston (at corresponding operating conditions). In the work using the Ruston engine, orifice sizes of 5, 7, and 9 mm were used for volume ratios of 7, 13, 17, and 25%.

The compression ratios chosen for tests were :- 6.4:1, 8:1, and 10:1. The 6.4:1 ratio was selected as this was the manufacturer's standard value for the Yamaha; the 8:1 ratio

was equal to that used in the Ruston engine study. The ratio of 10:1 was selected as the highest compression ratio that could be accommodated without running into severe problems associated with very small clearance volumes. Pre-chamber volume ratios of 17 & 25% were chosen to compare with the work of Al-Mamar, and 10% to compare with Desoky. The 7% volume ratio used by Al-Mamar would have entailed an extremely small pre-chamber, making filming and the use of lasers difficult, hence this case was not considered. Larger volume ratios would have made the main chamber height very small, reducing the thickness of the step in the cylinder head and making it very difficult to fit an orifice. As the orifice flow velocity during compression was found to have a controlling influence on combustion, it was decided that the orifice diameters used for the Yamaha should be scaled to reproduce the orifice flow velocities calculated for the Ruston at the compression ratio of 8 used in the earlier work. Scaling was also necessary to allow for greater flow rates at higher compression ratios. To avoid confusion when comparing results for the two engines at corresponding conditions, the orifice diameters for the Yamaha were termed no.5, no.7, and no.9 respectively. The resulting diameters of the scaled orifices are given in Table 3.1 for a range of compression ratios. The clearance between the piston crown and the cylinder head proved too small to allow the use of a no.9 orifice. Similarly, the no.7 orifice could be adopted for all volume ratios only at the lowest compression ratio; at the compression ratio of 8:1 it could only be used with the smallest volume ratio. This problem could have been overcome by using non-circular orifices; however, this was not considered initially as it would have made comparison of results between engines more difficult. Tests were principally carried out using a no.5 orifice; in later work the number and shape of the orifices were varied.

The cylinder barrel was machined down as shown in Fig. 3.6, enabling the new cylinder head to slide over the top and support this part of the liner. A further section of the barrel was cut away to give optical access to the lower pre-chamber window. A mirror was

	COMPRESSION RATIO			
	Yamaha			Ruston
	6.40	8.00	10.00	8.00
no.5	3.83	3.40	3.06	5.00
no.7	5.35	4.80	4.29	7.00
no.9	6.89	6.20	5.51	9.00

mounted in this space, supported by an arm remote from the engine so that it was unaffected by vibration.

During preliminary tests with the engine, leakage from the cylinder head was encountered. This occurred around the region where the orifice insert entered the cylinder head. The copper shims had a portion cut away to accommodate the insert; it was through this path that leakage occurred. The cylinder head was therefore re-designed so that the orifice size and the cylinder clearance height were controlled by a cylindrical insert (Figs. 3.7 & 3.8). Although this made the inserts larger and more time consuming to manufacture, it allowed the use of a complete ring of copper shim, so removing the leakage path.

Flush mounting of the two pressure transducers in the cylinder head was not possible because of the limited space available. These were therefore mounted as close as possible to the surface of their respective chambers; no problems with resonance in the connecting passage were encountered.

A second cylinder head was manufactured for single chamber operation (Fig. 3.9); copper shims were again used with this head to allow the compression ratio to be varied. However, the spark electrodes were re-designed so that the sealing surface created by the step in the cylinder head was not interrupted.

3.2.2. Piston Modifications

The piston crown of the Yamaha was originally curved; a flat crown was required to create the desired disc shaped chamber. This was needed to allow comparison of results with those of the Ruston engine; the uncomplicated geometry also simplified modelling. The Yamaha's piston crown was reasonably thick, so it was merely machined flat and used in its weakened state. It survived hydraulic testing at the anticipated maximum cylinder pressure; nevertheless for future continuous use at higher compression ratios it may prove necessary to incorporate a strengthening insert in the weakened central portion of the piston crown.

3.2.3. Lubrication

The Yamaha's standard lubrication system involved pumping oil, via a gearbox driven pump, into the inlet port of the engine; this then found its way onto the bearings and the cylinder liner. As installed on the test bed, the engine was driven via a coupling attached to the crankshaft at the clutch side of the engine with the clutch removed. As a result the gearbox and oil pump no longer rotated, necessitating an alternative lubrication system. In previous work on this engine (Panicker 1982, Carter and Hempstead 1982) lubrication was effected by feeding a petrol-oil mixture to the carburettor. However, when combustion was

filmed the results were not good, yellow patches appearing on the predominately blue flames, these being caused by burning oil droplets. To overcome this problem the engine was run on a petrol-oil mixture for five minutes to ensure adequate lubrication, and then switched to pure petrol for one minute prior to filming. Alternatives to this system considered were: (a) injection of oil directly into the crankcase to spray over the bearings, (b) blowing fuel-air mixture directly into the transfer ports, sealing the passage between the transfer ports and crankcase to allow the latter to be used as an oil sump. Eventually it was decided that it would be simplest to modify the system used by Panicker to allow separate petrol and oil flows. Oil was gravity fed directly to the intake manifold. This supply could be switched off just prior to filming, thus reducing the time that the engine was required to run without lubrication as the fuel line did not need clearing. This lessened the risk of engine seizure.

3.2.4. Fuel System

Fuel was fed to the air supply pipe through a nozzle which incorporated a number of 0.12 mm diameter holes. This produced a very fine spray which, when mixed with the air, was pre-heated to a constant inlet temperature of 30°C prior to entry into the engine. This was achieved using an electrical heating element wrapped around the inlet pipe; it ensured complete evaporation of the fuel.

The fuel was supplied from a constant head tank through a fine control valve and a rotameter to the injection nozzle (Fig. 3.10). The rotameter ensured more accurate metering of the fuel than that previously obtained using a calibrated control valve. The revised system still required calibration; this was achieved by removing the nozzle from the air supply pipe and measuring the time for a given quantity of fuel to pass through. A number of injection nozzles were found necessary; the maximum flow rate was limited by the available head. As the flowrate was reduced the fuel would start to drip out instead of spraying; these factors gave a flow range suitable for each nozzle. Calibration was performed on each nozzle, this however proved unnecessary as the flowrate was constant for a given rotameter reading. Atmospheric pressure and ambient temperature were also shown to have no effect on the volume flowrate. (The mass flowrate did of course vary with any change in fuel density associated with a change in ambient temperature; this was taken into account when setting the rotameter to give a chosen equivalence ratio.) The fuel used for all of the tests was a reference four star fuel supplied by BP having an octane number of 97.8 RON (Appendix A).

The air supply was metered by an Alcock viscous air flow meter coupled with an inclined manometer. The inlet mixture temperature was measured with a thermocouple fitted

close to the inlet port. In all tests the engine remained unthrottled. The arrangement of the fuel and air supply systems is illustrated in Figs. 3.10 and 3.11.

3.3. INSTRUMENTATION

3.3.1. Crank Angle Position

In order to use the pressure measurements taken from the engine it is necessary to know accurately the piston position at which they were recorded. In previous work on the Ruston engine the piston position at a given pressure sample was not known as accurately as one might wish. With that system a signal was sent to the on-line computer at TDC; this was generated by an electro-magnetic pickup which sensed a piece of ferrous metal mounted on the flywheel. Pressure samples were taken at time intervals chosen to approximate 1 crank angle degree. However since piston movement has been shown to be slower during the compression stroke than during the expansion stroke (Witze et al, 1983) it follows that pressure and other readings would need to be sampled at equal intervals of crank angle. This made it very difficult to accurately calculate quantities such as spark advance and mean effective pressure.

The Indicated Mean Effective Pressure (IMEP) was calculated by integrating the pressure-volume curve between start of compression and end of expansion. This calculation would of course be incorrect if the pressure readings were not exactly one crank degree apart; the change in volume would be smaller than calculated during compression and larger during expansion due to the variation in engine rotational speed during the cycle.

It was therefore considered more satisfactory, for the calculation of IMEP, to take samples at equal intervals in crank angle rather than time. This was done by using the output from a shaft encoder to trigger the ADC's instead of using a timer. The shaft encoder was required to produce 360 pulses per revolution so that samples were exactly one crank degree apart, irrespective of engine speed. A shaft encoder was manufactured; it consisted of a 12 inch diameter disc with 360 holes equally spaced around its circumference. This was mounted on the engine crankshaft. A slotted optical Schmidt switch was used in conjunction with this to give a square wave of wavelength equal to 1 crank angle degree.

A second switch was mounted at a different position; set to align with a single hole on a different diameter, this was used to supply a TDC signal. Both these signals were sent to the ignition unit and the on-line computer (described later). In practice difficulties were experienced with alignment of the disc as a close tolerance was required between the disc and the optical switch. Movement of the disc caused interference with the signal and led to less than 360 samples being taken per revolution. To overcome this the disc was replaced by a commercial shaft encoder (Hohner 320D/360). This was again connected to the crankshaft,

however a flexible coupling was needed between the two. Care was taken to ensure the coupling chosen was one which allowed movement only in the required directions and did not allow twisting, as this would cause the TDC signal to become misaligned.

3.3.2. Ignition System

The ignition system used on the Ruston engine consisted of a Mobelec Magnum contactless electronic ignition unit, a standard ignition coil and a 12 volt battery. For the Yamaha the Mobelec unit was replaced by a Sparkrite SX2000 Mk2; this provided an ignition energy of 45mJ @1400 rpm and a spark duration of 2 mSec. The triggering unit was designed by Mr L. Williams of the Electrical and Electronic Engineering Department at Leeds University. The control system counted pulses from the shaft encoder and triggered the spark at the required angle. The spark timing could be set to any crank angle between 90 degrees BTDC and 90 degrees ATDC. It could also be restricted to firing every alternate cycle or every 3rd, 4th or 5th cycle. In practice the engine was fired every 4th cycle to facilitate breathing, as scavenging of the pre-chamber was poor if fired more frequently. It also helped to prevent the engine accelerating beyond the required speed.

The system provided spark and TDC signals to feed to the on-line computer; it also 'gated' the once every degree clock pulse which triggered the computers data acquisition system. When operating in the firing 3rd, 4th or 5th cycle mode, some of the motoring cycles were not sampled. This was necessary to reduce the amount of data stored in the computer; the procedure is described in more detail later.

The spark electrodes consisted of two 1.6mm diameter brass rods inserted into the centre of the pre-chamber. In the Ruston engine one of the electrodes was at the centre of a 10mm diameter PTFE bar, while the second was inserted into a groove on the bar surface.

For the Yamaha engine, for single chamber operation, a separate head was used. In this head spark electrodes protruded into the main chamber, such that both central and side ignition were possible. However the Ruston's electrodes (described above) could not be used because of the Yamaha's small clearance height (between the piston crown at TDC and the cylinder head). Instead the electrodes were encased in 3mm diameter alumina tubes; these were of sufficiently small diameter to ensure that they could pass through the step in the cylinder head, thus avoiding cylinder head sealing problems (Fig.3.9). For the divided chamber head, the two electrodes and insulating alumina tubes were initially mounted in a 10mm diameter steel rod; this permitted adjustment of the electrode position so that the spark gap was always in the centre of the (various sized) pre-chamber inserts. However, the alumina tube proved unreliable; it only survived for one or two tests before cracking, allowing the spark to earth. The arrangement was replaced by the centre electrode from a

standard spark plug, and a brass rod was mounted into a hole in the pre-chamber insert to provide an earth electrode.

3.3.3. Pressure Measurement

Engine cylinder pressure is an important engine parameter; it provides information allowing estimation of the mass burning rate of the fuel. It also enables calculation of the indicated power output of the engine.

For the work reported in this thesis the pressure in each chamber was measured using piezo-electric pressure transducers. (Kistler model 701A). These transducers were considered to be particularly suitable for engine use, being capable of measuring rapidly varying pressure in the range 0 - 600 atm (while maintaining linearity and having very good frequency response). However, these transducers were sensitive to spark generated noise and so care had to be taken to prevent this occurring.

The transducers were mounted in the cylinder head as close as possible to the walls of their respective chambers. As discussed earlier, flush mounting of the transducers (as recommended by the manufacturers) was not possible in either chamber. In the pre-chamber it would have made the use of inserts extremely difficult. In the main chamber the clearance height above the piston at TDC was too small. Mounting of the transducer above the piston would have resulted in restricted optical access. The transducers were not water cooled; this was not necessary for the short engine running periods adopted in the tests.

It was necessary to calibrate the pressure transducer-charge amplifier combination to determine the relationship between applied pressure and voltage output. This was achieved by applying known pressure to the transducer, from a nitrogen gas cylinder, and measuring the voltage output using a Keithley 177 microvolt DMM Digital Voltmeter. The pressure was increased from 0 to 63 in steps of 7 Bar, the output voltage being noted at each point. During this procedure the charge amplifiers (Kistler type 5007), were used with the long time constant. When used in the engine under dynamic conditions the medium time constant was required. As the transducer was calibrated statically, inadequate transducer response could lead to spurious results.

3.3.4. On Line Data Acquisition

It was necessary to store the pressure measurements and other signals for subsequent processing to determine, for example, IMEP. In the work reported here the pressure signals from both chambers, together with spark and TDC signals, were converted to digital form using a Micro-Consultants very high speed analogue to digital converter (ADC) unit. This unit was capable of sampling up to 8 channels simultaneously, at a maximum rate of

400 kHz. It was interfaced to a VAX 8600 minicomputer via a direct memory access interface (DR-11B), which permitted a maximum of 32767 samples to be stored.

The sampling rate was controlled by an external clock. This comprised the 360 pulse shaft encoder and ignition unit described earlier. A square wave pulse was generated with a wavelength equal to 1 degree crank angle of the engine. Each time the ADC's received a pulse they would simultaneously sample all 4 channels; the digital signals were then stored in an array in the form 1234 1234 1234 Sampling stopped when the array was full or the 32767 point limit was reached.

The ADC system also allowed an external 'gate' input; this only allowed sampling to occur when an external supply of +5 volts was applied to the gate channel. The ignition system incorporated a means of triggering the gate and clock pulses so that sampling always started at BDC of a firing cycle. If there was more than one motoring cycle between firing cycles then the extra motoring cycles were not sampled. This resulted in ten firing cycles being sampled, irrespective of how often firing occurred. When sampling started a signal was fed to the event marker on the camera; this put a mark on the film so that film and computer data could be synchronised. When the film ran out a signal was fed back from the camera control unit to the ignition unit; this closed the gate to the ADC's. The output from the charge amplifier could then be switched off and sampling completed with no pressure signal. This was used as a second method of achieving synchronous film and pressure data. The layout of the control and data acquisition system is shown in Figs. 3.12 and 3.13.

The signal range of the ADC's was 0-10 volts; 10 volts gave a value of 8192. The pressure signals were fed direct from the charge amplifiers to the ADC's. The TDC signal from the shaft encoder was amplified and fed to the ADC's. When the spark occurred a signal was also fed to the ADC's by the ignition unit. This signal, like the TDC signal, was of zero volts except when the event occurred. Then it was of square wave pulse form, of amplitude 5 volts and duration 1 crank angle degree. Once the signal was sampled the information could be immediately processed into pressure-crank angle and pressure-volume diagrams. These could be displayed on a computer terminal. The area under the P - V diagram could also be calculated to give the IMEP. The processed data could be stored on magnetic tape for later reference, if required. The computer programme used for this work is described in Hynes (1986d).

Since the ignition unit-ADC system allowed the camera to trigger sampling, it was possible to relate the film sequence to the pressure trace for each firing cycle; the spark being visible on both, and the camera and engine speeds being known.

3.3.5. Engine Speed Measurement

A disadvantage associated with the shaft encoder system was that the engine speed could no longer be determined from the signals collected by the ADC's. Previously, when samples were taken at a given time interval, it was possible to calculate engine speed from the number of samples taken between consecutive TDC signals.

Initially this problem was overcome by feeding TDC and BDC signals to an LSI 11/03 microcomputer which was programmed to measure the time interval between signals. This gave a measurement of the engine speed during the compression and expansion strokes. These measurements were fed back to the main computer and stored with the data sampled by the ADC's. In later work the microcomputer was replaced by purpose built hardware, as this was more accurate; the microcomputer was still necessary to transfer the data from the hardware to the VAX when required.

3.4. PHOTOGRAPHIC EQUIPMENT

A Hitachi 16HM high speed camera capable of photographing at up to 10,000 frames per second was employed in the experiments. The time between frames was calculated from timing marks put on the film at intervals of 100 microseconds. In the majority of tests a camera speed of 8000 frames per second was used. Both schlieren and conventional photographic techniques were employed; conventional photography covered both chambers, whereas schlieren was used in the pre-chamber only. Where light emission was poor (i.e. for lean mixtures or slow engine speed) the camera speed was reduced to 6000 frames per second. The camera arrangement for photographing is illustrated in Figs. 3.14 and 3.15.

The arrangement for schlieren photography is shown in Fig. 3.16. Illumination was initially provided by a 250 Watt white light, this was kept cool by a blower mounted underneath it. The light was focused by an objective lens onto a concave mirror (focal length 250mm). This was aligned to produce a parallel beam of light which passed, via a flat mirror, through the pre-chamber and onto a flat mirror. From the second mirror the light was focussed, using a lens, onto a knife edge and then passed to the camera. Insufficient light for filming purposes was experienced when this arrangement was used; it also proved difficult to focus the light onto a knife edge, as the light did not emanate from a point source (the element was relatively large). The light source was therefore replaced by a 3mm helium-neon laser, and later (to provide even more light) by a 35mm laser.

The camera was operated remotely by a Gordon type GC 1026 camera control system. The camera speed and timing mark spacing were set prior to the test; microswitches stopped the camera when the film ran out.

Eastman Ektachrome 16mm film (type 7250 tungsten balanced) was used for all tests. This was force processed to 1600 ASA for mixtures as weak as 0.8 equivalence ratio. For mixtures weaker than this a small quantity of sodium ethylate was dissolved in the petrol. This had the effect of making the flame more yellow, hence increasing its definition on film; weak mixtures burned naturally with a pale blue flame which did not show clearly on film.

The high speed films were analysed using a 16mm back projection screen. This allowed slow motion viewing of the film; this gave a useful insight into the combustion process. The film could also be examined frame by frame: each frame could be traced, and the resulting copy retraced on a Summagraphics Bitpad. This was connected to the on-line computer, which read in the x-y co-ordinates of the stylus at a rate of 10 Hz. The stylus was moved round the perimeter of the tracing from the film and the resulting co-ordinates were stored in a file. Points less than 0.5mm away from the last sampled point were ignored, avoiding excessive data storage. The software was written such that if the stylus was moved too fast with resulting data points more than 1.5mm apart, the terminal would emit an audible warning.

Once the x-y co-ordinates of each flame position were stored it was possible to process this data and calculate flame area and perimeter. The programs for doing this are reported in Hynes (1986c, 1986d). It was possible to estimate a flame speed between each frame by calculating the increase in radius of an equivalent spherical flame (having the same projected area) in the known time interval.

3.5. TEST PROCEDURES

Engine combustion is affected by a great number of variables. It was therefore important to ensure that all parameters, other than those required to vary, remained constant throughout the tests. In order to achieve this several precautions were taken before data was recorded.

The fuel system was calibrated at different ambient conditions to ensure the flowrate remained constant for a given rotameter reading; changes in fuel density were taken into account when calculating mass flowrate and equivalence ratio. The air flowrate was measured each time test data were recorded, the volumetric efficiency and corresponding intake pressure were similarly re-calculated each time.

The charge amplifiers were allowed to warm up for half an hour before tests were conducted. A motoring test was then performed to check for leakage from the cylinder head (by examination of the peak pressure value) and to check coincidence of the pressure traces for the two chambers. The pressure traces may not coincide exactly when using a large volume ratio and small orifice diameter (Al-Mamar). When firing the engine, data was not sampled until the inlet temperature was constant at 30°C and the engine running smoothly.

The capacity of the ADC's set a limit to how much data it was possible to sample (10 firing cycles); tests at the same conditions were required to examine the repeatability, and where this was poor the tests were repeated many times.

 - perspex

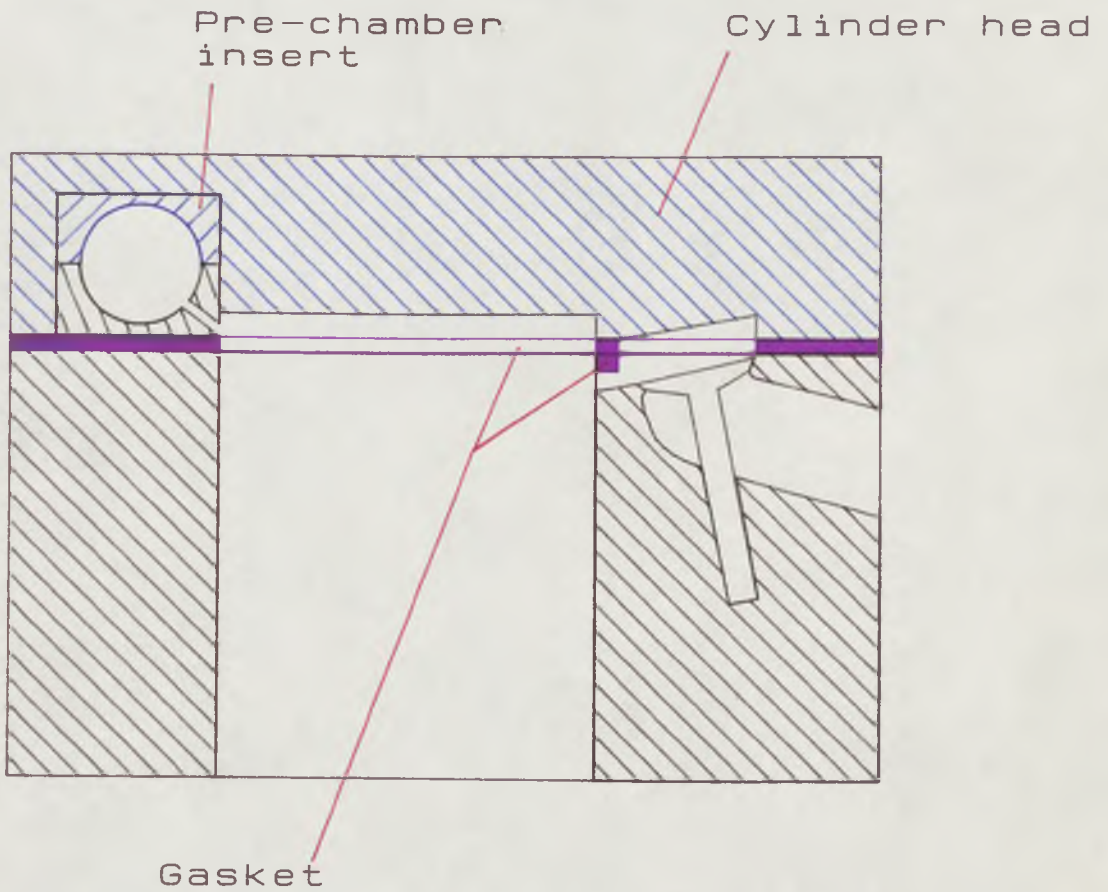


Fig.3.1

Cross section of cylinder on the Ruston engine, showing the gasket used to cut off the valve chamber at TDC.

orifice

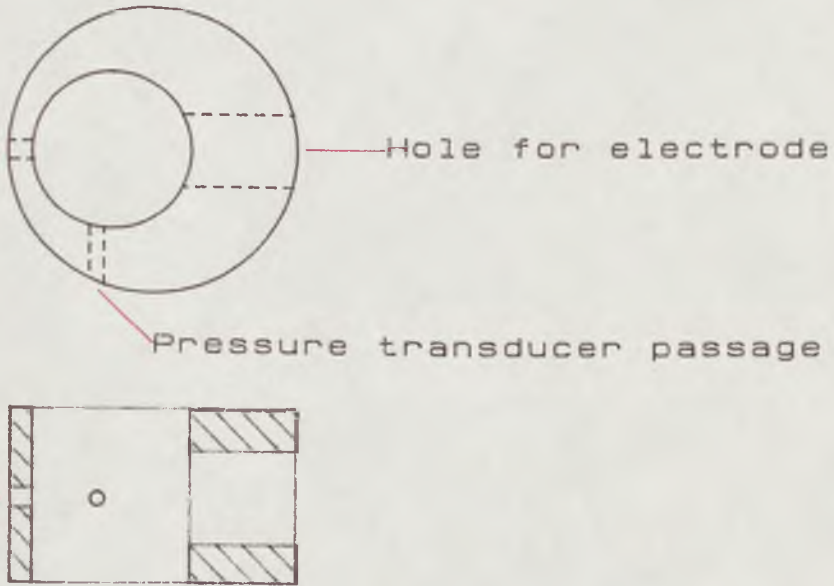


Fig.3.2 (a) Pre-chamber Inserts

orifice

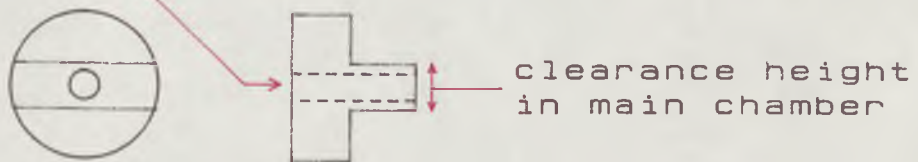


Fig.3.2 (b) Orifice Inserts

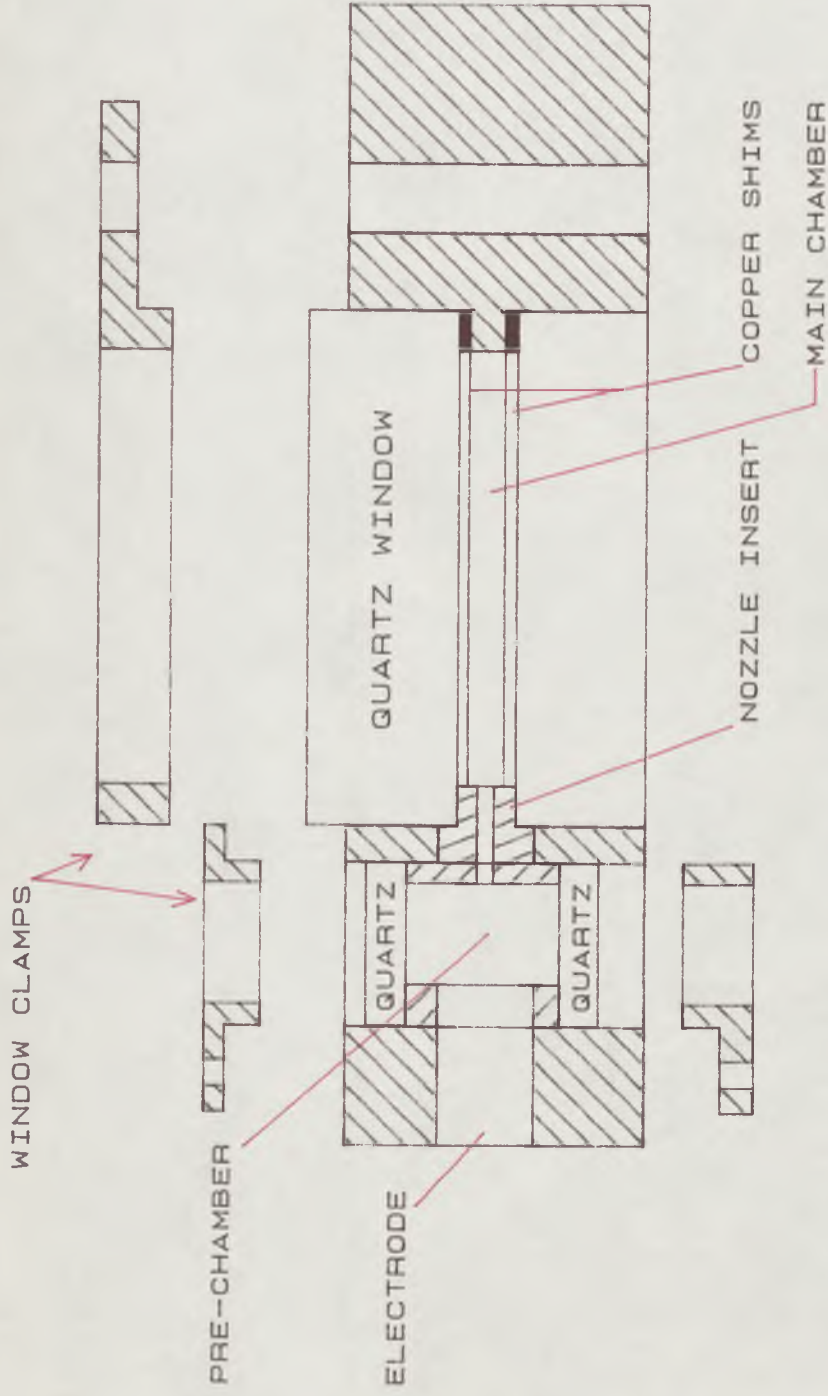


Fig. 3.4 Cylinder head design

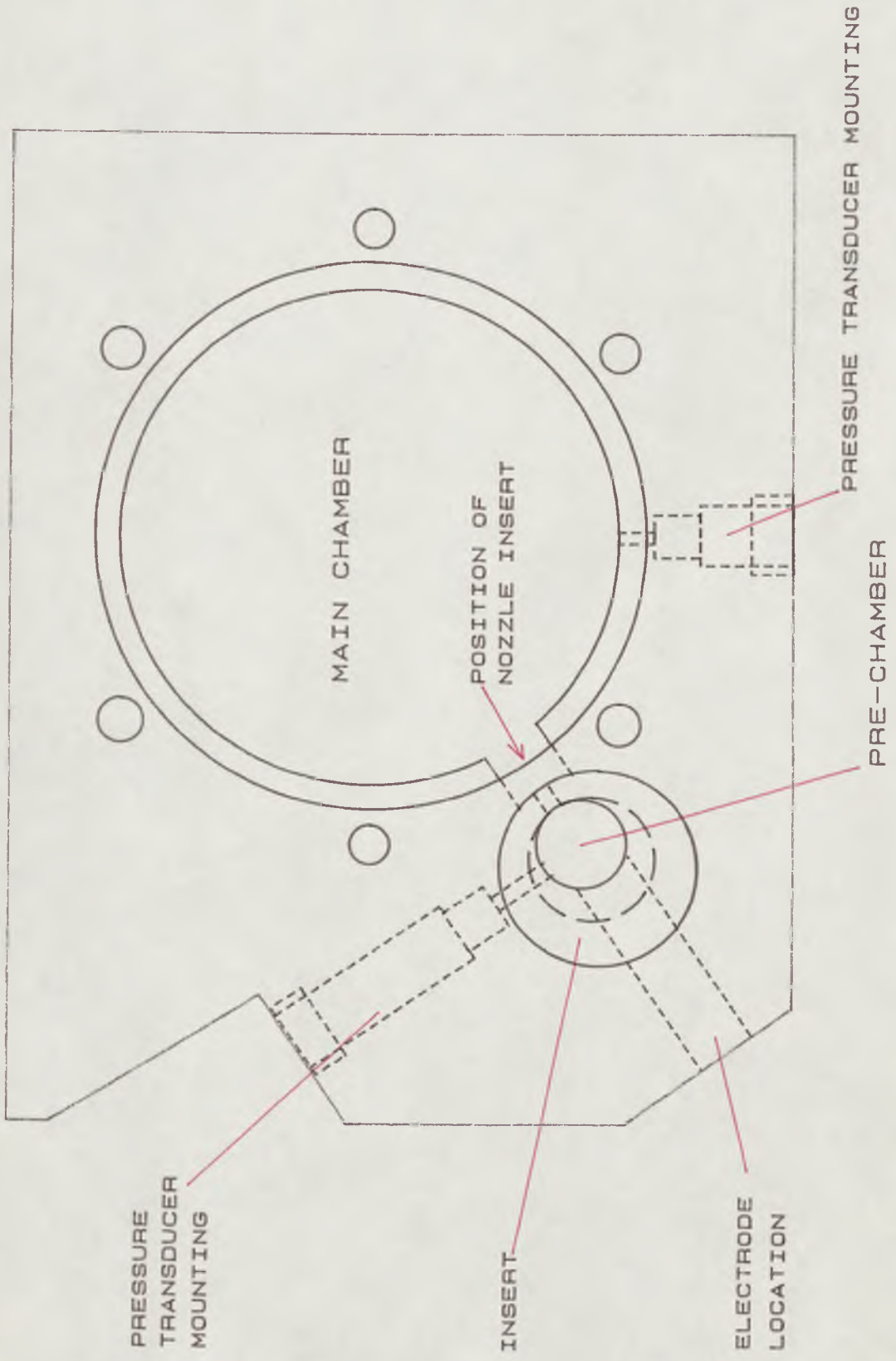


Fig.3.5 Cylinder head (plan view)



Fig.3.6

Modifications to the cylinder barrel

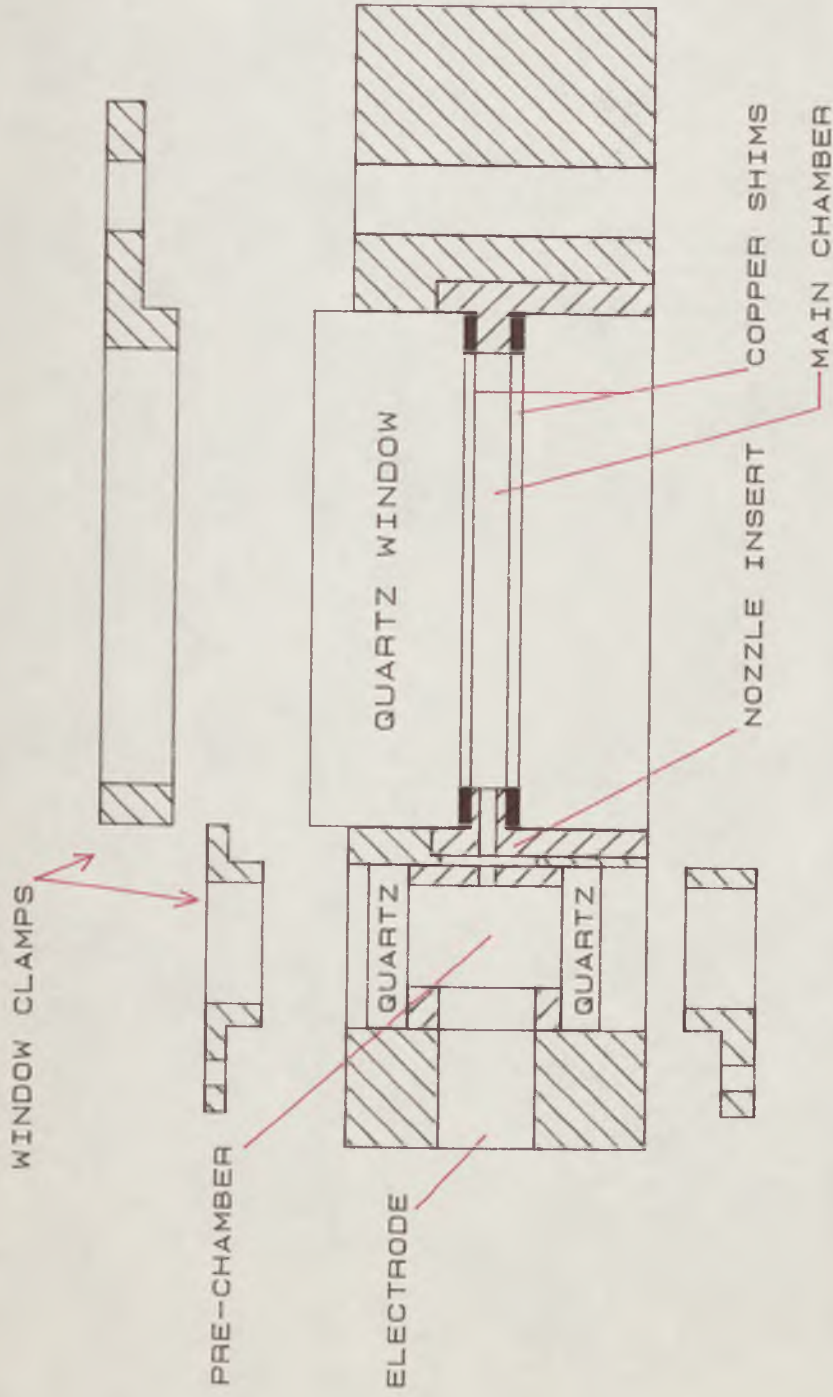


Fig.3.7 Modified cylinder head design

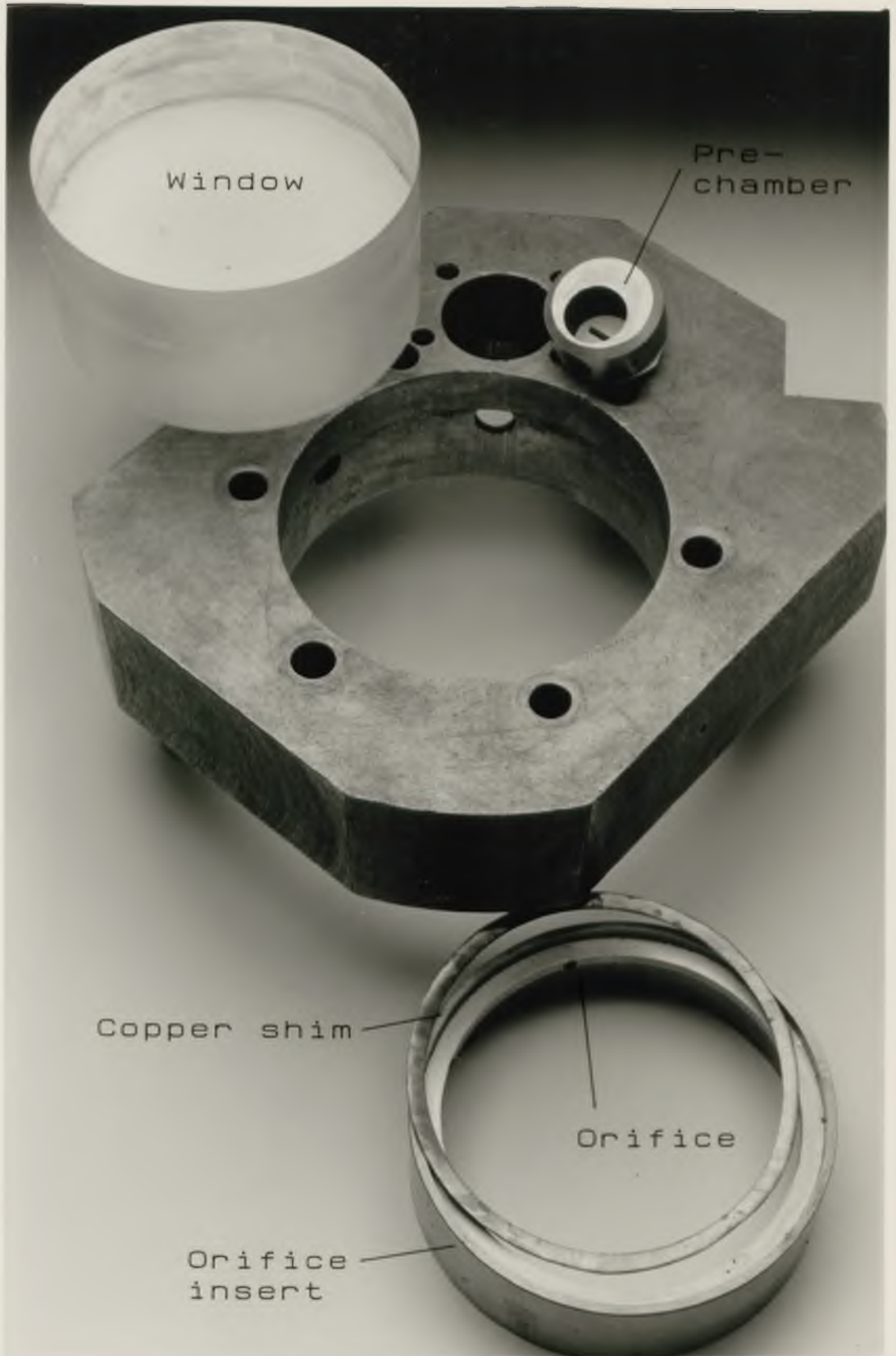


Fig.3.8

The divided chamber cylinder head.



Fig.3.9

The single chamber cylinder head.

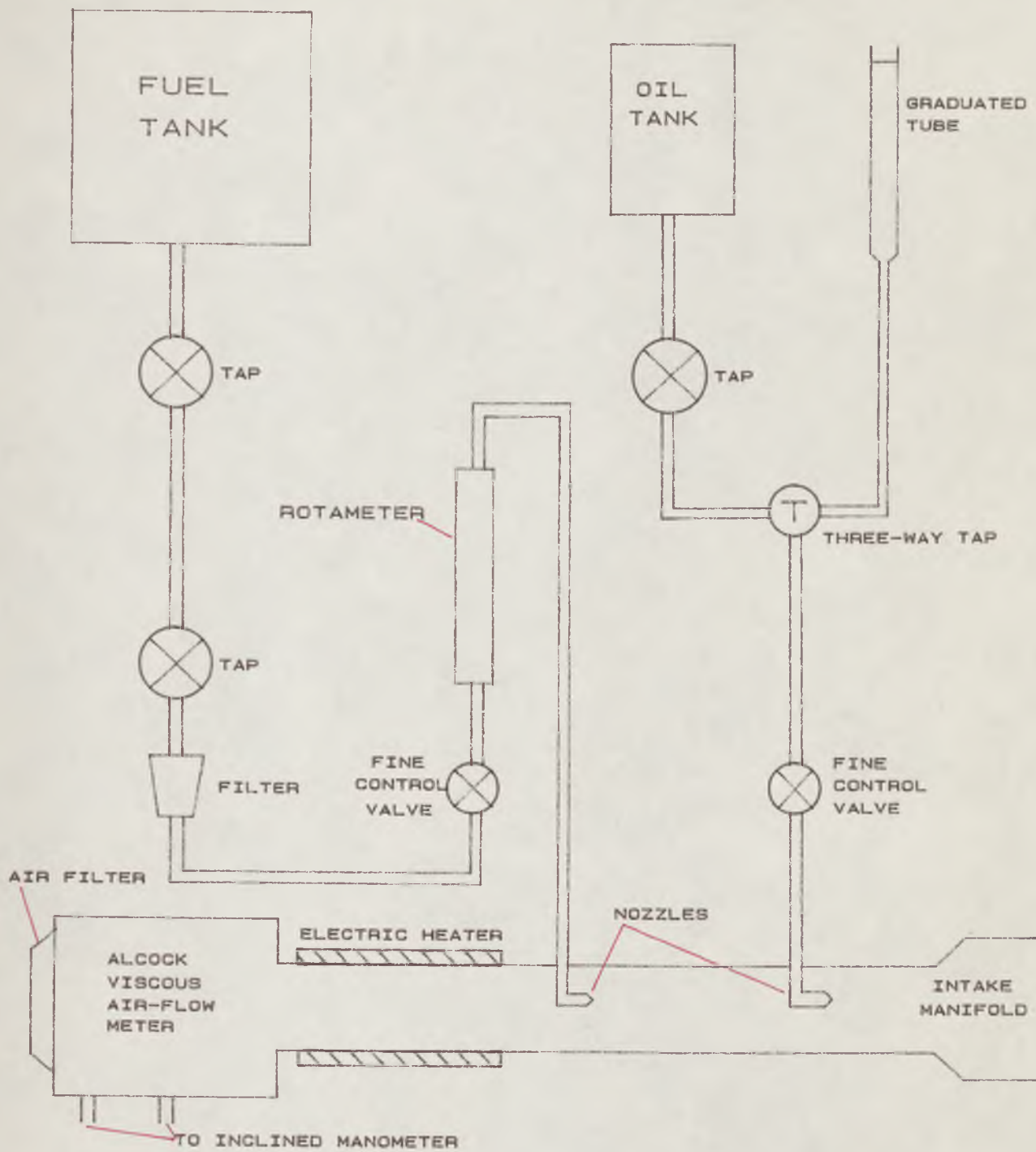


Fig.3.10

Diagram showing the layout of the fuel, lubrication and air supply systems

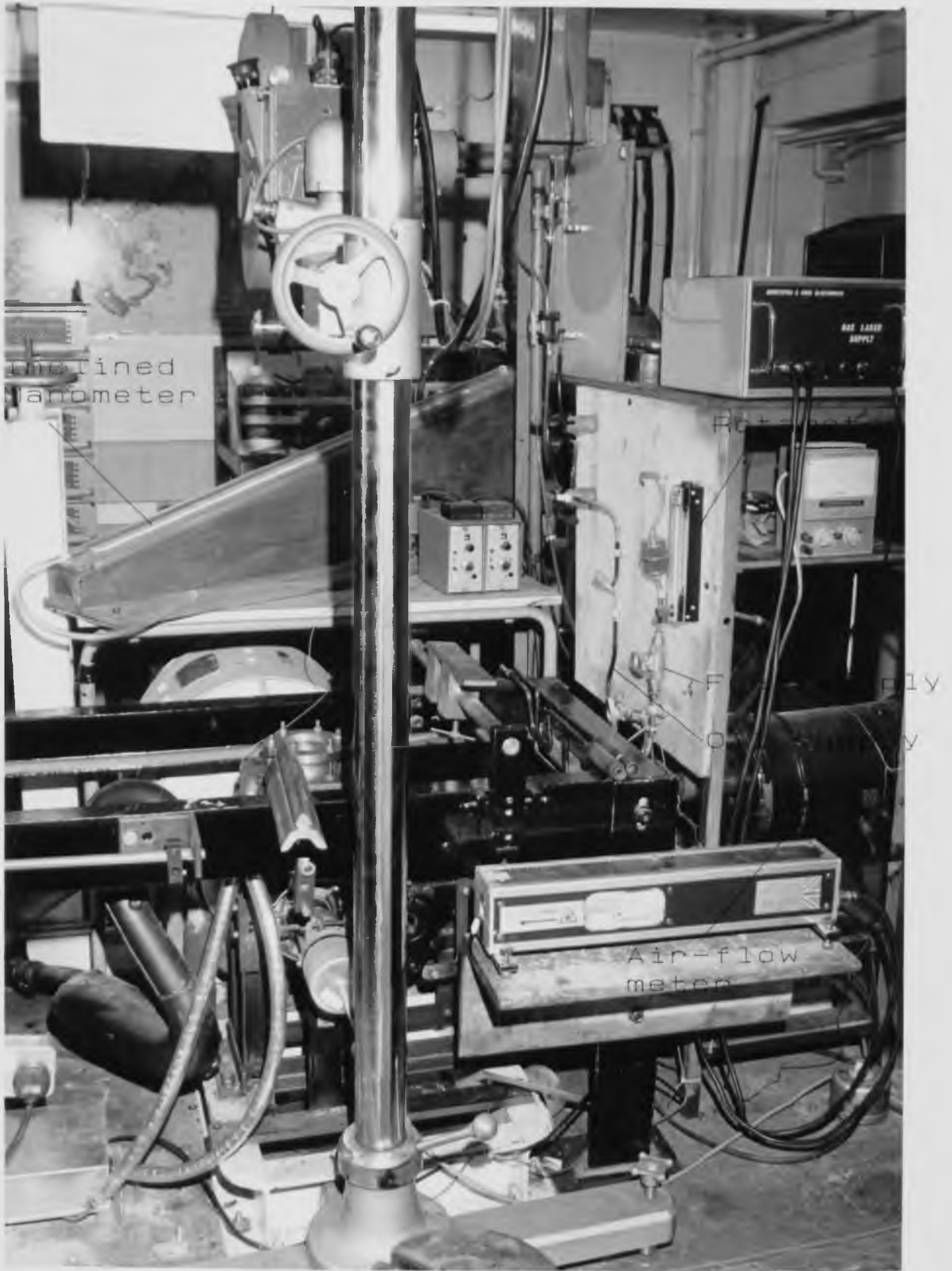


Fig.3.11
Layout of the experimental Rig

Inclined
Manometer



Rotameter



Fuel supply
Oil supply



Air-flow
meter



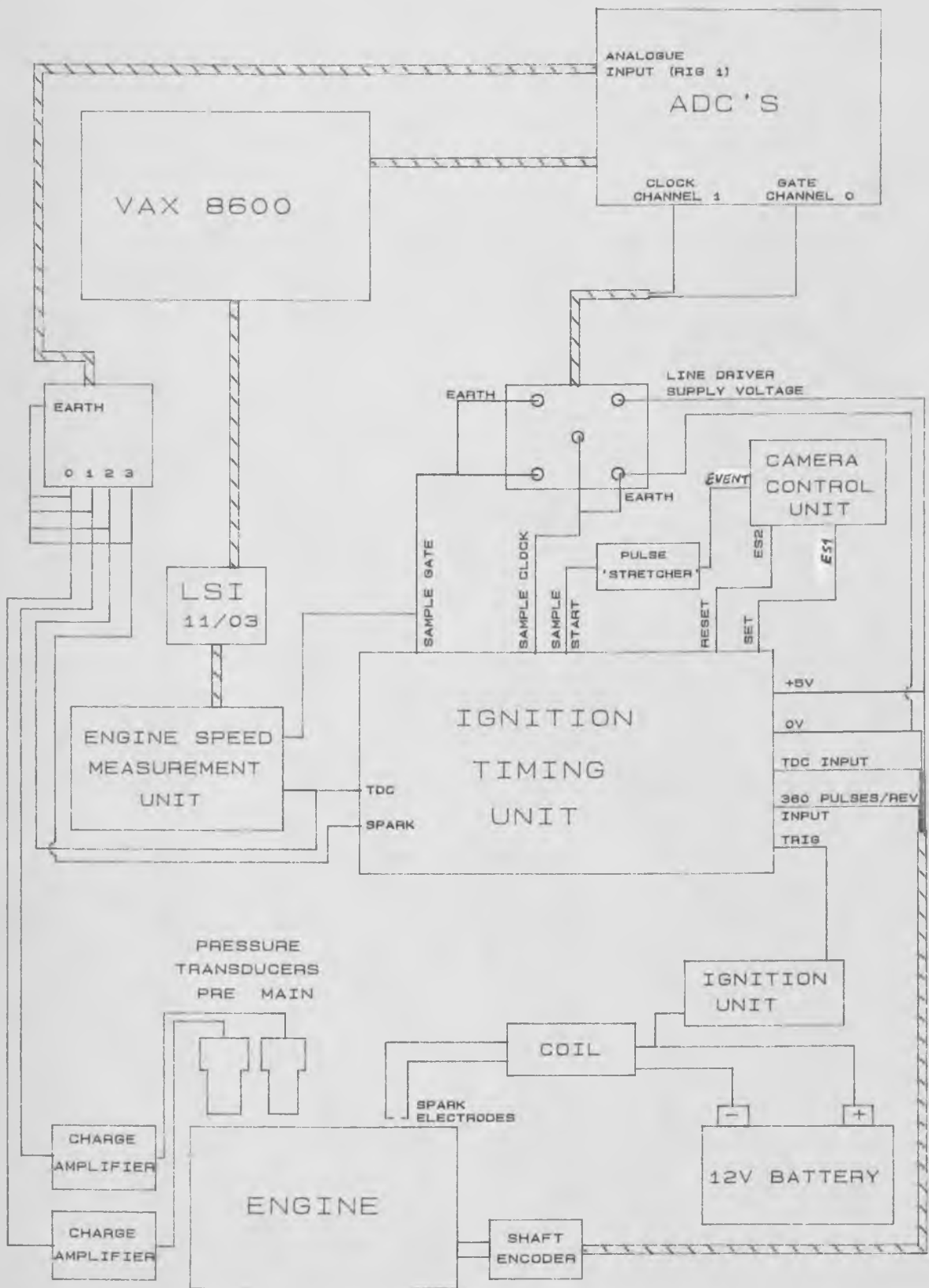


Fig.3.12 Diagram showing the electronic control and data acquisition system

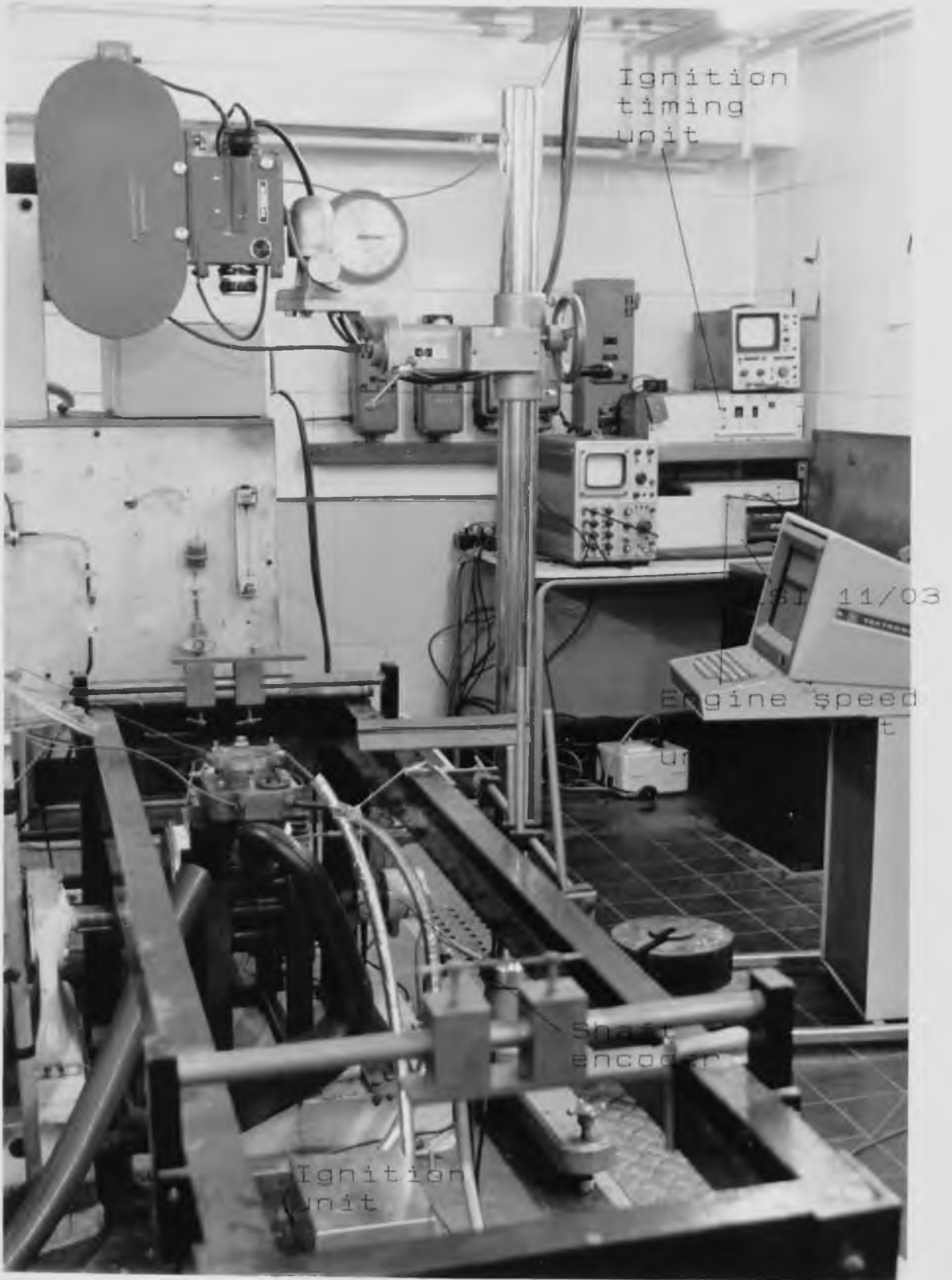
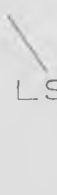


Fig.3.13
Layout of the experimental rig

Ignition
timing
unit



LSI 11/03



Engine speed
measurement
unit



Shaft
encoder

Ignition
unit

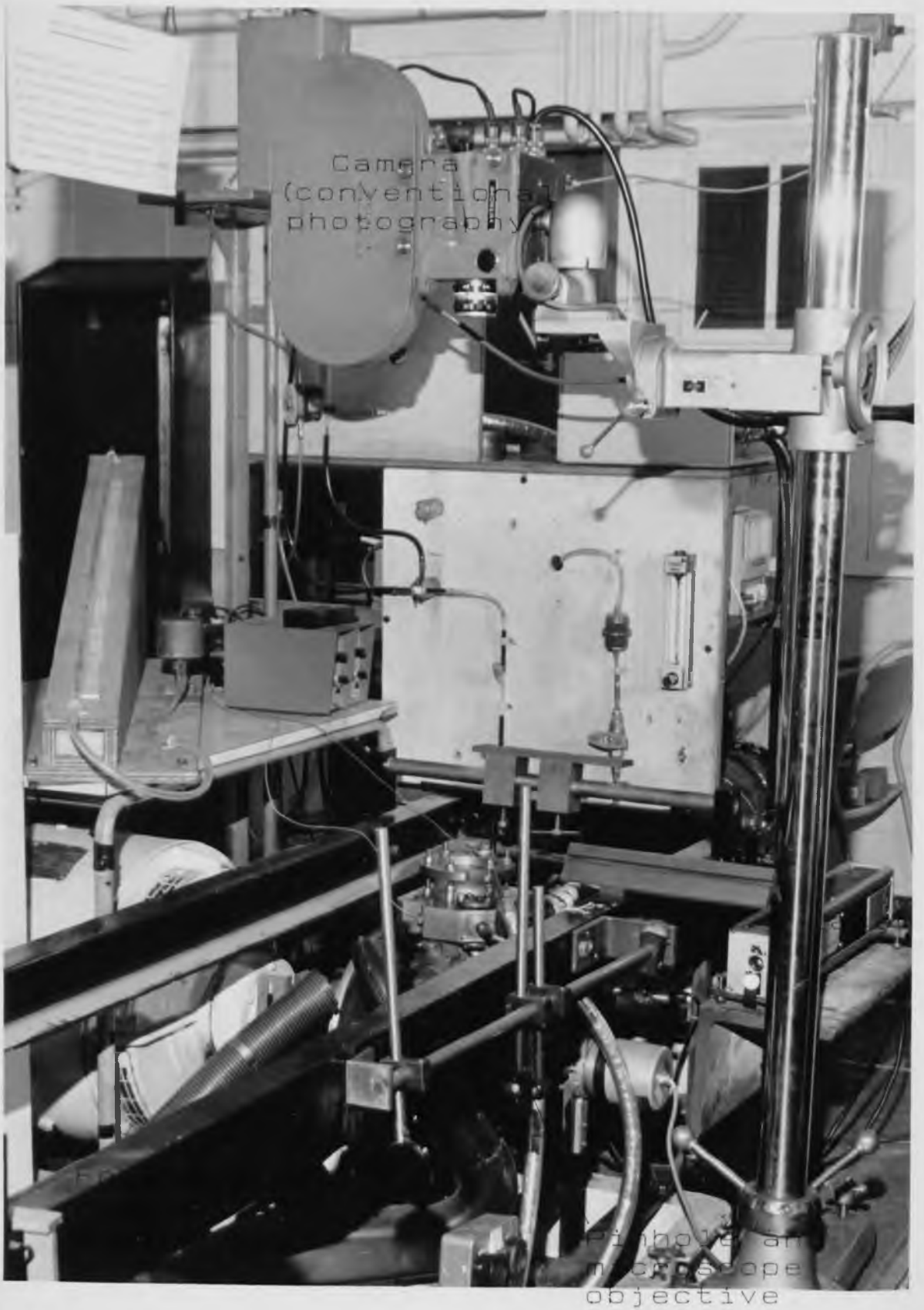


Fig.3.14
Layout of the experimental rig

Camera
(conventional
photography)

Laser

Focusing
mirror
(schlieren)



Pinhole and
microscope
objective



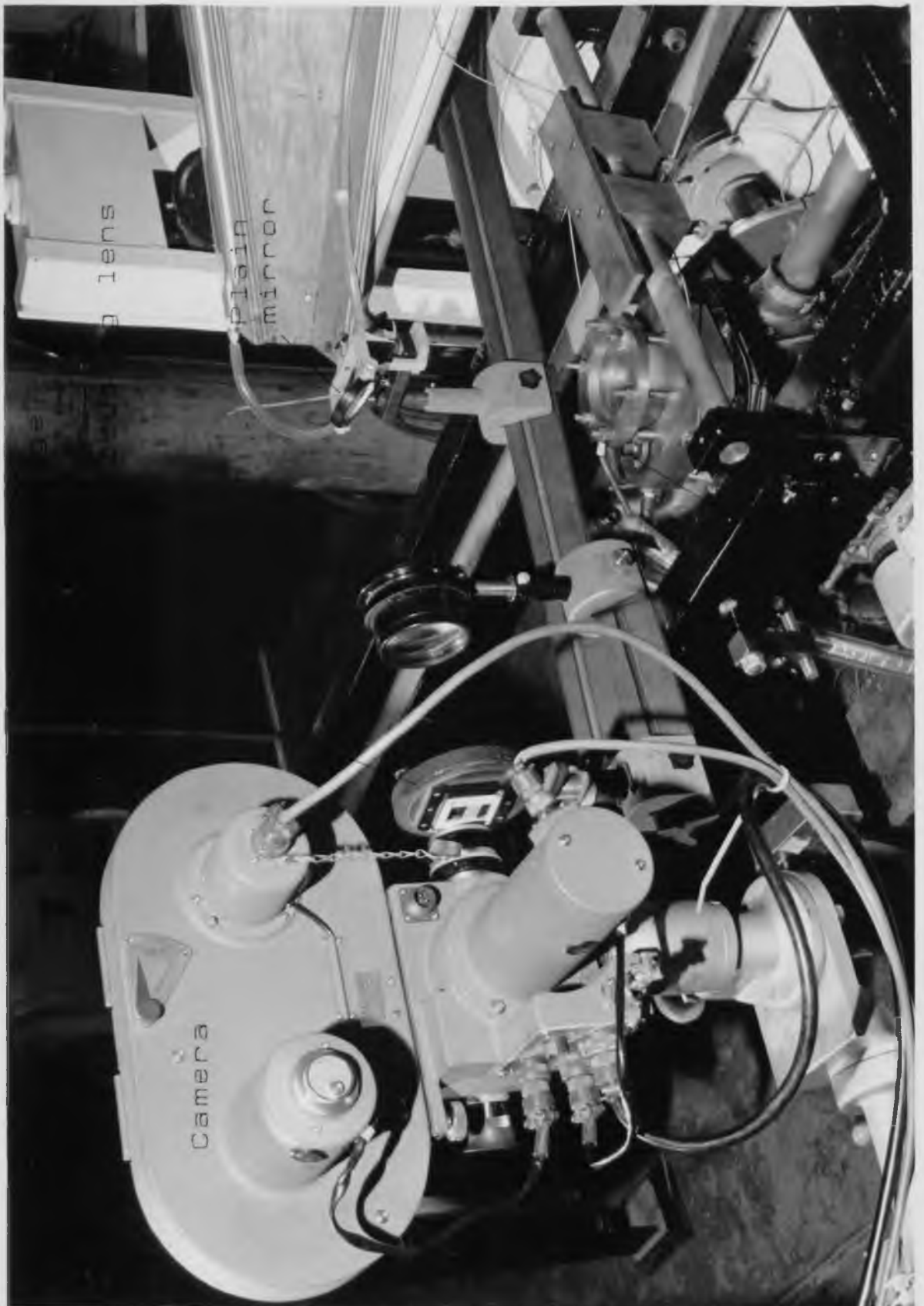


Fig. 3.15
Layout for schlieren photography

Knife edge

Focusing lens

Plain
mirror

Camera

Pre-chamber



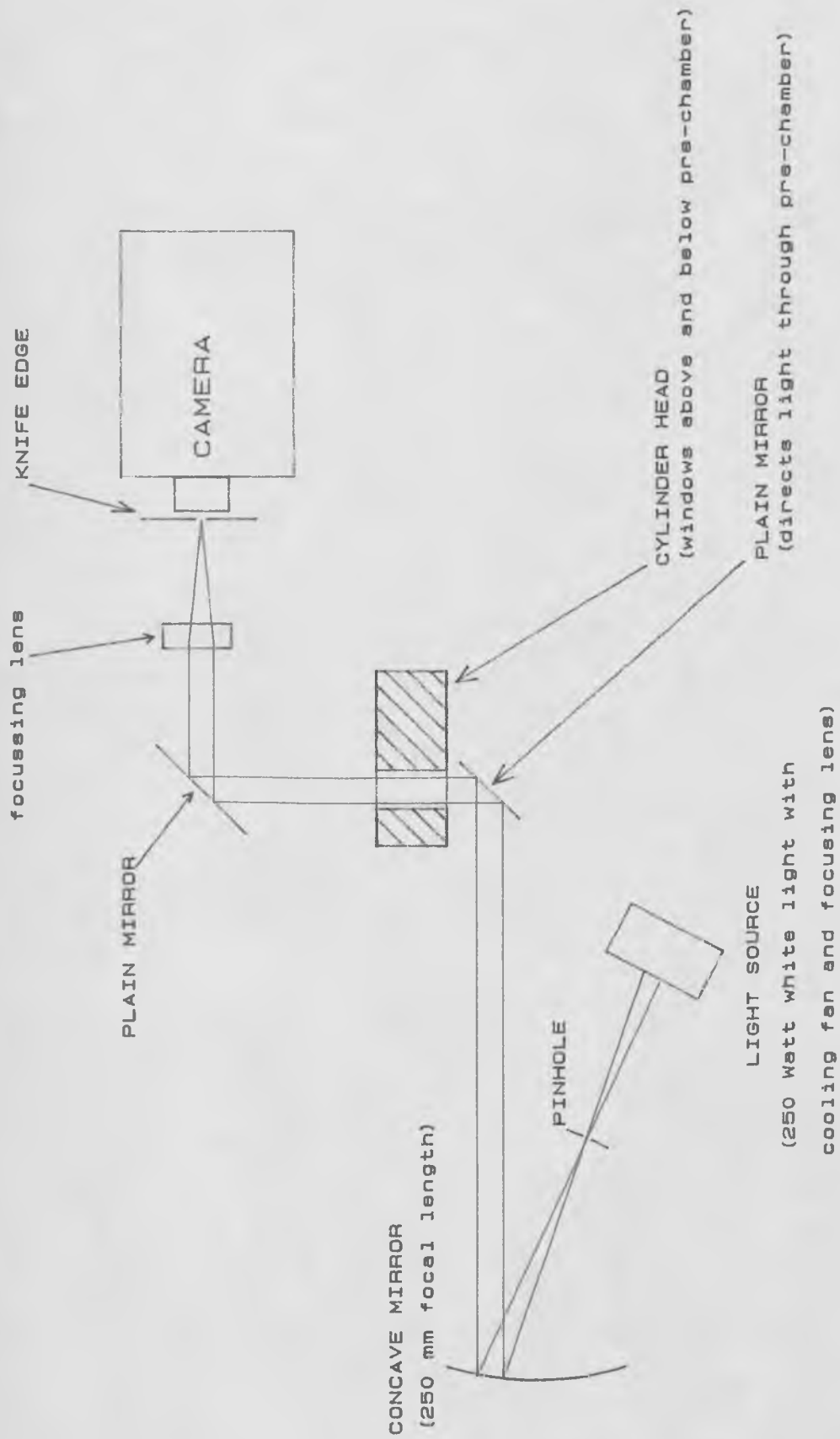


Fig. 3.16 Layout for Schlieren photography

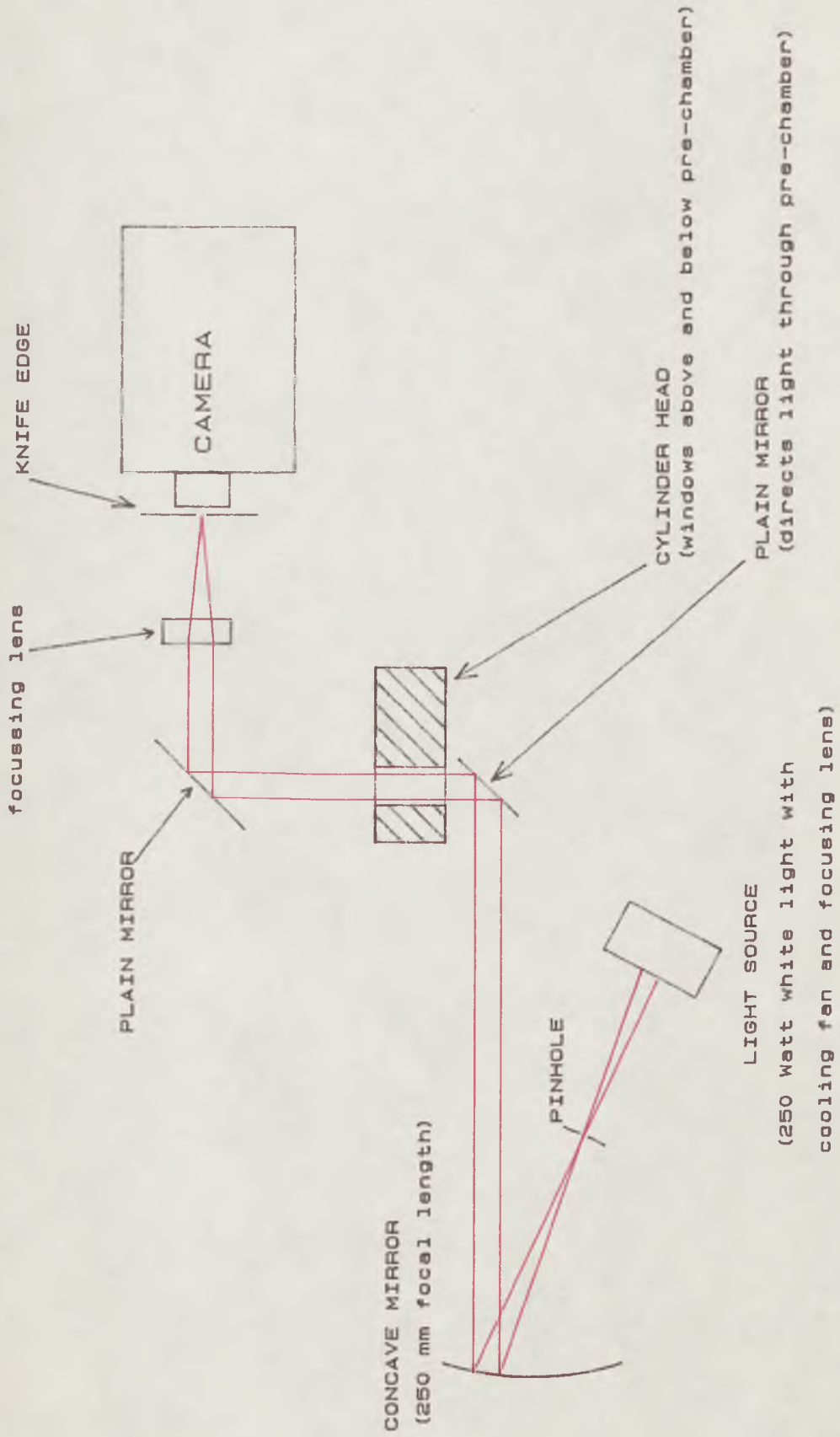


Fig. 3.16 Layout for Schlieren photography

CHAPTER 4

Experimental Results

CONTENTS

4.1	INTRODUCTION	50
4.2	RUSTON ENGINE	50
4.2.1	Pressure Records at 800 rpm	50
4.2.2	Flame Propagation	51
4.2.3	Effect of Gas Flow Velocity Through the Orifice	51
4.3	YAMAHA ENGINE - SINGLE CHAMBER	52
4.3.1	Film Analysis	53
4.3.2	Effect of Equivalence Ratio	53
4.3.3	Effect of Spark Plug Location	55
4.3.4	Effect of Engine Speed	55
4.3.5	Effect of Compression Ratio	56
4.3.6	Comparison of Results With Those of the Ruston Engine	57
4.4	YAMAHA ENGINE - DIVIDED CHAMBER	58
4.5	CONCLUSIONS	60

4.1. INTRODUCTION

In an earlier study at Leeds University, Al-Mamar (1983) conducted a series of tests on the Ruston (four-stroke) engine described in Chapter 3. These tests involved comparison of engine performance, with divided and single chamber geometries, at a constant engine speed of 1400 rpm. The divided chamber geometry was shown to produce faster combustion rates than obtained with the single chamber design. The combustion rate, as characterized by optimum ignition timing and flame propagation rate, was shown to increase with flow velocity through the connecting orifice; as this flow velocity is a function of engine speed, Al-Mamar conducted a second series of tests at a higher speed (2100 rpm) to examine the effect on performance. A third series of tests, at a slower speed (800 rpm), were conducted by the present author. The results of these tests were in the form of colour photographs and simultaneous pressure records. When these results were processed, the effect of charge being pushed into the valve chamber during the combustion process (and therefore allowing higher unburnt gas velocities and flame speeds) made comparison of results with predictions from the computer model (described in Chapter 6) difficult. Further work was therefore conducted on a Yamaha two-stroke engine (described in Chapter 3), which eliminated the valve chamber problem.

Initial tests on the Yamaha engine were concerned with single chamber operation; compression ratios of 6.4:1, 8:1 and 10:1 were used, with engine speeds of 800, 1400 and 2100 rpm and equivalence ratios of 0.8, 0.9, 1.0 and 1.1. Later work involved using the divided chamber concept. Lack of time unfortunately restricted the number of tests that were performed; the engine speed, compression ratio and equivalence ratio were fixed at 1400 rpm, 8:1 and stoichiometric respectively. Attempts to run the Yamaha engine at lean mixtures proved difficult, due to misfiring; this will be discussed in more detail later.

4.2. RUSTON ENGINE

As previously mentioned, the tests conducted on the Ruston engine were at an engine speed of 800 rpm. The volume ratios used were 13% (with 5 and 9 mm orifice diameter) and 25% (with only 5 mm orifice diameter) at equivalence ratios of 1.0 and 0.7. All other variables were held constant; these were : compression ratio (8:1), inlet mixture temperature (30°C), and wide open throttle setting.

4.2.1. Pressure Records at 800 rpm

Shown in Fig. 4.1 are curves of Indicated Mean Effective Pressure (I.M.E.P.) against ignition timing for the test conditions mentioned above. As the orifice diameter was reduced, or the volume ratio increased, the ignition advance for optimum power output was reduced.

This effect was noted by Al-Mamar at higher engine speeds. It is well established that engine combustion rates increase with enhanced in-cylinder turbulence. In the divided chamber engine the turbulence generated is likely to be a function of the gas flow velocity through the orifice; this flow velocity will increase as the orifice diameter is reduced, or as the volume ratio is increased. Hence, it is likely that the turbulence would have been greatest in those tests where the optimum ignition setting was noted to be least advanced.

Al-Mamar showed the power output at optimum ignition timing to be virtually independent of the geometry used. This also pertained at the lower engine speed of the currently reported study. The power output was, however, lower than that observed at 1400 rpm. Al-Mamar demonstrated that this could be attributed to changes in volumetric efficiency with engine speed.

The pressure records for the engine geometry giving the highest orifice flow velocity (25% volume ratio, 5 mm orifice diameter), are shown in Fig. 4.2, for both stoichiometric and lean ($\phi = 0.7$) mixtures. The difference obtained between the main and pre-chamber pressures during combustion was very small. At 1400 rpm this difference was considerably larger; the combustion rate at 800 rpm was clearly much slower than that at 1400 rpm, as there was time for pressure equalisation to occur.

4.2.2. Flame Propagation

No films of flame propagation at 800 rpm were taken. However a number of films of the combustion process, at both 1400 and 2100 rpm engine conditions, were taken by the current author. Charted in Fig. 4.3 and Fig. 4.4 are the successive positions of the flame front, for 13% and 25% volume ratio respectively (stoichiometric mixture, 1400 rpm, optimum ignition timing, and 5 mm orifice diameter). The time taken by the flame, to traverse the cylinder, was less with the 25% volume ratio (and its higher gas flow velocity through the orifice) than the 13% volume ratio; the flame propagation speed in each chamber is also higher with the 25% geometry (Fig. 4.5).

4.2.3. Effect of Gas Flow Velocity Through the Orifice

The films of the combustion process clearly showed that flame propagation rate increased with orifice flow velocity. Al-Mamar noted that although the flame propagation rate (when measured in terms of time) increased with engine speed, it decreased slightly when measured in terms of crank angle. The optimum spark advance also increased slightly with engine speed; the increase in combustion rate with engine speed was therefore not quite as large as the decrease in time available for the combustion event. To examine the above effects in more detail it was necessary to use the pressure data, as films were not available

for all the test conditions.

Shown in Fig. 4.6 is the optimum ignition advance plotted against maximum flow velocity through the orifice. The flow velocity during combustion was calculated in an incremental manner using the computer model described in Chapter 7; compression of the charge in the main chamber due to piston motion was assumed to be followed by isentropic expansion and compression of the main and pre-chamber gases respectively, until pressure equality was achieved. Then, for a known engine speed, the average mass flowrate in the increment was calculated, and the mean flow velocity determined from the continuity equation.

It can be seen from Fig. 4.6 that the observed rate of burning, as expressed by the optimum angle of ignition advance, correlated quite well with the maximum orifice flow velocity. For a stoichiometric mixture, the ignition advance reduced as the computed orifice velocity increased. This was considered to be a function of increased turbulence level associated with higher orifice velocity. The effect of engine speed was to increase the optimum ignition advance; this is shown by the separate curves for each speed. At a lean mixture the trends were similar; however, the scatter on the results proved much larger.

The rate of pressure rise in an engine can be used as a measure of combustion rate; a faster combustion process will produce a higher rate of pressure rise. In Fig. 4.7 the maximum rate of pressure rise in the pre-chamber is shown plotted against calculated maximum flow velocity through the orifice during the compression stroke. There is a considerable amount of scatter in the results obtained. However, one may note a general increase in rate of pressure rise with increasing orifice velocity. The maximum rate of pressure rise in the main chamber is shown plotted in Fig. 4.8. Again considerable scatter is evident; the effect of piston motion on the rate of pressure rise would be likely to have a greater effect on the rate of change of pressure in this chamber. It was not considered sensible to attempt further processing of these data, e.g. to determine mass rate of burning, given the inconsistency in the values of rate of pressure rise obtained, and the uncertainties associated with the late burning of fuel which had been trapped in the valve chamber at TDC.

4.3. YAMAHA ENGINE - SINGLE CHAMBER

Initial experiments on the Yamaha engine were centred on single chamber operation. Al-Mamar (1983) demonstrated the importance of ignition timing on engine power output; hence for each operating condition, a series of tests were performed to determine the minimum spark advance necessary to give the maximum power output (MBT timing). All subsequent tests were then carried out at the relevant optimum ignition advance.

The engine was operated at wide open throttle, with a constant inlet mixture temperature of 30°C, throughout.

4.3.1. Film Analysis

At each condition, the combustion process was filmed at the optimum spark advance. Since the engine was fired only once every fourth cycle (as described in Chapter 3), and a high filming speed (8000 f.p.s.) was employed (to ensure enough frames showing the details of the flame growth were available), only three or four cycles were recorded on each film. The first two cycles were neglected as the camera was still accelerating rapidly. Hence only one or two cycles could be analysed from each film. Since the high film processing costs restricted filming to one film per engine condition, it was necessary to interpret the results with caution - as the engine was subject to considerable cyclic variation.

Shown in Fig. 4.9 is the flame projected area for each frame during one cycle on a film. (The photographs of the cycle traced are shown in Fig. 4.10). The films were traced, first on paper from a back projection screen, and then on a bitpad (described in Chapter 3) to produce digital maps of the flame position. A Weibe function was then fitted to the flame areas (Fig. 4.11; Hynes, 1986d), to give smoothed data for further analysis.

Given the flame projected area, the radius of a circle with the same area was calculated. This was assumed to be equal to the flame radius; from this it was possible to calculate flame speeds, as the camera speed was known. It can be seen from Fig. 4.9 that the assumption of circular flame growth is reasonably valid in the early stages. However, late in the propagation process, the flame growth appears to be influenced by a swirl motion; this might have introduced errors in the calculated flame speed towards the end of the combustion event.

4.3.2. Effect of Equivalence Ratio

The first series of tests conducted on the Yamaha engine was to study the effect of varying equivalence ratio. The engine speed and compression ratio were held constant at 1400 ± 30 rpm and 8:1 respectively. Shown in Fig. 4.12 is the I.M.E.P., plotted against ignition advance, for each of the equivalence ratios used. Power outputs at equivalence ratios of 1.0 and 1.1 were almost identical. At the stoichiometric mixture a slightly smaller optimum angle of advance was required (24 degrees compared with 25 at 1.1); however, given the scatter of the results, it would be unwise to conclude that the stoichiometric mixture burned faster. In the results presented here the points shown on the graph were chosen as typical cycles, while the curves were chosen as the best fit to the average of approximately fifty engine cycles recorded at each condition.

As the equivalence ratio was reduced, the power output obtained from the engine also fell. Earlier ignition timing was correspondingly necessary for maximum power. This effect was due to the lower burning velocities associated with leaner mixtures.

The variation in cylinder pressure during a typical engine cycle at optimum spark timing, is illustrated in Fig. 4.13(a). Although there was a variation in the value of peak pressure with equivalence ratio, the crank angle at which this peak pressure occurred, was always in the range of 10 - 14 degrees after T.D.C. The effect of ignition timing, for the stoichiometric case, is demonstrated in Fig. 4.13(b). If the ignition timing were advanced, then combustion occurred too early; the peak pressure was higher, since more of the combustion event occurred before the piston reached the top of its stroke. Consequently the peak pressure also occurred sooner. If the ignition timing were retarded, then combustion was late; the peak pressure was reduced and happened later in the cycle.

The effect of equivalence ratio on flame propagation rate can be seen in Fig. 4.14. At each condition, a film of the combustion process was taken (with central ignition). The fastest flame growth and the highest flame speed occurred with the richest mixture used, whilst the leanest mixture gave the slowest flame propagation rates. This was not surprising, as the burning velocity increases with mixture strength for the range of equivalence ratios used. However, the results for the two intermediate mixture strengths were unexpected. In order to explain why the leaner mixture (0.9) gave higher burning rates than the stoichiometric mixture, it is necessary to study the pressure results which were taken simultaneously. Shown in Fig. 4.15(a) are the pressure vs crank angle graphs for the filmed cycles. Comparison of these with the pressure traces shown in Fig. 4.13(a) (which were chosen as being an average condition from a number of tests) illustrates clear discrepancies. The peak pressure is lower as the equivalence ratio increases from 0.9 to 1.1; this is likely to be caused by cyclic variation. To overcome this problem it would be necessary to take many more films and only analyse cycles which might qualitatively be considered to have an average pressure trace. Shown in Fig. 4.15(b) are the range of I.M.E.P. noted at each test condition; the results obtained when using the cylinder head with steel and perspex window inserts (Section 3.2.1) are shown separately. One may note that:

- (i) The power output obtained when using a head with the perspex window was lower than that with the steel head. As the perspex window permitted only short experimental runs of the engine, it is likely that the cylinder wall and piston crown temperatures were lower during the filmed tests than during tests involving the steel head. Heat losses might therefore have been greater, despite the smaller effective surface area available for heat transfer (perspex having lower thermal conductivity).

- (ii) The power output, for the cycle where the combustion process was filmed and traced, was very low for the stoichiometric and rich mixtures. However the cycle at 0.9 equivalence ratio was within the range of power associated with operation using the steel head. It is therefore perhaps not surprising that the flame growth, in this particular case, was faster than that obtained filming with a stoichiometric mixture.

4.3.3. Effect of Spark Plug Location

Tests were conducted with both side and central ignition. The location of the spark plug in the centre of the chamber gave reduced flame travel distance; the optimum spark timing was therefore less advanced than with side ignition (Fig. 4.16). With increased mixture strength, optimum ignition timing was found to be less advanced, as a result of the increased burning velocity. There was little difference between optimum ignition settings for the stoichiometric and slightly rich (1.1) mixtures, with central ignition. Since the burning velocity of a fuel/air mixture is generally maximum at an equivalence ratio of about 1.05, this would seem reasonable. The optimum ignition timing for the rich mixture with side ignition proved considerably less advanced than for the stoichiometric case. This was unexpected; since the power output and peak pressure obtained were also lower in this test, it is likely that the ignition timing was too far retarded.

For optimum ignition timing, the power output of the engine and the peak cylinder pressure were relatively insensitive to ignition location. However, with lean mixtures, the peak pressure occurred earlier in the cycle.

4.3.4. Effect of Engine Speed

A further series of tests was conducted to examine the effects of engine speed. The engine speeds employed were 800, 1400 and 2100 rpm, as used by Al-Mamar. In these tests only two mixture strengths were used, those corresponding to equivalence ratios 0.8 and 1.0. This was done to restrict the considerable number of engine tests otherwise required. It proved impossible to run the engine with a stoichiometric mixture at the highest engine speed, as the fuel system was unable to deliver at an adequate rate.

The effect of spark advance on power output, for each engine speed and mixture strength, is shown in Fig. 4.17. A greater ignition advance was required as the engine speed was increased, for the lean mixture. Although the combustion rate increased with engine speed, due to increased turbulent motion, it did not increase fast enough to compensate for the shorter time available. Hence, when measured in terms of crank angle, the combustion duration was greater at the higher engine speeds. The power output was maximum at 1400 rpm. These results were consistent with those observed by Al-Mamar (using the Ruston engine). He reasoned that his variation in power output was due to change in

volumetric efficiency. In the case of the Yamaha engine used in the currently reported work, scavenging efficiency would similarly affect performance. At high engine speeds, it would be possible for charge entering the intake port to go directly out through the exhaust port, without scavenging any of the residual charge in the cylinder. As the piston crown was machined flat this effect may have been much worse than in a standard Yamaha engine (where the piston is crowned).

The power output obtained with the stoichiometric mixture is also given in Fig. 4.17. Output was considerably lower at the lower engine speed. However, there proved little noticeable difference in optimum spark timing. The increase in burning velocity obtained with increased turbulence (i.e. engine speed) seems clearly dependent on equivalence ratio. Results obtained with the divided chamber Ruston engine, Fig 4.6, also showed a much larger effect of engine speed on optimum spark timing with leaner mixtures.

Shown in Fig. 4.18 are the flame radii and flame speed, plotted against crank angle after ignition, for each of the tests. For both mixture strengths, the flame speed increased considerably with engine speed; however, the shape of the curves proved similar. The peak flame speed occurred when the flame radius was approximately 2 cm. With the stoichiometric mixture, there was very little difference in the flame size (at a given crank angle after ignition), with engine speed. However, at the lean mixture strength, the flame size was smaller (at a given crank angle) at increased engine speed. This explained the need for a greater ignition advance at the higher speeds.

4.3.5. Effect of Compression Ratio

The engine was tested at compression ratios of 6.4:1, 8:1 and 10:1. At an equivalence ratio of 0.8 the optimum ignition timing was found to decrease, and hence combustion rate to be enhanced, with increasing compression ratio. Increased compression ratio is accompanied by an increase in the temperature of the charge in the chamber, and a reduction in the quantity of residual charge present. Both these effects would cause an increase in the burning velocity of the charge (see Section 6.3.1). An increased cylinder pressure ought to cause a reduction in burning velocity; however, this is obviously not as dominant as the temperature and residual charge effects.

The peak pressure in the cylinder, at optimum ignition timing, increased as the compression ratio was increased from 6.4 to 8 (Fig. 4.19); however, a further increase in compression ratio caused a reduction in peak pressure, and power output. The combustion chamber shape was a flat, disc shaped cylinder; as the compression ratio was increased the height of this cylinder was reduced (to approximately 3mm at 10:1). This shape of chamber had a very large surface area to volume ratio. Heat losses would therefore be large,

especially at the high compression ratio, where a large proportion of the cylinder volume at TDC could possibly have been occupied by quench layers.

Shown in Fig. 4.20 are the flame position and speed during combustion for each compression ratio, at optimum ignition timing. At the stoichiometric mixture there was little difference exhibited in flame propagation rate for the two lower compression ratios. As the optimum spark advance was the same in both cases, this does not seem unreasonable. The flame propagation rate at the high compression ratio was considerably slower; this suggests that the temperature was lower than for the other two compression ratios, and supports the argument that excessive heat transfer is responsible.

With the leaner mixture (of equivalence ratio 0.8), the flame propagation is slower with the lower compression ratio; more ignition advance was necessary for optimum power at this condition. The graphs presented in Fig. 4.20 for this case are plotted against actual crank angle (rather than crank angle after ignition). It is interesting to note that the flame growth is almost identical. At the lower compression ratio, the flame growth needs more time in the early stages (to reach 0.5cm flame radius, for example), but once it has started, flame propagation continues in a manner similar to that at the 8:1 compression ratio. The higher temperatures, associated with the higher compression ratio, are obviously important in the early stages of the combustion process.

It was not possible to take a film for the lean mixture at the high compression ratio. Flame propagation was slow, and even with reduced camera speed, the flame was not bright enough to allow reliable tracing.

4.3.6. Comparison of Results With Those of the Ruston Engine

Single chamber tests conducted by Al-Mamar on the Ruston engine were for side ignition only; central ignition is therefore not included in the current comparisons. The optimum spark advance required, at each equivalence ratio, was greater in the Yamaha engine than was found in the Ruston (Fig. 4.21). This suggests that the combustion rate was slower. A lower turbulence level in the Yamaha engine could be responsible for this; there are a number of possible causes:

- (i) The side valve region in the Ruston engine could have acted as a squish region (even though it was cut off at TDC) and so generated turbulence during compression.
- (ii) The effective swept volume (after the valves/ports have shut) was considerably smaller in the Yamaha engine (exhaust port closes 91° BTDC) than in the Ruston engine (exhaust valve closes 138° BTDC). This would result in lower mass flow

rates into the engine for the Yamaha, giving lower flow velocities on intake for a fixed cross-sectional intake area.

- (iii) The transfer ports on the Yamaha engine were considerably larger than the cross-sectional valve flow area on the Ruston; this would cause an even greater reduction in intake flow velocity than the effect discussed under heading (ii) alone.

The mean effective pressure in the Yamaha engine was lower than that observed in the Ruston. This is because mean effective pressure is defined as the work done per CC swept volume. If it were, instead, defined in terms of the effective swept volume then there would be little difference in the mean effective pressure (with the exception of the rich condition in the Yamaha engine; the reason for this anomaly was discussed in Section 4.3.3).

In general the peak pressure noted in the Yamaha engine tests was lower than that observed with the Ruston engine. A lower turbulence level and slower burning rate could be responsible for this. The crank angle at which the peak pressure occurred was, however, approximately the same in each engine.

4.4. YAMAHA ENGINE - DIVIDED CHAMBER

As previously mentioned, dual chamber tests on the Yamaha engine were conducted at a fixed engine speed of 1400 rpm, a compression ratio of 8:1, and a stoichiometric mixture. Shown in Fig. 4.22 is the effect of spark advance on mean effective pressure, for each of the volume ratios used, and a no. 5 orifice. In each case the optimum ignition timing was considerably retarded when compared with results from the Ruston engine. The pressure diagrams for the two larger volume ratios are shown in Fig. 4.23. In both cases, pre-chamber combustion was very fast; it produced a very high rate of pressure rise, and a peak pre-chamber pressure in excess of the main chamber pressure. One may also note that the pre-chamber pressure during compression was considerably lower than that in the main chamber; this suggests that the flow from the main chamber through the orifice into the pre-chamber was restricted, possibly choked. These effects were not observed in the Ruston engine; they suggest that the orifice flow velocity (and hence turbulence) was considerably higher in the Yamaha engine. Although the Yamaha orifice sizes were scaled to match the calculated orifice flow velocities with those estimated for the Ruston engine, it is clear that this was unsuccessful. In the Ruston engine, some of the charge could have been pushed into the valve chamber more easily than into the pre-chamber, during compression. This could have led to orifice flow velocity being lower than calculated using the method outlined in Section 4.2.3.

Shown in Fig. 4.24 is a print from the film of the combustion process for the 10% volume ratio case. It can be seen that pre-chamber combustion was completed extremely

rapidly (within four frames), while main chamber flame growth was clearly very different from that observed in the Ruston engine. To process these results by assuming spherical flame growth would obviously be invalid.

Severe misfiring was experienced when attempts were made to run the Yamaha engine on leaner mixtures. The very high orifice flow velocity was obviously inhibiting reliable ignition; a lower jet velocity would be necessary to study leaner mixtures, and to analyse films on the same basis as had been done previously (i.e. by calculating flame speeds on the basis of spherical flame growth). To achieve this, the pre-chamber volume would have to be reduced, or the orifice area increased. Photography of the pre-chamber combustion process set a lower limit to the acceptable pre-chamber size, while the main chamber clearance height set an upper limit to orifice diameter. The review in Chapter 2 suggested that orifice shape or number had little effect on performance, for a given cross-sectional area. A test was therefore conducted with the smallest pre-chamber, and two no. 5 orifices. The additional orifice resulted in an increase in the ignition advance necessary for maximum power, from 12° to 20° BTDC (Fig. 4.22). The effect of the reduced orifice flow velocity on cylinder pressure is illustrated in Fig. 4.25. The high peak pre-chamber pressure, produced by pre-chamber combustion, was considerably reduced; the increased rate of mass transfer between chambers did not allow a large pressure differential to develop. The resultant flame growth is shown in Fig. 4.26. The flame growth, and cylinder pressure with the two orifices was in accord with results from the Ruston engine; this supports the suggestion that orifice flow velocities were too high with the single orifice.

Attempts were made to film the pre-chamber combustion process using the Schlieren technique. Initially a white light source was adopted; however, focusing of the light onto a knife edge proved impossible, due to the size of the element in the bulb. The light source was therefore replaced by a 3mw helium-neon laser, as this could provide a point source of light. The photographs produced were of very poor quality. When the engine was started, it would misfire for a considerable length of time before a smooth running condition was obtained. During this period the quartz windows became covered by an oil film (even though the lubrication oil was turned off for a few minutes prior to filming). This oil film cut out most of the laser light, hence any image on the film was barely visible.

In an attempt to overcome this problem by reducing initial misfiring, a cylinder head with a 17% volume ratio and a slotted orifice of 10mm length and 3.40mm (no.5) height was adopted. It was hoped that the reduced orifice flow velocity given by this larger orifice would lead to more consistent ignition. With this head in place the optimum ignition advance was 19° BTDC (c.f. 2° BTDC for a single no.5 orifice). The pressure trace for this condition is shown in Fig. 4.27, together with a single chamber pressure trace. Although the

peak cylinder pressure and time of its occurrence were similar in both cases, the initial rate of pressure rise was considerably greater in the divided chamber case; as more of the mass was burning before the piston reached the top of its stroke. Schlieren photographs of this condition were still poor, and the engine still misfired for a period before running smoothly. In an attempt to increase the definition on the film, the laser power was increased from 3mw to 35mw. This resulted in a much brighter image; however, due to refraction of the laser light by the oil film, the definition of the flame surface was not clear enough to be of any use. It became clear that for successful application of schlieren photography it would be necessary to prevent oil from entering the combustion space. This would necessitate the use of graphite piston rings, and re-direction of the intake charge so that it would not enter the crank case; the crank case could then be filled with oil to lubricate the crank bearings. No time was available for such extensive modifications in the programme of work presented in this thesis; consequently schlieren photography was abandoned at this point.

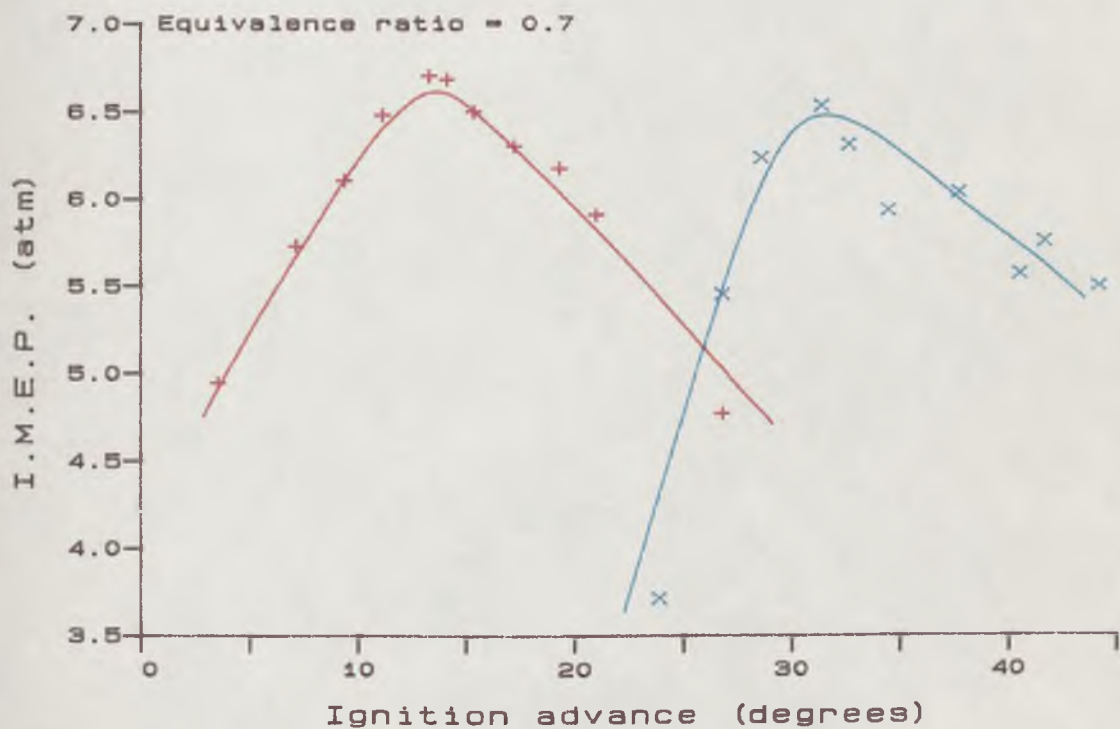
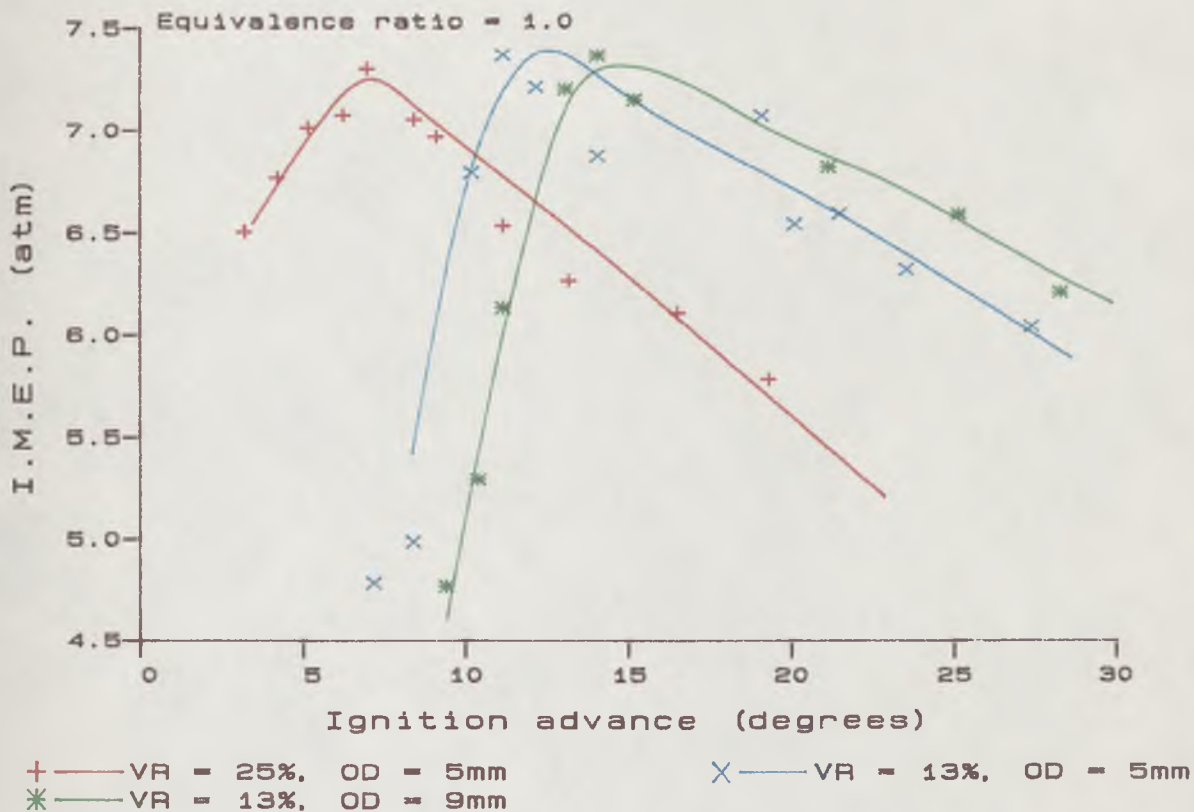
A conventional film of the combustion process, when using the cylinder head with the slotted orifice, was taken (Fig. 4.28). The wide slot produced a very wide torch effect in the main chamber. Subsequent flame growth appeared approximately circular on the film; this could have been the result of either spherical or cylindrical flame growth. The flame was very yellow in comparison with those seen for single chamber combustion; the main chamber window was perspex and, since subsequent examination revealed that the surface was considerably burnt, it is possible that the colouration might have been associated with perspex combustion. Although the wide slot produced circular flame growth in the main chamber, the misfiring and low power output noted with this configuration suggested that the turbulence level in the pre-chamber was still rather high (*vis à vis* the Ruston engine). The turbulence produced by a long thin slot is likely to be different from that produced by a circular hole; one cannot be sure that the effect of the orifice shape was not significant without comparing results with those using a circular orifice. To do this would require a new engine as the limitation in available clearance height in the Yamaha's main chamber at TDC would not allow such a comparison.

4.5. CONCLUSIONS

Both the Yamaha and Ruston engines used in the work suffered from a number of problems which precluded the range of tests originally envisaged. Nevertheless a number of conclusions can be drawn from the results obtained:

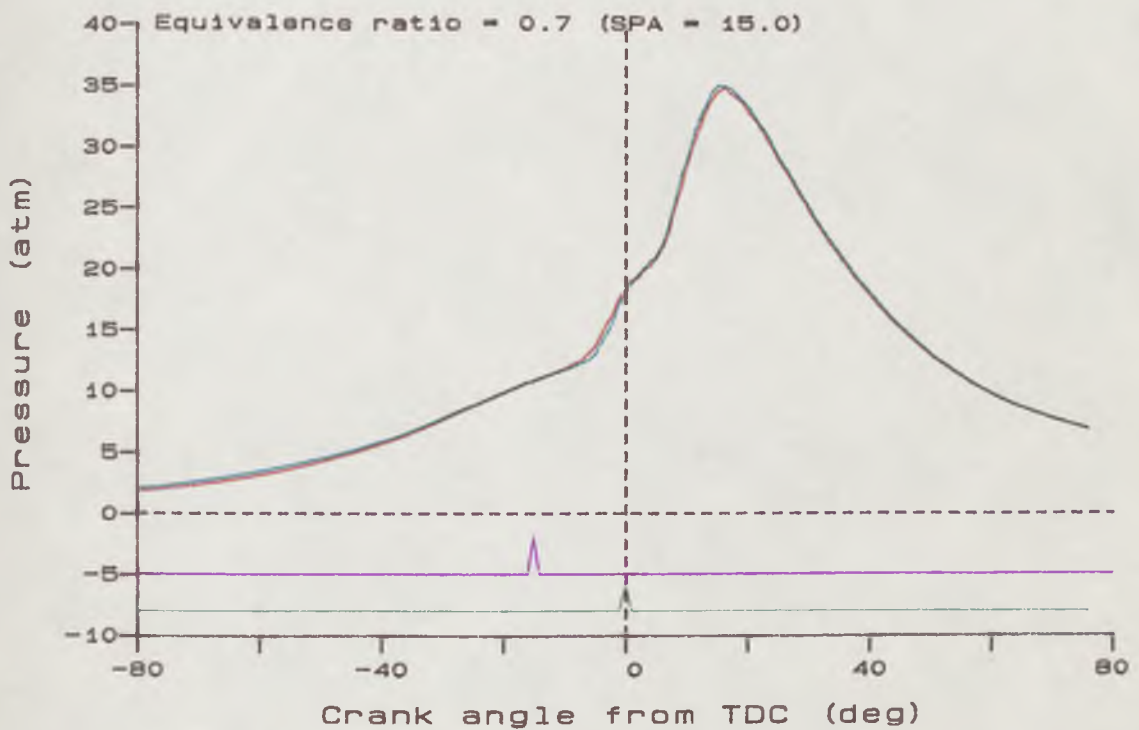
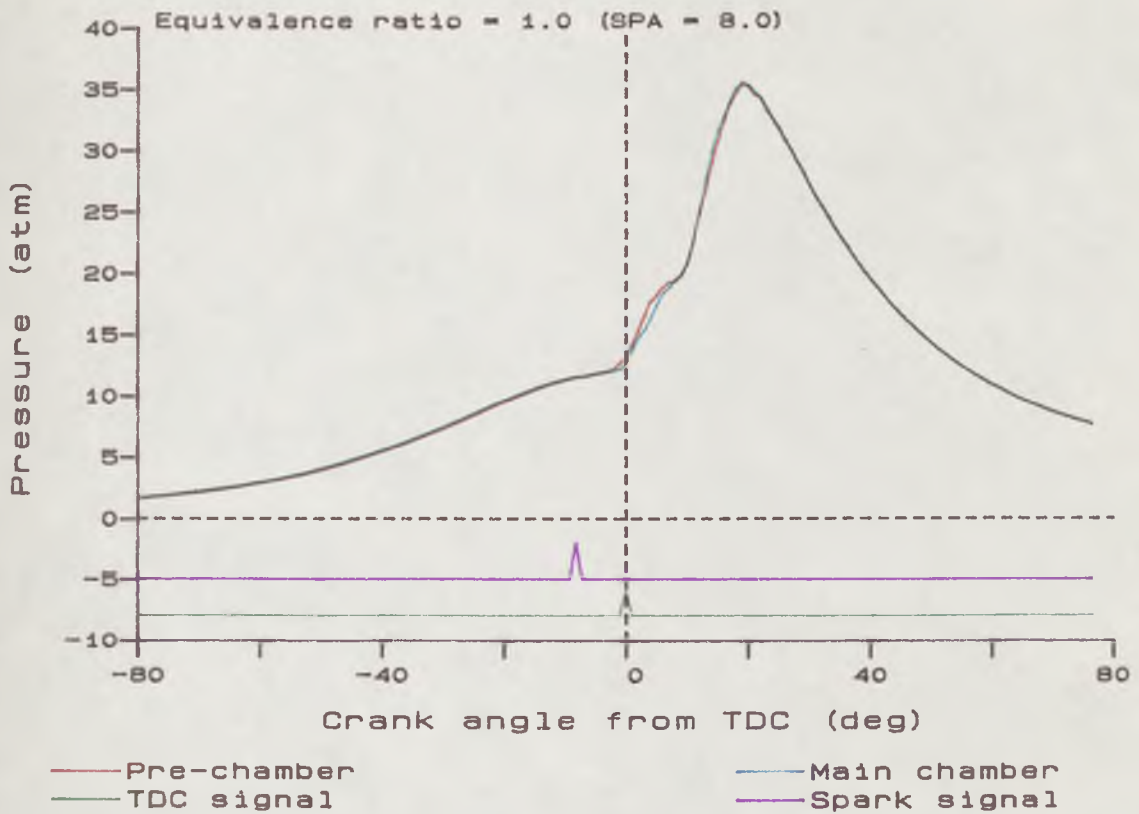
- (1) For single chamber operation in the Yamaha engine, the assumption of spherical flame growth (adopted in the computer model in Chapters 5 and 6) proved reasonably valid - except in the late stages of flame propagation.

- (2) With ignition timing set to give maximum power output, peak cylinder pressure always occurred at between 10-14 degrees ATDC; this finding was independent of engine speed, compression ratio, equivalence ratio and chamber geometry.
- (3) Both Engines were subject to considerable cyclic variation effects. A large number of films would therefore be required in order to study the effect of the various operating conditions on flame propagation rate.
- (4) The recorded power output of the Yamaha engine was lower when its cylinder head was fitted with a perspex window than when equipped with a steel head. This was considered to be a function of the different heat transfer characteristics of the two materials, and the adoption of an abbreviated engine warm up period in the perspex case.
- (5) Power output was generally little affected by ignition location, or pre-chamber/orifice geometry; however, when a long thin interconnecting orifice was used power output was much reduced. This was thought to be due to the different turbulence characteristics generated by the different orifice geometries.
- (6) Changes in power output with engine speed could be explained in terms of variation in volumetric efficiency. Combustion duration, measured in terms of crank angle, decreased with increased engine speed.
- (7) Increased compression ratio resulted in increased combustion rate and power output in the single chamber Yamaha engine. However, for a disc shaped chamber there proved to be a limit to this trend; above a certain compression ratio, heat losses from the consequent wide thin chamber became excessive.
- (8) Flame propagation rates in the Yamaha engine, when operating in single chamber mode, were considerably slower than in the Ruston engine. This was thought to be due to lower turbulence levels. In divided chamber mode, flame propagation was, however, considerably faster. This was considered to be a result of higher orifice flow velocities, and hence higher turbulence, in the Yamaha engine vis à vis those of the Ruston engine
- (9) High peak pre-chamber pressure, prior to main chamber combustion, was associated with those dual chamber volume ratios and orifice diameters which resulted in high orifice flow velocity. Misfiring was also more significant under these conditions.
- (10) The presence of lubricating oil films on engine windows causes refraction of light passing through the windows; hence the resultant image is distorted. Attempts to adopt schlieren photography in the currently reported work had to be abandoned because of such effects.



ENGINE SPEED = 800 rpm
 COMPRESSION RATIO = 8.0

Fig.4.1 Effect of Ignition advance on mean effective pressure



COMPRESSION RATIO = 8.0
ORIFICE DIAMETER = 5 mm
ENGINE SPEED = 800 rpm

VOLUME RATIO = 25%
OPTIMUM SPARK ADVANCE

Fig.4.2 Pressure - crank angle diagram

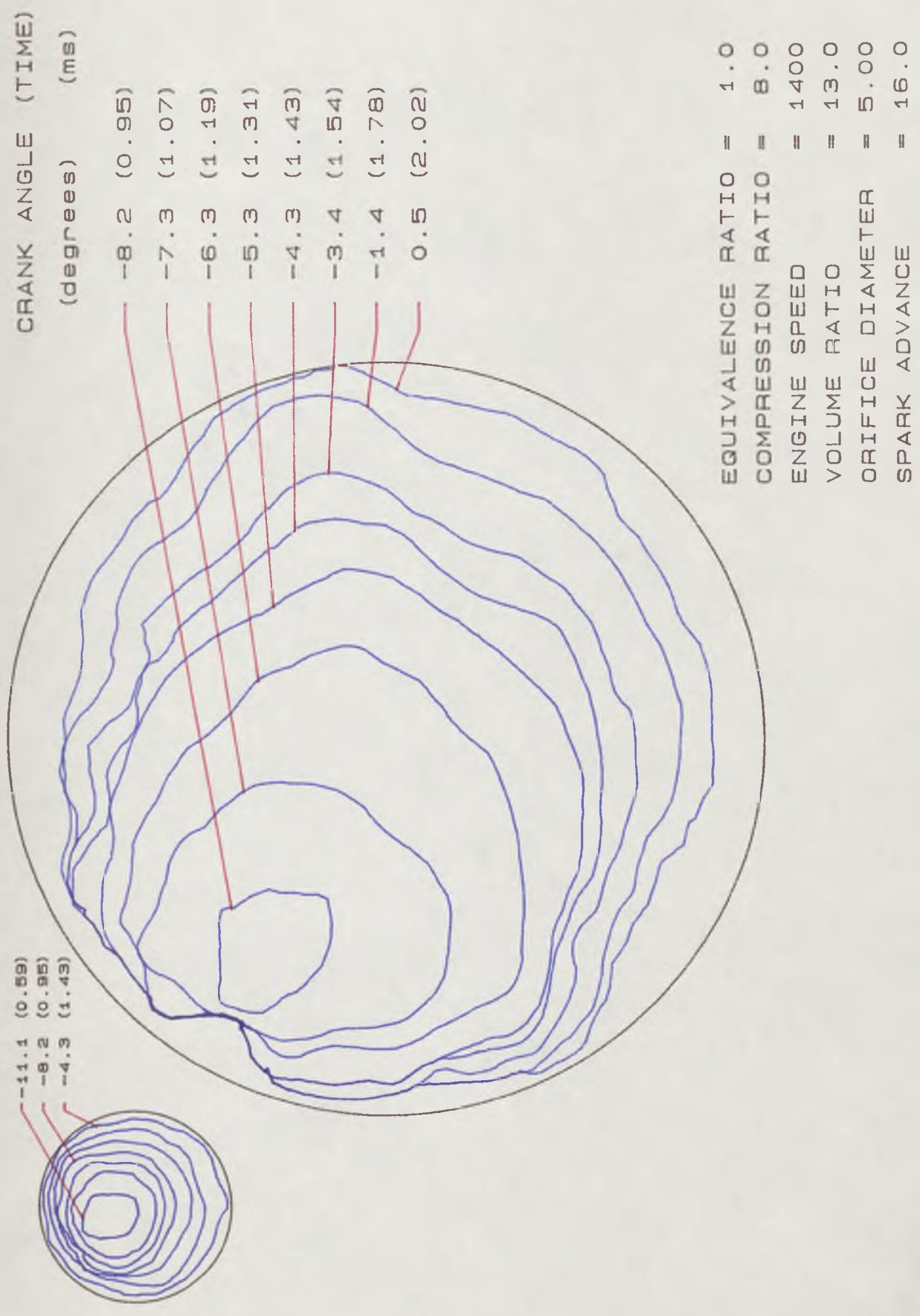


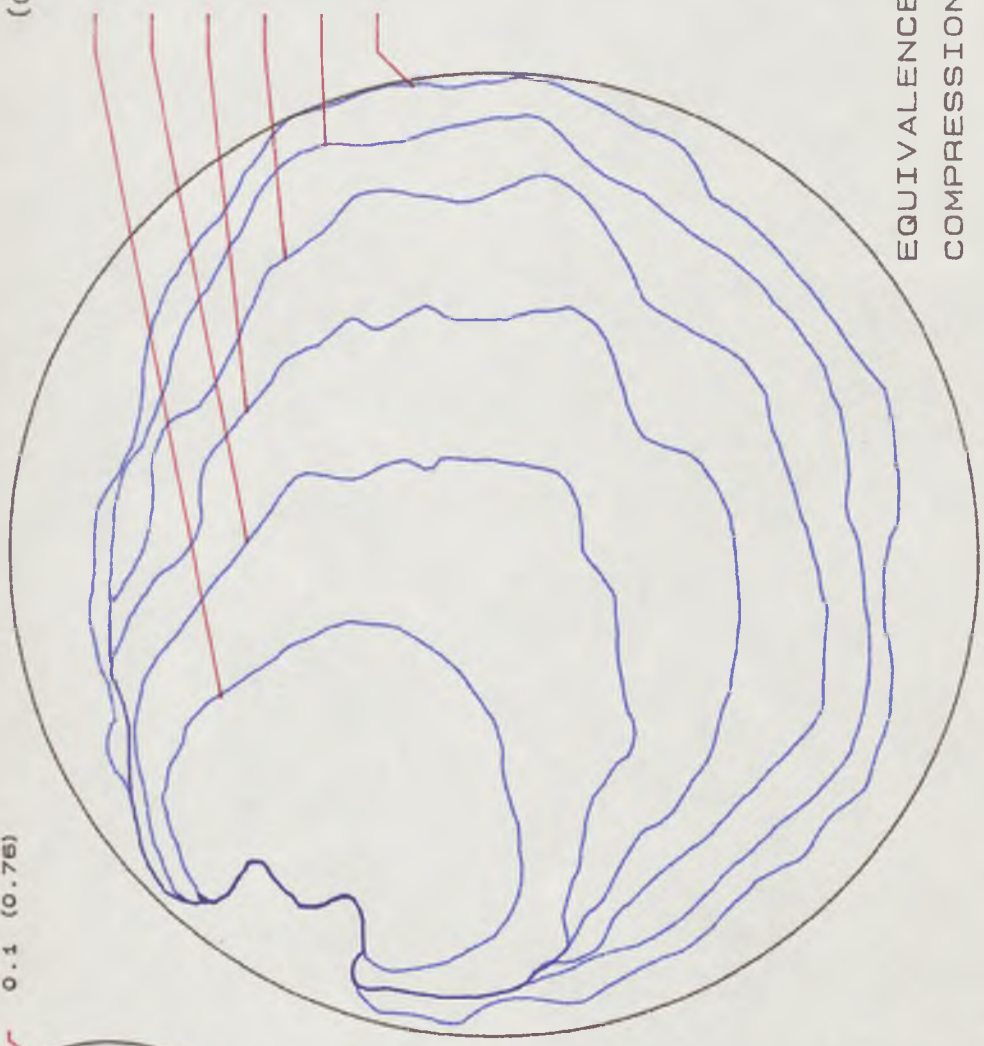
Fig. 4.3 Flame projected area shown by film

-4.0 (0.25)
 -2.0 (0.51)
 0.1 (0.76)



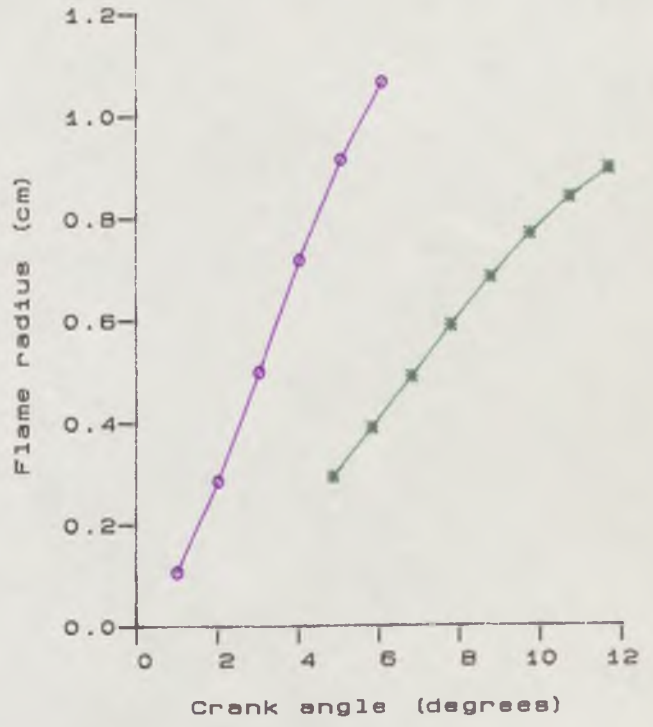
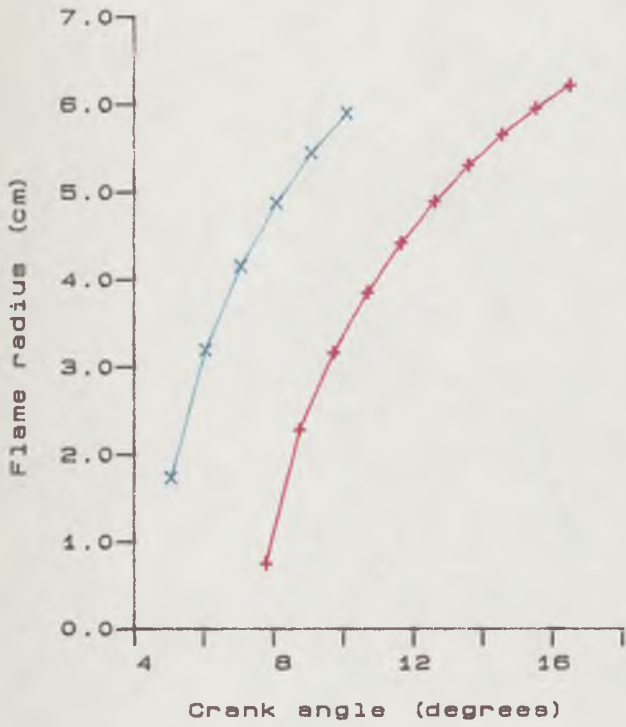
CRANK ANGLE (TIME)
 (degrees) (ms)

-1.0 (0.64)
 0.1 (0.76)
 1.1 (0.89)
 2.1 (1.02)
 3.1 (1.14)
 4.1 (1.27)



EQUIVALENCE RATIO = 1.0
 COMPRESSION RATIO = 8.0
 ENGINE SPEED = 1400
 VOLUME RATIO = 25.0
 ORIFICE DIAMETER = 5.00
 SPARK ADVANCE = 6.0

Fig.4.4 Flame projected area shown by film



+ — Main chamber 13%VR
* — Pre-chamber 13%VR

x — Main chamber 25%VR
o — Pre-chamber 25%VR

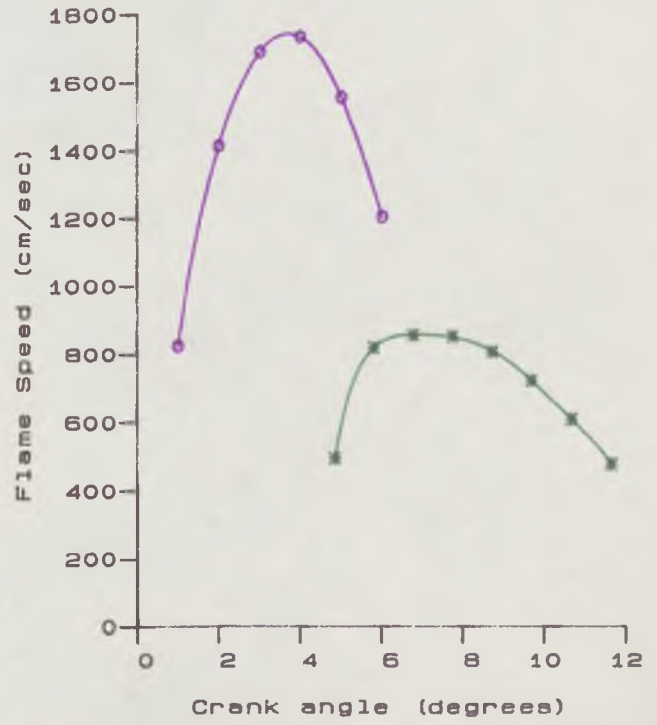
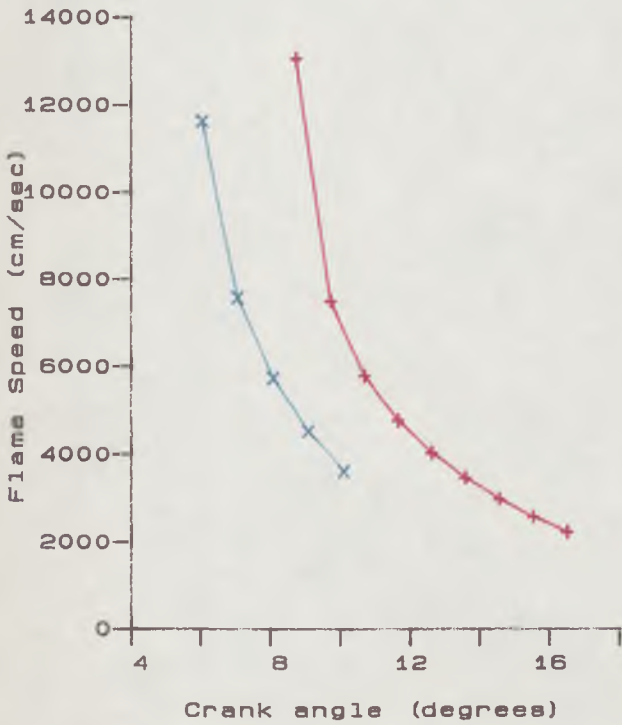


Fig.4.5

Comparison of flame propagation rates with varying volume ratio.

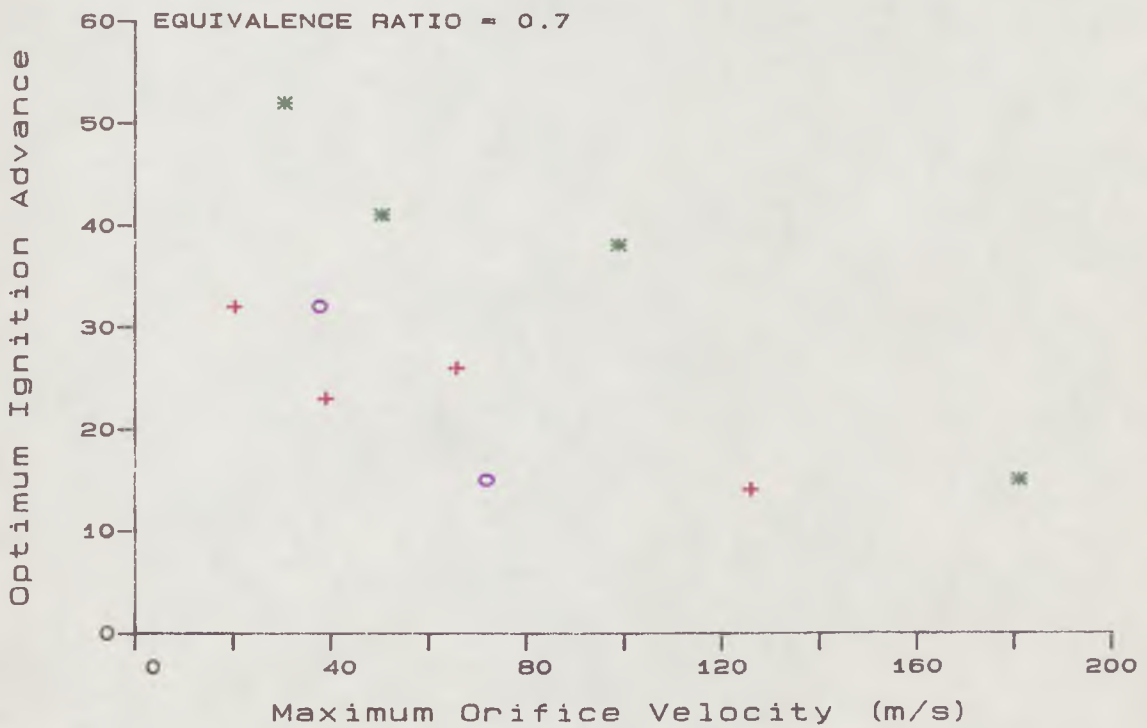
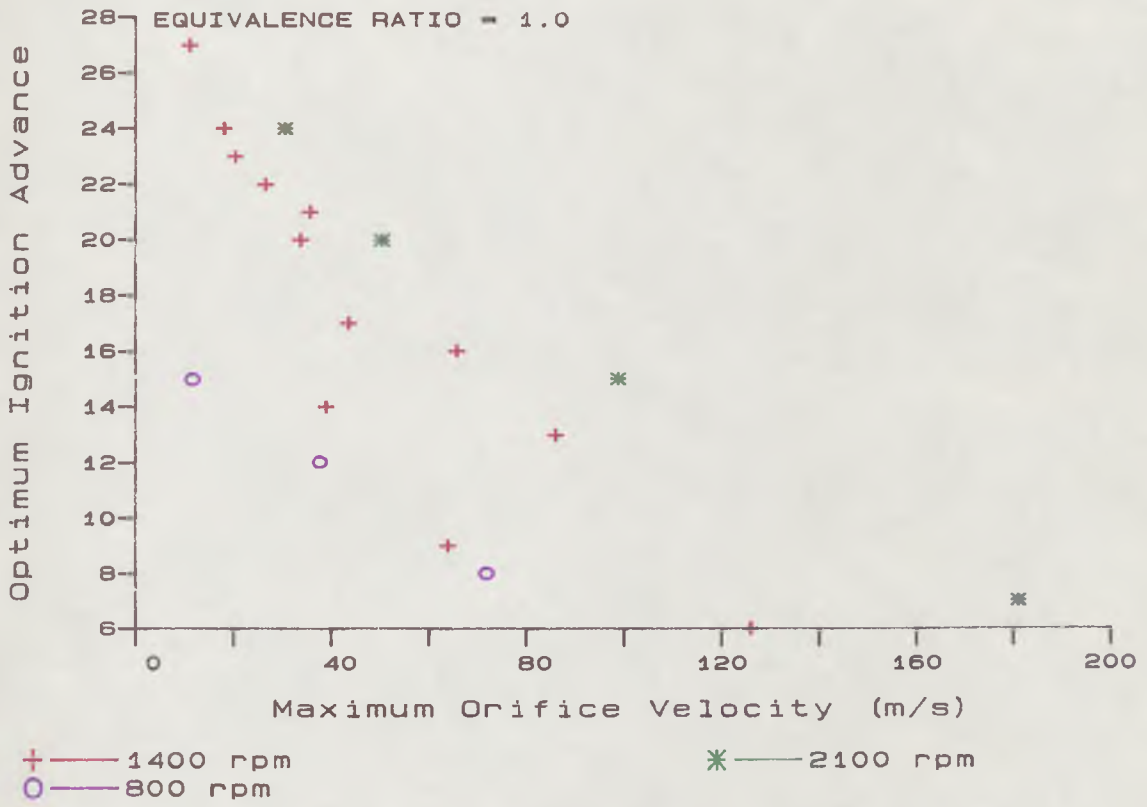


Fig. 4.6

Effect of Maximum Orifice Velocity on Optimum Ignition Advance

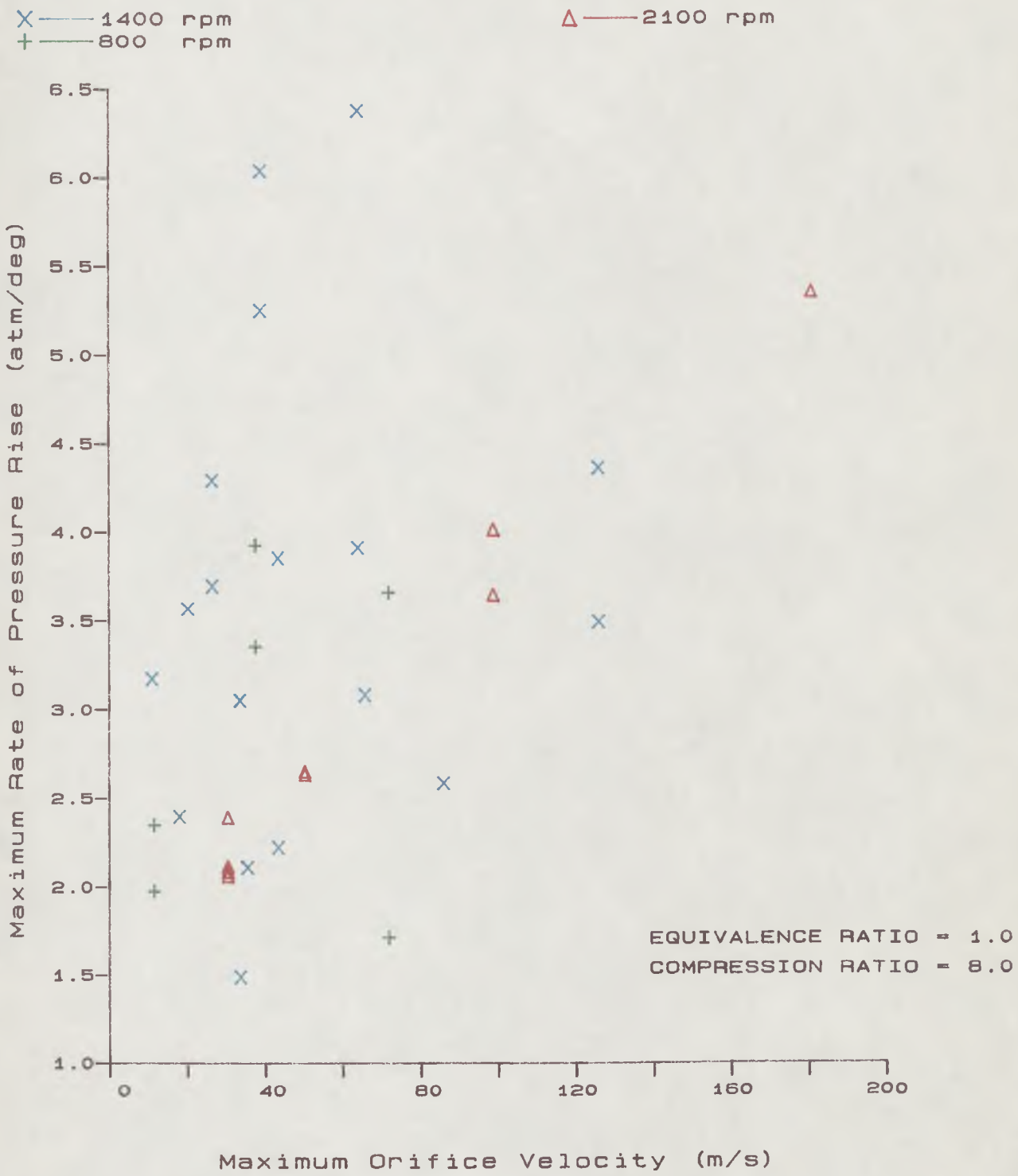


Fig.4.7

Effect of Maximum Orifice Velocity on Maximum Rate of Pressure Rise in the Pre-Chamber

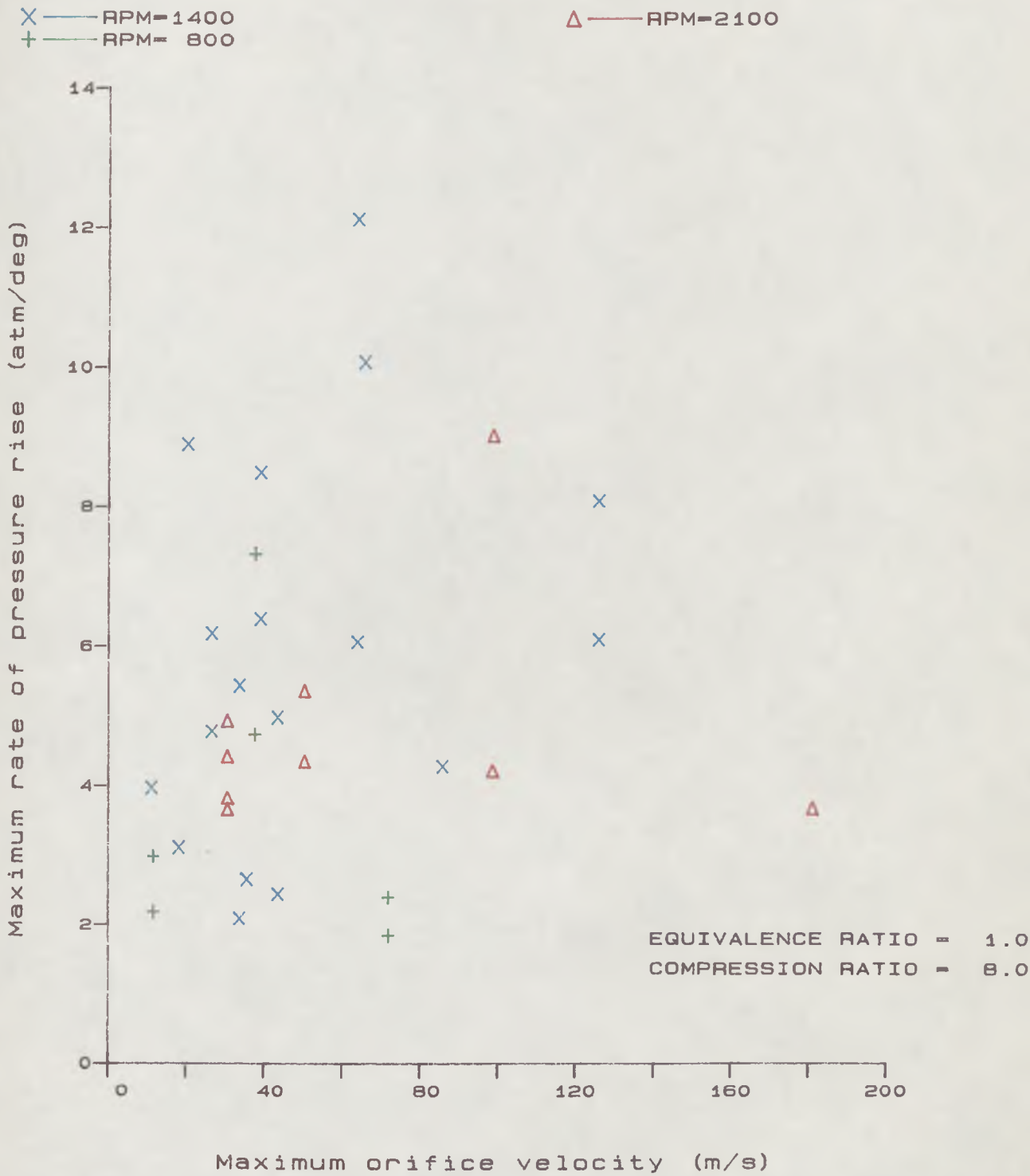


Fig.4.8

Effect of Maximum Orifice Velocity on Maximum Rate of Pressure Rise in the Main Chamber

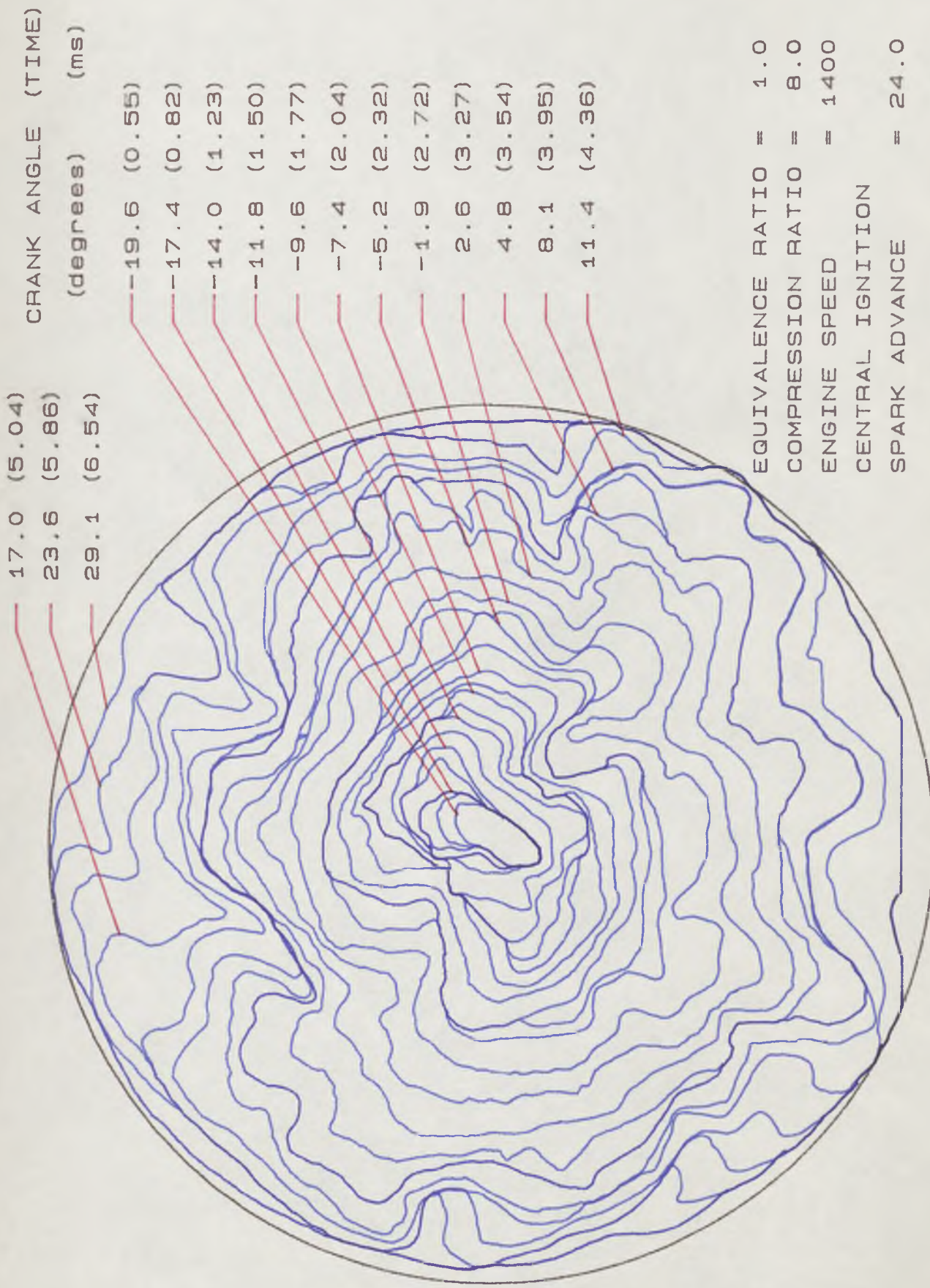


Fig. 4.9 Flame projected area shown by film

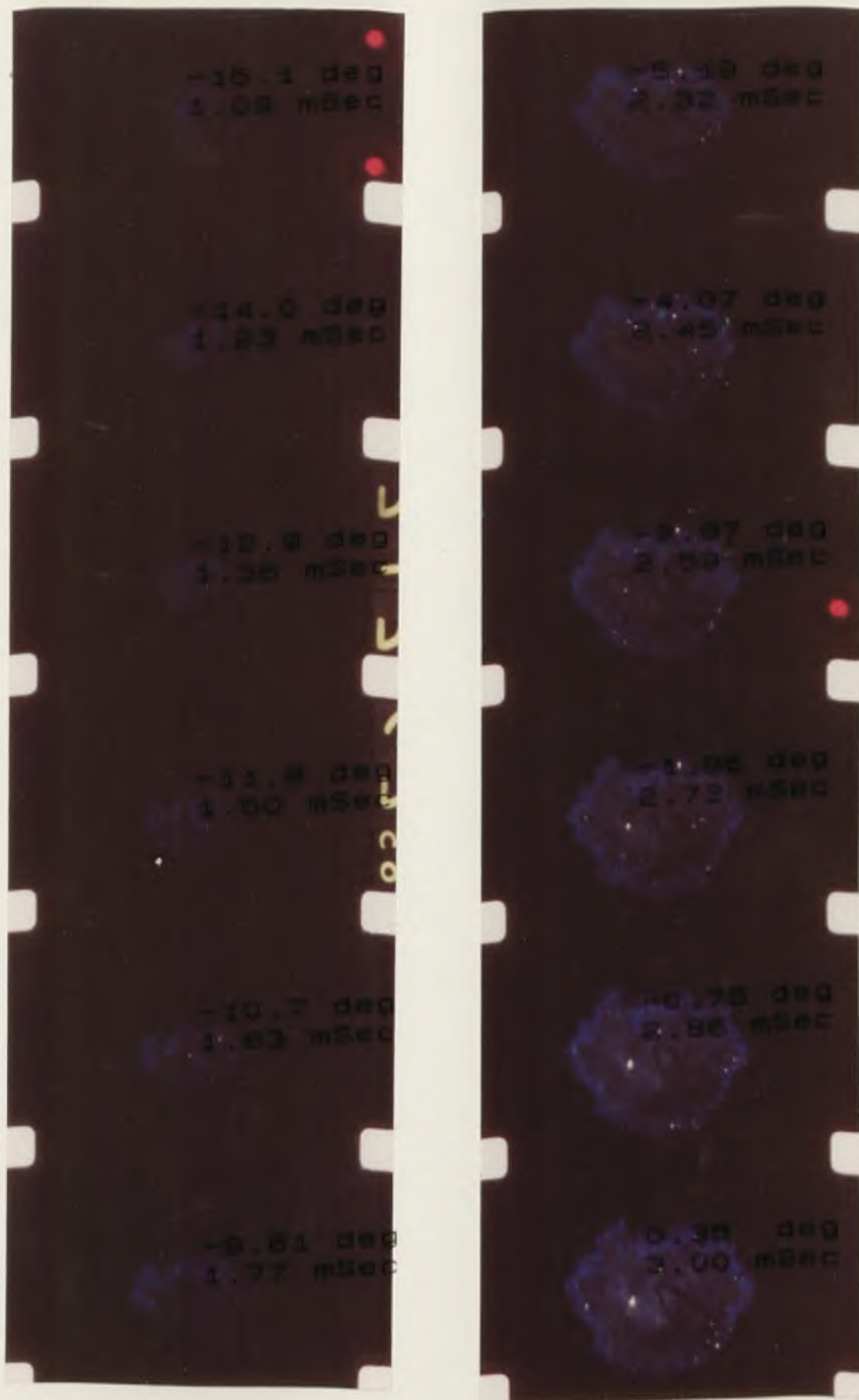


Fig. 4.10
 Flame propagation photographs
 (Single chamber, $\text{PHI} = 1.0$)

-15.1 deg
1.09 mSec

-5.19 deg
2.32 mSec

-14.0 deg
1.23 mSec

-4.07 deg
2.45 mSec

-12.9 deg
1.36 mSec

-2.97 deg
2.59 mSec

-11.8 deg
1.50 mSec

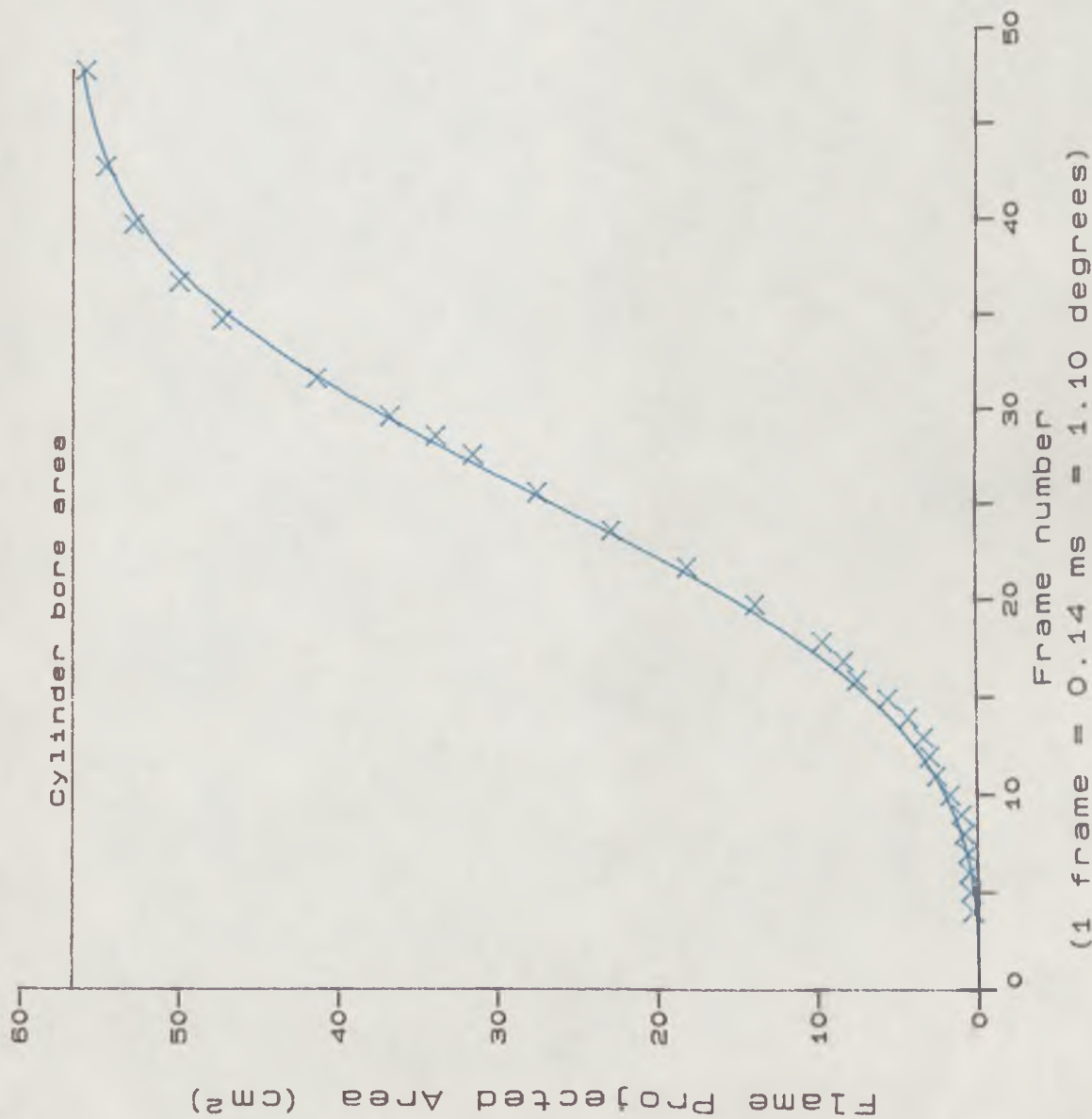
-1.86 deg
2.72 mSec

-10.7 deg
1.63 mSec

-0.75 deg
2.86 mSec

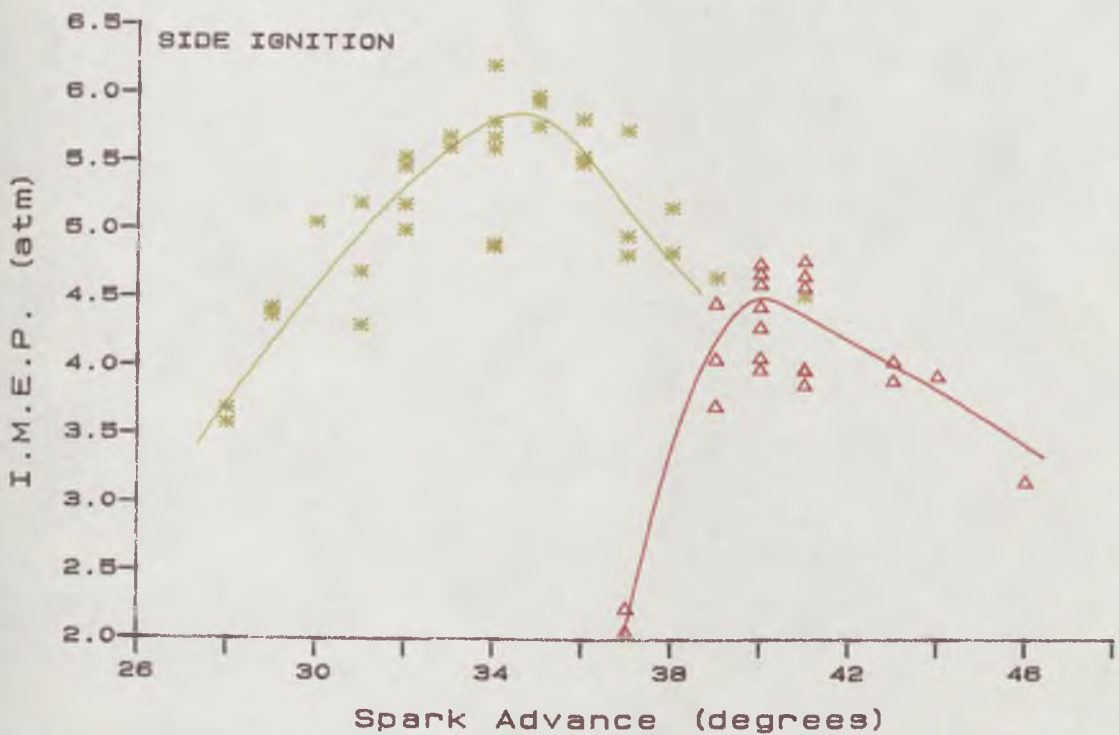
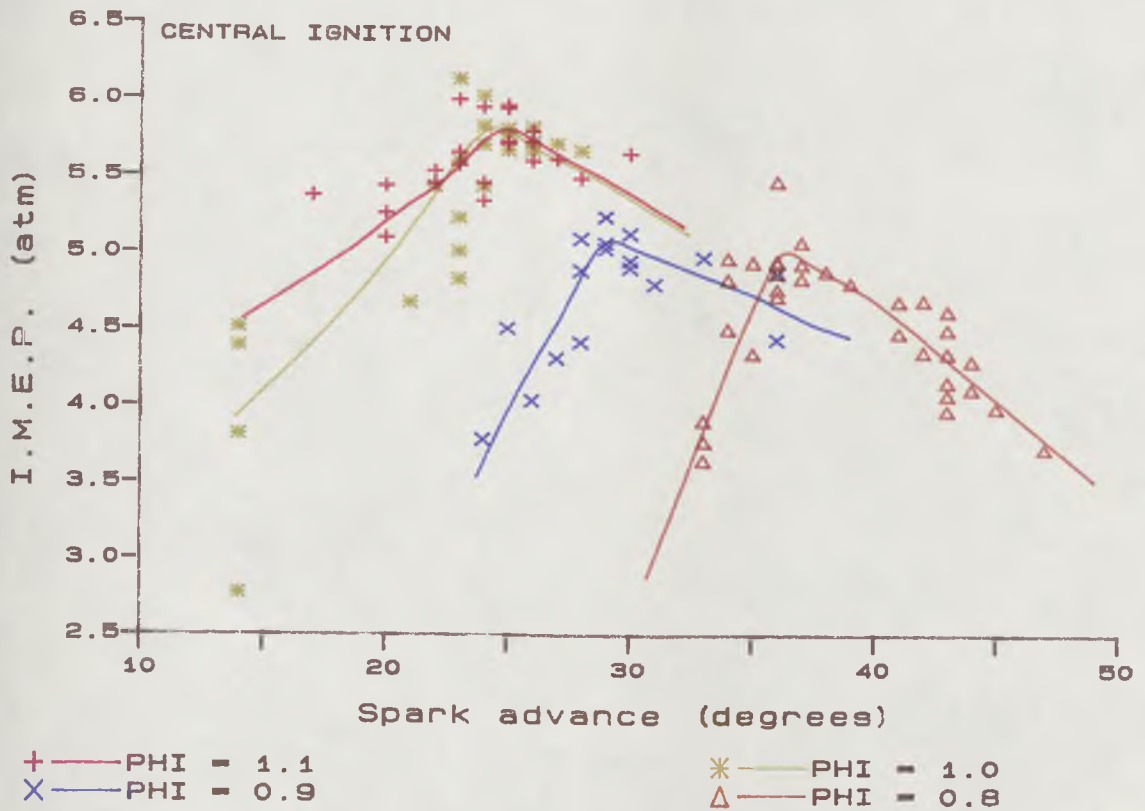
-9.61 deg
1.77 mSec

0.35 deg
3.00 mSec



EQUIVALENCE RATIO = 1.0
 COMPRESSION RATIO = 8.0
 ENGINE SPEED = 1400
 CENTRAL IGNITION
 SPARK ADVANCE = 24.0

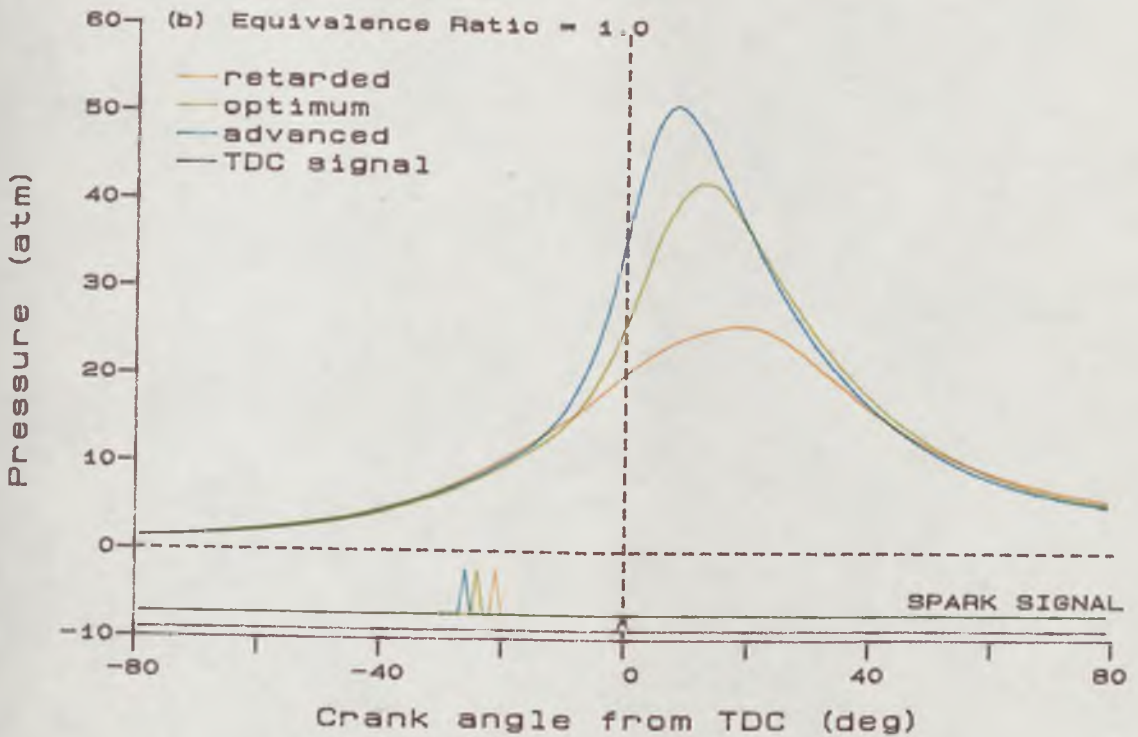
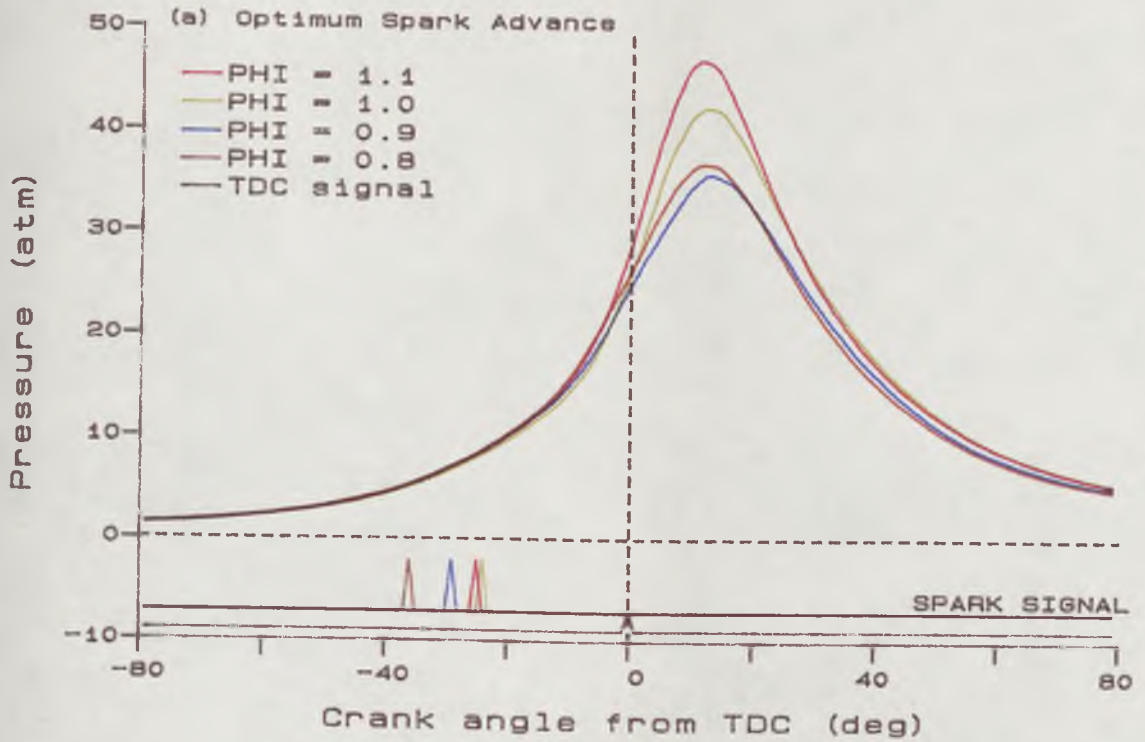
Fig. 4.11 Weibe function fit to flame area data



OPTIMUM SPARK ADVANCE
 ENGINE SPEED = 1400 rpm
 COMPRESSION RATIO = 8.0

Fig. 4.12

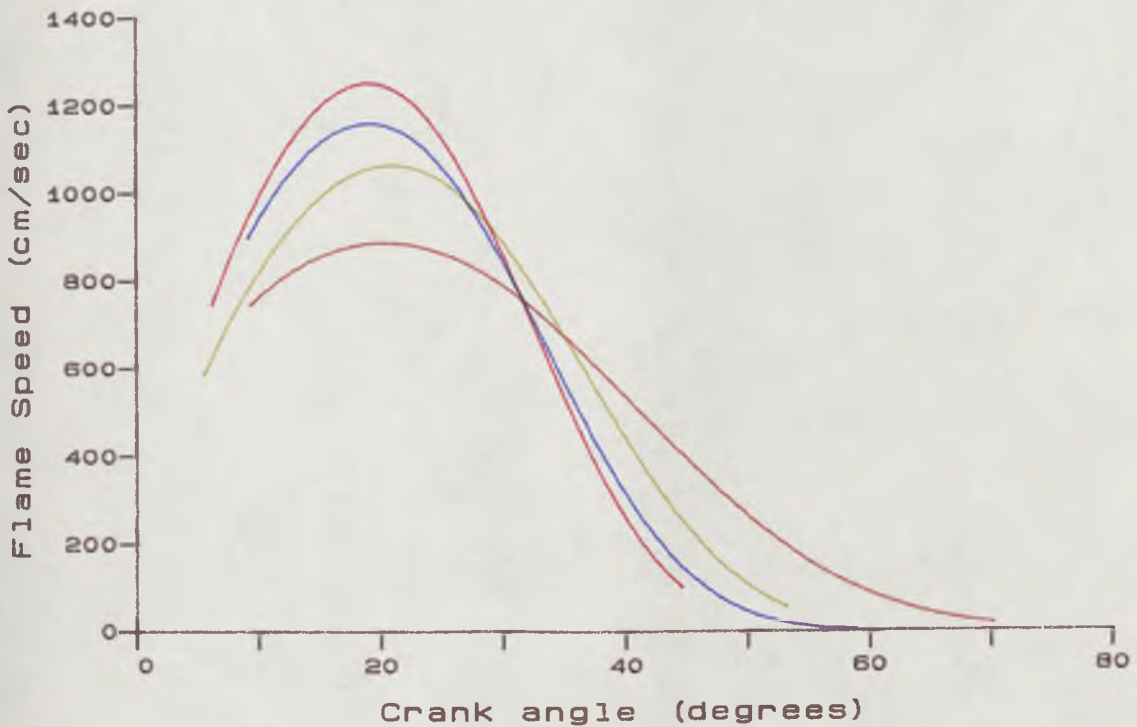
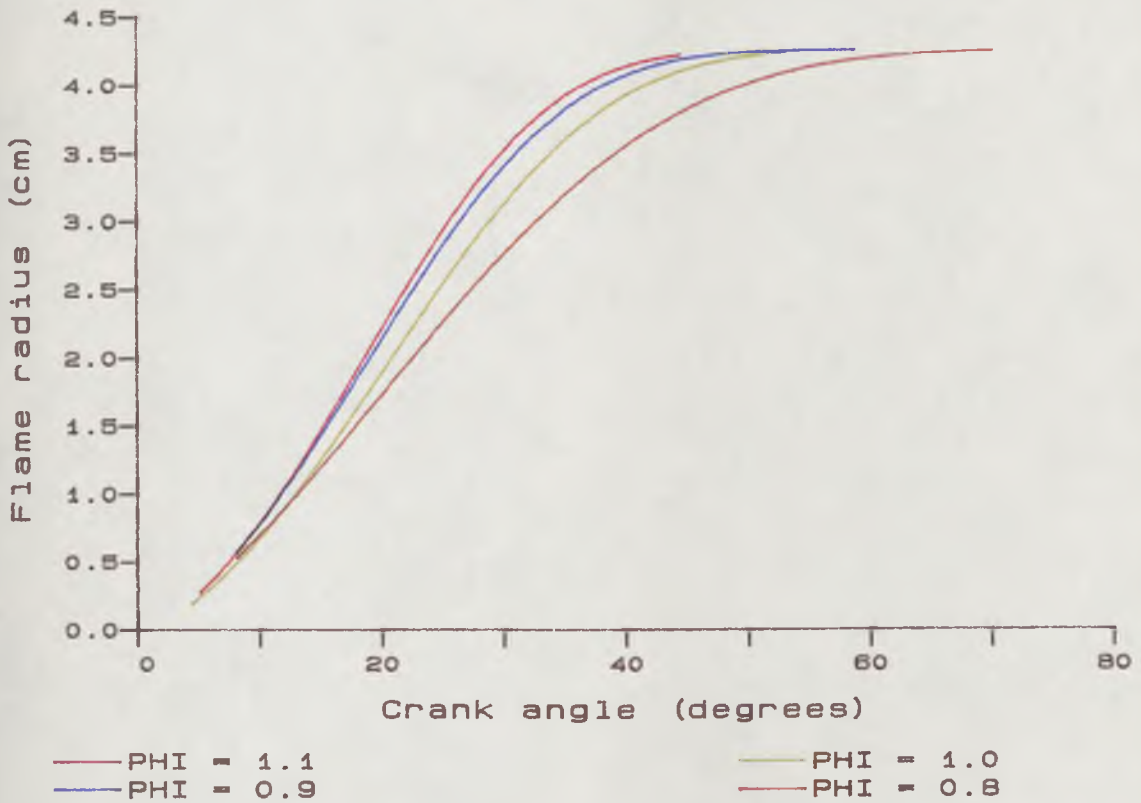
Effect of Equivalence Ratio and Ignition Timing on Power Output



CENTRAL IGNITION
COMPRESSION RATIO = 8.0
ENGINE SPEED = 1400 rpm

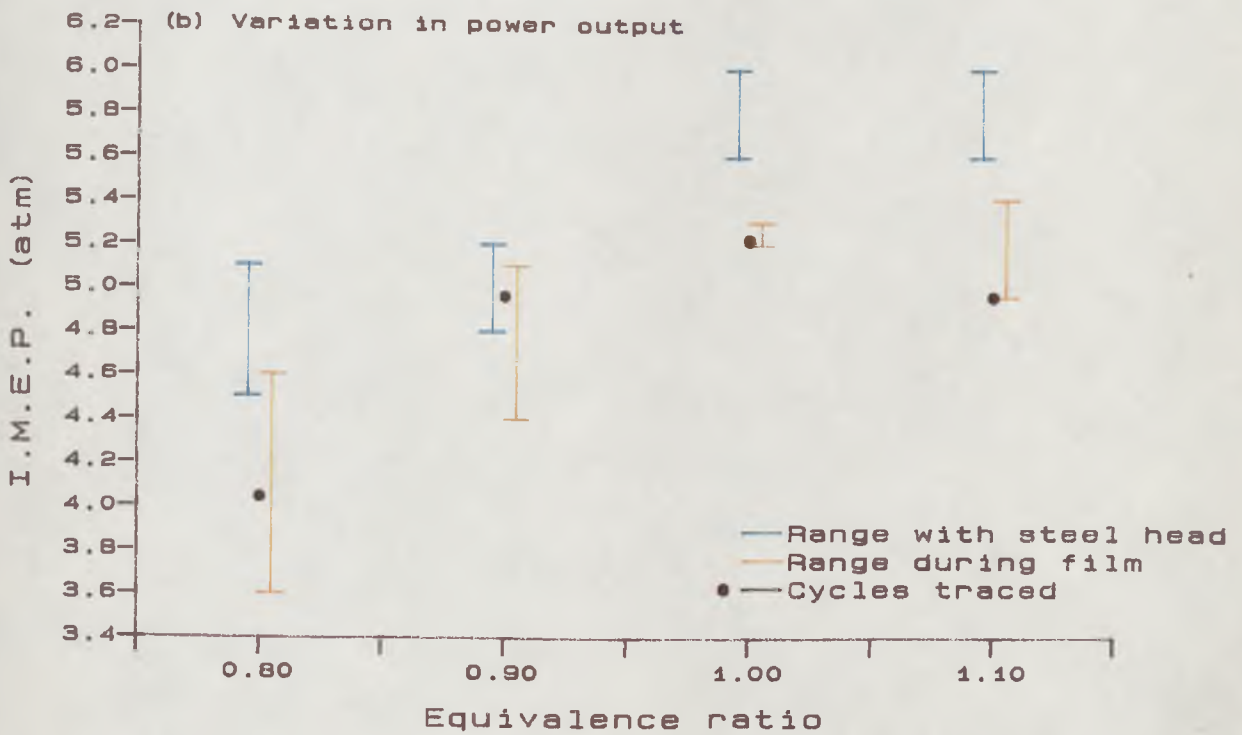
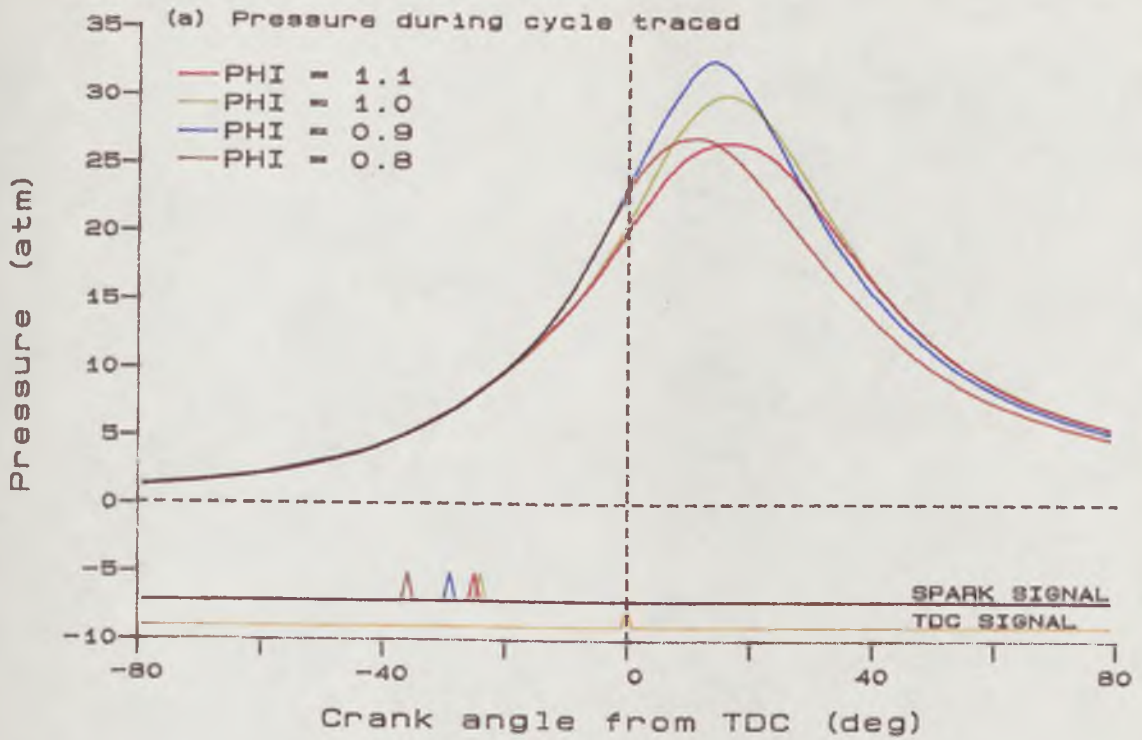
Fig. 4.13

Effect of equivalence ratio and ignition timing on cylinder pressure



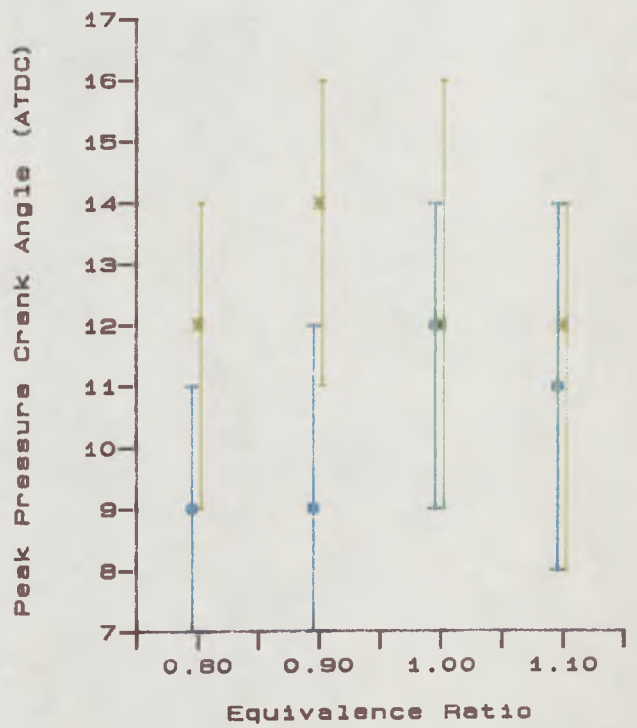
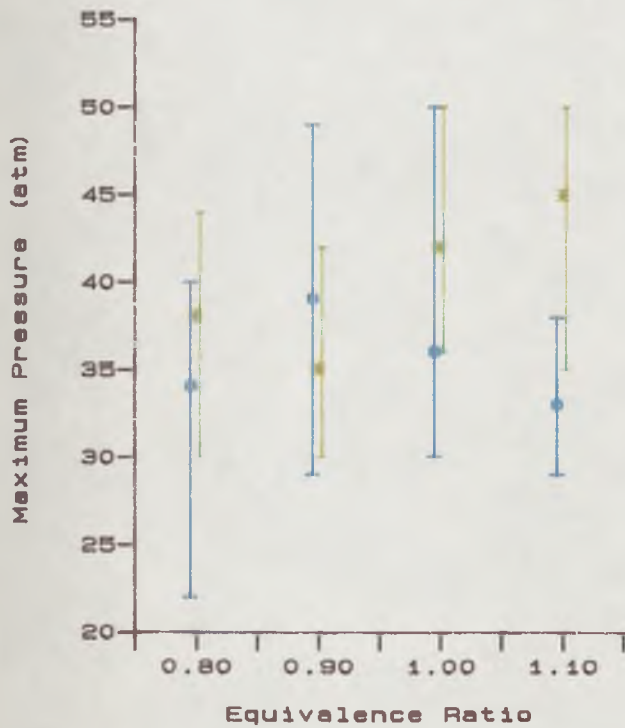
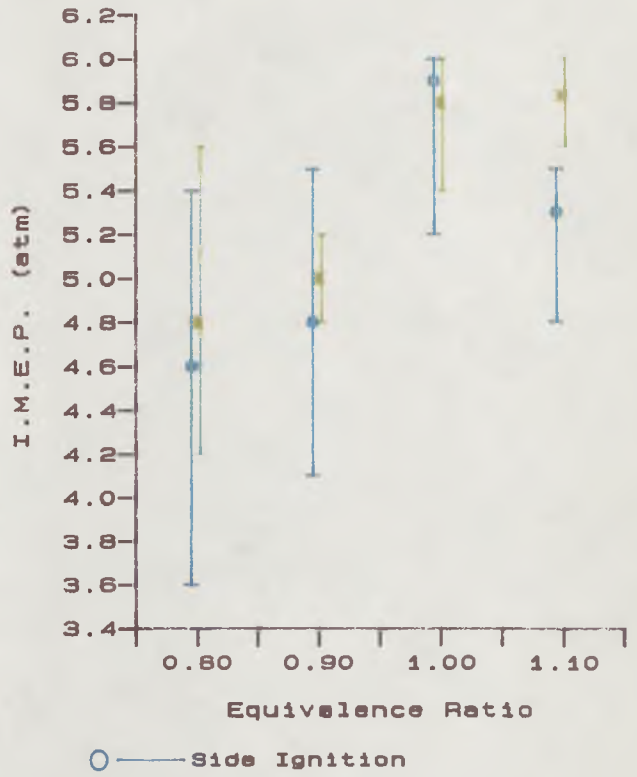
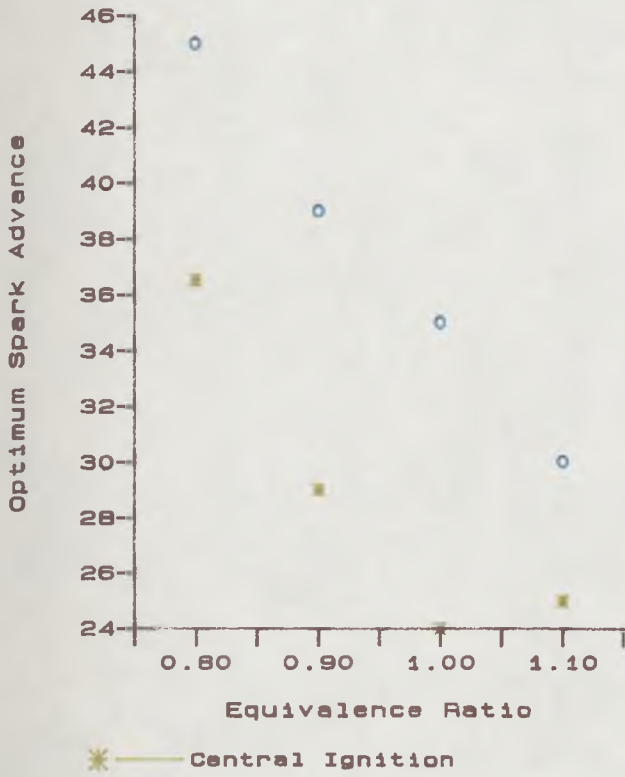
CENTRAL IGNITION
 OPTIMUM SPARK ADVANCE
 COMPRESSION RATIO = 8.0
 ENGINE SPEED = 1400 rpm

Fig. 4.14 Effect of Equivalence Ratio on flame propagation rate



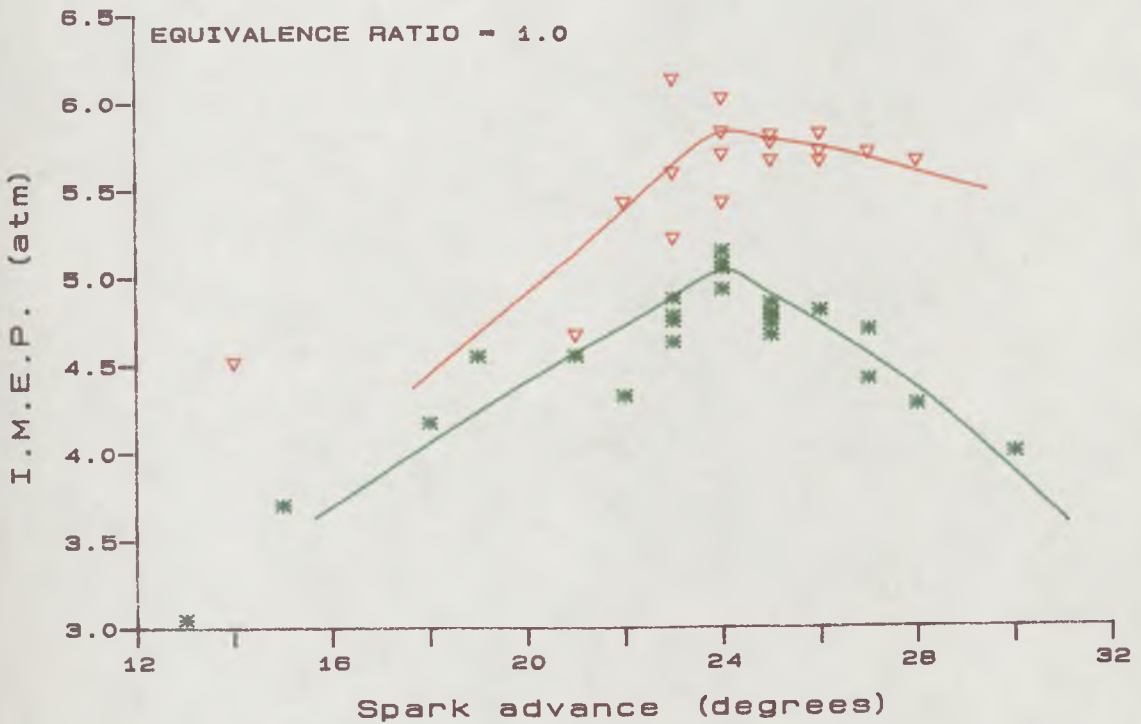
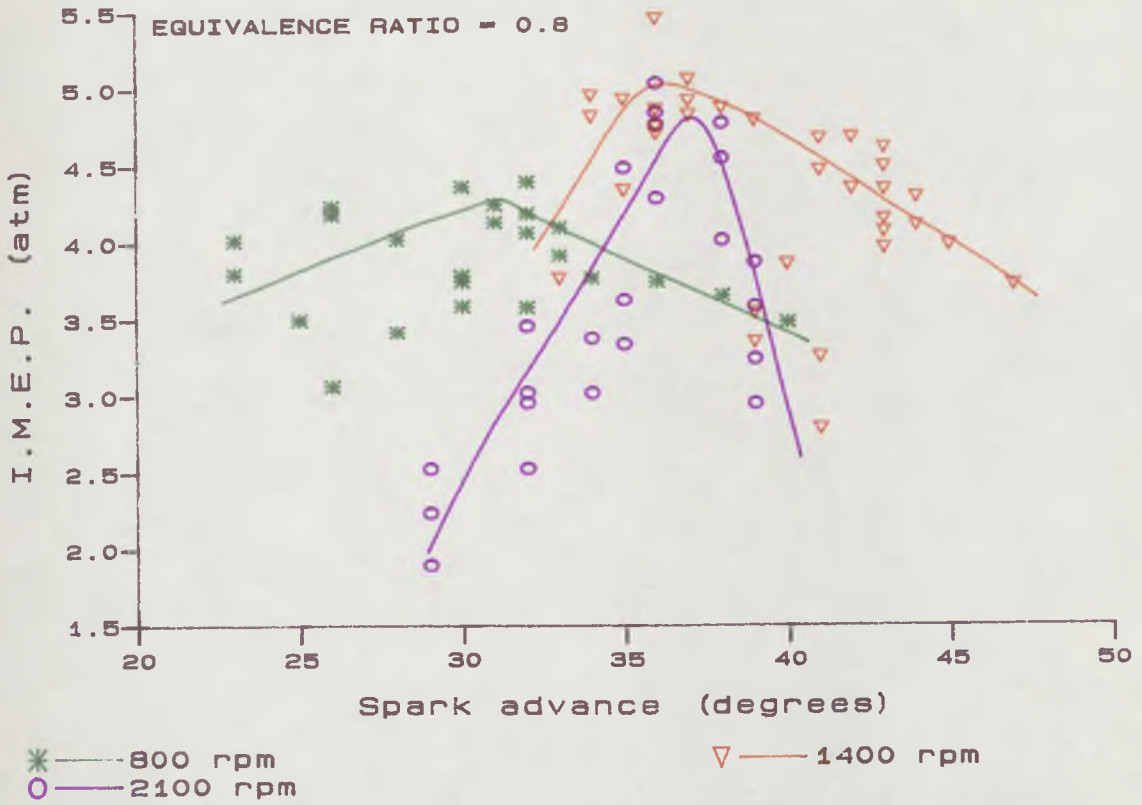
CENTRAL IGNITION
OPTIMUM SPARK ADVANCE
COMPRESSION RATIO = 8.0
ENGINE SPEED = 1400 rpm

Fig. 4.15 Pressure and power variation for cycles which were filmed



COMPRESSION RATIO - 8.0
ENGINE SPEED - 1400 rpm

Fig.4.16 Effect Of Spark Plug location



COMPRESSION RATIO = 8.0
 OPTIMUM SPARK ADVANCE
 CENTRAL IGNITION

Fig. 4.17
 Effect of Engine Speed and
 Ignition Timing on Power Output

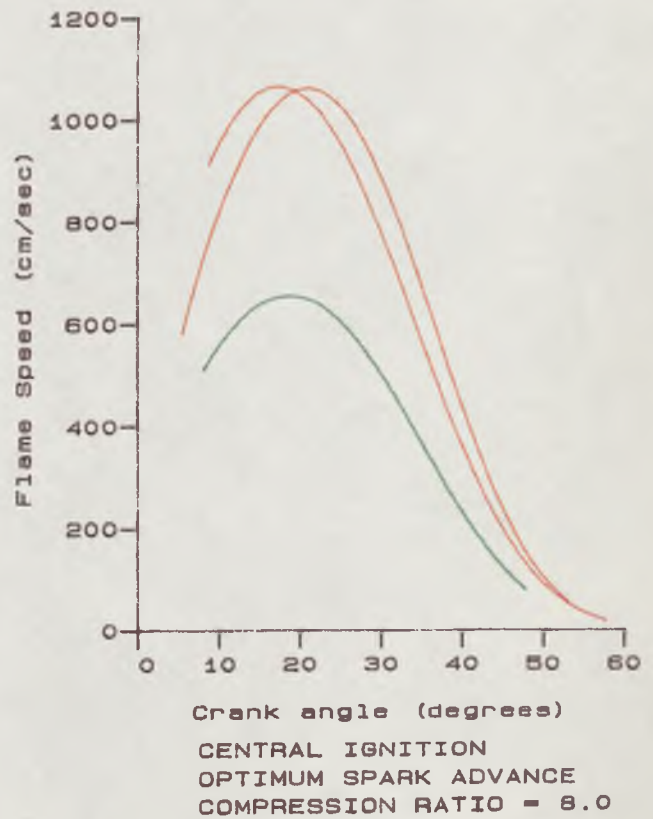
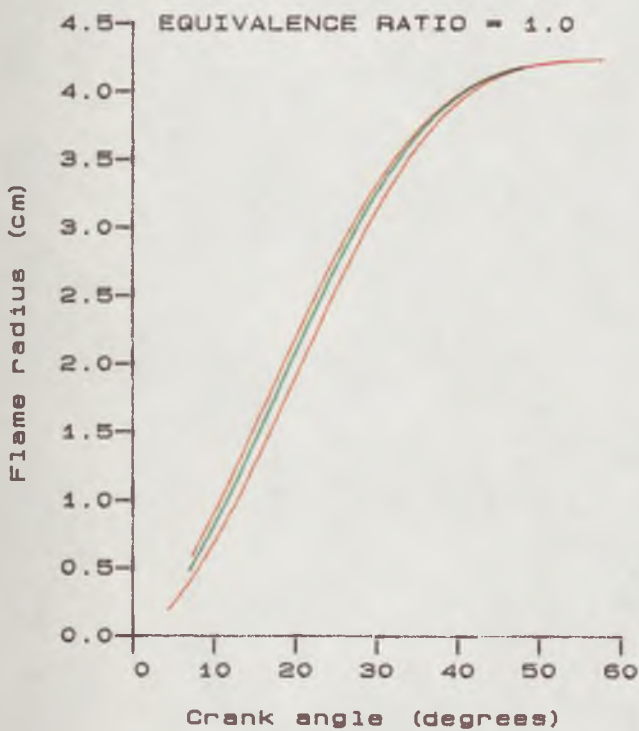
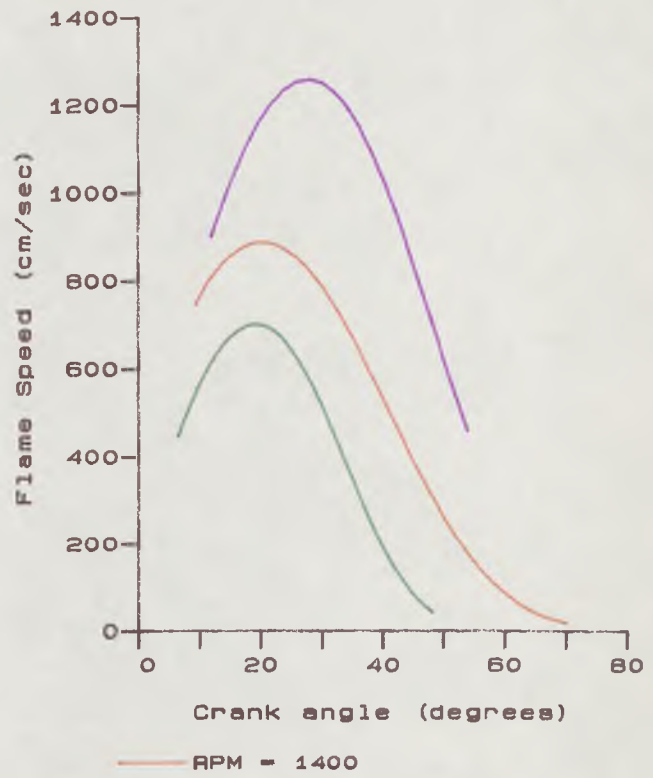
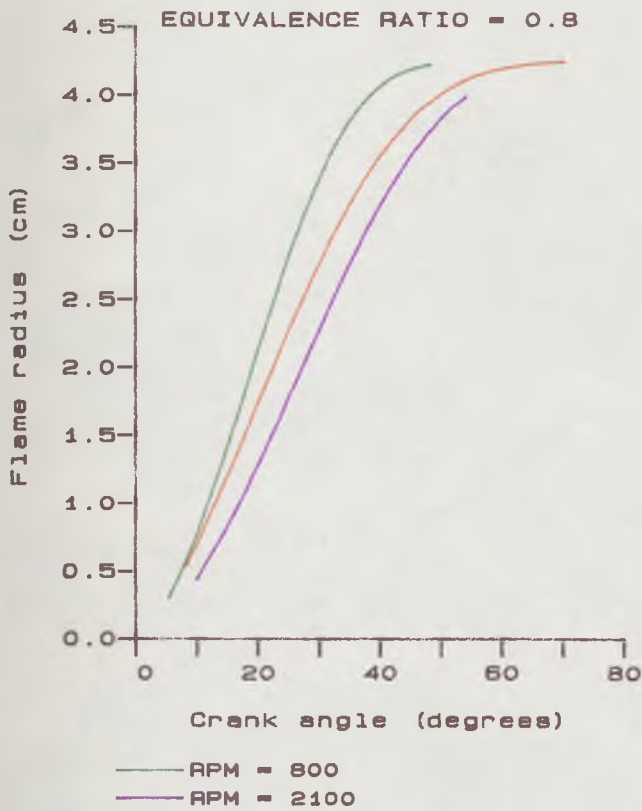
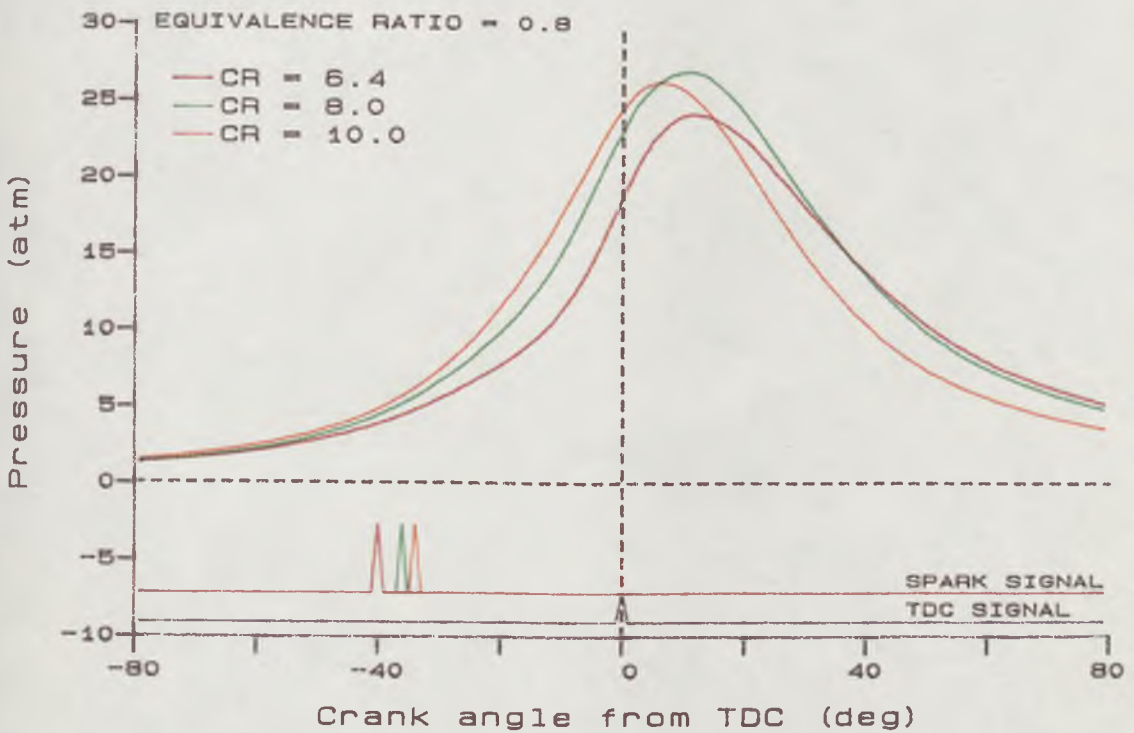
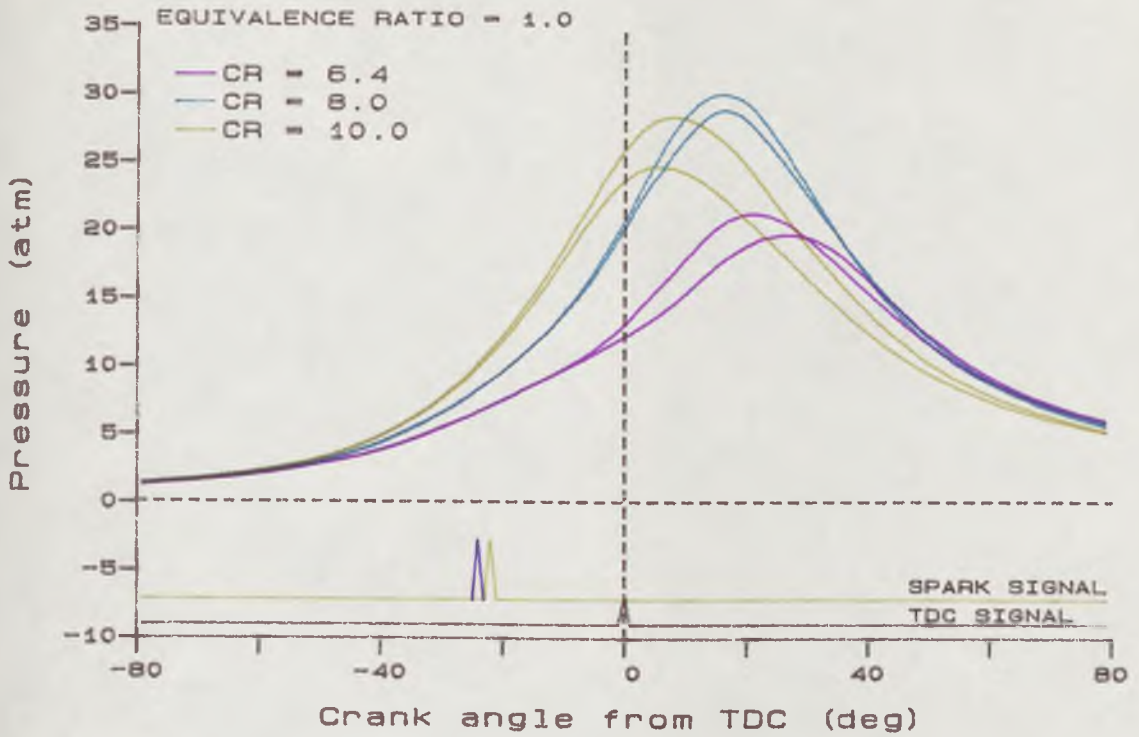
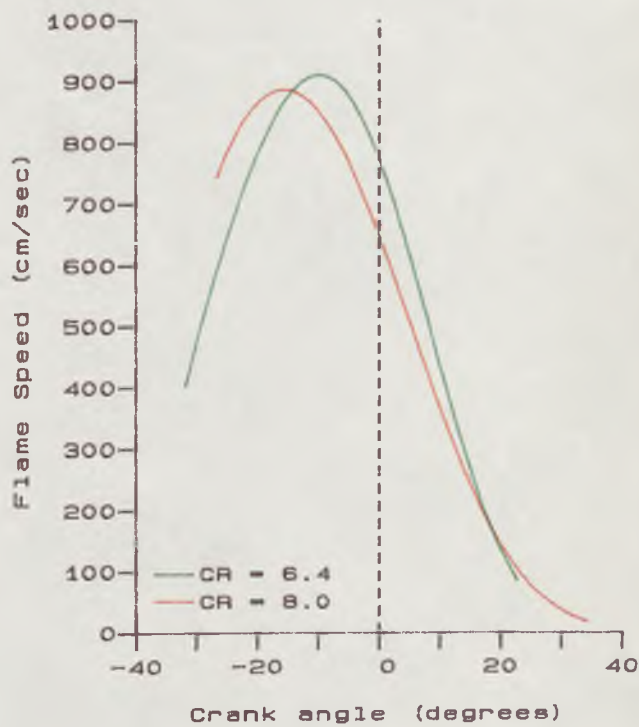
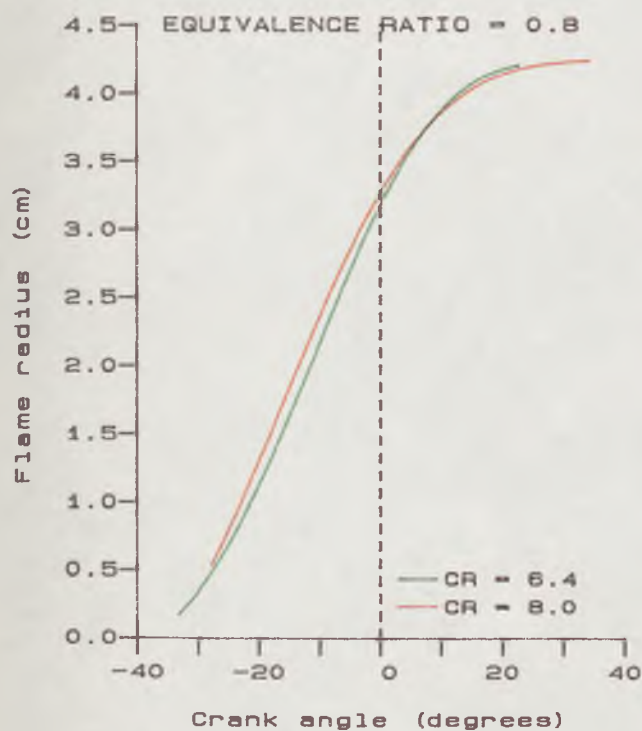
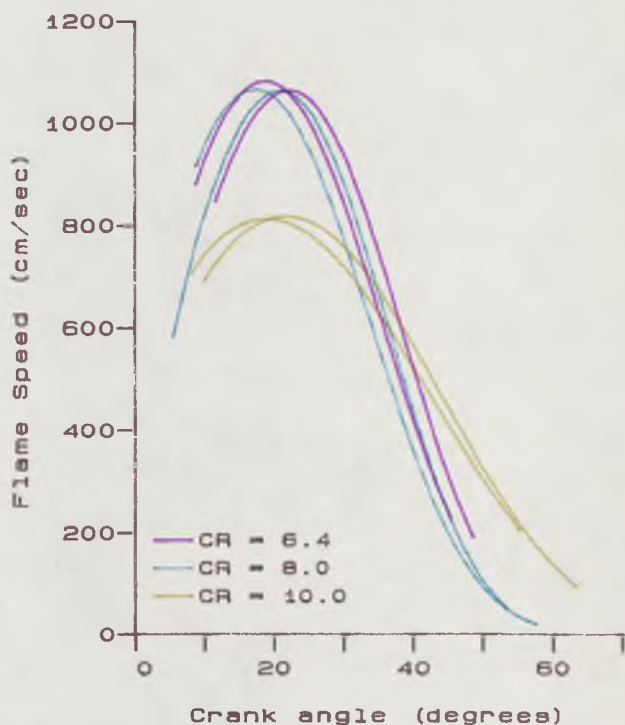
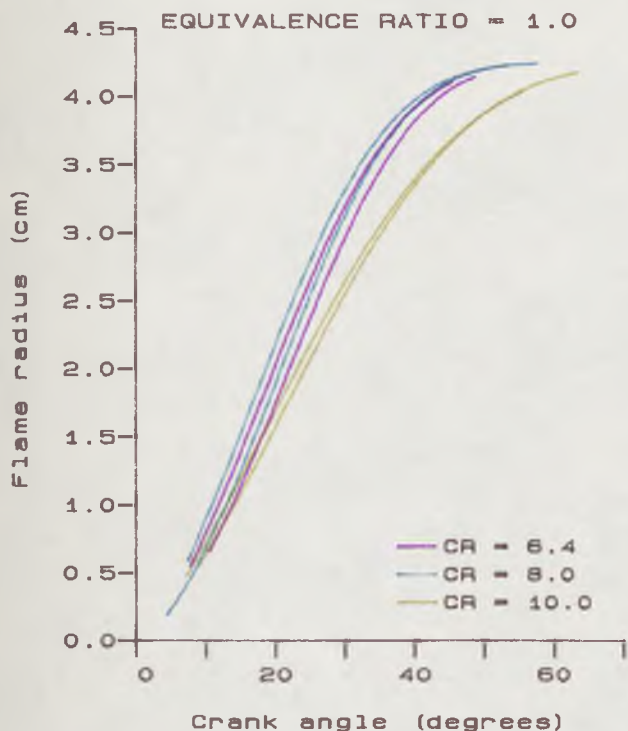


Fig. 4.18 Effect of Engine Speed on flame propagation rate



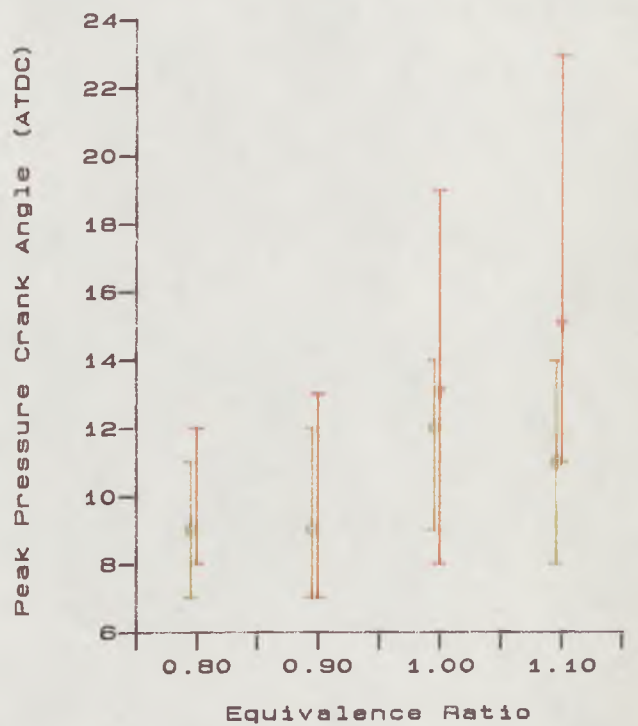
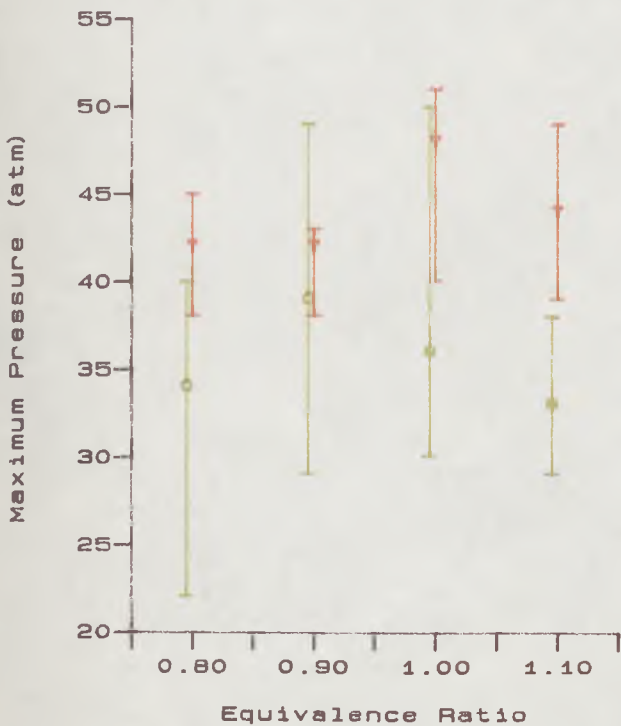
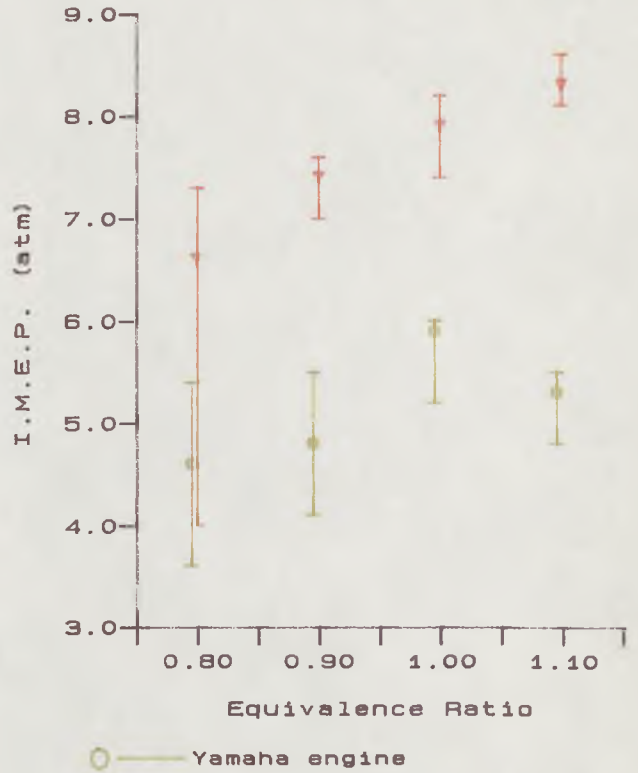
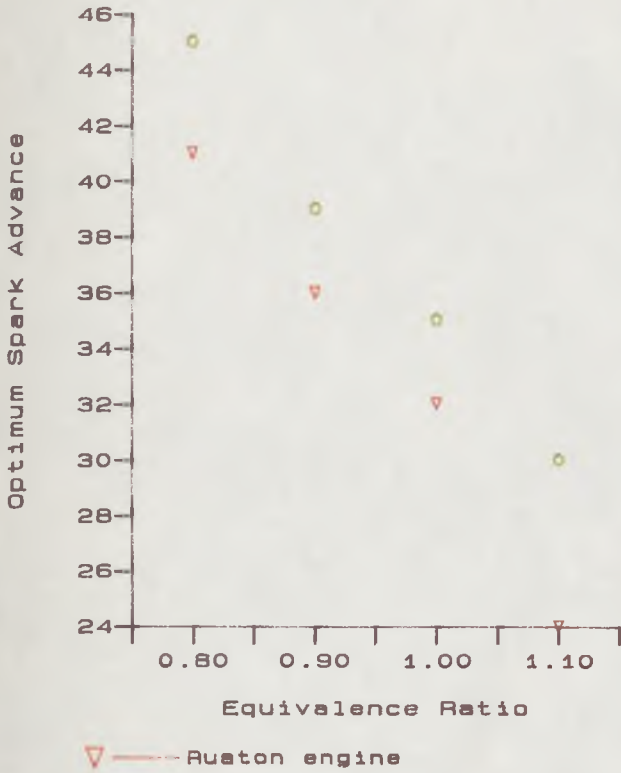
CENTRAL IGNITION
OPTIMUM SPARK ADVANCE
ENGINE SPEED = 1400

Fig. 4.19 Effect of Compression Ratio on cylinder pressure



CENTRAL IGNITION
OPTIMUM SPARK ADVANCE
ENGINE SPEED = 1400

Fig. 4.20 Effect of Compression Ratio on flame propagation rate



SIDE IGNITION
 COMPRESSION RATIO = 8.0
 ENGINE SPEED = 1400 rpm

Fig. 4.21

Comparison of experimental results from the Ruston and Yamaha engines

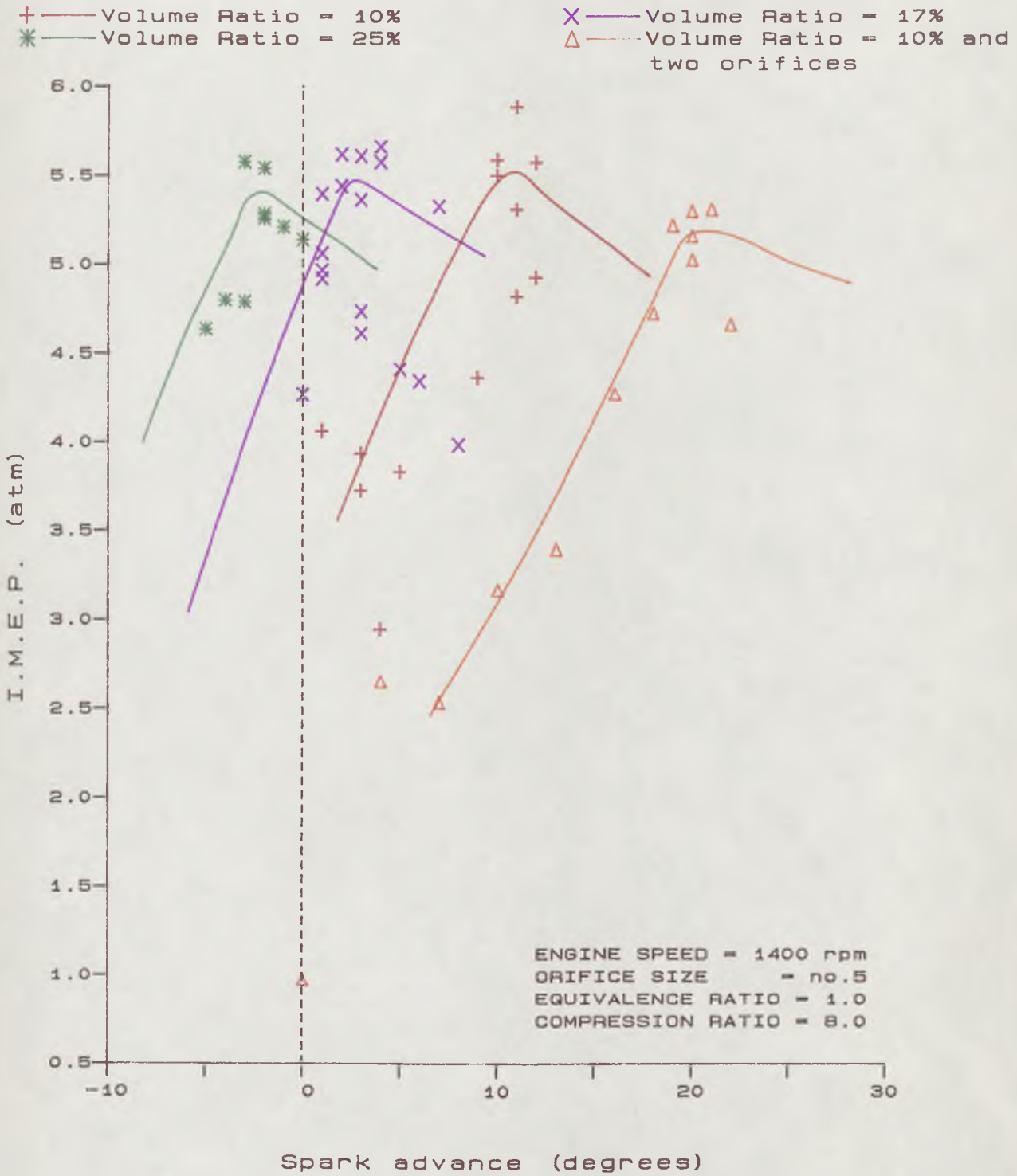


Fig. 4.22 Effect of Volume Ratio on Optimum Ignition Timing

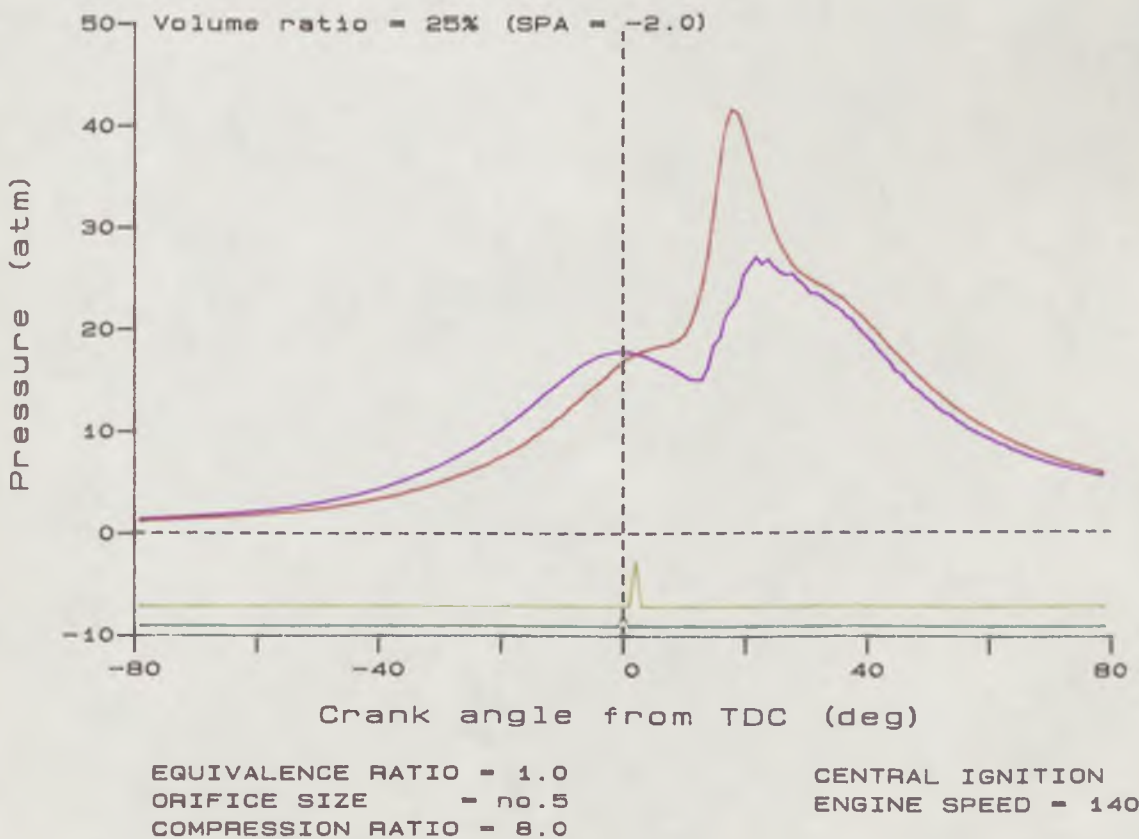
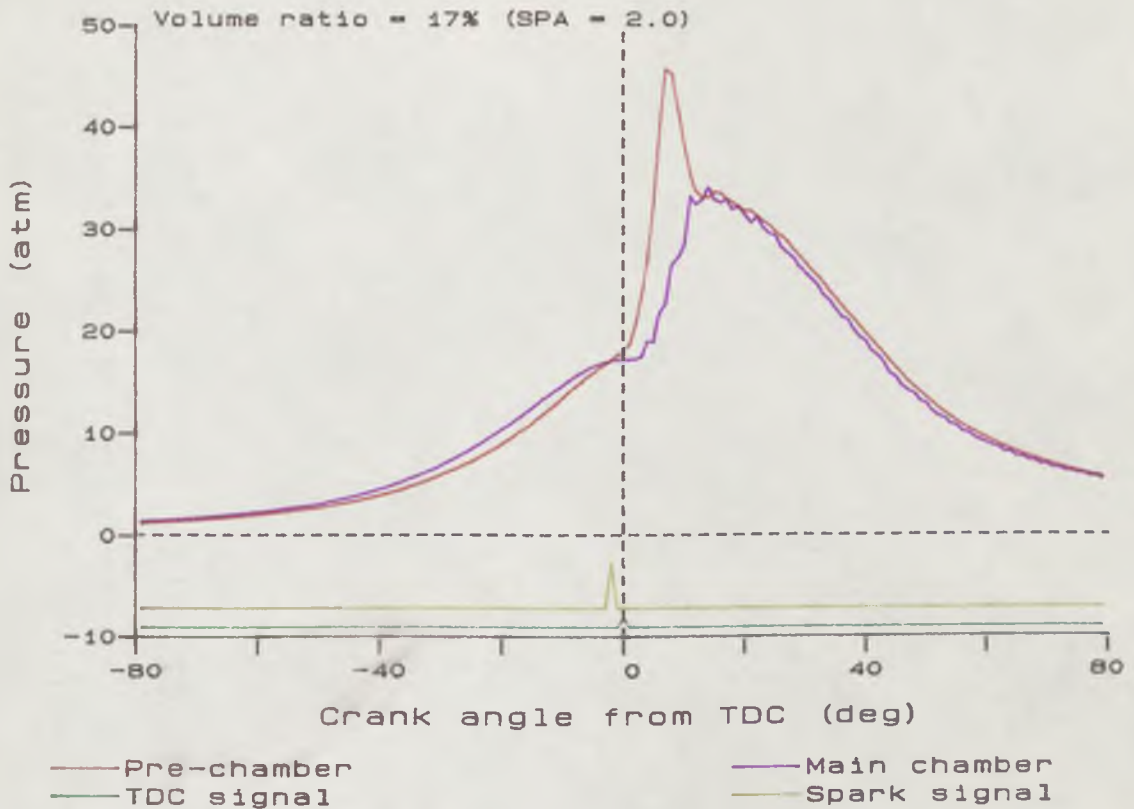


Fig.4.23
Effect of Volume ratio on Cylinder pressure

-6.36 deg
0.43 mSec

5.77 deg
1.86 mSec

-5.15 deg
0.57 mSec

6.98 deg
2.00 mSec

-3.93 deg
0.71 mSec

8.19 deg
2.14 mSec

-2.72 deg
0.86 mSec

9.40 deg
2.29 mSec

-1.51 deg
1.00 mSec

10.6 deg
2.43 mSec

-0.30 deg
1.14 mSec

11.8 deg
2.57 mSec

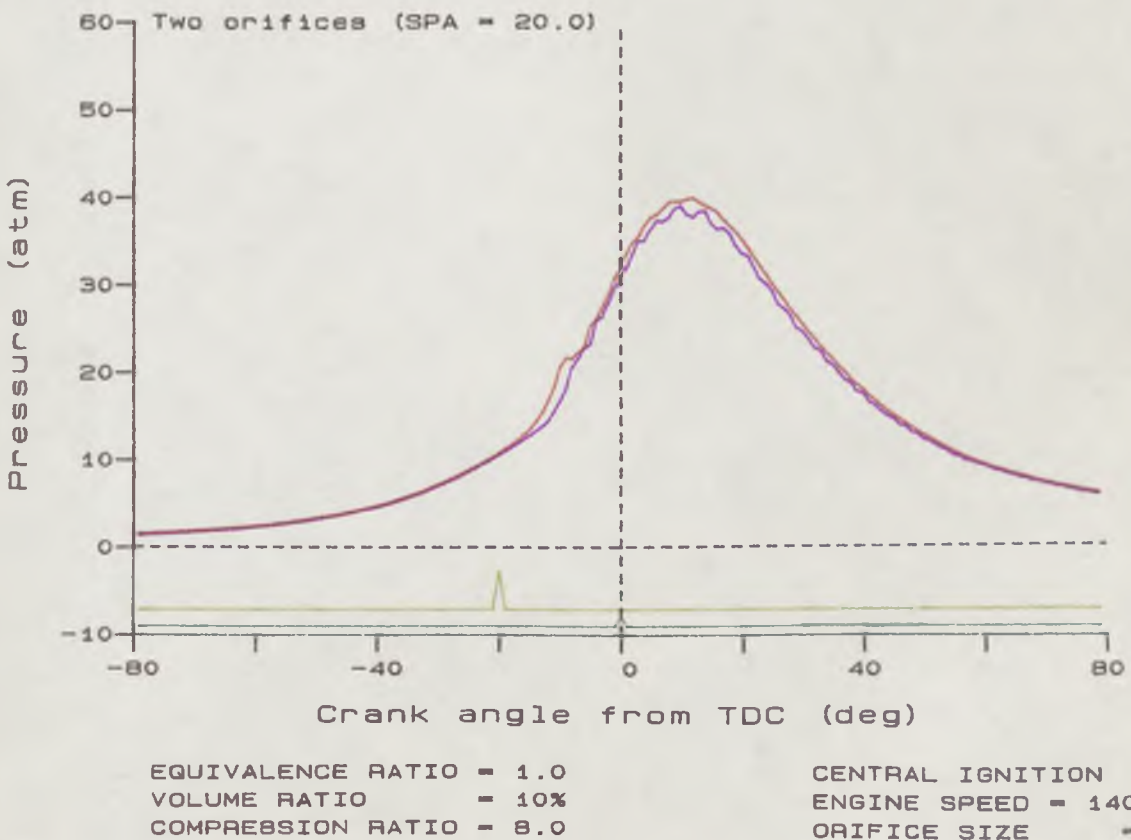
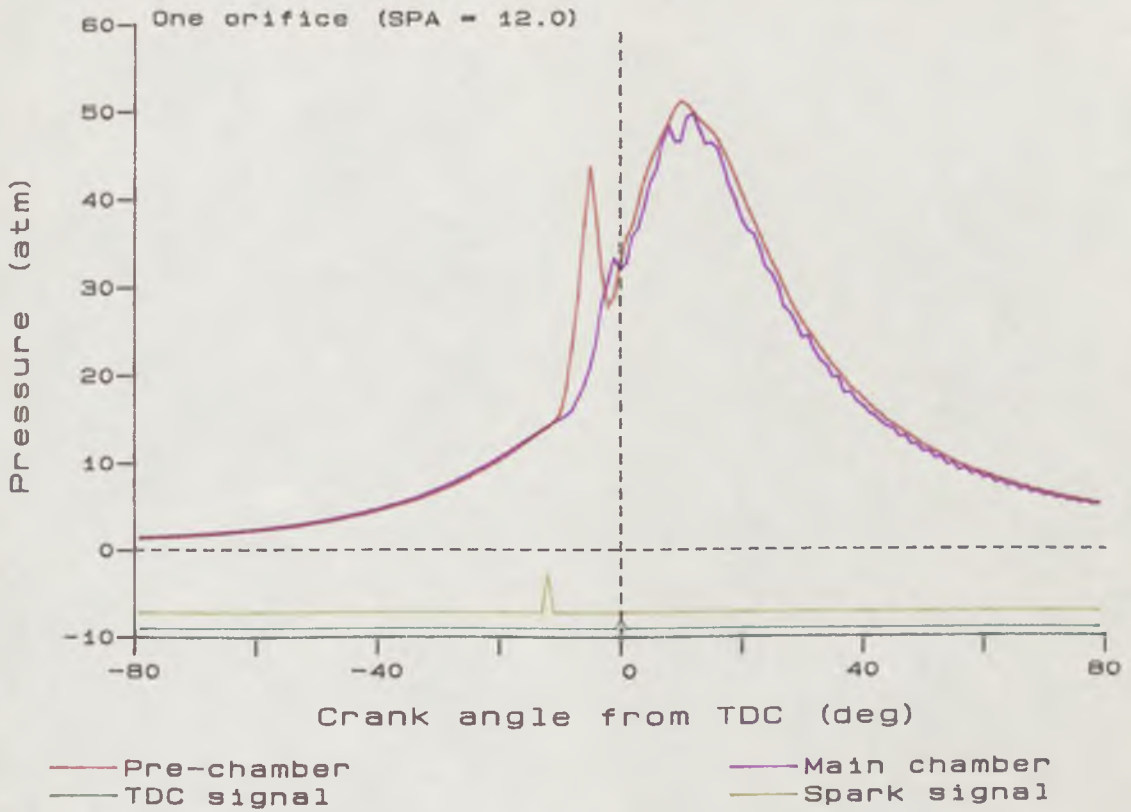


Fig.4.25 Effect of number of orifices on Cylinder pressure

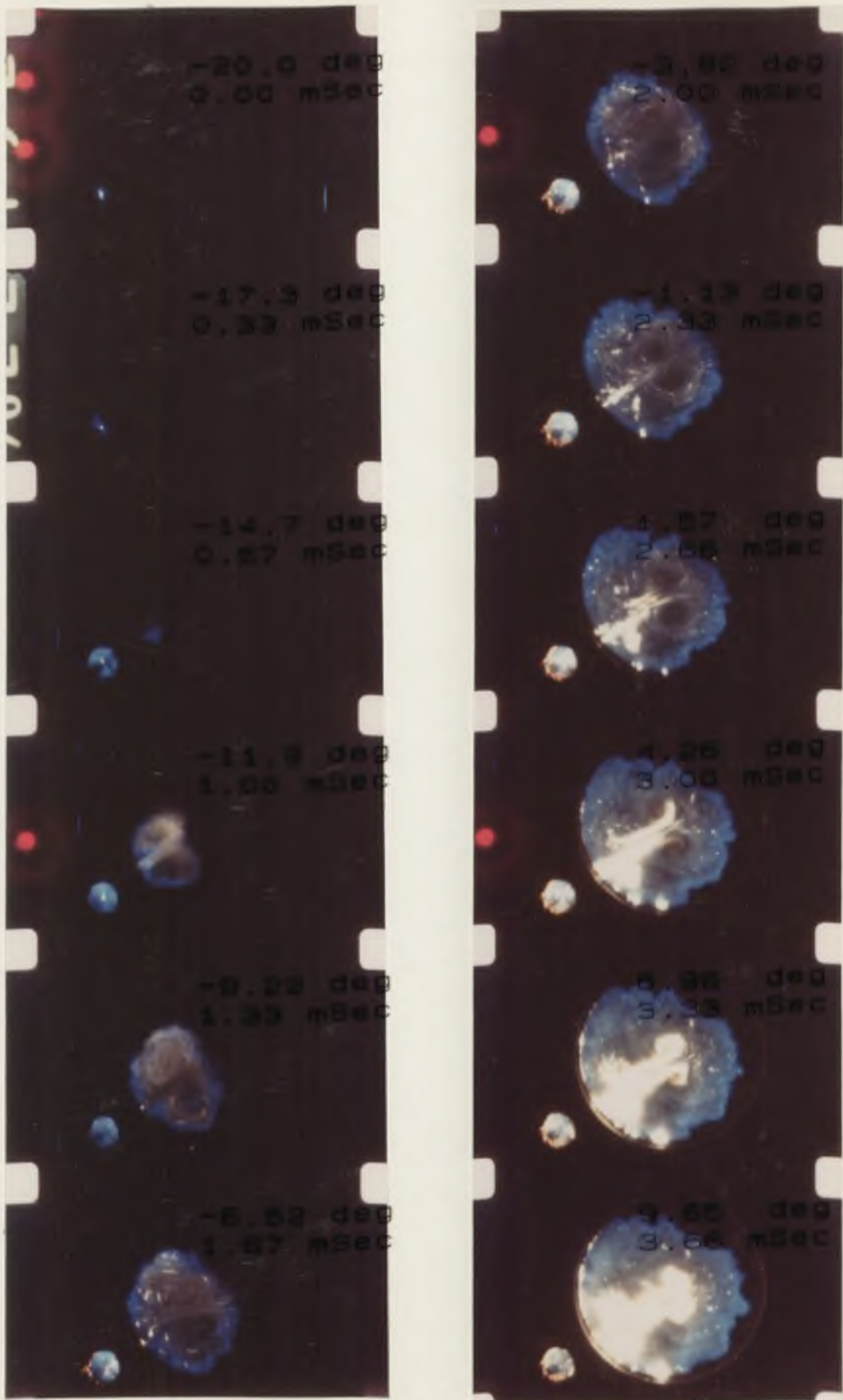


Fig.4.26

Flame propagation photographs
 (VR = 10%, 2 x no.5 Orifices)

-20.0 deg
0.00 mSec

-3.82 deg
2.00 mSec

-17.3 deg
0.33 mSec

-1.13 deg
2.33 mSec

-14.7 deg
0.67 mSec

1.57 deg
2.66 mSec

-11.9 deg
1.00 mSec

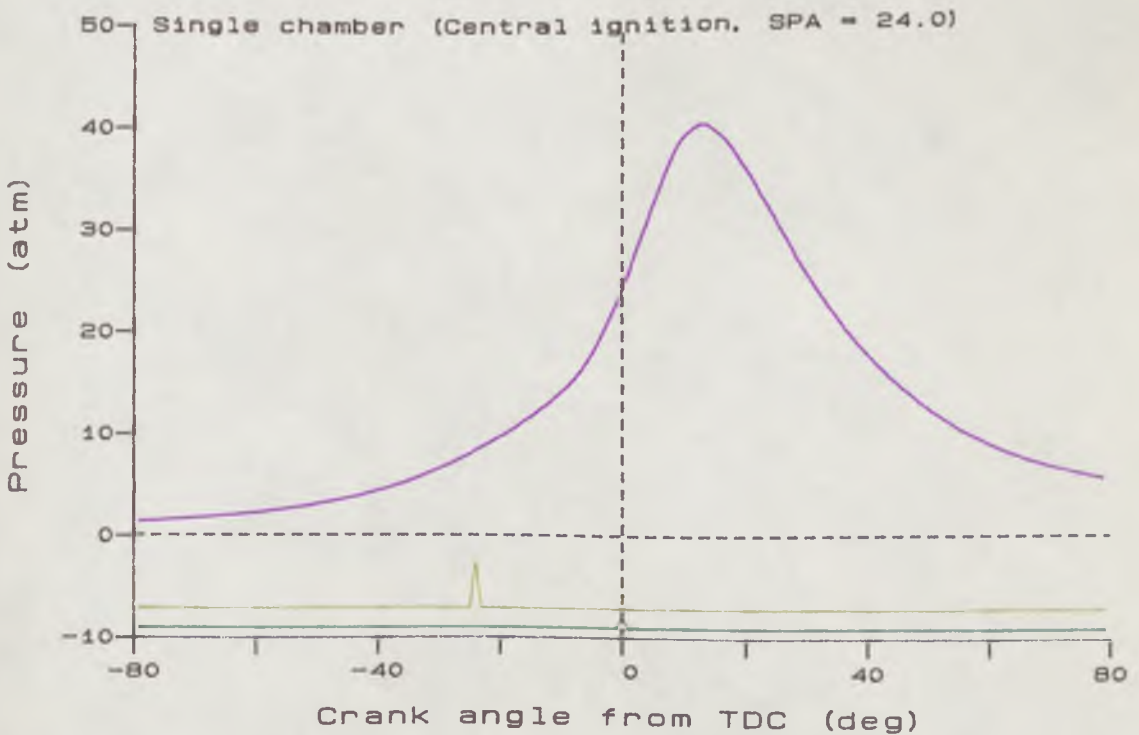
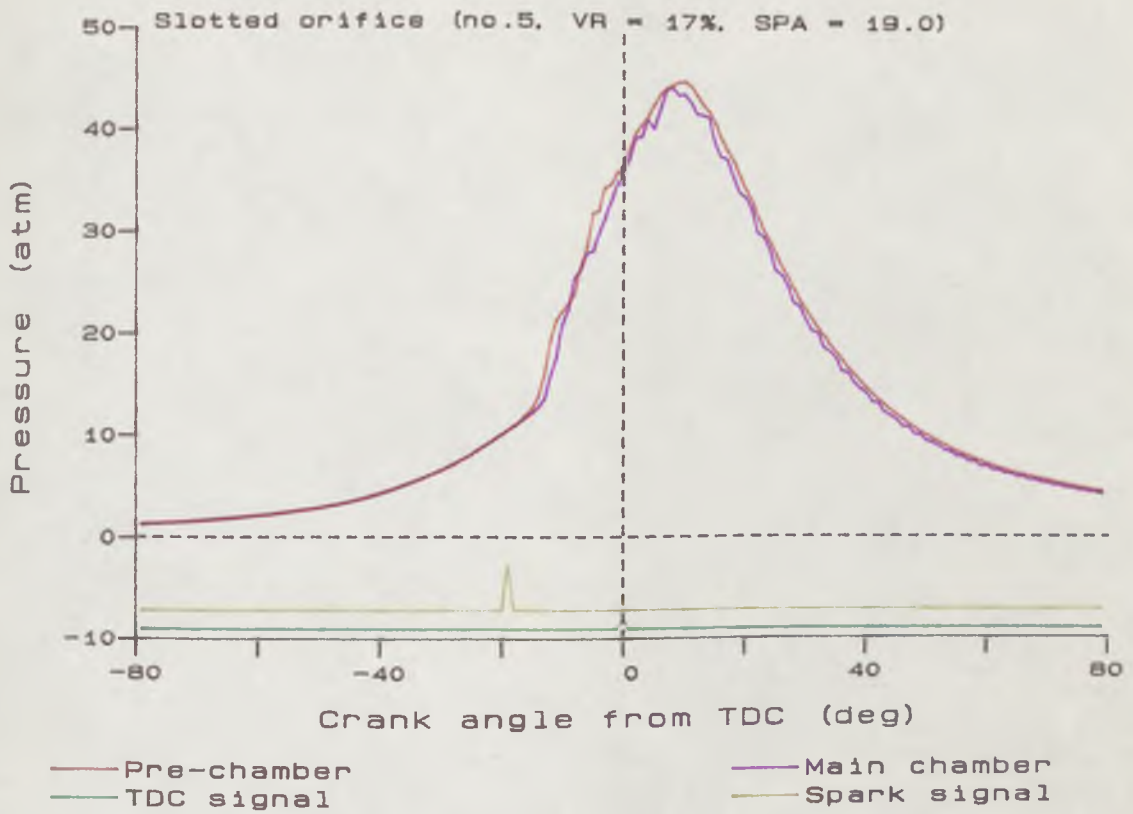
4.26 deg
3.00 mSec

-9.22 deg
1.33 mSec

6.96 deg
3.33 mSec

-6.52 deg
1.67 mSec

9.65 deg
3.66 mSec



ENGINE SPEED = 1400 rpm
EQUIVALENCE RATIO = 1.0
COMPRESSION RATIO = 8.0

Fig.4.27

Cylinder pressure with slotted orifice compared with single chamber.

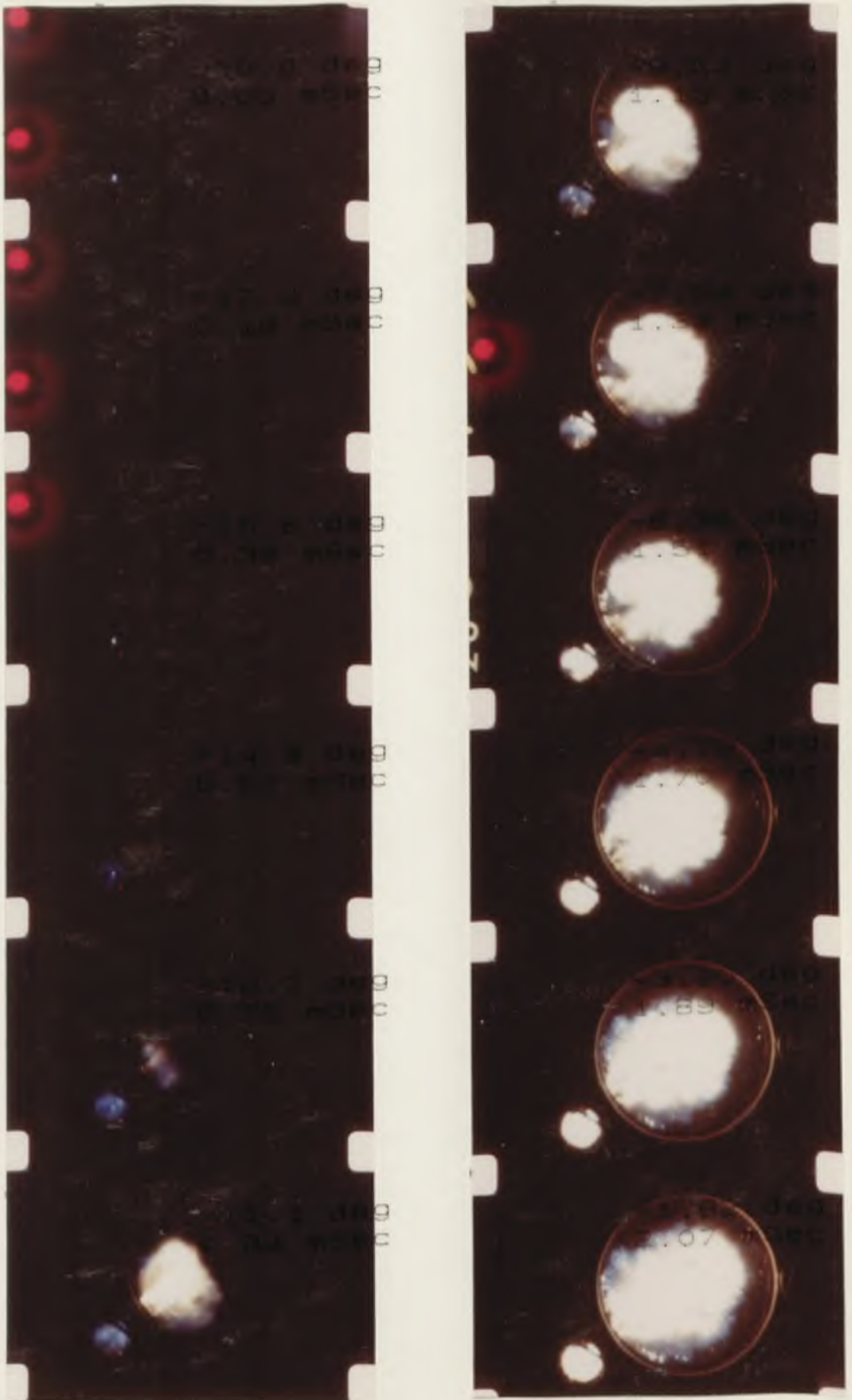


Fig.4.28
Flame propagation photographs
(VR = 17%. 10mm x no.5 slotted orifice)

-19.0 deg
0.00 mSec

-9.52 deg
1.13 mSec

-17.4 deg
0.19 mSec

-7.94 deg
1.32 mSec

-15.8 deg
0.38 mSec

-6.36 deg
1.51 mSec

-14.3 deg
0.57 mSec

-4.79 deg
1.70 mSec

-12.7 deg
0.75 mSec

-3.20 deg
1.89 mSec

-11.1 deg
0.94 mSec

-1.62 deg
2.07 mSec

CHAPTER 5

Single Chamber Computer Model

CONTENTS

5.1	INTRODUCTION	92
5.2	WORKING FLUID AND ITS PROPERTIES	93
5.3	COMPRESSION PROCESS	93
5.4	HEAT TRANSFER	95
5.5	COMBUSTION PROCESS	97
	5.5.1 Instantaneous	97
	5.5.2 Rate Controlled - Empirical	97
5.6	EXPANSION	100
5.7	CALCULATION OF NO AND CO CONCENTRATIONS.	101
5.8	EXHAUST PROCESS.	103
	5.8.1 Exhaust Blowdown	103
	5.8.2 Exhaust Stroke	104
5.9	INTAKE PROCESS	104
5.10	PERFORMANCE CALCULATIONS	105
5.11	RESULTS AND DISCUSSION	106
	5.11.1 Effect of Progressive Combustion	106
	5.11.2 Effect of Heat Transfer	106
	5.11.3 Effect of Nature of Empirical Rate Expression	106
	5.11.4 Effect of Ignition Advance	107
	5.11.5 Effect of Combustion Duration	107
	5.11.6 Effect of Engine Speed	108
	5.11.7 Some Comparisons With Experimental Results	108
5.12	CONCLUSIONS	109

5.1. INTRODUCTION

Early attempts to model the combustion process of internal combustion engines were traditionally based on air-standard cycles. The advent of high speed computers allowed these models to be improved to include a chemical equilibrium composition approximation (see Edson, 1961; Vickland et al, 1962). The development of modelling of engine combustion is reviewed by both Desoky (1981) and Al-Mamar (1983).

At Leeds, Desoky (1981) used equilibrium cycle models, for single and divided chamber engines, to demonstrate the higher thermal efficiencies obtainable by burning leaner mixtures. The models also showed that higher compression ratios could be used to compensate for the lower power output associated with lean burn. These programs were modified by Al-Mamar (1983) so that they would simulate power modulation by throttling at a constant equivalence ratio. However both programs still suffered from the inadequacy of not including a combustion rate; combustion was assumed to occur instantaneously at constant volume when the piston reached the top of its stroke. Al-Mamar did devote a chapter in his thesis to a discussion of possible methods of incorporating a combustion rate into the model, although he made no attempt to so modify his own program.

Reported in this chapter and the next are the efforts of the current author to include expressions for rate of burning into the model. The present chapter is concerned with methods based on empirical expressions for the mass fraction burned at any given time. Outlined in Chapter 6 are subsequent attempts to develop more complex and realistic models which employ the concepts of turbulent burning velocity and turbulent entrainment.

Described below are the changes made to the Desoky/Al-Mamar program to incorporate a combustion rate. These involved modifications to allow variation of spark advance, the addition of heat transfer subroutines, and numerous program improvements and corrections. Routines described in detail by Desoky or Al-Mamar are only outlined here; new routines and major modifications are described in greater detail. The exhaust and intake routines adopted were for a four stroke engine as this configuration was easier to model than a two stroke; two stroke engine modelling requires consideration of flowrates through ports, and scavenging efficiency (see Adachi et al, 1985; Baudequin and Rochelle, 1980). The principal objective of the work reported here was to investigate the effect of turbulence on combustion, therefore detailed modelling of the intake process was not considered. Where comparison with the experimental data for the Yamaha two-stroke engine was required, the modelled pressure at intake was adjusted to agree with experimentally measured values.

5.2. WORKING FLUID AND ITS PROPERTIES

As outlined by Al-Mamar the working fluid was assumed to be composed of either:-

- (i) combustion products in thermochemical equilibrium at the adiabatic flame temperature,
- (ii) combustion products in equilibrium at some other prescribed pressure and temperature, resultant from combustion and piston motion, or
- (iii) a mixture of combustion products of 'frozen' composition and/or fresh reactants.

In the model described here it was possible for there to be two distinct regions in the chamber, one of fresh reactants and one of combustion products, separated by a thin reaction zone (flame front). These regions could be at different temperatures; no heat transfer was allowed between them. However, the pressures in the two regions were assumed to be equal.

The model was programmed for iso-octane or methanol fuels; it could be readily modified for any other hydrocarbon fuel. In later comparisons with experimental data the program was also used to model engine behaviour with regular 97.8 octane rating gasoline. For this exercise unknown fuel properties (e.g. burning velocities, specific heats) were assumed to be similar to those of iso-octane. This was considered justifiable for specific heat capacity and enthalpy etc., as the model required these quantities only for the fuel/air mixtures; since the fuel was only present in relatively small concentrations errors in these fuel properties would have little effect on the values of the properties of the mixture.

Entropy and enthalpy data can be related to specific heat capacity at constant pressure (Prothero, 1969). The specific heat data used in the program were calculated using sixth order polynomials given by Prothero. Such polynomials were not available for the fuels. For methanol a similar polynomial expression was fitted to data from Svehla (1962); for iso-octane a polynomial was generated using data from the American Petroleum Institute (A.P.I., 1983). Viscosities were evaluated using polynomials fitted to the experimental data of Watson (1972); where such data were unavailable, they were calculated theoretically. The procedure for calculating these properties for individual species and mixtures of gases is described in Appendix B.

5.3. COMPRESSION PROCESS

Initially, the cylinder was assumed to contain a general hydrocarbon $C_xH_yO_z$, defined by x,y,z , and air at a given equivalence ratio (ϕ). On subsequent cycles a residual fraction of exhaust gases was also included in the mixture at the start of the compression process.

This mixture was then considered to be isentropically compressed until that crank angle at which combustion was assumed to be initiated (i.e. the spark advance) as shown by process 1-2 in Fig. 5.1. The compression process was considered in a succession of 5 degree crank angle increments, the final increment being shorter if the spark advance was not a multiple of 5 degrees. Increments of 5 degrees were selected as optimum; longer increments gave significantly reduced accuracy, shorter increments involved more computing time.

Pressure and temperature estimates at the end of each increment were initially calculated from isentropic relationships, on the basis of the change in cylinder volume over the crank angle increment (known from geometrical relationships).

$$P_i = P_{i-1} \left[\frac{V_{i-1}}{V_i} \right]^\gamma \quad (5.1)$$

$$T_i' = T_{i-1} \left[\frac{V_{i-1}}{V_i} \right]^{\gamma-1} \quad (5.2)$$

where the cylinder volume ($V(\theta)$) at a given crank angle(θ) is given by:-

$$V(\theta) = V_s \left[\frac{1}{CR-1} + \frac{1}{2} \left[\frac{l}{r} + 1 - \cos(\theta) - \sqrt{\frac{l^2}{r^2} - \sin^2(\theta)} \right] \right] \quad (5.3)$$

and V_s is the total swept cylinder volume

l is the connecting rod length

r is the crank shaft throw

Heat transfer was allowed to occur at the end of each increment. The quantity of heat transferred (Q) was calculated on the basis of the difference in temperature between the gas at the start of the increment and the cylinder wall temperature. The work done during an increment for an isentropic process was found from:-

$$W = U_{i-1} - U_i' \quad (5.4)$$

where U_i' is the internal energy calculated from the isentropic temperature T_i' . The actual temperature at the end of the increment was then found by an iterative process, given the required internal energy:-

$$U_i = U_{i-1} + Q - W \quad (5.5)$$

The procedure adopted was to estimate the temperature and then calculate the internal energy at this temperature and at set increments (10°C) above and below this value. A

quadratic was then fitted to the temperature-internal energy values and solved to provide a revised estimate of temperature. The process was repeated until the internal energies agreed within a set accuracy (0.05%). The pressure was then calculated from the ideal gas law.

5.4. HEAT TRANSFER

Those engine cycle models that incorporate heat transfer between the cylinder and working fluid, usually use heat transfer expressions based on the work of Annand (1963) or Woschni (1967). On the basis of their experiments these workers showed that heat transfer is mainly by forced convection and obeys the law:-

$$Nu \propto Re^n \quad (5.6)$$

Annand suggested a value of 0.7 for n ; he also included the effect of radiation into his heat transfer expression. He defined the overall heat transfer rate as:-

$$\dot{Q} = \frac{a\kappa(Re)^{0.7}}{B} \times [T_g - T_w] + C [T_g^4 - T_w^4] \quad (5.7)$$

where a was in the range 0.35 to 0.8, increasing with increasing charge motion in the cylinder. The constant C had the value zero during compression and 2.1×10^{-13} during combustion and expansion in spark ignition engines. The mean piston speed was taken as the characteristic velocity in the calculation of Reynolds number.

Woschni considered the effect of radiative heat transfer to be negligible, and suggested a value of 0.8 for the exponent n :-

$$Nu = 0.035 Re^{0.8} \quad (5.8)$$

He also took the characteristic velocity proportional to mean piston speed, and for the combustion and expansion phases he included an additional term to allow for combustion induced gas motion. Hassan (1970) conducted experiments with a motored engine and generated an equation similar to Woschni's; however his constant of proportionality was in the range 0.0276 - 0.0184. Later work by Annand (1971,1980) included an additional term to account for the phase lag between heat transfer rates and driving temperature difference caused by boundary layer effects.

Borgnakke et al (1980) were the first to develop a theory for the heat transfer across an unsteady boundary layer in an engine cylinder. In later work (Davis and Borgnakke, 1982; Borgnakke, 1984) it was shown that this theory could be considerably simplified, for a sufficiently thick boundary layer, giving:-

$$\dot{Q} = \dot{q}_b A_b + \dot{q}_u A_u \quad (5.9)$$

where the heat transfer rates per unit area in the burned and unburned zones are:-

$$\dot{q}_u = C \frac{\kappa_{l_u}}{B} \text{Re}_u^n (T_u - T_w) \quad (5.10)$$

$$\dot{q}_b = C \frac{\kappa_{l_b}}{B} \text{Re}_b^n (T_b - T_w) \quad (5.11)$$

The characteristic velocity used in calculation of the Reynolds number was similar to that of Woschni:

$$\text{Re} = \frac{(S_p + S_e) B}{\nu} \quad (5.12)$$

where the expansion velocity (S_e) was related to the motoring pressure (P_{mot}) by:-

$$S_e = 3.24 \times 10^{-3} \left[\frac{V T_{in}}{V_{in}} \right] \left[\frac{P - P_{mot}}{P_{in}} \right] \quad (5.13)$$

with the assumption of ideal gas behaviour, this reduced to:-

$$S_e = 3.24 \times 10^{-3} \left[\frac{V}{n_r R} \right] (P - P_{mot}) \quad (5.14)$$

(where V is the instantaneous cylinder volume and n_r is the number of moles of reactant in the cylinder, prior to combustion).

Actual heat transfer rates are affected by charge motion, chamber shape and spark plug position (Heywood, 1984). Therefore the constants in such equations for any particular engine really need to be determined by comparing model and experimental results for the engine in question (or one of very similar geometry).

An estimate of the surface temperatures was also required. Alkidas (1982) and Yoshida et al (1982) have investigated the effect of varying engine operating parameters on local surface temperatures (piston crown, cylinder wall and cylinder head) and heat fluxes. They showed that equivalence ratios and spark advance had only small effects on local surface temperature, whereas engine speed and volumetric efficiency had significantly large effects. Alkidas showed the cylinder wall temperature to be much less sensitive (than the piston crown and cylinder head), to the factors discussed above; they reasoned that the walls were in contact with the hot gases for rather less time and that cooling was more efficient in this region.

In the computations reported in this thesis (using equations 5.9 - 5.14) the cylinder wall temperature at all operating conditions was taken to be 470K for that part of the wall exposed at TDC, decreasing linearly to 303K at BDC. The cylinder head and piston crown

were assumed to be 370K and 470K respectively at standstill, and to increase by 40K per 1000 rpm engine speed. These values were typical of those given in the above papers and those of Ricardo and Hempson (1968) and Benson and Whitehouse (1979).

5.5. COMBUSTION PROCESS

5.5.1. Instantaneous

In the instantaneous combustion version of the program, the compression process was followed by an instantaneous and adiabatic constant volume combustion process at T.D.C. (Process 2'-3' in Fig. 5.1). Following combustion the products were assumed to comprise ten species (CO, CO₂, O₂, H₂, H₂O, OH, H, O, NO, N₂) in chemical equilibrium at the adiabatic flame temperature. The mole fractions of these products were calculated from atom balance and chemical equilibria equations as described by Al-Mamar (1983). The adiabatic flame temperature was calculated by successive approximation for equivalence of internal energy for the reactants and products, system pressure being determined on the assumption of ideal gas behaviour.

5.5.2. Rate Controlled - Empirical

In practice the rate of burning, which varies with time, will be a function of the rate at which unburned mixture is engulfed by the flame and the rate at which it subsequently burns. These rates will be complex functions of turbulence, chemical reaction rate and cylinder geometry. The modelling of these complex processes is considered in more detail in Chapter 6. However in an attempt to assess the effects of progressive combustion and burn rate (and to provide a means of calculating mass fraction burned from experimental engine data), the program was initially modified to incorporate an empirical burning rate expression along the lines suggested by a number of previous workers (Tabaczynski and Klomp, 1974; Hires et al, 1976; Wall et al, 1978). These empirical burning rate expressions describe the mass fraction of mixture burned at any given crank angle ($n(\theta)$) as a function of time (or crank angle) elapsed since ignition and the total combustion duration (usually expressed in terms of crank angle $\Delta\theta_b$). In such empirical burning rate expressions the overall rate of combustion can be varied by changing the (assumed) combustion duration; the variation in burning rate during the combustion period being described by (somewhat arbitrary) mathematical functions. The simplest such function is a linear one, as described by Eqn. 5.15, Fig. 5.2. This merely states that the proportion of mixture burned is directly proportional to fraction of total combustion duration elapsed.

$$n(\theta) = \frac{(\theta - \theta_i)}{\Delta\theta_b} \quad (5.15)$$

However, combustion photographs show that flame propagation starts off slowly, increases and then slows down as the process nears completion. This variation is better described by other functions such as the cosine law (Eqn. 5.16, Fig. 5.2) and the Weibe function (Eqn. 5.17, Fig. 5.2).

$$n(\theta) = \frac{1}{2} \left[1 - \cos \left[\pi \left[\frac{\theta - \theta_i}{\Delta\theta_b} \right] \right] \right] \quad (5.16)$$

$$n(\theta) = 1 - \exp \left[-A \left[\frac{\theta - \theta_i}{\Delta\theta_b} \right]^{M+1} \right] \quad (5.17)$$

The Weibe function is the most versatile method as the constants (A and M) can be chosen to give different mass burning rates. (Fig. 5.2 shows the Weibe function with $A=5$, $M=1$ (WB51), and $A=5$, $M=3$ (WB53)).

In the model the burned and unburned gases at any instant in time (crank angle θ), the proportions of which being calculated from one of the burning rate expressions, were considered to exist in two discrete zones separated by an infinitely thin flame (Fig. 5.3). After a given time interval the flame front was assumed to have moved forward (Fig. 5.4), and the new mass entrained and burnt considered to be at equilibrium at the adiabatic flame temperature and pressure. This zone of newly burnt charge was then allowed to expand and compress the unburnt and 'old' burnt charge; the flame front hence moved forward because of the compression of the unburnt gas. The flame growth was assumed to be spherical for the heat transfer calculation.

Calculation Procedure

In the program the combustion process was considered in two degree increments (chosen as an optimum for computer time and accuracy). During each increment the charge was first compressed by piston motion until the crank angle at the end of the increment was reached. This process was initially considered to be isentropic, so:-

$$P_i = P_{i-1} \left[\frac{V_{i-1}}{V_i} \right]^\gamma \quad (5.18)$$

and for the unburnt region, since $PV=nRT$

$$T_i = T_{i-1} \left[\frac{V_{i-1}}{V_i} \right]^{\gamma-1} \quad (5.19)$$

However this relationship was not true for the burnt region as it was assumed to be in chemical equilibrium. The equilibrium composition of the charge was of course temperature dependent, hence the number of moles of burnt charge changed. In order to find the

temperature of the burnt charge an iterative procedure was employed; the entropy of the charge was calculated at two different temperatures and interpolation-extrapolation used to find the temperature at which the entropy change during the process was negligible. The two regions could now be at different pressures due to the differing values of the index of compression (γ). To equalise pressures, the higher pressure (burnt) region was allowed to expand to an average pressure:-

$$P_{av} = \frac{n_b P_b + n_u P_u}{n_b + n_u} \quad (5.20)$$

where n_u and n_b represent the number of moles of charge present in the unburnt and burnt regions respectively. The volume and temperature of the burned zone were calculated from isentropic assumptions and its equilibrium composition re-calculated. The volume of the unburnt region was found by subtraction of the burnt volume from the total cylinder volume. This volume was used to calculate the temperature and pressure; the pressure was compared with that of the burnt region and, if the two did not agree within a set accuracy (0.05%), then the process was repeated.

Combustion of a small increment of fuel was then allowed to occur; the mass of fuel was calculated from the empirical law described above. This process was considered to be instantaneous and at constant volume. After completion of combustion there were considered to be three regions present; the unburnt and 'old' burnt regions at the same pressure but different temperatures, and a newly burnt region at the adiabatic temperature and pressure. Pressure equalisation was then considered to occur; this was computed exactly as described earlier, except for the complication of the third region.

The two burnt regions were then allowed to mix. This process was assumed to occur at constant internal energy since no work is done. The internal energy of the two separate regions was calculated, the temperature of the resultant mixture estimated, and its composition and internal energy calculated. The latter should have remained constant:-

$$\text{i.e. } (n_1 + n_2)U_3 = n_1U_1 + n_2U_2 \quad (5.21)$$

where U is the internal energy per mole and n is the number of moles. If this relation was not satisfied within a set accuracy (0.05%) then the composition and internal energy were re-calculated at set increments (10°C) above and below. A quadratic equation was fitted to the temperature-internal energy values and solved to give a new estimate of temperature. The process was repeated until agreement was reached; in practice convergence was fast. The pressure of the mixture was calculated from the ideal gas law (assuming the volume had remained constant); if it was different from the unburnt pressure then equalisation of the two regions was permitted to occur on the same basis as before.

At this stage in the procedure there were two regions of charge present, burnt and unburnt. Heat transfer was then considered. As with the compression process, the calculation of the heat flux out of the cylinder was based on the temperature of each region at the start of the increment. This heat flux would cause a reduction in temperature of both regions, and a possible change in volume of each region as heat loss from the burnt region could be greater. The surface area of cylinder wall in contact with each region was calculated (Appendix D). As with the compression process the energy equation could be applied to each region separately. The burnt region would have done work by expanding, whereas the unburnt region would have had work done on it by the burnt gas and possibly by piston motion. The temperature of each region was calculated by iteration; then their respective volumes were calculated, assuming the pressure remained constant. If the sum of the volumes of each region did not equal the total cylinder volume (V_c), then the pressure must have changed; the new pressure could be calculated from the ratio of cylinder volume to the sum of volumes of each region.

$$\text{i.e. } P_i = P_{i-1} \frac{(V_u + V_b)}{V_i} \quad (5.22)$$

NO and CO concentrations were then calculated in the burnt region (described later), and the entire combustion process was repeated until all the fuel was burnt.

5.6. EXPANSION

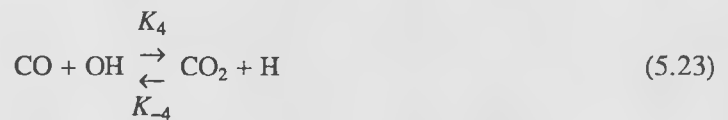
The expansion process (which was considered to start when all the charge was burnt) was treated in a manner similar to that for the compression process. Five degree crank angle increments were adopted (the first being shorter if necessary). The process was considered to start at the end of combustion, this being dependent on spark advance and combustion duration (3-4, Fig.5.1). It was possible for combustion to be completed before the piston reached the top of its stroke, in which case some compression also had to be considered during this procedure.

Changes in the thermodynamic state of the gas were initially assumed to be isentropic. Since the charge was assumed to be in thermochemical equilibrium, the temperature and composition again had to be calculated by an iterative method. This involved calculation of the entropy at three temperatures and fitting a quadratic to give a better estimate of temperature. At the end of each iteration, heat transfer and the 'kinetic' concentration of the pollutants (as described below) were calculated.

5.7. CALCULATION OF NO AND CO CONCENTRATIONS.

Experimental measurements of CO and NO concentrations in the exhaust of engines have been shown to be considerably larger than computed equilibrium values. This is due to there being insufficient time for the chemical reaction to be completed before the temperature falls to a value too low to sustain it; the reactants are therefore 'frozen' at non-equilibrium concentrations.

CO is formed predominately by fast reactions early in the combustion process and then oxidised to CO₂ by the reaction:-



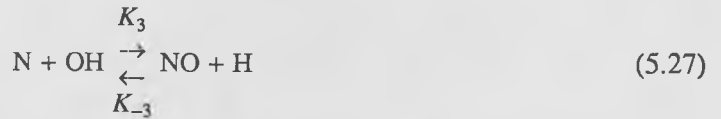
The rate of oxidation of CO is therefore given by:-

$$-\frac{d[\text{CO}]}{dt} = K_4[\text{CO}][\text{OH}] - K_{-4}[\text{CO}_2][\text{H}] \quad (5.24)$$

In the model all the carbon present in the products when the mixture first burns was assumed to be in the form of CO (i.e. CO concentration was taken as the sum of the equilibrium values of CO & CO₂ produced by the instantaneous combustion routine, while the initial concentration of CO₂ was taken as zero). The OH and H species concentration were taken to be the equilibrium values at the given temperature and pressure. On these premises, the 'kinetic' concentrations of CO and CO₂ could therefore be found by integration, following Al-Mamar (1983).

The 'non-equilibrium' concentrations of CO and CO₂ were calculated during the expansion process (as reported by Desoky); they were also computed for the burnt gas region during combustion. Since combustion was assumed to occur at the end of each increment, in the rate controlled combustion routines the quantity of CO oxidised during each increment was based on the CO and CO₂ concentrations at the start of the increment; any equilibrium CO and CO₂ formed during the instantaneous combustion routine was then added to the kinetic concentration of CO. A crank angle increment of 1 crank degree was employed for all 'kinetic' calculations, the final values were converted to (gm/Ikwh) as described by Al-Mamar (1983).

It is generally accepted that NO formation is governed by the extended Zeldovich mechanism:-



This gives an overall rate of production of NO:-

$$\frac{d[\text{NO}]}{dt} = \left[K_1[\text{O}][\text{N}_2] - K_{-1}[\text{NO}][\text{N}] + K_2[\text{N}][\text{O}_2] - K_{-2}[\text{NO}][\text{O}] + K_3[\text{N}][\text{OH}] - K_{-3}[\text{NO}][\text{H}] \right] \text{ cc/gmole-sec} \quad (5.28)$$

In the current program the species [O], [H], [OH], [O₂], [N₂] were assumed to be at their equilibrium levels, and the concentration of [N] was found by invoking the steady state assumption (Westenberg, 1971):-

$$[\text{N}]_{\text{ss}} = \frac{K_1[\text{O}][\text{N}_2] + K_{-2}[\text{NO}][\text{O}] + K_{-3}[\text{NO}][\text{H}]}{K_{-1}[\text{NO}] + K_2[\text{O}_2] + K_3[\text{OH}]} \quad (5.29)$$

The kinetic NO concentration could be found by combining the above equations and solving by integration (Al-Mamar, 1983). The initial concentration of [NO] was taken to be zero and subsequent concentrations were calculated at 1 degree crank angle increments throughout the combustion and expansion phases. The calculation procedure used was similar to that for the calculation of 'kinetic' CO; the final exhaust concentration was again converted to (gm/lkwh).

A simplified method for NO calculation, employing only the first two reactions for the Zeldovich scheme, was also tried.

This gives:-

$$\frac{d[\text{NO}]}{dt} = \left[K_1[\text{O}][\text{N}_2] - K_{-1}[\text{NO}][\text{N}] + K_2[\text{N}][\text{O}_2] - K_{-2}[\text{NO}][\text{O}] \right] \quad (5.30)$$

$$[N]_{sr} = \frac{K_1[O][N_2] + K_{-2}[NO][O]}{K_{-1}[NO] + K_2[O_2]} \quad (5.31)$$

This method gave considerably different results with little saving in computer time. Since this method was considered to be the more unreliable of the two, its use was discontinued.

5.8. EXHAUST PROCESS.

A very simplified treatment of both the exhaust and intake processes was considered; the model was principally concerned with the combustion process and a detailed analysis of the exhaust and intake processes was therefore considered inappropriate.

The process was assumed to be irreversible, and to occur in two stages. Initially the exhaust valve was considered to open, and the cylinder pressure fall to that of the exhaust (4-5, Fig. 5.1); this was termed the exhaust blowdown period. The pressure difference across the valve was assumed to fall to zero while the cylinder volume remained constant. Then the piston was considered to travel upwards, displacing exhaust gases from the cylinder; this was termed the exhaust stroke. During this period heat transfer was allowed to occur as the process was not instantaneous. When the piston reached the top of its stroke the exhaust valve was allowed to close and the inlet valve open. If the pressure in the inlet manifold was less than atmospheric then some of the residual gases would enter the manifold (6-7, Fig. 5.1). These residual gases were assumed to re-enter the cylinder at the start of the intake stroke, prior to entry of fresh charge.

The intake manifold was assumed to have an infinitely large area; pressure was not increased when the inlet valve opened. No valve overlap was allowed to occur, as mass flowrates through the valves would then have to be considered. Exhaust valve closing and inlet valve opening were assumed to occur at TDC.

5.8.1. Exhaust Blowdown

This was considered in two stages; firstly, isentropic expansion to an intermediate pressure ($\sqrt{P_4}$) occurred. This pushed some charge out of the cylinder and resulted in a change in composition. Secondly, a further expansion to atmospheric pressure took place, again resulting in a change in composition; this necessitated an iterative procedure to calculate the temperature. The gas remaining in the cylinder was considered to have undergone the process 4-4' (Fig. 5.1), ending at state 5 due to the reduction in mass of charge present.

The residual mass fraction at this point was calculated from the gas properties:-

$$RF = \frac{m_5}{m_4} = \frac{\rho_5}{\rho_4} \quad (5.32)$$

5.8.2. Exhaust Stroke

The piston was then allowed to travel up the cylinder, pushing out most of the charge at a constant pressure of one atmosphere. This process was considered in 5 degree increments; at the end of each increment the mass remaining in the cylinder was calculated from the change in volume:-

$$m_i = m_{i-1} \left[\frac{V_i}{V_{i-1}} \right] \quad (5.33)$$

The heat flux out of the cylinder during this period was calculated from the temperature at the start of the increment. If there were no heat transfer from the system the temperature and volume of the charge remaining in the chamber would not change, therefore no work would be done on this remaining charge (although pumping work would be done by the engine to produce the change in mass in the cylinder). The energy equation reduced to:-

$$h_2 = Q(T_1) + h_1 \quad (5.34)$$

The temperature of the charge having this enthalpy was calculated iteratively. The heat transfer process resulted in a fall in temperature, and therefore an increase in density of the charge; consequently the mass remaining in the chamber was slightly greater than that assumed by isentropy (and was calculated from the density).

The inlet valve was then considered to open, and the pressure allowed to fall to the intake manifold pressure. This was again assumed to occur instantaneously and (therefore) isentropically. Any reactions occurring in the residual fraction were assumed to be instantly frozen prior to the intake stroke.

5.9. INTAKE PROCESS

As with the exhaust stroke, this process was considered in five degree crank angle increments. The pressure during the process was assumed to remain constant, and to be equal to the manifold pressure. The fresh charge was assumed to be at 30°C unless the engine had exhaust gas recirculation, in which case the temperature was calculated by assuming the enthalpy had remained constant during the mixing process:-

$$\text{i.e. } h_{in} = (1-MF_{egr}) h_{in} + MF_{egr} h_{egr} \quad (5.35)$$

where MF_{egr} is the mole fraction of recirculated charge and h_{egr} is its enthalpy.

At the end of the increment the heat transfer from the residual fraction was calculated on the basis of the cylinder wall area at the start of the increment. The temperature of the residual fraction was then found by an iterative procedure similar to that for the exhaust stroke. The fresh charge and residual fraction were then considered to mix. The temperature

of this mixture could only be found by an iterative method; the enthalpy was assumed to remain constant during the mixing process. First the temperature was estimated, and the volume of the residual charge calculated at this temperature. The volume and mass of fresh charge were then calculated, and the enthalpy of the mixture calculated at this temperature and at equal increments above and below it. A quadratic was fitted to these values to give a new approximation for the temperature where the mixture enthalpy (h_m) was equal to the sum of enthalpies of fresh charge (h_{in}), and the products (h_f):-

$$(n_f + n_{in})h_m = n_f h_f + n_{in} h_{in} \quad (5.36)$$

This process was repeated until enthalpies agreed within a set accuracy (0.05%).

The next increment was then considered. When the piston reached the crank angle of inlet valve closing, any further charge entrained (as the piston moved down to BDC) and pushed out again (as it moved back up to the crank angle at which the inlet valve closed) was assumed not to mix with the other charge. Heat transfer during this period would result in a decrease in density of the mixed charge, hence some of this charge would also be pushed out of the cylinder.

The whole calculation procedure was then repeated (starting with the compression stroke) for the revised conditions at position 1 (Fig. 5.1) until property values on successive cycles were approximately the same. When deriving data for comparison with that generated using the Yamaha engine, the cycle of computations was only carried out once (in experiments the Yamaha was only fired every fourth cycle; the residual fraction present was therefore considered negligible).

5.10. PERFORMANCE CALCULATIONS

The net work done during the cycle could be found by applying the second law of thermodynamics (assuming internal reversibility):-

$$W_{net} = \int_1^4 P dV - W_{loop} \quad (5.37)$$

where W_{loop} is the work done during the exhaust and intake strokes

The indicated mean effective pressure is defined as:-

$$I.M.E.P. = \frac{\int_1^4 P dV}{V_{sw}} \quad (5.38)$$

As this quantity was also calculated from the P - θ data collected in the experimental work it was useful to output its value from the theoretical program for comparative purposes.

However, in deriving this quantity no account is taken of work done during the exhaust and intake strokes, and hence a net mean effective pressure was also calculated, where:-

$$(MEP)_{net} = \frac{W_{net}}{V_{sw}} \quad (5.39)$$

The thermal efficiency and specific fuel consumption were also calculated. These are defined as:-

$$\eta_{th} = \frac{W_{net}}{LCV \times MF_{(fuel)} \times MW_{(fuel)}} \quad (5.40)$$

$$I.S.F.C. = \frac{MF_{(fuel)} \times MW_{(fuel)} \times 1000 \times 3600}{W_{net}} \quad gm/kWhr \quad (5.41)$$

5.11. RESULTS AND DISCUSSION

5.11.1. Effect of Progressive Combustion

Shown in Fig. 5.5 are the pressure and temperature diagrams for instantaneous combustion, and also for an empirical method (cosine law with 60 degrees combustion duration and 30 degrees spark advance). The progressive nature of the empirical method produces a gradual rise in pressure; this leads to a much lower peak pressure and temperature, and will therefore have a considerable effect on model predictions of power output and emissions of pollutants. The pressure history predicted by the empirical method is much closer to that found experimentally in a real engine. To assume that combustion is instantaneous is clearly invalid.

5.11.2. Effect of Heat Transfer

The effect of heat transfer on model predictions is demonstrated in Fig. 5.6. Heat losses have little effect during compression as the driving temperature difference between gas and cylinder wall is relatively low. During combustion and expansion the heat loss from the cylinder charge has little effect on cylinder pressure but an increasingly large effect on the charge temperature. At the end of expansion the temperature of the charge, when heat transfer is included, is considerably lower than that predicted by an adiabatic model. Model predictions without heat transfer are therefore unlikely to give accurate predictions of pollutant concentrations, although (since pressure is less affected) power output should be relatively insensitive to heat transfer.

5.11.3. Effect of Nature of Empirical Rate Expression

The disadvantage of the empirical rate method is that it needs a combustion duration to be specified. Without some knowledge of how the combustion duration varies, this method is

not very useful for studying effects where the variation in combustion duration is large (such as changes in equivalence ratio). Experimental results show that engine speed and spark advance have little effect on combustion duration (in crank angle degrees), and so the effects of varying these can be studied qualitatively without an accurate knowledge of the combustion duration. The method can also be used to study the importance of combustion duration on performance.

Shown in Fig. 5.7 is the mass fraction burned against crank angle for a number of different empirical burning rate expressions, for the same spark advance (30 degrees BTDC) and combustion duration (60 degrees). The Weibe function expressions are identified by the values of A and M in the governing equation, Eqn. 5.17. The pressure-crank angle diagrams are also shown; these are considerably different. The rate at which mass is consumed by the flame front, and the timing of maximum heat release greatly affect the power output. Clearly, by adopting appropriate values of A and M in the Weibe function it would be possible to generate a pressure diagram close to any particular engine experiment; these same values would not necessarily give a universally good fit to other engine experiments. In all subsequent computations the cosine rate was used; this method is that most widely used in the literature by exponents of the empirical expressions.

5.11.4. Effect of Ignition Advance

Shown in Figs. 5.8 & 5.9 is the effect of varying spark advance on output and emissions for fixed engine conditions and an assumed combustion duration of 60° crank angle. The I.M.E.P. is maximum with 30 degrees of spark advance; the maximum pressure at this condition is 44 atmospheres and occurs at twelve degrees after TDC. This is in accord with results obtained experimentally in the Ruston engine. As the spark timing is retarded the peak pressure and NO emissions are reduced, while CO emissions increase. The late spark timing results in there being less time spent at the high temperatures necessary for NO formation and CO burn up.

5.11.5. Effect of Combustion Duration

Shown in Figs. 5.10 - 5.12 is the effect that combustion duration has on performance and emissions for a stoichiometric mixture, for a set spark advance of 30° crank angle. As the combustion duration is increased, the rate of pressure rise decreases - as mass is being consumed at a slower rate. As a consequence of this, the mean effective pressure reaches a maximum when the combustion duration is approximately 55 degrees (Campbell (1979) gives 60 degrees for this value, however the curve shows that there is little difference in the IMEP in the range 50 - 60 degrees). The shortest combustion duration gives a longer

period when the temperature is high enough for NO and CO reactions to occur; CO emissions are therefore lower, while NO are higher. When combustion is slow, the peak pressure and temperature are lower; hence the NO formation, and CO burn up, reactions are slower. Emissions of NO are therefore low, while CO emissions are high. The ideal combustion duration will be a compromise between the emissions of these pollutants.

The output values presented above are functions not only of combustion duration, but also of timing of the combustion event. A further series of computations were performed, for each of the combustion durations, in order to determine the optimum spark advance. In each case, at the optimum advance, 50% of the charge was burnt at 2-3 degrees after TDC (Fig. 5.13). The IMEP at optimum ignition advance is almost constant; it decreases slightly as the combustion duration is increased, as there is more time for heat loss to occur. The concentration of pollutant emissions follow similar trends to those at a fixed spark advance, however, the variation is considerably reduced.

5.11.6. Effect of Engine Speed

The predicted effects of engine speed on engine performance and emissions are presented in Figs. 5.14 and 5.15. Engine speed has very little effect on computed pressures and temperatures (with the volumetric efficiency assumed constant). The predicted equilibrium concentrations of NO and CO are therefore almost identical. The kinetic concentrations of these pollutants are not only dependent on temperature, but also on the time available for reactions to occur. Concentrations of CO are higher than the equilibrium values, and increase with engine speed; this is due to less time being available for oxidation to occur before the temperature falls to a level too low to support chemical reactions. The same argument can be used to explain the reduction in emissions of NO as the engine speed is increased.

5.11.7. Some Comparisons With Experimental Results

Finally, a set of calculations were performed for each of the different expressions for representing combustion rate, at equivalence ratios of 0.8 and 1.1. The combustion duration was varied until the peak pressure, predicted by the model, agreed with those obtained in an experimental cycle for the Ruston engine (as described in Chapter 4). The experimental cycles chosen were from tests where a film of the combustion process had been taken. The flame area had been traced from the film, and the flame radii at each frame had been calculated for a circle having the same projected area. In the model tests, at both equivalence ratios, the crank angle at which peak pressure occurred was only predicted correctly by the Weibe function with both constants equal to 3 (WB33). This relation is obviously the only one that correctly predicted the mass burning rate. When the flame radii

predicted by the model (assuming spherical flame growth and that all charge behind the flame front is burnt) are compared with the experimental measurements (Fig. 5.16), there are considerable discrepancies. These are worse for the weaker mixture. The flame position predicted is too far advanced across the chamber; this implies that the combustion process cannot be complete behind the flame front.

5.12. CONCLUSIONS

The tests conducted with the model show the importance of a progressive combustion model, and the need for heat transfer calculations, in modelling spark ignition engine combustion. Simple equilibrium cycle models, and models which do not incorporate heat transfer, cannot predict the cylinder pressure and temperature with any degree of accuracy. These types of models, therefore, have little chance of predicting pollutant emissions and performance, although they may be useful for giving some insight into engine behaviour.

The use of an empirical mathematical equation is not, however, a good method. This is because:

- (a) A combustion duration needs to be specified, and this can only really be found from experimental tests, and
- (b) It must be remembered that the purpose of a mathematical model is to evaluate the performance of new engine designs, without the expense of building and testing the various possible alternatives.

An ideal model must be able to predict the effect of changes in cylinder geometry. In the model tests performed here, the Weibe function with a specific set of constants (WB33) gave mass burning rates similar to one particular set of experimental results. However, the chamber used was a flat disc shaped chamber, and side ignition was employed. In an engine with a more compact chamber geometry, employing central ignition, the mass burning rate is unlikely to be similar. Different constants in the empirical formula would probably be necessary. To model changes in cylinder geometry, it is necessary to be able to predict the flame position at any given time, and also the mass fraction burnt behind the flame front at that instant. This is beyond the capabilities of a model which uses empirical mathematical formulae to describe the mass burning rate. A more complex description of the combustion process is therefore required; a model which allows for some unburnt charge behind the flame front is described in the following chapter.

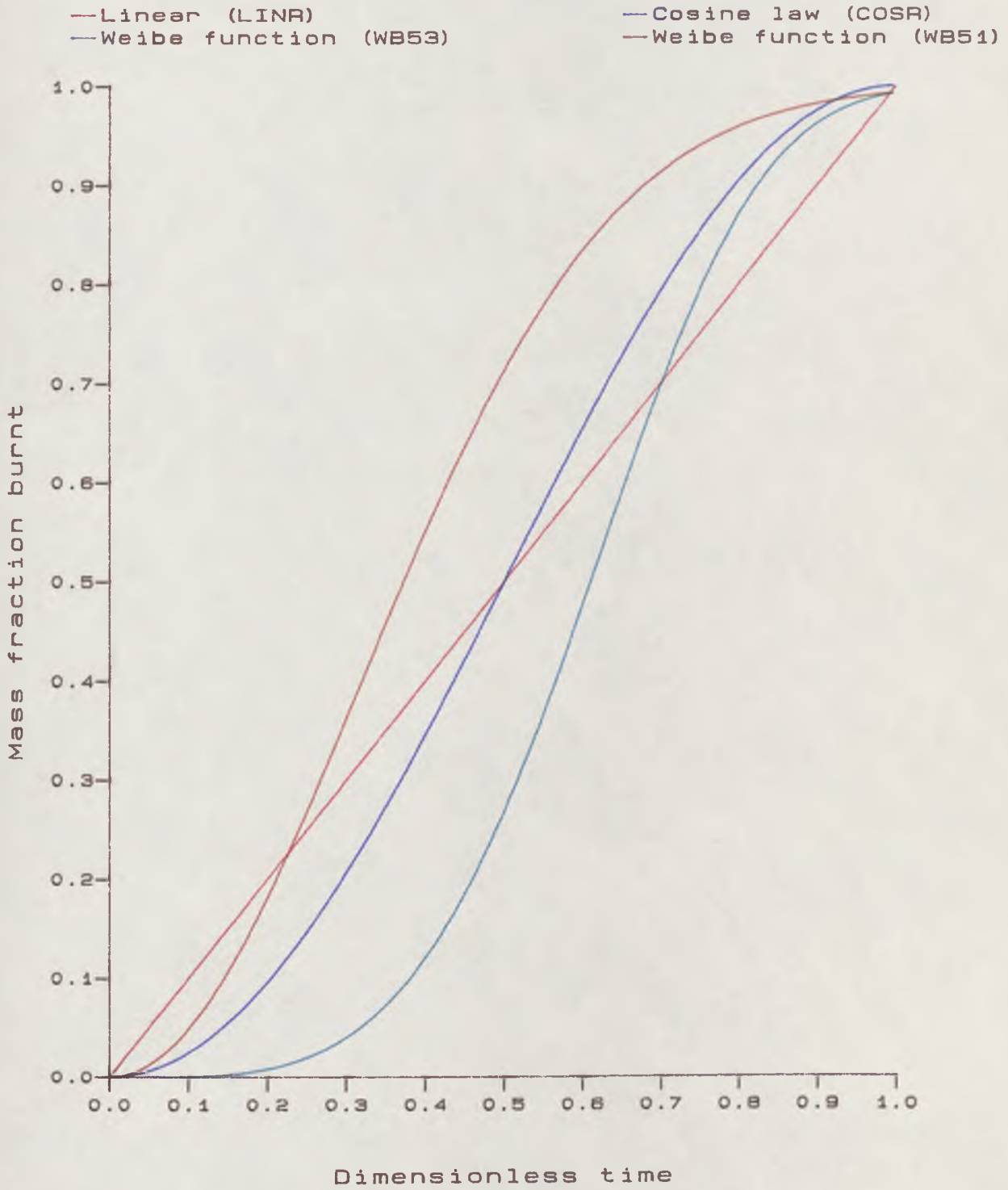


FIG.5.2 The empirical functions used to describe mass burning rate

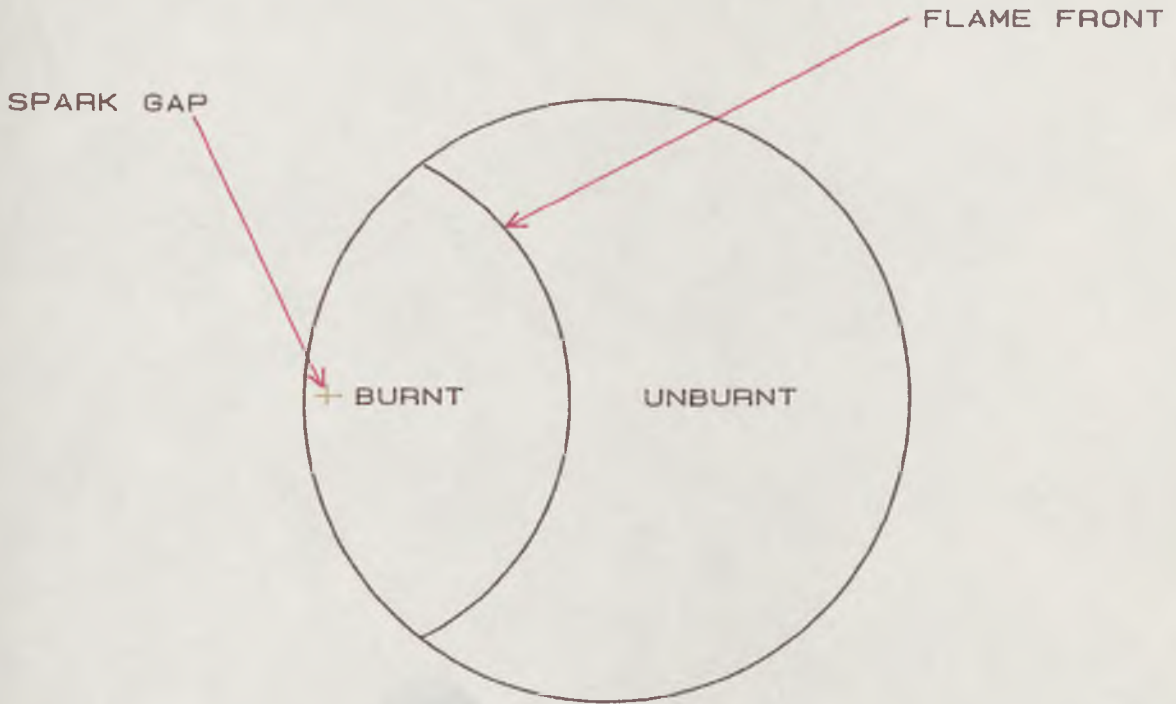


FIG.5.3 Flame position at a given time

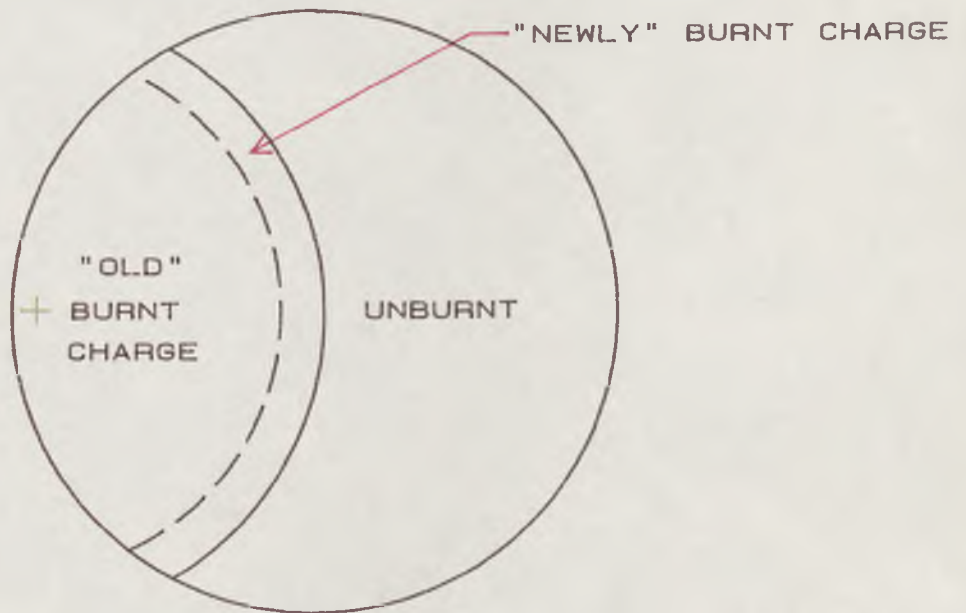
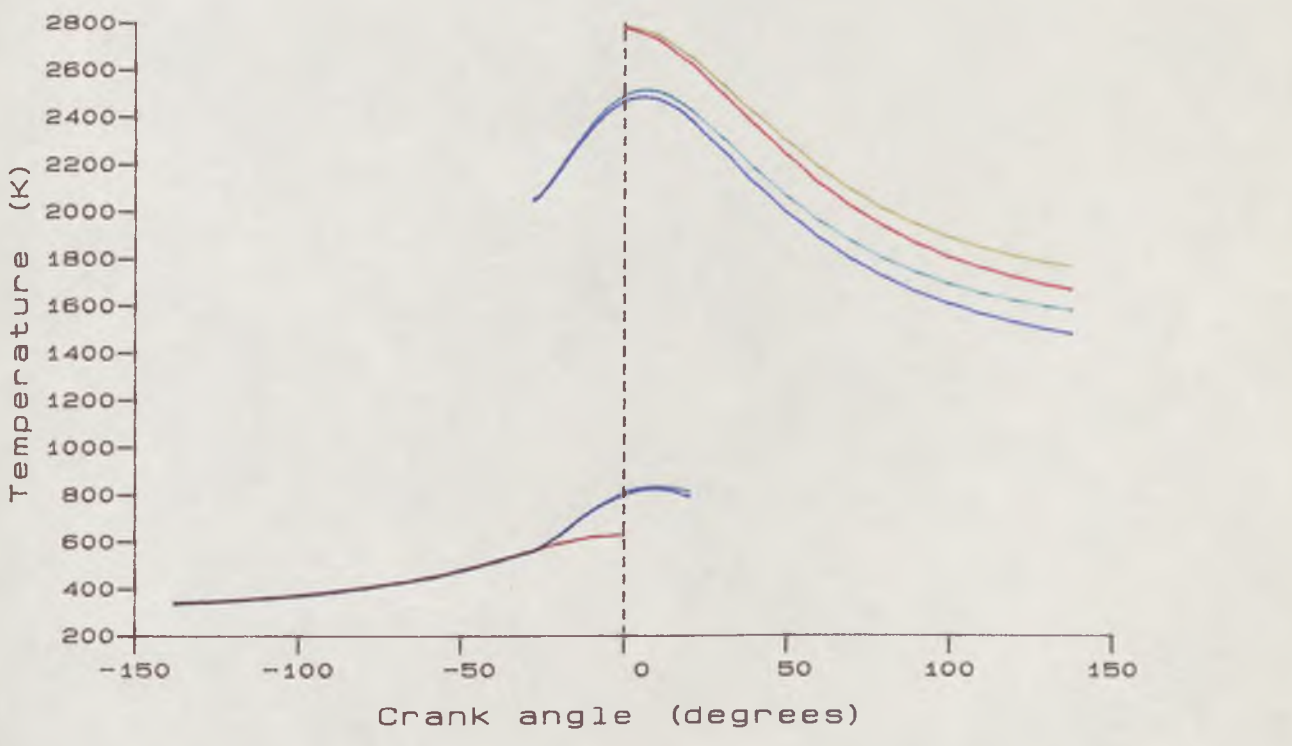
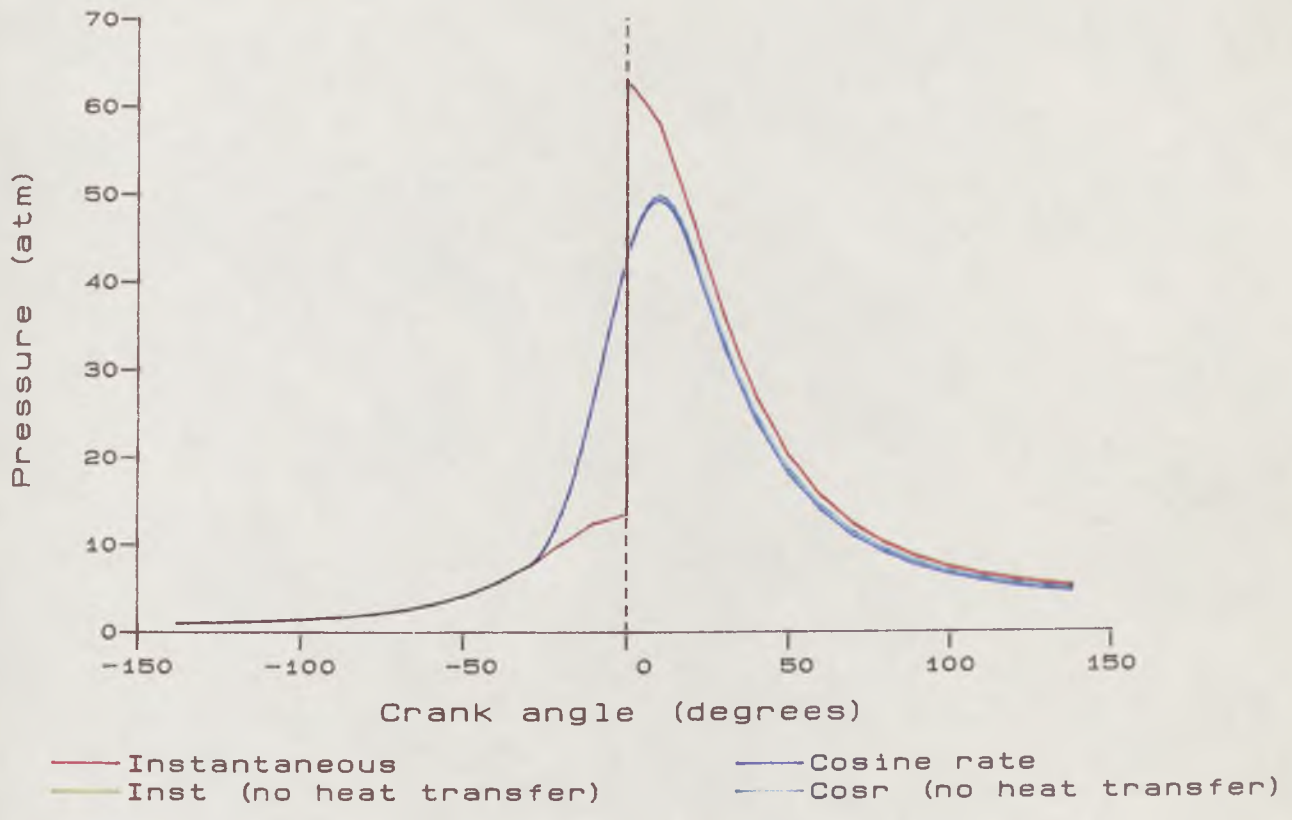
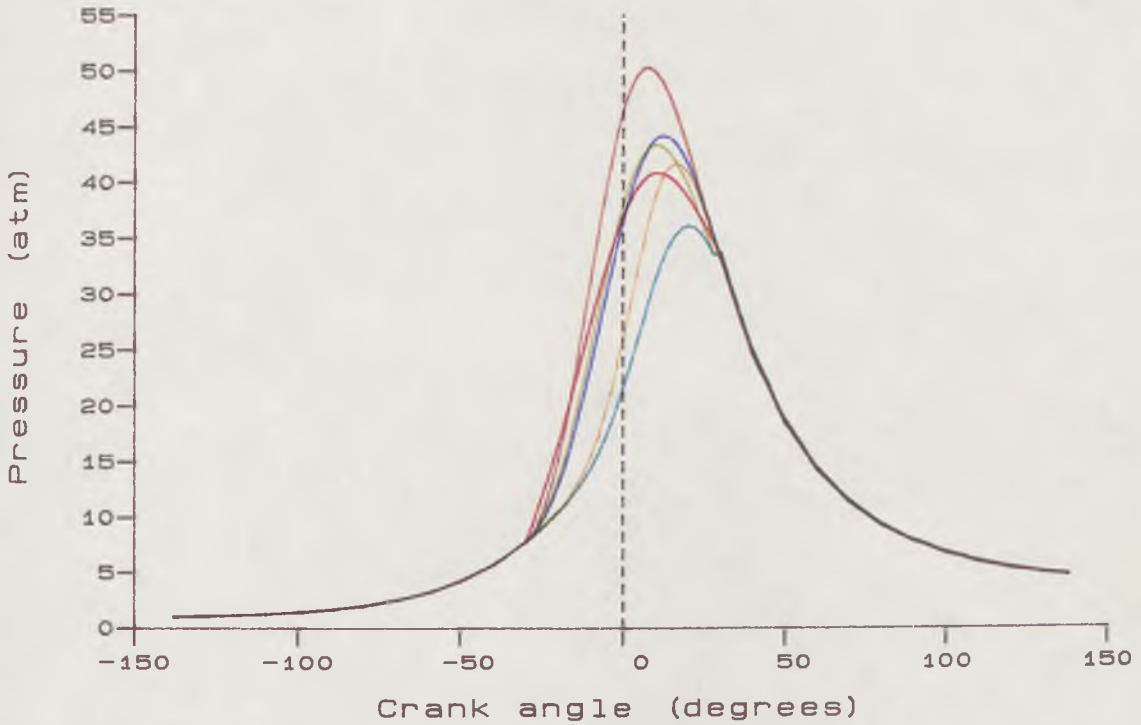


FIG.5.4 Flame position at a later time showing newly entrained charge

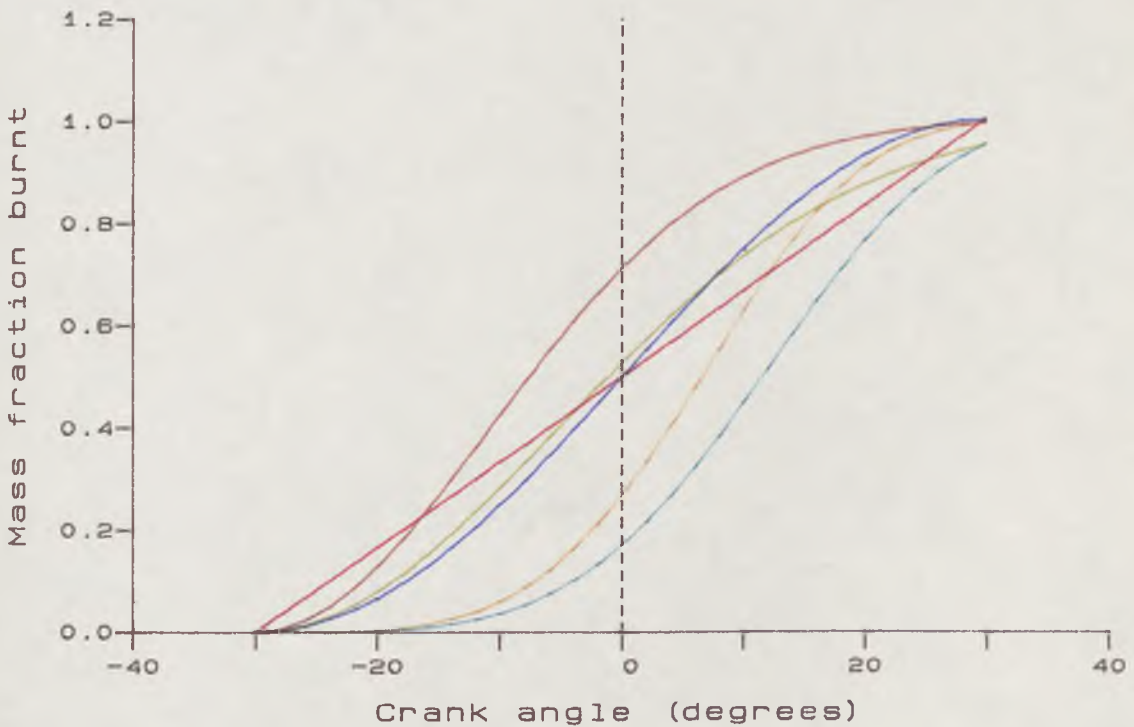


EQUIVALENCE RATIO = 1.0 ENGINE SPEED = 1400 rpm
 COMPRESSION RATIO = 8.0 SINGLE CHAMBER (SIDE IGN.)
 MANIFOLD PRESSURE = 1.0 FUEL BP-4STAR

FIG.5.6 Effect of heat transfer



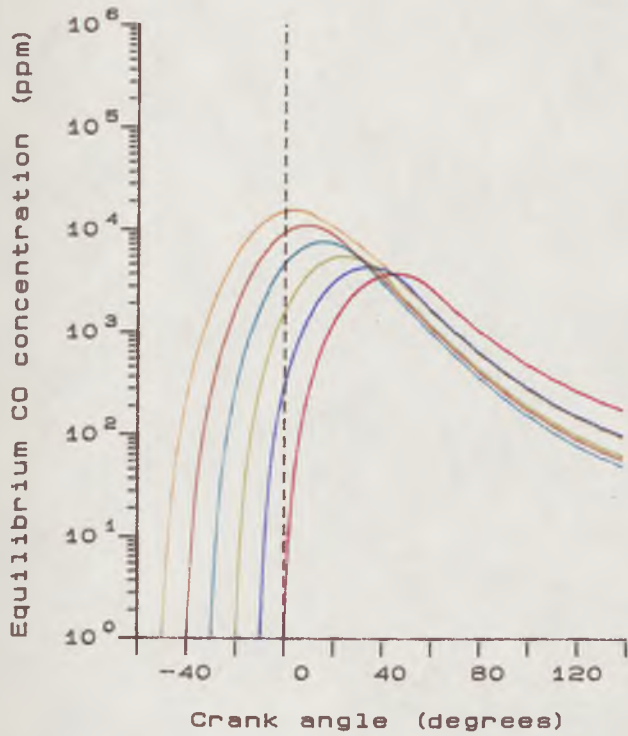
- Linear (LINR)
- Weibe function (WB31)
- Weibe function (WB51)
- Cosine rate (COSR)
- Weibe function (WB33)
- Weibe function (WB53)



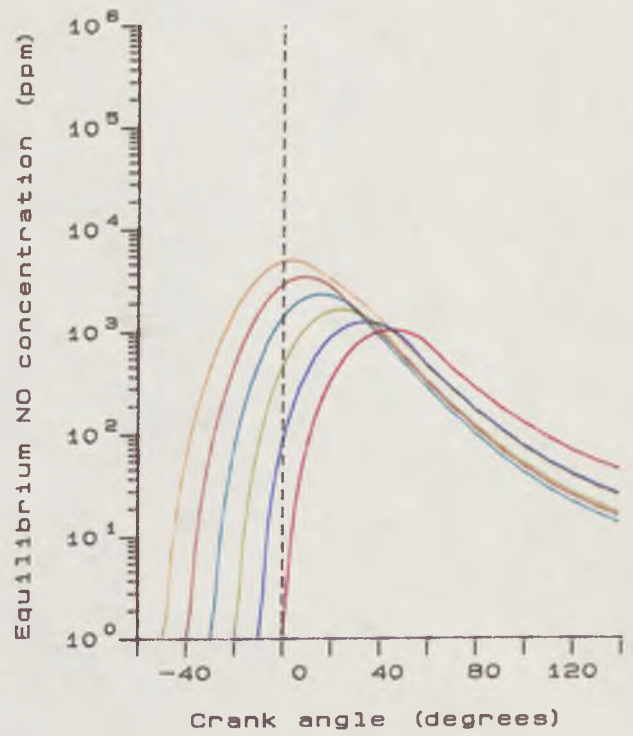
COMPRESSION RATIO = 8.0	SINGLE CHAMBER (SIDE IGN.)
EQUIVALENCE RATIO = 1.0	ENGINE SPEED = 1400 rpm
MANIFOLD PRESSURE = 1.0	FUEL BP-4STAR
SPARK ADVANCE = 30.0	COMBUSTION DURATION = 60.0

FIG.5.7

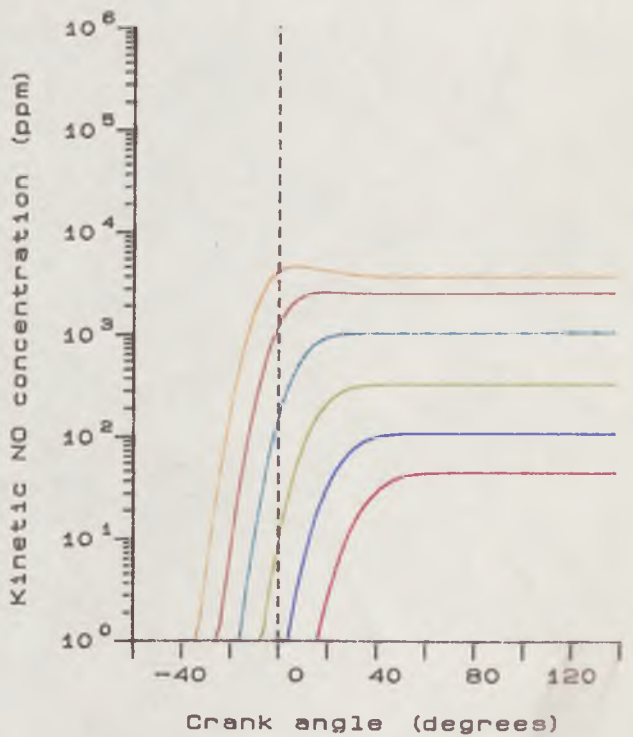
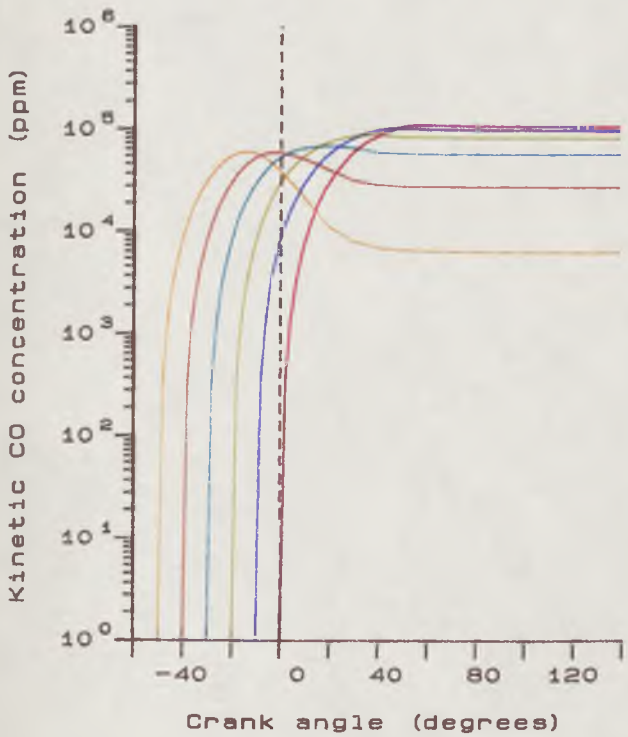
Effect of varying calculation method



— SPA= 0.0
 — SPA=20.0
 — SPA=40.0



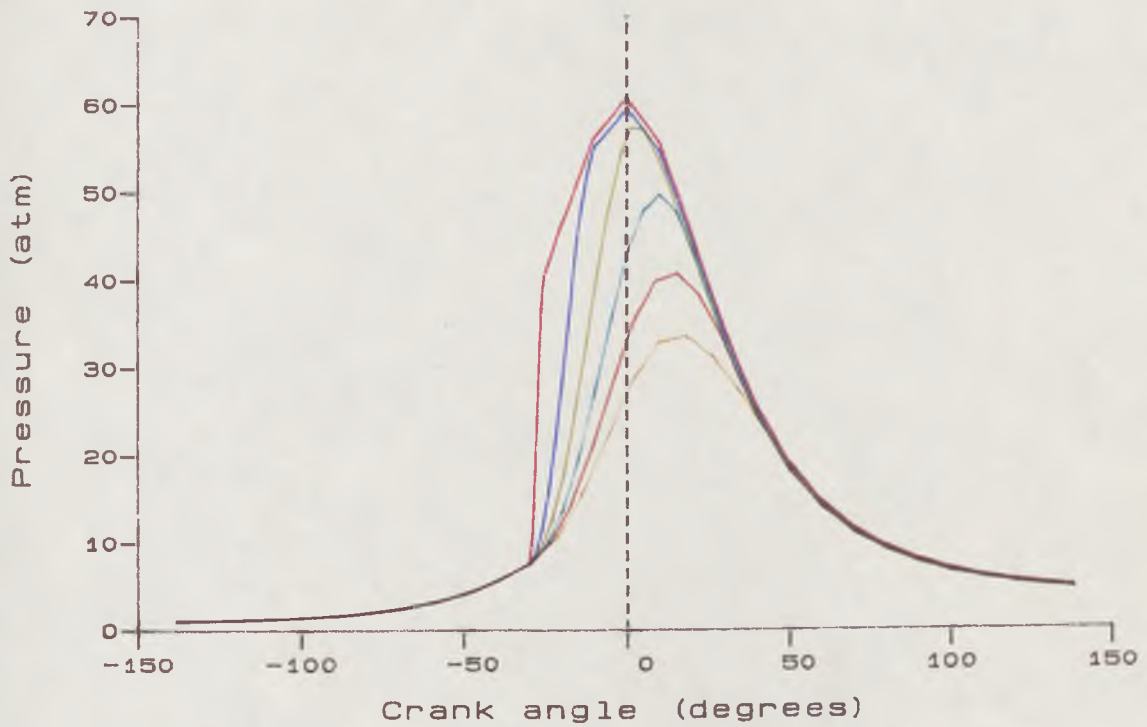
— SPA=10.0
 — SPA=30.0
 — SPA=50.0



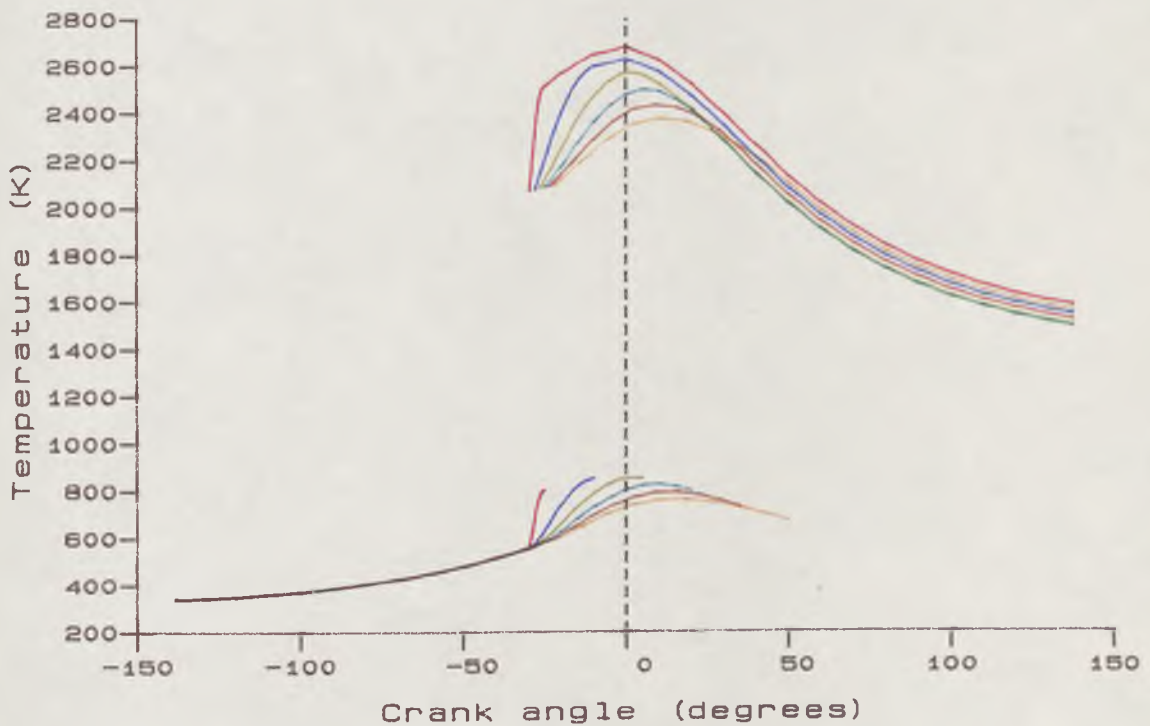
SINGLE CHAMBER (SIDE)
 MANIFOLD PRESSURE = 1.0
 FUEL BP-4STAR
 ENGINE SPEED = 1400 rpm

COSINE MASS BURN RATE
 COMPRESSION RATIO = 8.0
 EQUIVALENCE RATIO = 1.0
 COMBUSTION DURATION = 60.0

Fig.5.9 Effect of Varying Spark Advance

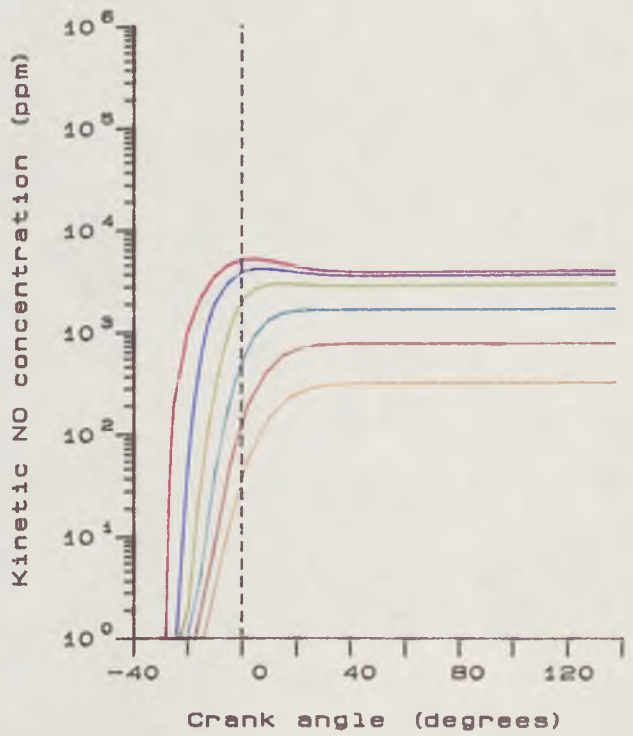
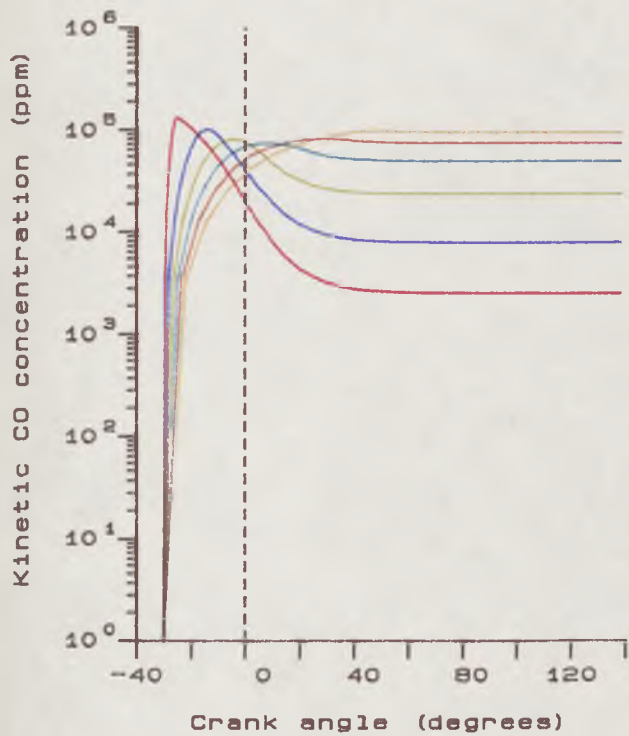
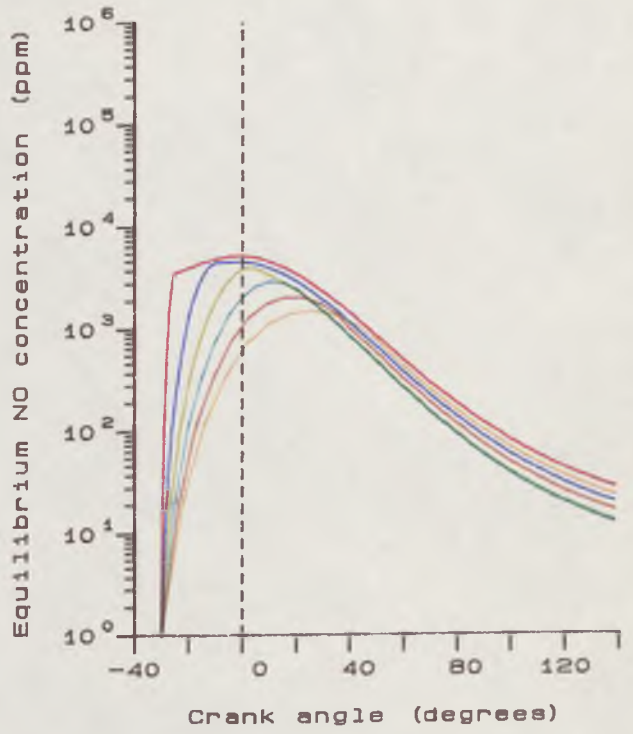
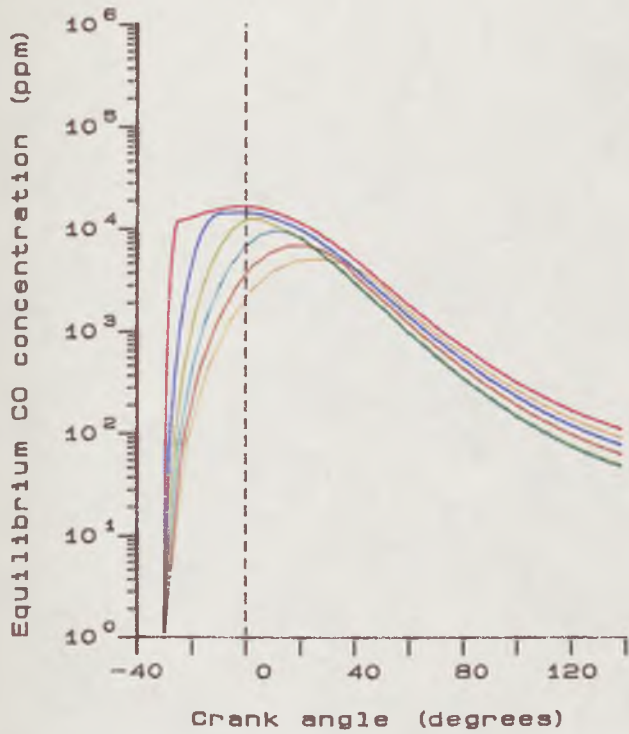


— CDR = 5.0	— CDR = 20.0
— CDR = 35.0	— CDR = 50.0
— CDR = 65.0	— CDR = 80.0



SINGLE CHAMBER (SIDE)	COSINE MASS BURN RATE
MANIFOLD PRESSURE = 1.0	COMPRESSION RATIO = 8.0
FUEL BP-4STAR	EQUIVALENCE RATIO = 1.0
ENGINE SPEED = 1400 rpm	SPARK ADVANCE = 30.0

Fig.5.10 Effect of varying combustion duration

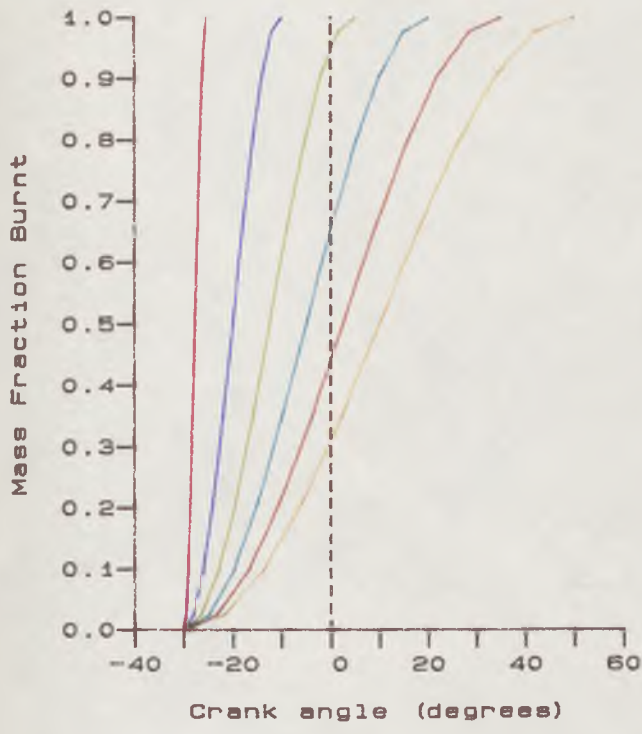


SINGLE CHAMBER (SIDE)
MANIFOLD PRESSURE = 1.0
FUEL BP-4STAR
ENGINE SPEED = 1400 rpm

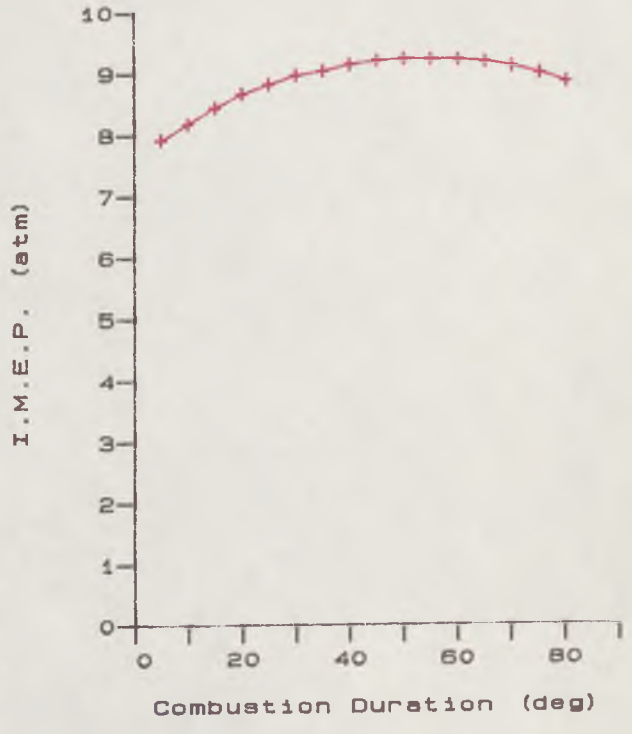
COSINE MASS BURN RATE
COMPRESSION RATIO = 8.0
EQUIVALENCE RATIO = 1.0
SPARK ADVANCE = 30.0

Fig.5.11

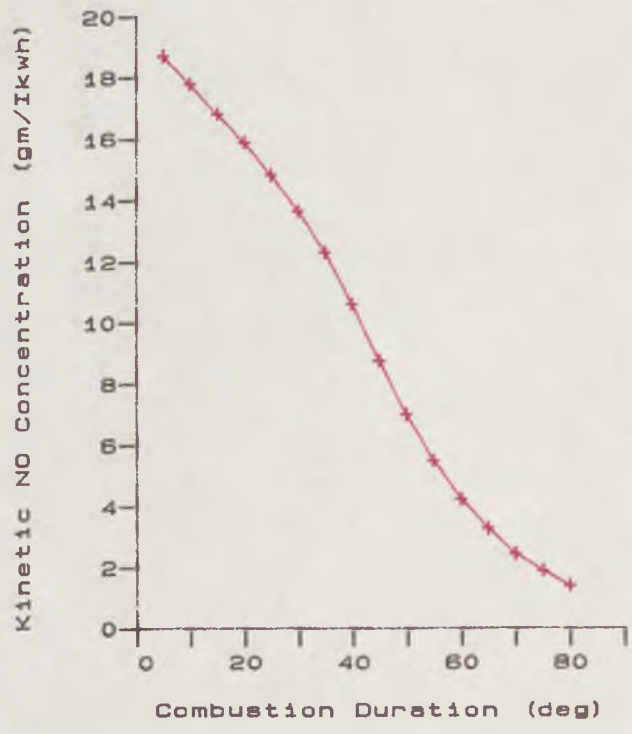
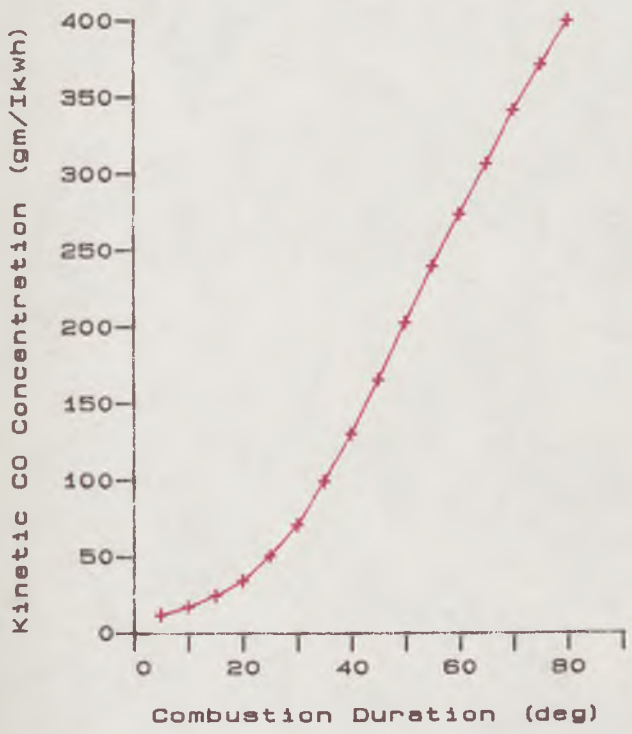
Effect of Varying Combustion Duration



— CDR= 5.0
 — CDR=35.0
 — CDR=65.0



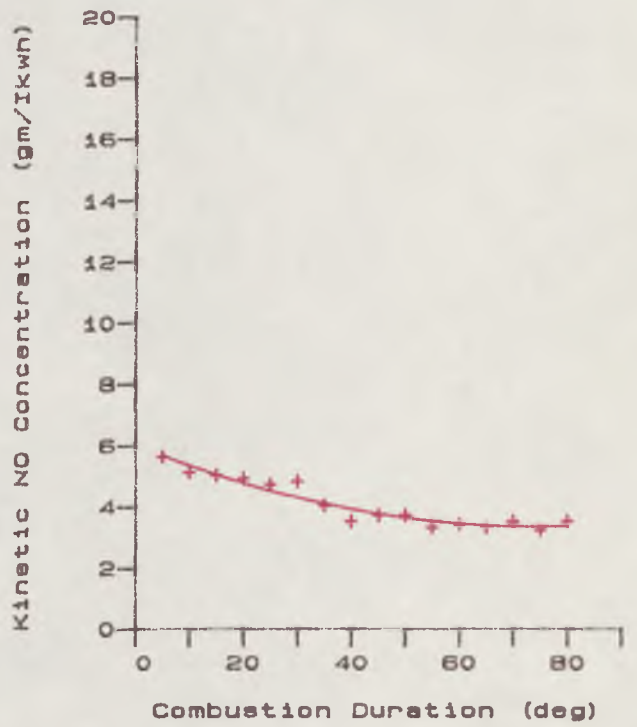
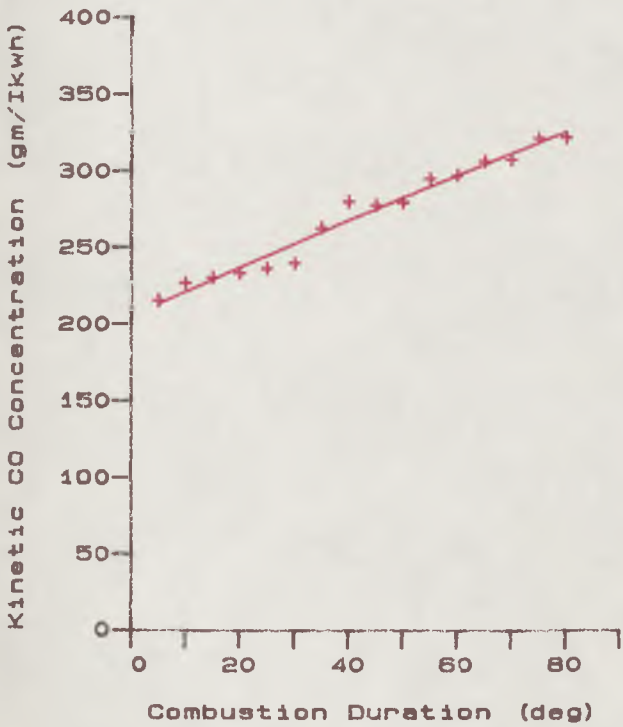
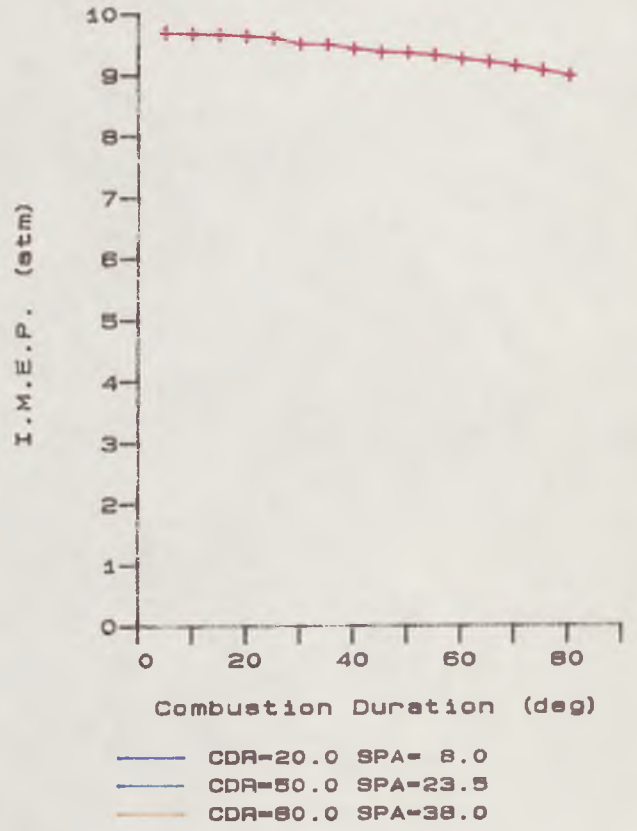
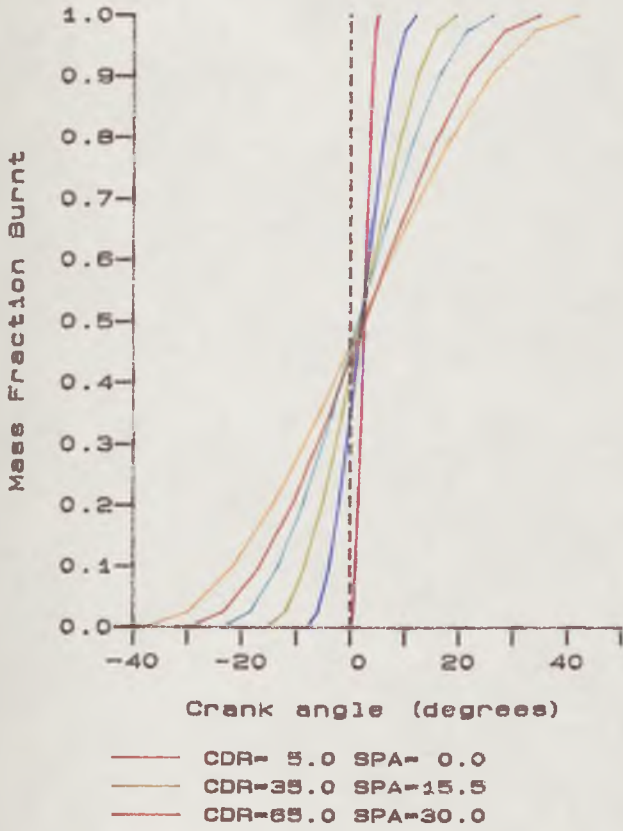
— CDR=20.0
 — CDR=50.0
 — CDR=80.0



SINGLE CHAMBER (SIDE)
 MANIFOLD PRESSURE = 1.0
 FUEL BP-4STAR
 ENGINE SPEED = 1400 rpm

COSINE MASS BURN RATE
 COMPRESSION RATIO = 8.0
 EQUIVALENCE RATIO = 1.0
 SPARK ADVANCE = 30.0

Fig.5.12
 Effect of Varying Combustion Duration

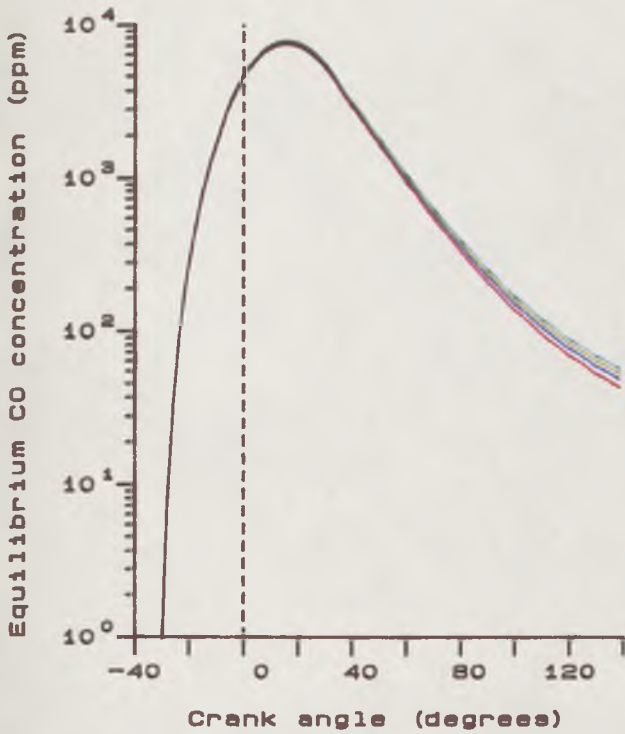


SINGLE CHAMBER (SIDE)
 MANIFOLD PRESSURE = 1.0
 FUEL BP-4STAR
 ENGINE SPEED = 1400 rpm

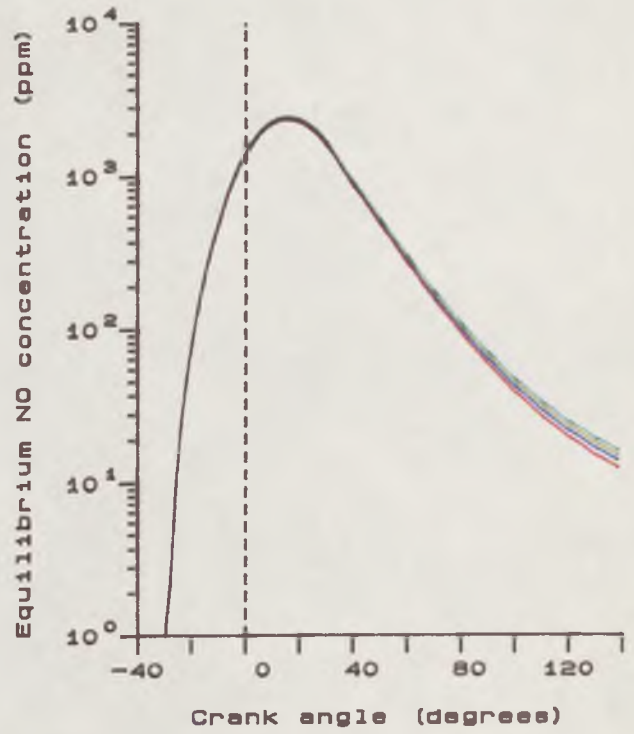
COSINE MASS BURN RATE
 COMPRESSION RATIO = 8.0
 EQUIVALENC RATIO = 1.0
 OPTIMUM SPARK ADVANCE

Fig.5.13

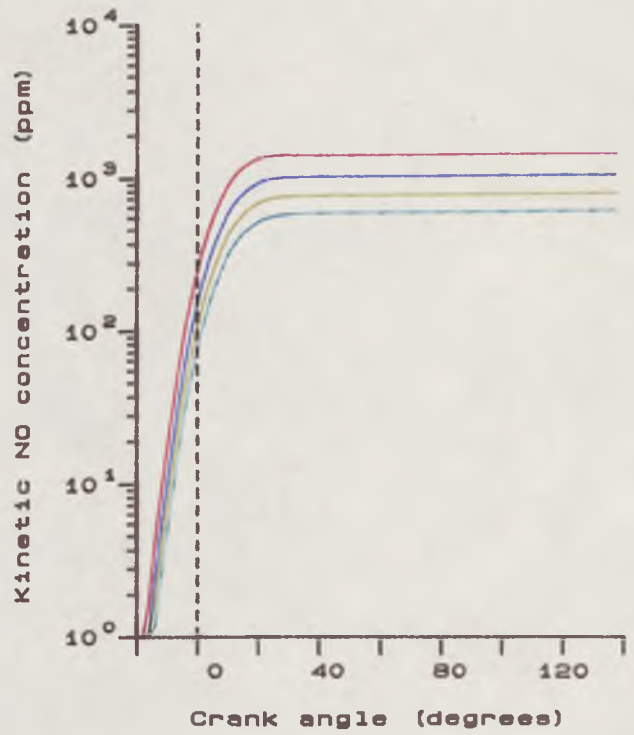
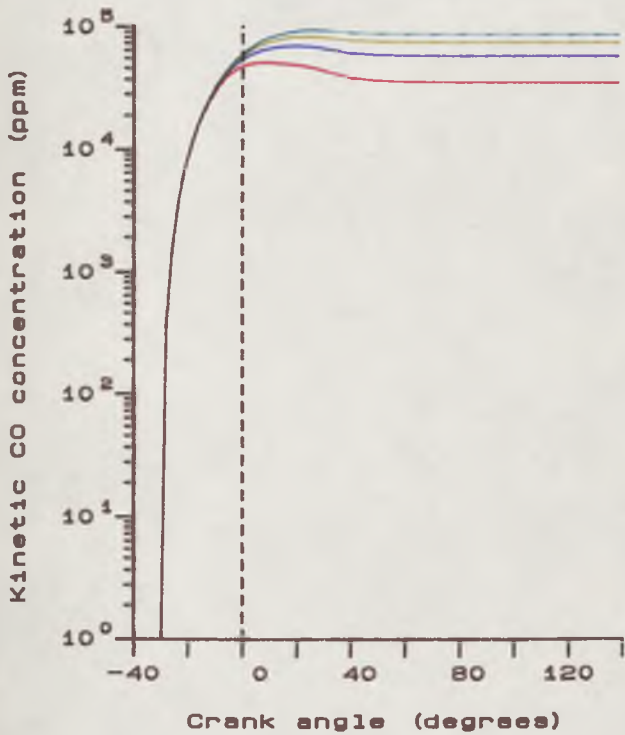
Effect of Varying Combustion Duration



— 800 rpm
— 2100 rpm



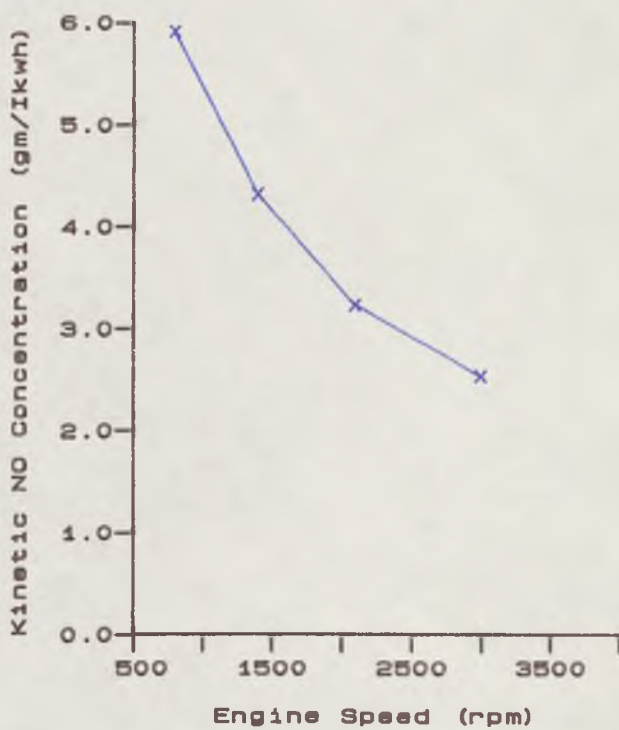
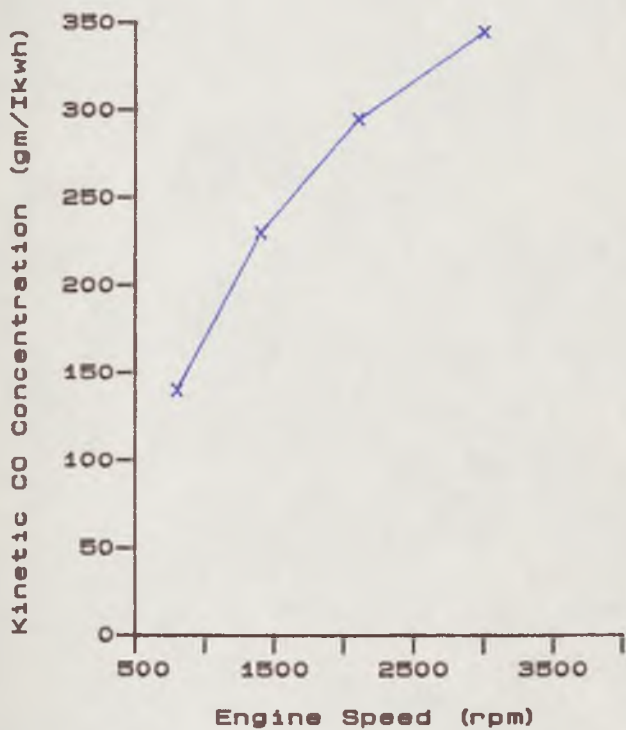
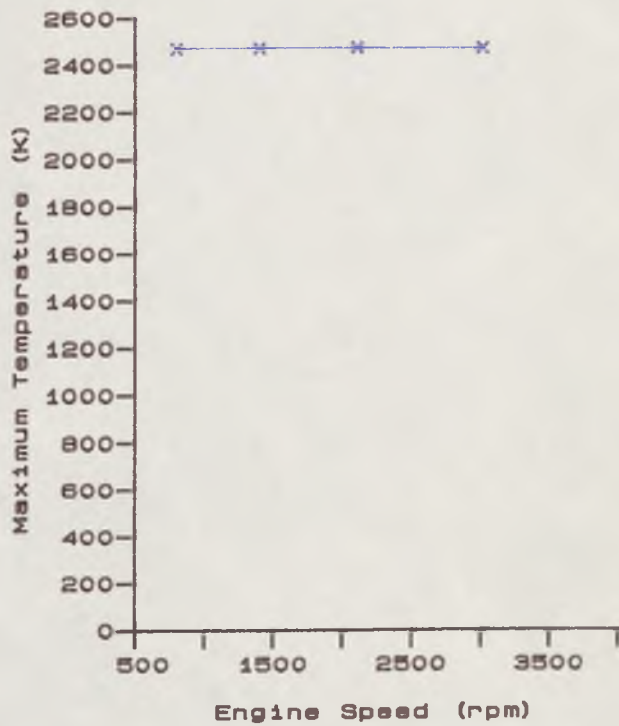
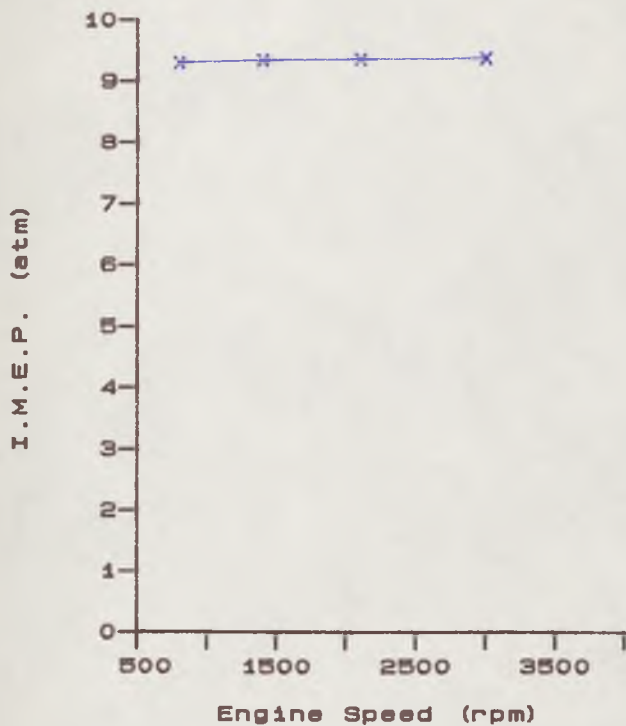
— 1400 rpm
— 3000 rpm



COMPRESSION RATIO = 8.0
MANIFOLD PRESSURE = 1.0
EQUIVALENCE RATIO = 1.0
COMBUSTION DURATION = 60.0

SINGLE CHAMBER (SIDE)
COSINE MASS BURN RATE
FUEL BP-4STAR
SPARK ADVANCE = 30.0

FIG. 5.14 Effect of Varying Engine Speed



SINGLE CHAMBER (SIDE)
 MANIFOLD PRESSURE = 1.0
 FUEL BP-4STAR
 SPARK ADVANCE = 30.0

COSINE MASS BURN RATE
 COMPRESSION RATIO = 8.0
 EQUIVALENCE RATIO = 1.0

Fig.5.15 Effect of Varying Engine Speed

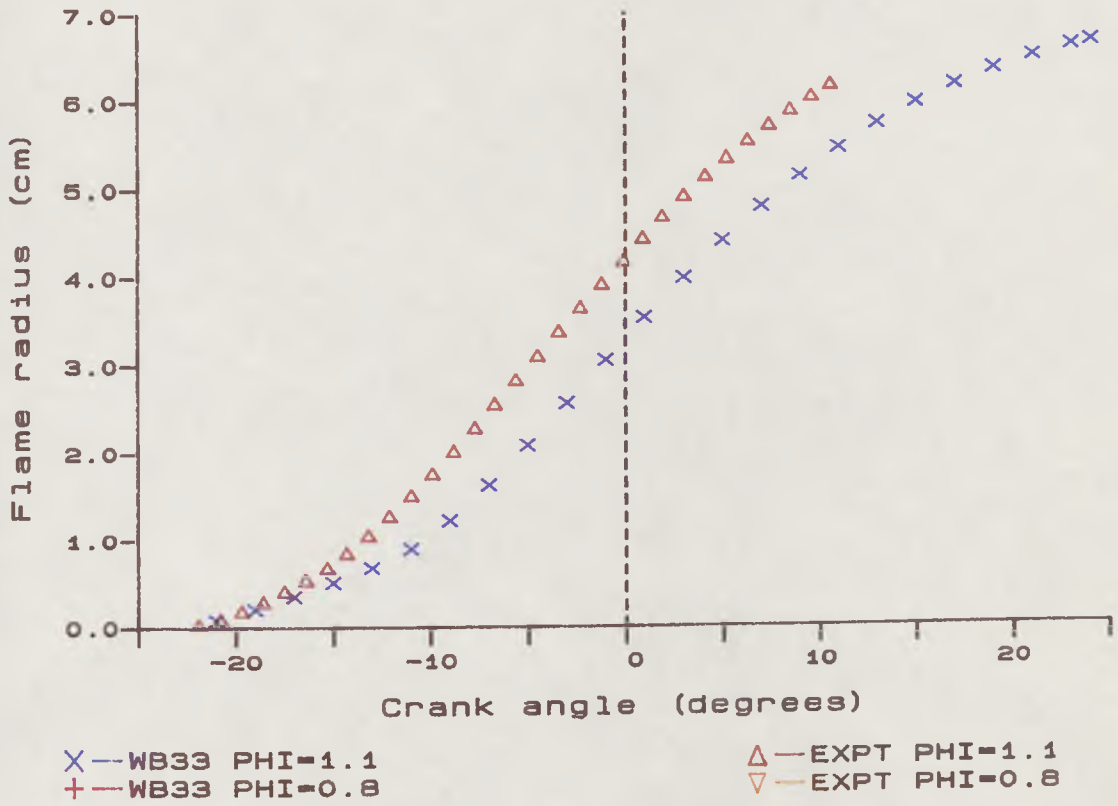


Fig. 5.16 Comparison of Experimental And Predicted Flame Radii

CHAPTER 6

Single Chamber Model - Burning Velocity Method

CONTENTS

6.1	INTRODUCTION	128
6.2	DETERMINATION OF TURBULENCE PARAMETERS	129
6.2.1	Integral Length Scale (L)	129
6.2.2	Turbulence Intensity (u')	130
6.2.3	Taylor Microscale (λ)	130
6.2.4	Eddy Lifetime	130
6.3	DETERMINATION OF BURNING VELOCITIES AND FLAME STRUCTURE	131
6.3.1	Laminar Burning Velocity	131
6.3.2	Turbulent Burning Velocity	131
6.3.3	Developing Flame	133
6.3.4	Flame Thickness (δ)	133
6.3.5	Chemical Lifetime	134
6.4	MODELLING OF THE COMBUSTION PROCESS	135
6.4.1	Ignition	135
6.4.2	Rate of Entrainment	135
6.4.3	Rate of Burning	136
6.5	RESULTS AND DISCUSSION	137
6.5.1	Some Comparisons With Experimental Results (Ruston Engine).	139
6.5.2	Comparison With Experimental Results (Yamaha Engine)	140
6.5.3	Effect of EGR	140
6.6	CONCLUDING REMARKS	141

6.1. INTRODUCTION

When a pre-mixed fuel-air mixture is ignited, a flame propagates through the mixture; this flame entrains unburnt charge, which is subsequently burnt. It is this effect which causes the progressive nature of the combustion process. The velocity with which the flame travels, relative to the unburnt gas ahead of it, is termed the burning velocity. If the mixture is quiescent, the flame propagation is laminar, and the burning velocity is called the laminar burning velocity (u_l). As the mass entrained by the flame front burns, it expands and pushes the unburnt gas ahead of the flame forward (at the unburnt gas velocity u_g). To a stationary observer the flame appears to move forward at a velocity (u_f) equal to the sum of the burning velocity and the unburnt gas velocity ($u_f = u_l + u_g$).

If the mixture motion is turbulent the flame propagation rate is increased. Turbulent motion is characterised by velocity fluctuations, superimposed on the mean flow, associated with eddies of various sizes. The upper limit of eddy size will be dependent on vessel size, while the lower limit will be defined by viscosity effects (Hinze, 1959). Large eddies create velocity gradients, which in turn create smaller eddies; eventually all the kinetic energy in the turbulent flow is dissipated into random molecular motion (heat) by the smallest eddies. The turbulent scale is a representative size of these eddies; the integral length scale (L) is a characteristic mixing length associated with the large eddies, while the Taylor microscale is a measure of the small eddies associated with velocity fluctuations at high frequencies, and the Kolmogorov scale is a measure of the smallest eddies (vortices) in which dissipation occurs. The intensity of the turbulence (u') is defined as the root mean square of the velocity fluctuations.

The turbulence enhances the flame propagation rate by distorting the flame front and assisting the transport of reactive species. The way in which this process occurs is not well understood; the diversity of opinion is shown in the many different models of flame propagation reviewed by Andrews et al (1975). Pavinelli and Fuhs (1962) suggested that the large scale eddies increased the flame surface area, while small scale eddies enhanced turbulent transport. Experimental studies suggest that the reaction zone is thick compared to laminar values (Beretta et al, 1983; Smith, 1982a). Ballal and Lefebvre (1975) noted that at high turbulence, flame wrinkling was replaced by a fragmented reaction zone. Using a Rayleigh scattering technique, Smith (1982a) conducted measurements of flame thickness, and showed pockets of unburnt charge to exist behind the flame front. The probability of occurrence of these pockets increased with engine speed (and therefore turbulent intensity), as did the mean flame thickness. Namazian et al (1980), using schlieren photography in a perspex engine, found that only 50-70% of the mixture behind the flame front was burnt.

The importance of small scale turbulent structure on flame propagation was noted by Abdel-Gayed and Bradley (1977). In a study on flame structure Smith (1982b) observed that the size of the flame structures was of the order of the Taylor microscale, and decreased as the flame propagation progressed or the engine speed increased (i.e. as the turbulence intensity increased, and therefore the Taylor microscale decreased).

Early work involving burning velocities (eg. Lucas and James, 1973) assumed that all mass behind the flame front was burnt. Blizzard and Keck (1974) extended the ideas of Damköhler (1940) to spark ignition engines. They modelled the turbulent flame propagation process as the entrainment and subsequent laminar burning of discrete, coherent, turbulent eddies. The rate at which mass was entrained by the flame was described in terms of the turbulent burning velocity, while the rate at which this entrained mass subsequently burnt was assumed to occur at an exponential rate.

Described in this chapter is a model based on the entrainment concept used by Blizzard and Keck. The combustion rate was calculated in an incremental fashion very similar to that outlined in the previous chapter, when an empirical burn rate expression was used. The main computational difference involved was in the calculation of mass fraction burnt during each increment. This was found from considerations of burning velocity and rate of entrainment. Unlike the method used previously, in Chapter 5, the combustion duration did not need to be specified; it was determined by the program.

6.2. DETERMINATION OF TURBULENCE PARAMETERS

In the model described here the turbulence in the engine cylinder has been assumed to be isotropic and homogeneous; Witze et al (1983) showed engine turbulence to be isotropic, but non-homogeneous.

6.2.1. Integral Length Scale (L)

The integral length scale at ignition has been assumed proportional to the instantaneous cylinder height. This assumption has been made by many workers for engine models; a few workers, however, have preferred to use inlet valve lift instead (e.g. Davis et al, 1984). Abdel-Gayed and Bradley (1980) showed that, for pipe flow, the length scale is 0.08 times the pipe diameter. Abdel-Gayed et al (1986b) showed that for turbulence in a bomb the length scale is approximately one tenth of the vessel diameter, while Tabaczynski chose a constant of proportionality of 0.15, as this gave the closest agreement between his engine model and experimental results. A value of 0.1 was adopted in the work reported here.

6.2.2. Turbulence Intensity (u')

The turbulence intensity is defined as the root mean square of the fluctuating velocity of the turbulent flow. For conventional (single chamber) engines, at the time of ignition, this has usually been assumed to be proportional to the mean piston speed (although some workers have preferred to use intake flow velocity through the inlet valve). Witze et al (1983, 1984a) and Rask (1979) showed, from LDA measurement, the constant of proportionality to be of the order of 1-1.1. Liou et al (1984) reviewed the correlation for a number of workers and showed the constant to vary in the range 0.4-1.3. Results from LDA measurements gave a constant at the higher end of the range, and as LDA has been shown to be more accurate than hot wires (Witze, 1980a), the constant chosen for the currently reported work was a value near to the top of this range (1.1). After ignition, as the charge burns, it expands; this expansion changes the turbulence characteristics of the unburnt charge as it is pushed ahead of the flame front. To allow for this effect the eddies were assumed coherent; the integral length scale was therefore governed by conservation of mass of an eddy:-

$$L = L_{ig} \left[\frac{\rho_{u_{ig}}}{\rho_u} \right]^{\frac{1}{3}} \quad (6.1)$$

and the turbulent intensity was governed by conservation of angular momentum (rapid distortion theory, Wong and Hoult 1979):-

$$u' = u'_{ig} \left[\frac{\rho_u}{\rho_{u_{ig}}} \right]^{\frac{1}{3}} \quad (6.2)$$

where subscript ig denotes conditions at the time of the spark.

6.2.3. Taylor Microscale (λ)

The Taylor microscale, for isotropic turbulence, can be calculated from the relationship (Hinze, 1959) :-

$$\lambda^2 = C \frac{L^2}{R_L} \quad (6.3)$$

where Hinze gave a value of 15 for the constant, C . Abdel-Gayed and Bradley (1981) suggested that the constant to be used in the above equation should be 40.4. Both values were used in the work reported here, in order to determine the effect of this constant.

6.2.4. Eddy Lifetime

This is a characteristic time defined as (L/u' or λ/u'); it can be considered to be the time that an eddy will exist, before it is broken down and dissipated by the turbulent motion.

6.3. DETERMINATION OF BURNING VELOCITIES AND FLAME STRUCTURE

6.3.1. Laminar Burning Velocity

The laminar burning velocity is an important parameter, since it is an expression for the global chemical reaction rate of the mixture concerned. Its importance, even at very high turbulence levels was noted by Karlovitz et al (1951). In order to use the expressions for the turbulent burning velocity available in the literature, it is necessary to know the laminar burning velocity at the relevant temperature, pressure and equivalence ratio. These data are not available at the temperatures and pressures typically found in engines; however, many papers have been published giving data at lower pressures and temperatures - together with equations for extrapolating it. (eg. Gulder, 1982; Ryan & Lestz, 1980; Metghalachi & Keck, 1982; Babkin et al, 1967)

These laminar burning velocity data have usually been generated from experiments conducted in constant volume bombs or on burners; the data tend to be subject to wide numerical variation (see Andrews and Bradley, 1972). A number of sources of laminar burning velocity data were used in the currently reported model, in order to identify that set of data which was most consistent with the experimental results for the engines used. Laminar burning velocity data derived from experiments in the Leeds bomb (Hamid, 1986) were also used. As these data were only available for atmospheric pressure, they were extrapolated using the relations presented by Gulder, and Metghalachi and Keck. The data of Babkin were only available for stoichiometric mixtures; for other equivalence ratios, the percentage change in burning velocity with equivalence ratio was assumed to be the same as that found for the Leeds data at atmospheric pressure.

6.3.2. Turbulent Burning Velocity

As described previously, turbulence enhances burning velocity by distorting the flame front and assisting the transport of reactive species. A number of relationships have been developed to express the enhancement of laminar burning velocity in terms of turbulence characteristics (principally u') within the engine cylinder at any instant. Four such relationships have been investigated in the present study :

- (i) It could be argued that reactive species will be carried from the flame front (by turbulent eddies) into the unburnt mixture, at a velocity equal to the turbulent intensity (u'), such that u_t (the total burning velocity relative to the unburnt mixture) would be given by: $u_t = u_l + u'$. This simple approach was first suggested by Damköhler (1940) (in his wrinkled flame model) and has since been adapted for engine models by Tabaczynski et al (1977) and Borgnakke et al (1980).

- (ii) A second possibility considered was to take the burning velocity to be the sum of the unburnt gas velocity (ahead of the flame front) and the laminar burning velocity.

$$\text{i.e. } u_t = u_l + u_g \quad (6.4)$$

This approach assumes that the unburnt gas velocity ahead of the flame generates turbulence which enhances the flame propagation rate. Although this may be true to some extent, it is likely that a constant of proportionality should be included.

- (iii) The ratio of turbulent burning velocity to laminar burning velocity (u_t/u_l), often termed the flame speed ratio, has been studied in engines by a number of workers (Lancaster, 1976; Groff and Matekunas, 1980). Groff and Matekunas used photographs of flame propagation, together with pressure records and a computer model, to determine the turbulent burning velocity in an engine. They related this burning velocity to turbulence intensity measurements, using data from hot wire probes, in the engine under motoring conditions. The results of this correlation were expressed as a flame speed ratio :-

$$\frac{u_t}{u_l} = 2 + 1.21 \times S \times \left[\frac{u'}{u_l} \right] \times \left[\frac{P}{P_{mot}} \right]^{0.82} \quad (6.5)$$

$$\text{where } S = 1.0 + 0.05\theta_{ig}^{0.4}$$

$$\theta_{ig} = \text{spark advance}$$

$$P_{mot} = \text{motoring pressure}$$

To use this correlation in the model, the turbulent intensity during motoring was taken to be that measured by Groff and Matekunas - as their engine was of similar geometry to that assumed in the current study.

- (iv) An alternative expression used for the flame speed ratio was taken from the work of Hamid (1986). He correlated all published data (from constant volume bombs and burners) of flame speed ratio against u'/u_l , for varying turbulent Reynolds number and Lewis number. To use this data in the engine model, sixth order polynomials were fitted to it - for each range of Reynolds and Lewis numbers. Shown in Fig. 6.1 are the curves for high Lewis numbers (≥ 1.3); this Lewis number regime covers stoichiometric and lean iso-octane mixtures. The turbulent burning velocity could then be found, on the basis of estimated values of u' and u_l . Although these measurements were derived from bomb data, in which the length scales were larger than in the engines under consideration, it was considered that the data were still applicable to engines. Lancaster et al (1976) have shown that length scale has little effect on flame speed ratio.

6.3.3. Developing Flame

When a flame is small, it will not be affected by the full range of turbulent eddy sizes; eddies of a scale larger than the size of the flame kernel will only move it bodily, convecting it without significantly affecting its propagation rate. As the flame grows it will be affected by a larger spectrum of eddy sizes; its entrainment rate will increase until it reaches that given by the fully developed turbulent burning velocity (Lawes, 1986). In the program, the development of turbulent burning velocity was modelled by the inclusion of an exponential term :-

$$u_t = (u_t)_{dev} \times \left(1 - e^{-\frac{r}{\tau}} \right)^{1/2} \quad (6.6)$$

where τ is a characteristic time defined as $0.44L/u'$, Abdel-Gayed et al (1981). Other workers (Groff and Matekunas, 1980; Lancaster et al, 1976b; Mathur et al, 1983) have suggested that turbulence develops until the flame reaches a given critical radius.

Groff & Matekunas give:-

$$\frac{u_t}{u_l} = 1.07 \times \left[\frac{r}{r_{dev}} \right]^{1.04} \times \left[\frac{u_t}{u_l} \right]_{dev} \quad (6.7)$$

while Lancaster et al suggest:-

$$\frac{u_t}{u_l} = \left[\frac{u_t}{u_l} \right]_{dev} \times \left[\frac{r}{r_{dev}} \right]^{\frac{m-1}{2}} \quad (6.8)$$

and Mathur et al proposed:-

$$\frac{u_t}{u_l} = \left[\frac{u_t}{u_l} \right]_{dev} \times \left[\frac{r}{0.03} \right]^{0.5} \quad (6.9)$$

note: r is measured in metres

where r_{dev} is the minimum radius of the fully developed flame.

This approach was not adopted in the present study because its use requires knowledge of the (engine dependent) radius at which the flame becomes fully developed.

6.3.4. Flame Thickness (δ)

Turbulent combustion usually occurs in reaction zones which are thicker than those of laminar flames, but less thick than the integral length scale. In those reaction zones the flame propagation is thought to be laminar like (Abdel-Gayed et al, 1984a). Gaydon and

Wolfhard (1970) suggested that the flame thickness would be approximately given by:

$$\delta = \frac{v}{u_l} \quad (6.10)$$

6.3.5. Chemical Lifetime

The time that an eddy takes to burn is termed the chemical lifetime. If this is greater than the eddy lifetime, then an eddy will break up before combustion is complete; this can lead to quenching of the flame (Chomiak and Jarosinski, 1982; Quader, 1974, 1976).

Blizzard and Keck (1974) and McCuiston et al (1977) assumed that an eddy of characteristic radius (l_e) would, once entrained by the flame front, burn inwards from peripheral ignition sites at a rate given by the laminar burning velocity. Hence the time for it to burn would be given by:-

$$\frac{l_e}{u_l} \quad (6.11)$$

In their work, on the basis of comparison with experimental results, they took the radius l_e to be proportional to valve lift.

Tabaczynski et al (1977) considered the turbulent structure in greater detail. An eddy, size L , was assumed to contain a number of dissipative vortices, of the order of the Kolmogorov scale. These were considered to be separated by quiescent regions of dimension λ , the Taylor microscale. Diffusion of a laminar nature was assumed to occur in these regions, hence the time to burn each microcell was given by:-

$$\tau_c = \frac{\lambda}{u_l} \quad (6.12)$$

Dissipation along the vortex tubes, with the associated molecular transport, was taken to be the mechanism for flame propagation; ignition sites were assumed to be transported along the vortex tubes at a rate governed by turbulent intensity and laminar flame speed. The time to burn an eddy was shown to correlate with the ratio of the chemical lifetime of the Taylor microscale (λ/u_l) and the eddy lifetime (L/u'). Hires et al (1978) investigated this correlation over a wide range of turbulent parameters and showed that the chemical lifetime (τ_b , of an eddy size L) could be given by:-

$$\tau_b = 1.8 \times \left[\frac{L}{u'} \right]^{\frac{1}{3}} \times \left[\frac{\lambda}{u_l} \right]^{\frac{2}{3}} \quad (6.13)$$

In later work (Tabaczynski et al, 1980) this approach was discarded, as it did not allow a smooth transition from ignition to fully developed flame propagation. Instead, the relevant

chemical lifetime was taken as being that associated with the Taylor microscale (λu_i). All subsequent work reported in the literature (Davis et al, 1982,1984; Belaire et al, 1983; Arici et al, 1983) has used this value; it was therefore used in the model described in the current work.

The chemical lifetime can also be expressed as the ratio of flame thickness to laminar burning velocity. The chemical lifetime was calculated by this method (using the expression of Gaydon and Wolfhard (Eqn. 6.10) for flame thickness) for one set of tests; these tests showed no appreciable difference in the model results, when compared with λu_i .

6.4. MODELLING OF THE COMBUSTION PROCESS

6.4.1. Ignition

The ignition process was considered in a very elementary manner. A spherical kernel of diameter equal to the Taylor microscale (λ) was assumed to ignite at its centre, and burn at laminar burning velocity (u_i). The time for it to burn was therefore given by:-

$$\frac{\lambda}{2u_i} \quad (6.14)$$

This combustion process was considered to occur instantaneously (at the end of the time interval given in Eqn 6.14) at constant volume. Computationally this was followed by an isentropic expansion of the burnt charge and compression of the unburnt charge. The heat transfer rate from the unburnt charge during this period was calculated, and the temperature of the unburnt charge found.

6.4.2. Rate of Entrainment

The rate at which unburnt charge was subsequently entrained by the flame front was taken to be :-

$$\frac{dm_e}{dt} = \rho_u A_f u_e \quad (6.15)$$

where A_f is the instantaneous flame area and u_e is the entrainment velocity. This was taken as being equal to the turbulent burning velocity (u_t) calculated on the various bases discussed previously.

In the program the rate of entrainment was considered in incremental fashion. Shown in Fig. 6.2 is a flame in position (1), at a given time interval (t_i) after ignition; the flame growth was assumed to be spherical. At time $t_i + \Delta t_i$ the flame would have moved forward by a distance $u_i \Delta t_i$, and a volume ΔV_i would have been entrained.

The volume entrained at a given flame radius can be found from geometrical considerations (Appendix C) and hence :-

$$\Delta V_i = V(r_i + u_i \Delta t_i) - V(r_i) \quad (6.16)$$

The mass entrained during this increment was therefore given by :-

$$\Delta m_{b_i} = \rho_{u_i} \Delta V_i \quad (6.17)$$

Some of this mass entrained would burn during this increment, together with mass entrained during previous increments.

After burning it would expand, compressing the burnt and unburnt regions; this process was considered to be isentropic and resulted in the flame front moving forward (to (2) - Fig. 6.2). The distance moved can be defined as $u_{g_i} \Delta t_i$, where u_{g_i} is the unburnt gas velocity ahead of the flame front.

At the end of each increment values of u_i and τ_b were re-calculated.

6.4.3. Rate of Burning

Once entrained, the unburnt charge was assumed to burn at an exponential rate (as described by Blizzard and Keck). The mass burnt at a given time (t) after ignition was given by:-

$$m_b = \int_0^t \left[1 - e^{-(t-t')/\tau} \right] \rho_u A_f u_e dt' \quad (6.18)$$

where t' was the time after entrainment. The process was considered computationally in an incremental manner; if $\Delta m_e(i)$ is the mass entrained in the i th increment of time interval Δt , and, at the end of the increment the time after entrainment is taken as $\frac{1}{2}\Delta t$ then the total mass burnt (at the end of the increment) would be given by:-

$$m_b(i) = m_e(i) - \sum_{j=1}^i \Delta m_e(j) \times \exp \left[-(i-j+\frac{1}{2}) \frac{\Delta t}{\tau} \right] \quad (6.19)$$

The mass burnt in the increment was therefore given by:-

$$\Delta m_b(i) = m_b(i) - m_b(i-1) \quad (6.20)$$

Once the quantity of mass burned was evaluated, the numerical procedure was identical to that described previously for the empirical rate model. The mass was considered to be burned instantaneously at constant volume, then allowed to expand, compressing the 'old' burnt charge and unburnt charge. The burnt regions were mixed (the unburnt charge

behind and in front of the flame front was treated as one region for the purposes of pressure equalisation). Heat transfer was considered and pollutant concentrations were then calculated. The process was repeated until the enflamed volume was greater than 99% of the total cylinder volume. Any remaining unburnt charge at this time was then assumed to have been entrained; burning of this residual was considered numerically in one degree increments. The mass burnt in each increment was calculated as above. The process was repeated until 99% of the charge (by mass) was burnt.

After each increment of burning the appropriate values of the turbulence parameters and the burning velocities were calculated, on the basis of the new pressure and temperature.

6.5. RESULTS AND DISCUSSION

The effect of equivalence ratio on laminar burning velocity for each of the methods of calculation used, is plotted in Fig. 6.3. The first two graphs (a & b) are for low pressure and temperature (the conditions at which most of the measurements were taken); the second pair (c & d) are for higher temperature and pressure, more typical of engine conditions.

Ryan and Lestz conducted their measurements at 6 atmospheres pressure (Fig.6.3b); their results are in reasonable agreement with other workers at that pressure. However their equation for extrapolation (to other pressures and temperatures) gives unreasonable results at the other conditions shown; in particular one may note burning velocities higher with leaner mixtures at atmospheric pressure and no burning velocity at mixtures leaner than 0.8 at engine conditions. The experimental formula given by these workers has constants for equivalence ratios 0.85, 1.0, 1.15; for other equivalence ratios the burning velocity was found by fitting a quadratic equation to the velocities at the three given equivalence ratios, at the required temperature and pressure. This is obviously inadequate for extrapolating to leaner mixtures at typical engine conditions. The equation of Van Tiggelen and Deckers is a theoretical expression; at low pressures it gives burning velocities very much higher than experimental values, and at engine conditions it still gives values which are considerably higher.

Data from Leeds was only available at atmospheric pressure. It was extrapolated using the expressions of Keck and Gulder, to show the effect of the different laws of extrapolation. Using Keck's expression gave a much higher temperature dependence than that of Gulder; this led to much higher predicted burning velocities. Keck's expression also allowed for differing temperature effects on burning velocities at different equivalence ratios.

The experimental measurements taken by Babkin et al, and Metghalachi and Keck, were for a wide range of pressure and temperature. (323-650K, 6-60atm and 4-40atm respectively). The equations for extrapolation given by these two groups are therefore likely

to be the most accurate. Babkin, however, only investigated stoichiometric mixtures. (In the model, for other mixtures the variation with equivalence ratio was assumed to occur in the same proportions as that observed in the Leeds data.)

When the various expressions were used to predict burning velocities at temperatures and pressures likely to be found in engines, there was a considerable difference in the values predicted (Figs. 8.3c and d). This very large difference could lead to considerable errors in model predictions if the method chosen is not the most accurate.

Shown in Figs. 6.4 & 6.5 are model output data using the seven different expressions for laminar burning velocity incorporated into the Damköhler expression for turbulent burning velocity (This expression has been used for illustrative purposes, similar conclusions about the most valid laminar burning velocity data resulted when alternative turbulent burning velocity expressions were used). The model is based on the dimensions of the Ruston engine described in Chapter 3. Adoption of the Van Tiggelen and Deckers theory results in far higher burn rates and much higher peak pressure than the other methods. The effect on temperature with each of the other methods is small, so variations in predicted burning velocity are clearly more associated with the extrapolation of laminar burning velocity data with pressure rather than with temperature. Babkin's experimental data was obtained over the largest range of pressures (6-60 atm) of any of the methods; however, it only applied to stoichiometric mixtures. The expression given by Metghalachi and Keck gave values in reasonable agreement with Babkin (at stoichiometric mixture) at typical engine conditions. The former data were based on experimental pressures in the range 4-40 atm; the data have also been used by Tabaczynski (Milane et al, 1983) in engine models. The Keck values were therefore adopted in the computations described below. More data on the effect of pressure on laminar burning velocity are obviously required. Such effects may be difficult to measure, as the flame may not be truly laminar at high pressures; the large density gradients across the flame front are likely to generate considerable turbulence.

The effect of using the different methods of calculation of flame speed ratio is illustrated in Figs. 6.6 & 6.7. When the unburnt gas velocity ahead of the flame front was used to calculate the turbulent burning velocity (i.e. method (ii) in section 6.3.2), very high flame propagation rates resulted. The computed rate of pressure rise and flame speed proved very much faster than observed experimentally; the use of this method was therefore discontinued. Use of the other three methods described in section 6.3.2 gave basically similar trends. The flame speed ratio correlation (iii), of Groff and Matekunas, gave the fastest combustion rate; while (iv), that of Hamid, produced the slowest. The pressure trace resultant with the wrinkled flame method (i) gave values closest to those found experimentally; however, further comparisons are necessary before dismissing the other two

methods, since they could be made to agree with experimental cycles by a suitable choice of the constant used in the estimation of the turbulence intensity at ignition.

6.5.1. Some Comparisons With Experimental Results (Ruston Engine).

Shown in Fig. 6.8 are the I.M.E.P., maximum pressure and crank angle at which maximum pressure occurred, together with the crank angle when the enflamed area was 90% of the cylinder bore area, plotted against equivalence ratio. In each case the results using the four different flame speed ratio methods are shown, together with the average experimental values (and the range found in the experiments). The experimental conditions were for the optimum spark advance found experimentally; the model tests were also conducted using this spark advance.

The I.M.E.P. was lower in the experimental tests than predicted by the model using any of the methods. As previously mentioned, the Ruston engine had a gasket to cut off the valve chamber close to TDC. It is likely that a considerable quantity of fuel air mixture would be pushed into this chamber during compression (and the early stages of combustion); this would subsequently burn late in the expansion stroke and would therefore give a lower contribution to the I.M.E.P.

In general the effect of equivalence ratio on peak pressure shown by each of the methods was in reasonable qualitative agreement with the experimental observations. The best quantitative agreement was obtained using the wrinkled flame model (method (i)). However, the crank angle at which peak pressure occurred was overpredicted by this method; the correlation of Groff and Matekunas (method (iii)) gave a closer prediction. The fourth method (using correlations developed at Leeds) gave the best agreement with the crank angle where the enflamed area reached 90% of the cylinder bore area (although this method could not be used for the leanest (0.8) equivalence ratio as the value of u'/u_i for this condition was beyond the range of the correlation). The inability of any of the methods to correctly predict more than one of the above variables suggests that the flame propagation and burning rates predicted by the model are inaccurate. If the flame propagation rate was predicted correctly, then the peak pressure would be too low, and occur too late in the cycle, whichever turbulent flame speed model were used.

The flame propagation rate predicted by the model (using the wrinkled flame method (i)) is shown in Fig. 6.9 together with experimental measurements. For the richer mixture the optimum spark advance predicted by the model (37 degrees) did not agree with that found experimentally (24 degrees); curves are shown for model predictions using both values. In both cases the flame propagation rate predicted by the model was too slow in the later stages. This could be due to the unburnt charge ahead of the flame front being pushed

into the valve chamber; this would allow the burnt charge behind the flame to expand at a greater rate, and hence lead to increased flame velocity. This problem should not occur when modelling the Yamaha engine. For the weaker mixture the agreement was reasonable (compared with that using Weibe function - Fig. 5.16). The shape of the curve is, however, not accurate. The model underpredicts the flame growth in the early stages, and overpredicts in the later stages. This suggests that the experimental expression used to allow for the development of a turbulent flame (Eqn. 6.6) did not give a true representation of the process. Very recent work at Leeds by Bradley and his co-workers (Abdel-Gayed et al, 1986c) has produced an improved expression for the development process; this would give higher values in the initial stages of burning. Work is currently in progress to incorporate this expression in the model.

6.5.2. Comparison With Experimental Results (Yamaha Engine)

Experimental results from the Yamaha engine showed the peak pressure to be lower than it was, at the same operating conditions, in the Ruston engine. In Chapter 4, it was suggested that lower turbulence intensity (*vis à vis* that of the Ruston) was responsible for this effect. Since no measurements of turbulence in a two-stroke engine were available, a number of tests were performed with the model (using differing constants of proportionality to determine turbulence intensity at ignition) in an attempt to identify a turbulence level that would yield results close to the experimental ones. Shown in Figs. 6.10 and 6.11 are the model predictions (at varying levels of turbulence at ignition, defined in terms of mean piston speed S_p) compared to experimental results for side and central ignition respectively. In all cases the trends predicted by the model were reasonably good; quantitative agreement was not so good. In general, the model underpredicted the peak pressure with side ignition, and overpredicted the power output with central ignition. The best agreement was probably that with a value of 0.8 for the constant K_i (compared with 1.1 used in the Ruston engine). Experimental measurements of turbulent intensity in this engine would be very useful in order to verify if this was the cause of the discrepancy between the results from the two engines.

6.5.3. Effect of EGR

The computations using the model have shown that it can be used to predict, qualitatively, the effect of varying operating parameters. However, more detailed investigation is required before accurate quantitative predictions are possible. In response to a request from staff at B.L. Technology, the model was used in an attempt to predict the effect of exhaust gas recirculation on fuel economy and emissions. Shown in Fig. 6.12 is the predicted specific NO emissions plotted against fuel economy for varying air-fuel ratio without EGR; also

shown is the effect of dilution with EGR on a stoichiometric mixture. When a stoichiometric mixture was allowed to be diluted with air, the model predicted that fuel economy would be improved, whilst NO emissions would increase; due to the excess oxygen available. Further dilution with air would reduce the peak temperature and pressure; modelled emissions of NO were therefore reduced. At very lean mixtures the fuel consumption was shown to increase rapidly; this was due to inefficient combustion, partial quenching and misfire. (This phenomena was only shown when the flame speed ratio correlation of Hamid (Section 6.3.2, method (iv)) was employed in the model, since this method was the only one to predict a reduction in flame speed ratio at very high values of u'/u_1 (Fig. 6.1)). If the initial stoichiometric mixture was assumed to be diluted with inert exhaust gas instead of air, then modelled emissions of NO fell; the reduction in temperature, associated with dilution, would reduce the amount of dissociation and inhibit NO reactions. Predicted fuel economy was little affected as the mixture was still stoichiometric; the same quantity of fuel was therefore required to give the same power output. For high concentrations of EGR, the fuel consumption was shown to increase rapidly, in a manner similar to that for lean mixtures. The reason for this is, again, inefficient burning and partial quenching of the flame. This behaviour was in accord with the experimental experience of B.L. Technology (private communication).

6.6. CONCLUDING REMARKS

The burning velocity approach to modelling of progressive combustion in an engine has been shown to be a superior to more simplistic empirical methods. The combustion duration can be determined by the model; this allows the model to be used to predict the effect of parameters (such as equivalence ratio) which have a large effect on combustion duration. The following conclusions can be drawn from computations performed with the model reported here:

- (1) The computation of turbulence levels within the engine was rather primitive; this required a constant of proportionality to define the turbulence at ignition. Although a more complex turbulence model would be required, if the model were to be used to predict performance from new engine designs, insufficient time was available to develop this in the work currently reported here. The simple model used proved adequate for the work reported here; i.e. to qualitatively study the effect of turbulence on combustion. Measurements of turbulence in the cylinder would, however, be useful to validate the values used.
- (2) The heat transfer computation was also very simplified. Measurements of wall temperatures and exhaust gas temperature would be useful to validate the constants

used in the heat transfer expressions.

- (3) Once the constants in the model were determined, qualitative predictions by the model were reasonable. Good quantitative predictions of pressure and flame speed were possible, but not simultaneously. A possible reason for this was the inadequacy of the experimental law used to predict the effect of flame development. Recent work at Leeds has led to a revised expression; work is currently in progress to incorporate this expression into the model.
- (4) Further work is necessary to adapt the model to predict performance of the Yamaha engine. Since this engine does not have a valve chamber, model predictions of flame propagation and pressure rise should be more accurate than with the Ruston engine (with its valve chamber problems).
- (5) Further experimental data for the effect of pressure on laminar burning velocity is needed. The data values available in the literature vary considerably; uncertainties in the values assumed inhibit the validation of the (more complex) turbulent combustion model.

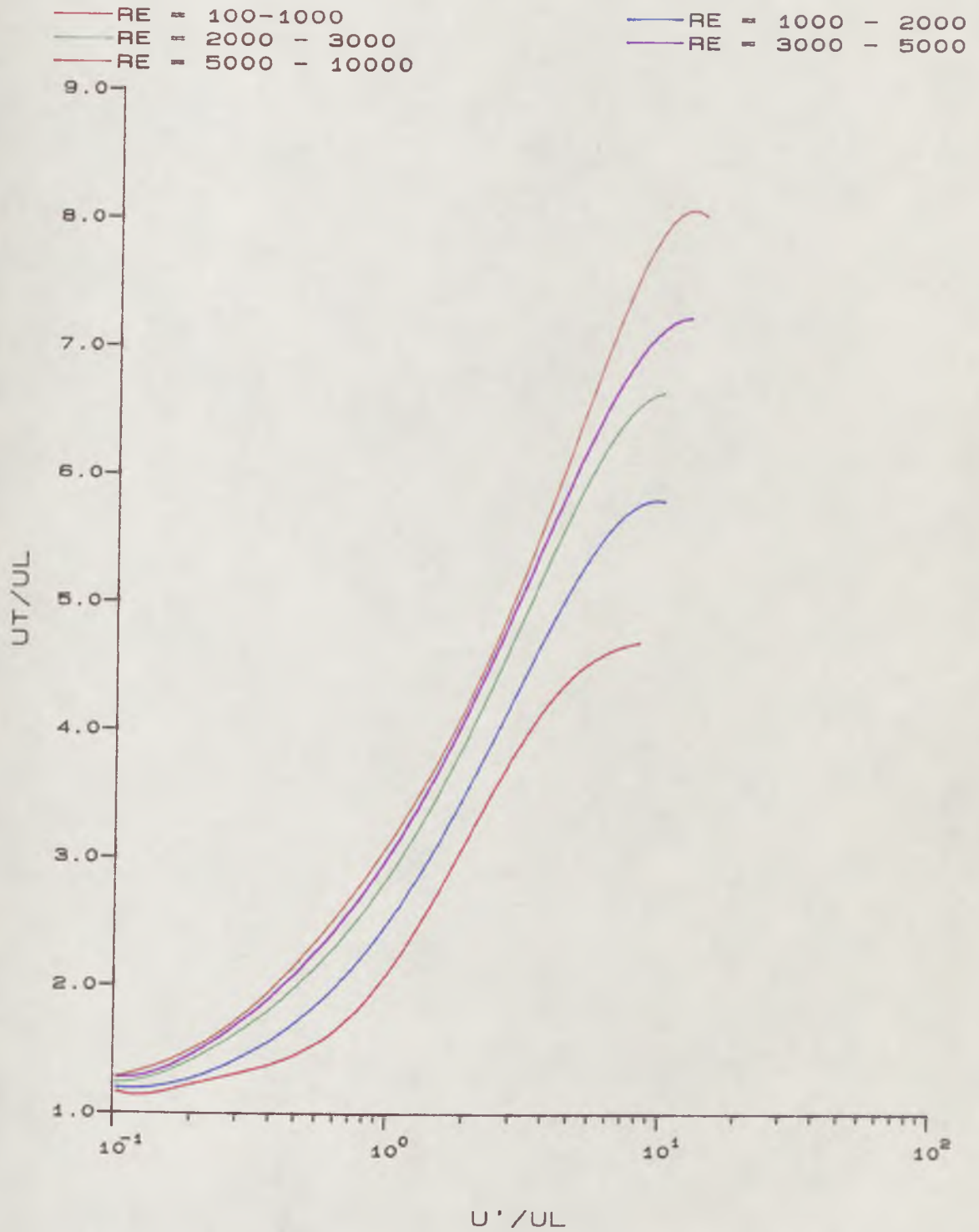


Fig. 6.1

Effect of Laminar Burning Velocity and Reynolds number on Flame Speed Ratio (For High Lewis numbers)

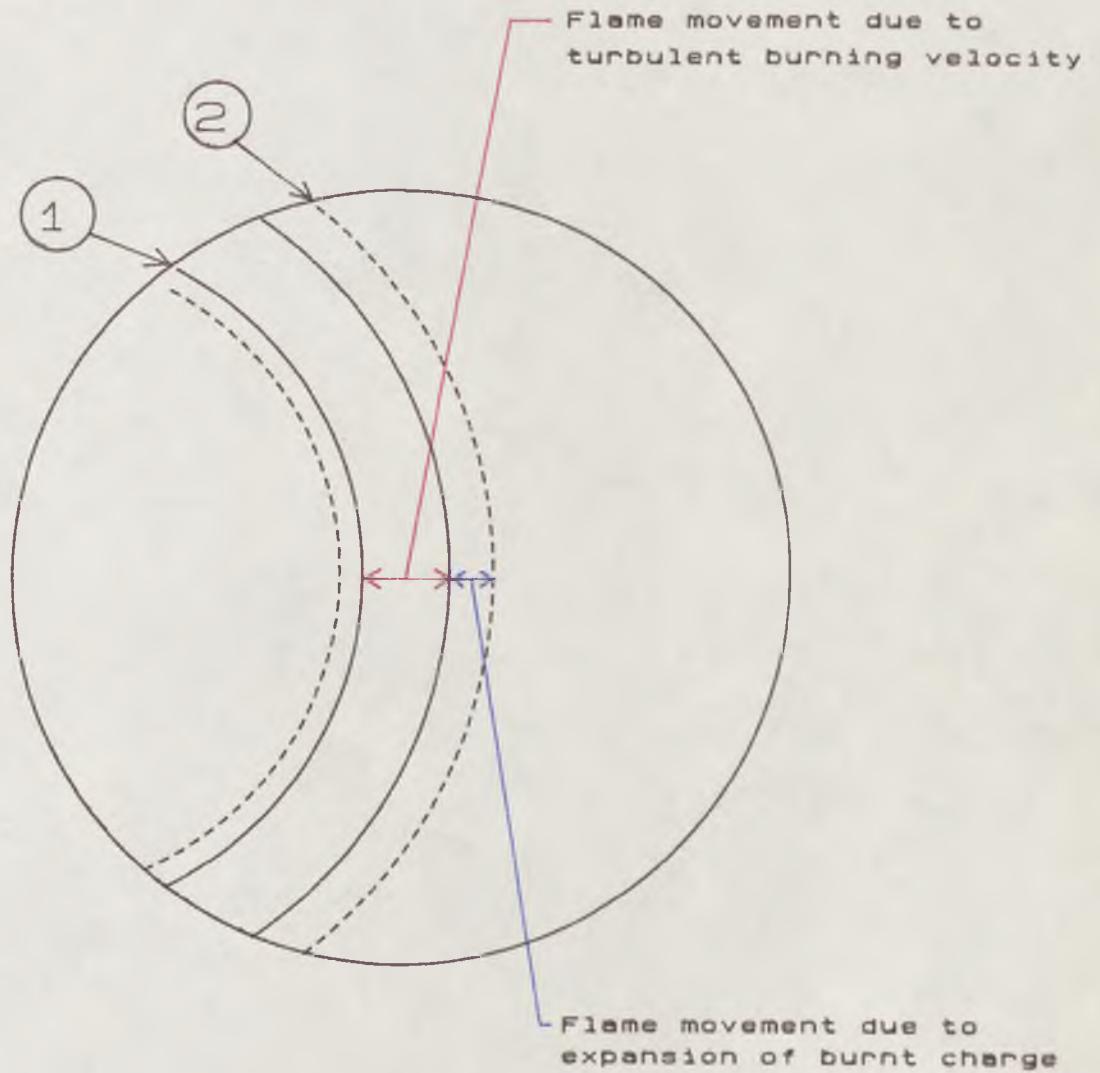


Fig.6.2

Contribution of burning velocity and burnt charge expansion to flame movement

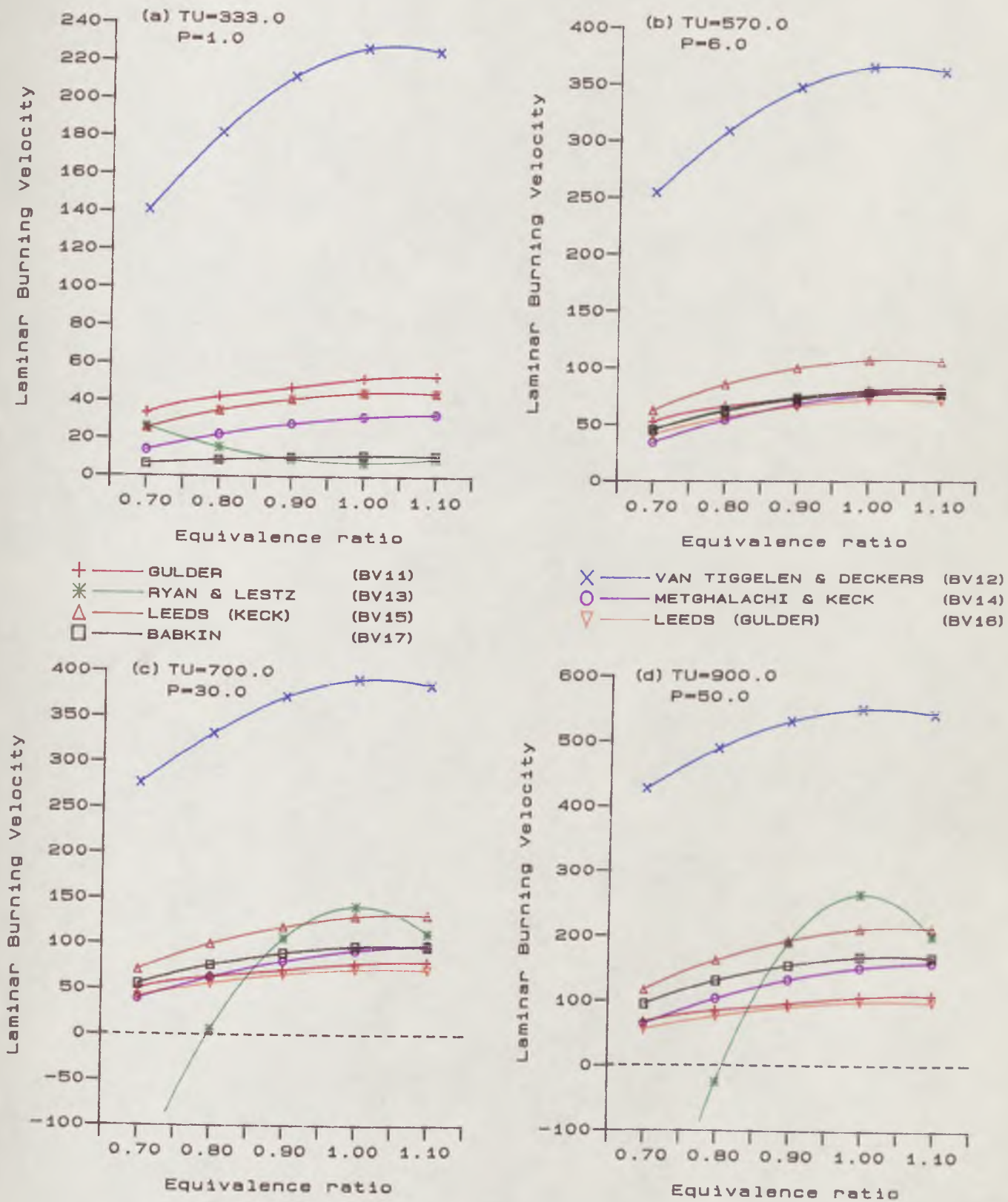
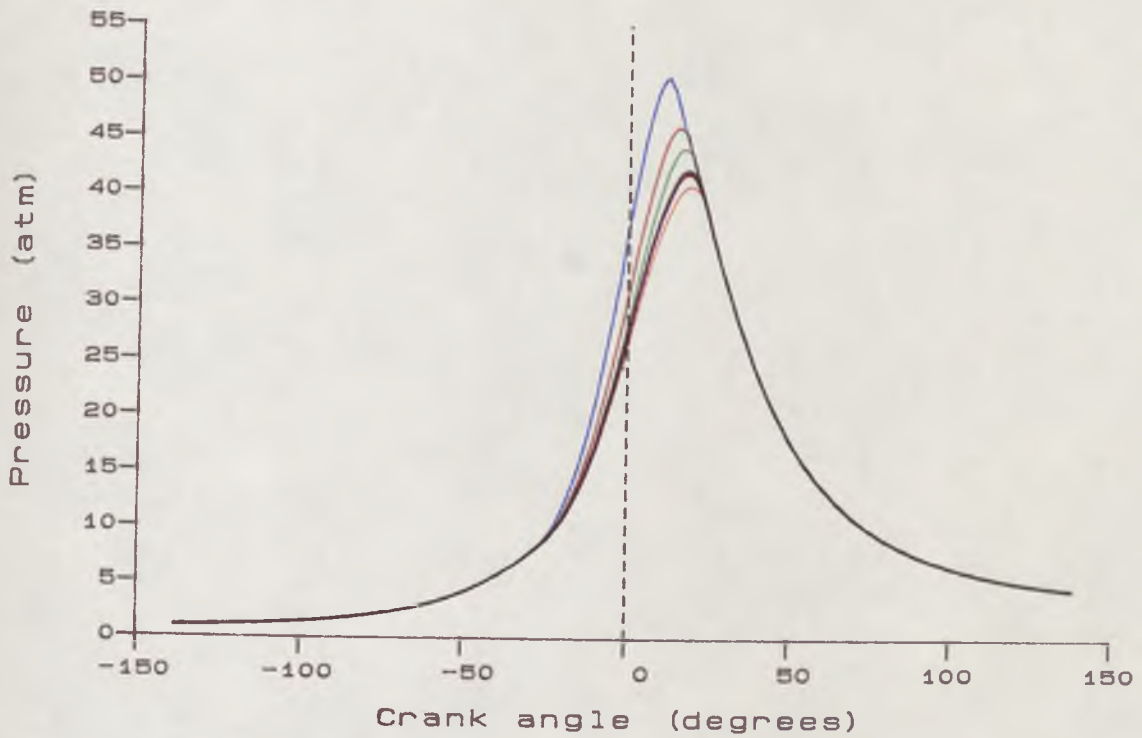
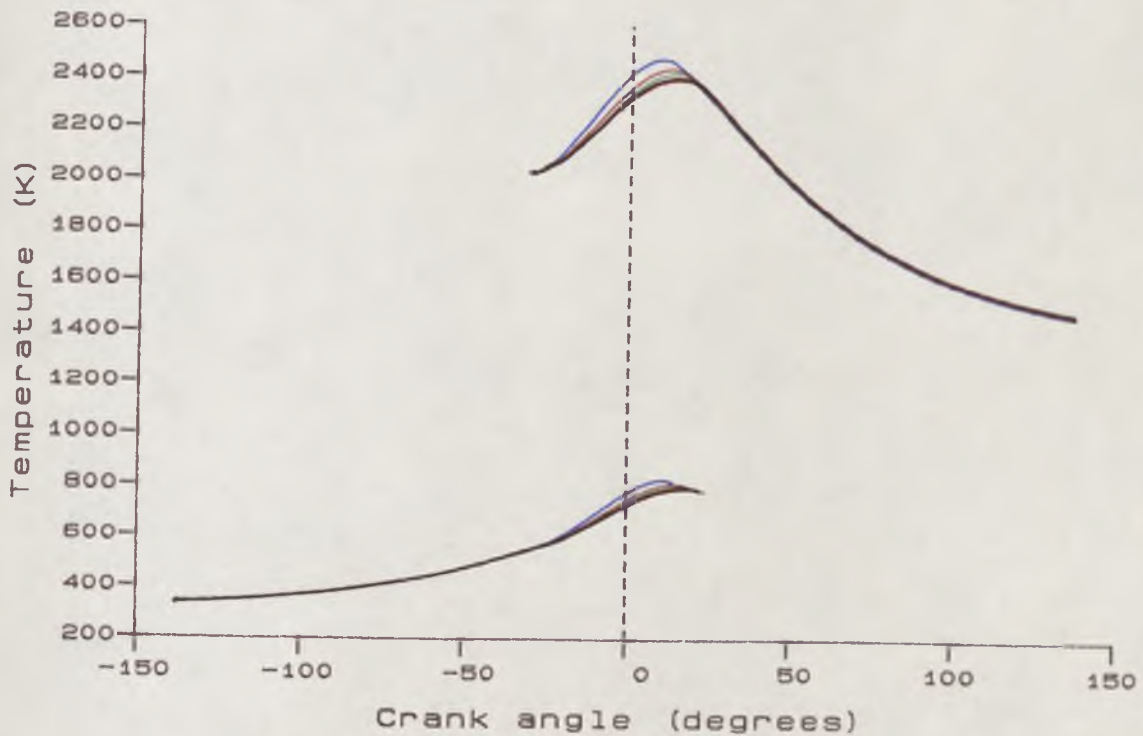


Fig.6.3
Comparison of laminar burning velocity correlations given by different workers.

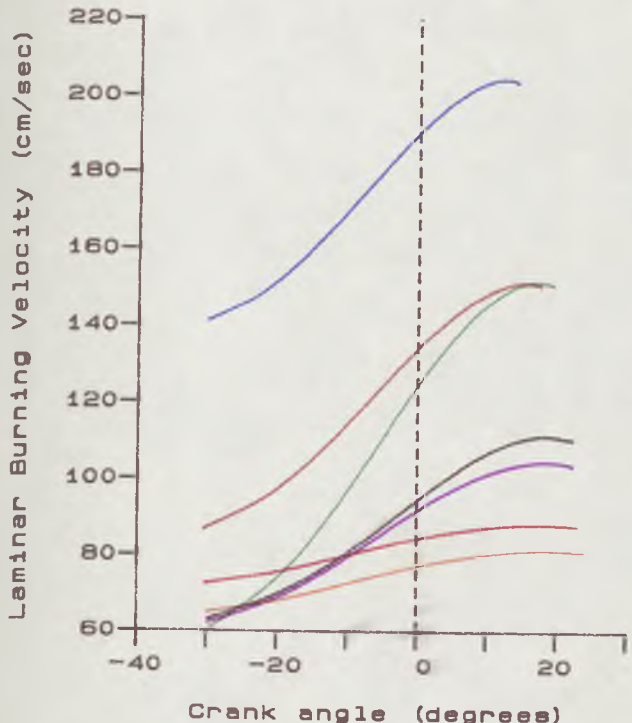


— BV11 (GULDER) CDR=54.9	— BV12 (V.T & D) CDR=46.0
— BV13 (R & L) CDR=51.4	— BV14 (M & K) CDR=54.2
— BV15 (LDS K) CDR=49.6	— BV16 (LDS G) CDR=56.1
— BV17 (BABKIN) CDR=54.2	

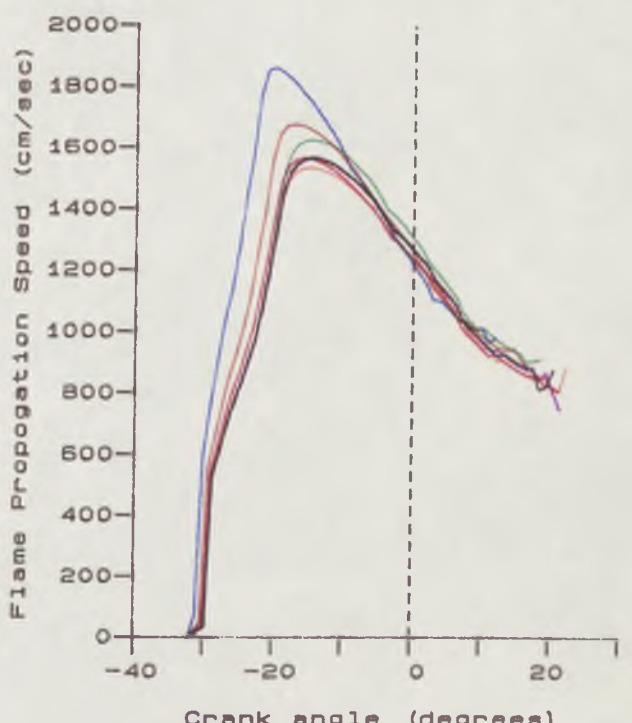


SINGLE CHAMBER (SIDE)	MANIFOLD PRESSURE = 1.00
COMPRESSION RATIO = 8.0	FUEL BP-4STAR
EQUIVALENCE RATIO = 1.00	ENGINE SPEED = 1400 rpm
OPTIMUM SPARK ADVANCE (32.0)	

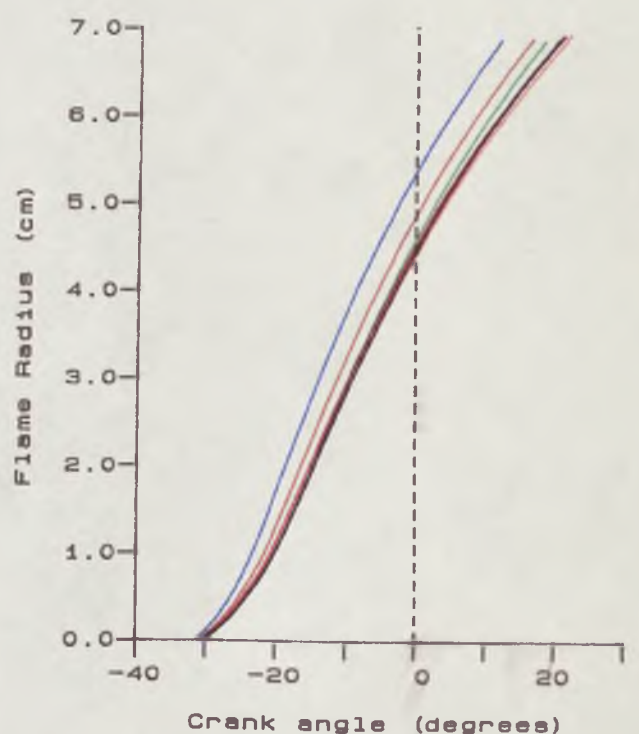
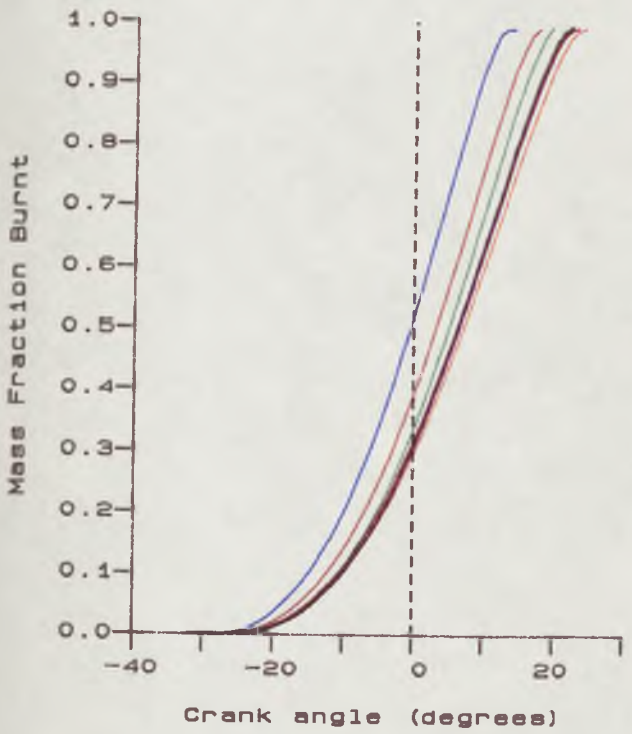
Fig.6.4 Effect of Laminar Burning Velocity



- BV11 (GULDER) CDR=54.9
- BV13 (R & L) CDR=51.4
- BV15 (LDS K) CDR=49.6
- BV17 (BABKIN) CDR=54.2



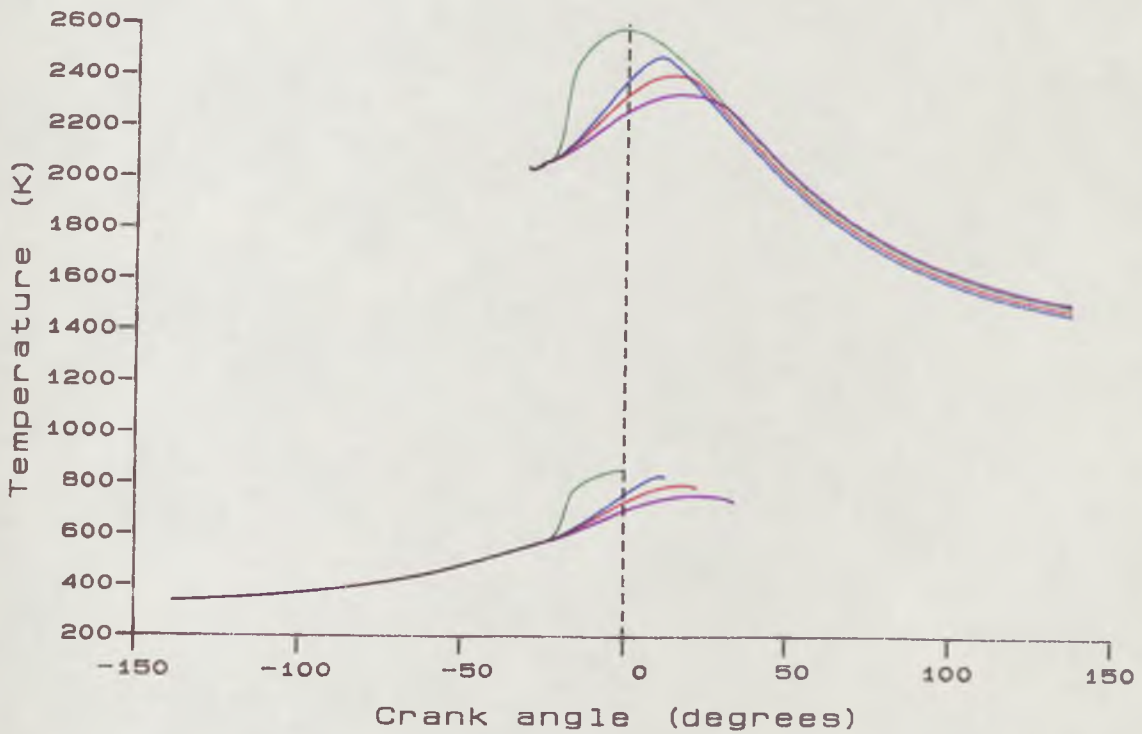
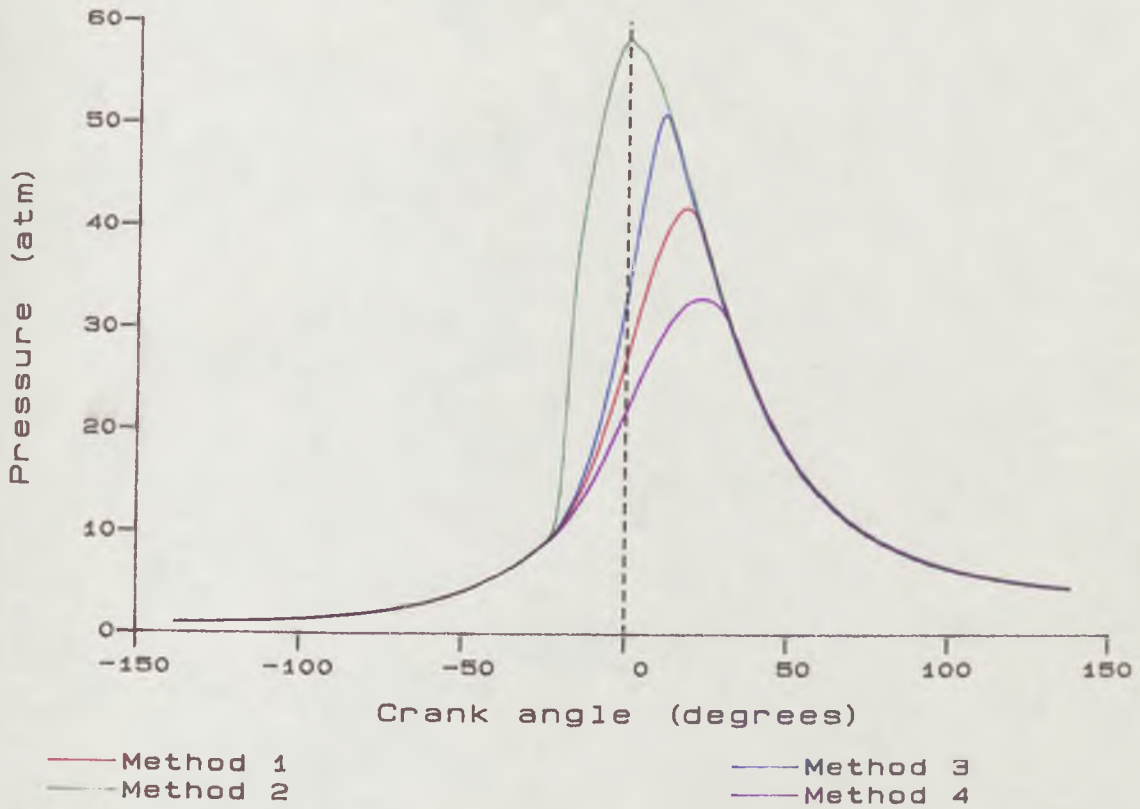
- BV12 (V.T & D) CDR=46.0
- BV14 (M & K) CDR=54.2
- BV16 (LDS G) CDR=56.1



SINGLE CHAMBER (SIDE)
 COMPRESSION RATIO = 8.0
 EQUIVALENCE RATIO = 1.00
 OPTIMUM SPARK ADVANCE (32.0)

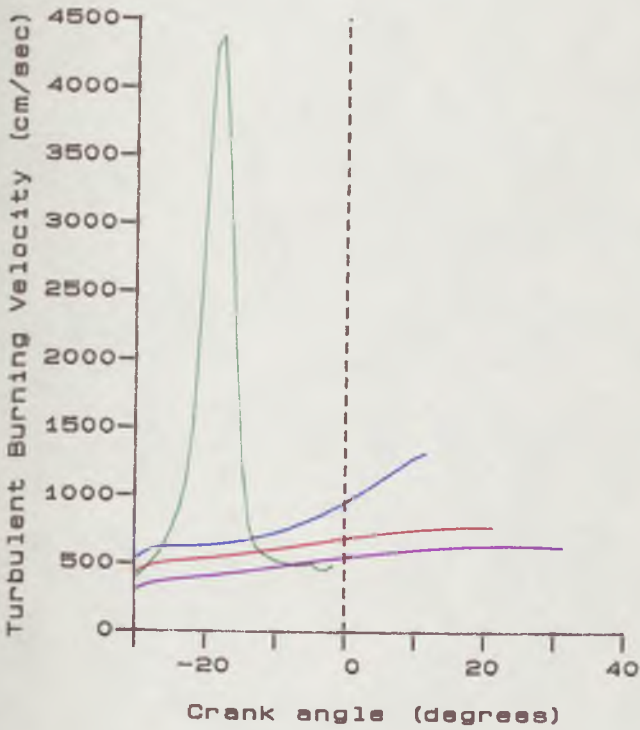
MANIFOLD PRESSURE = 1.00
 FUEL BP-4STAR
 ENGINE SPEED = 1400 rpm

Fig.6.5 Effect of Laminar Burning Velocity

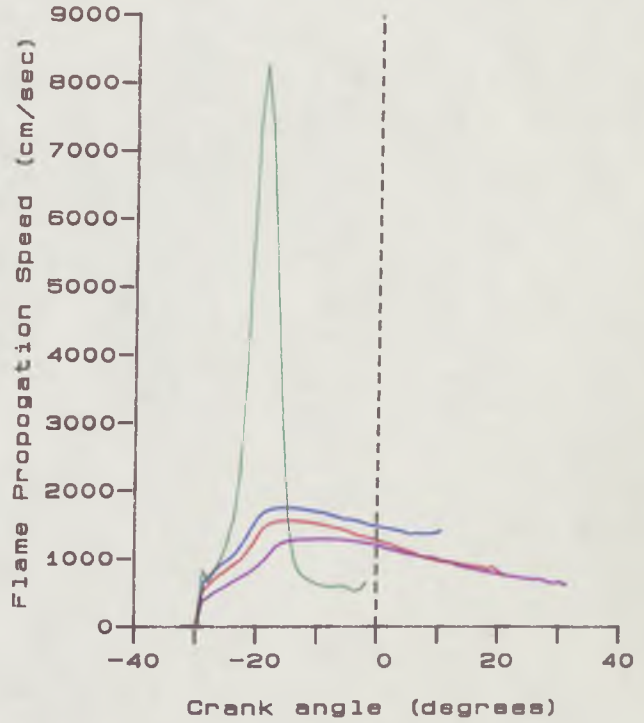


SINGLE CHAMBER (SIDE)	MANIFOLD PRESSURE = 1.00
COMPRESSION RATIO = 8.0	FUEL BP-4STAR
EQUIVALENCE RATIO = 1.00	ENGINE SPEED = 1400 rpm
SPARK ADVANCE = 32.0	

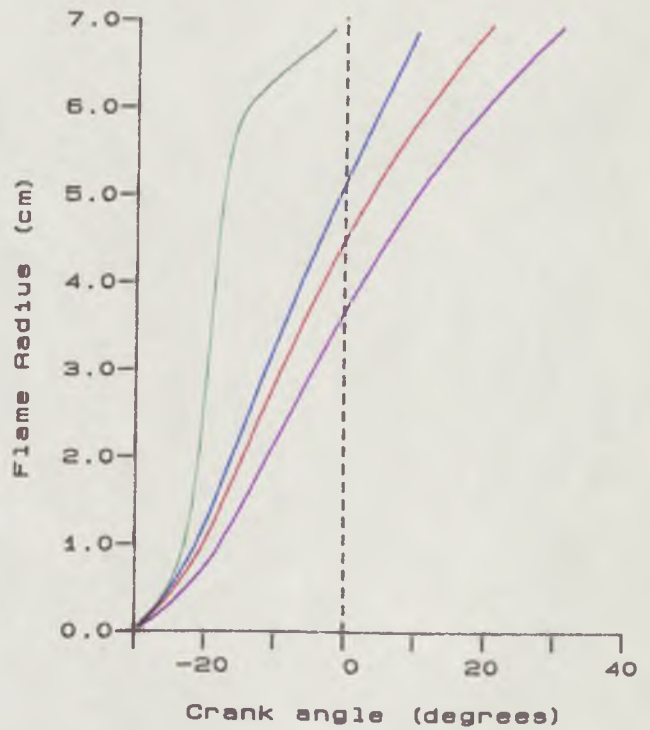
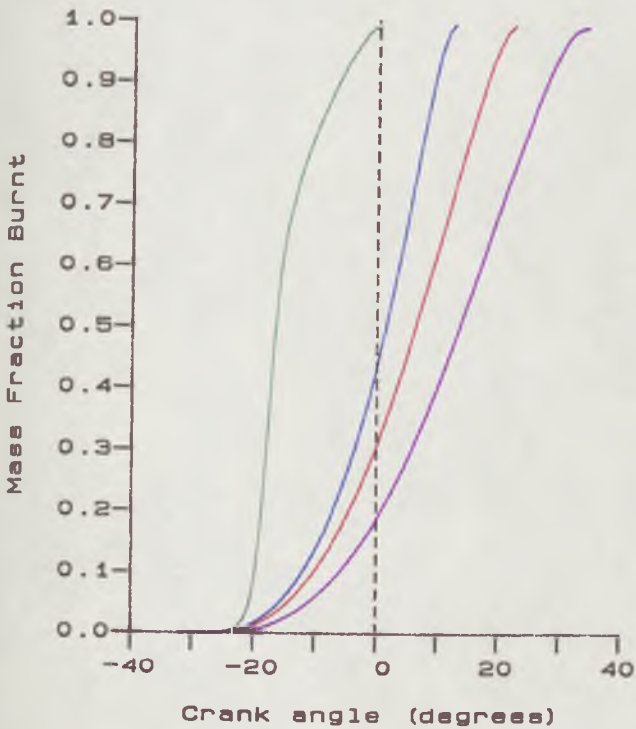
Fig.6.6 Effect of Varying Flame Speed Ratio



Method 1
Method 2



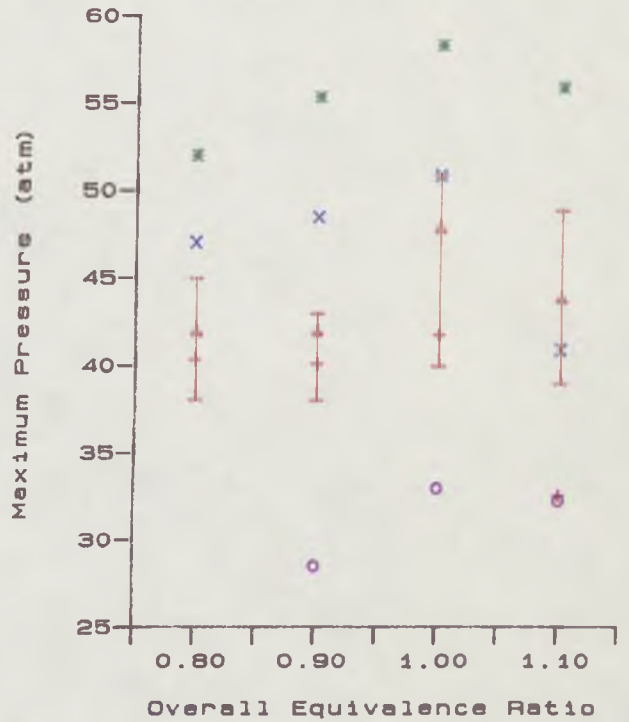
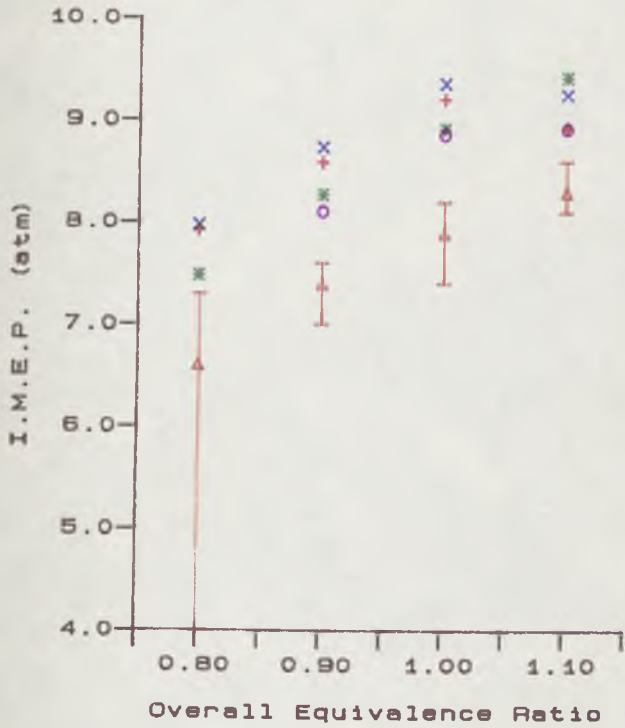
Method 3
Method 4



SINGLE CHAMBER (SIDE)
COMPRESSION RATIO = 8.0
EQUIVALENCE RATIO = 1.00
SPARK ADVANCE = 32.0

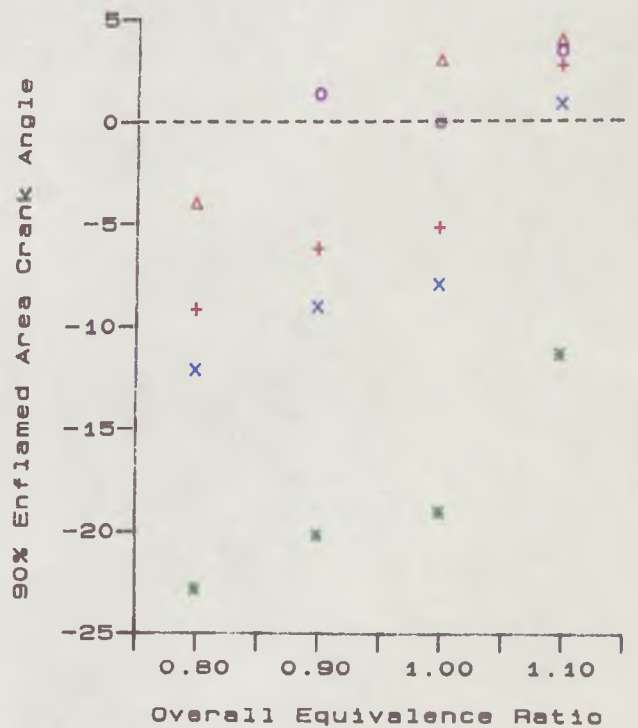
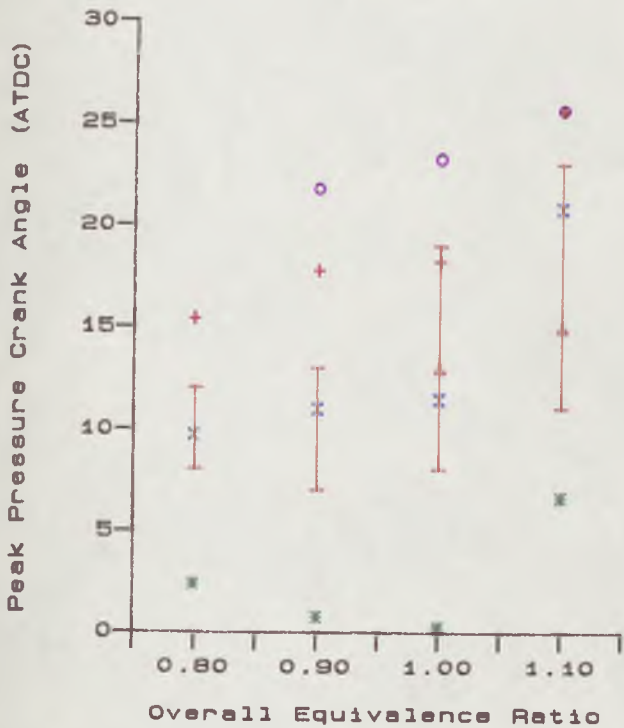
MANIFOLD PRESSURE = 1.00
FUEL BP-4STAR
ENGINE SPEED = 1400 rpm

Fig.6.7 Effect of Varying Flame Speed Ratio



+ Method 1
 * Method 2
 Δ experimental

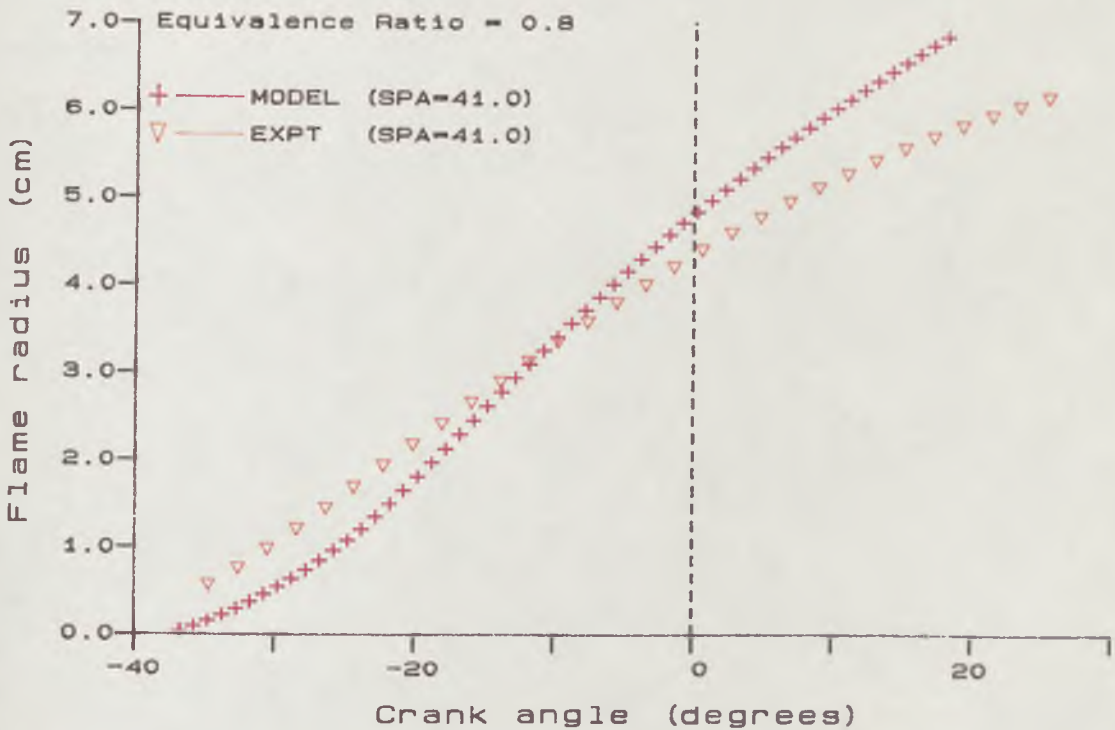
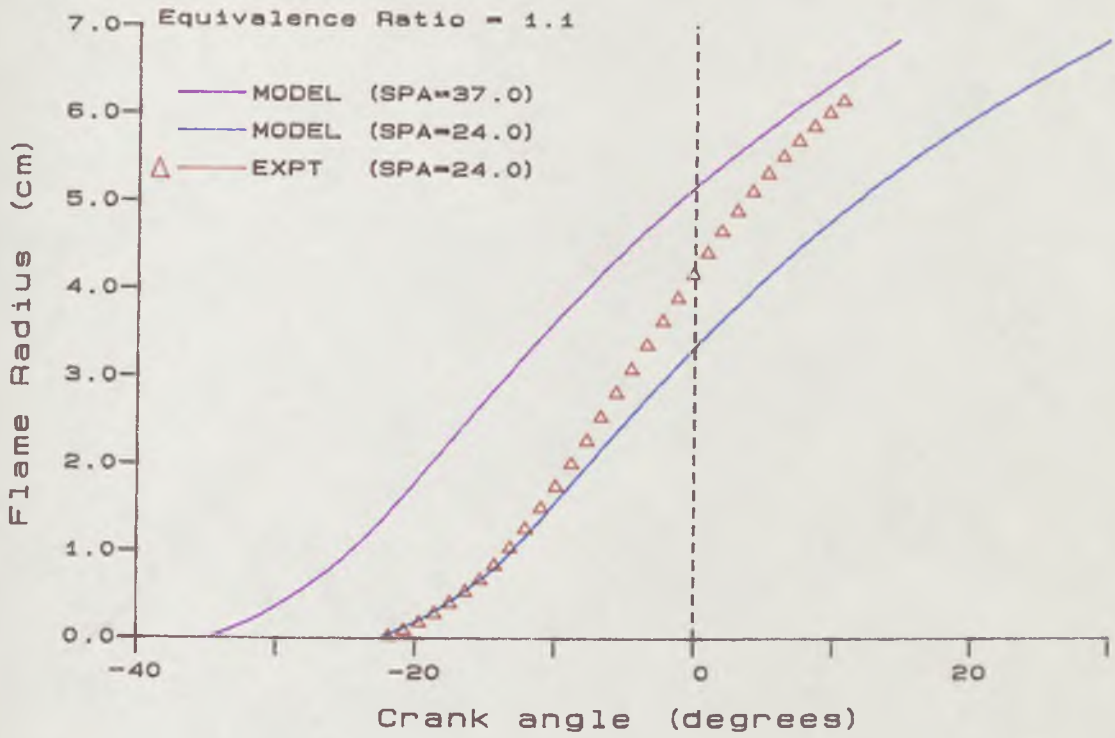
X Method 3
 O Method 4



SINGLE CHAMBER (SIDE)
 COMPRESSION RATIO = 8.0
 ENGINE SPEED = 1400 rpm

MANIFOLD PRESSURE = 1.00
 FUEL BP-4STAR
 OPTIMUM SPARK ADVANCE

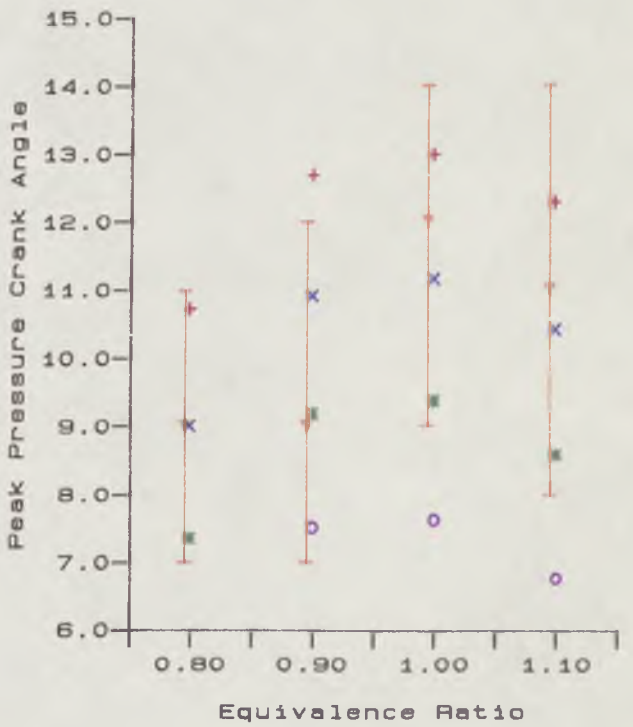
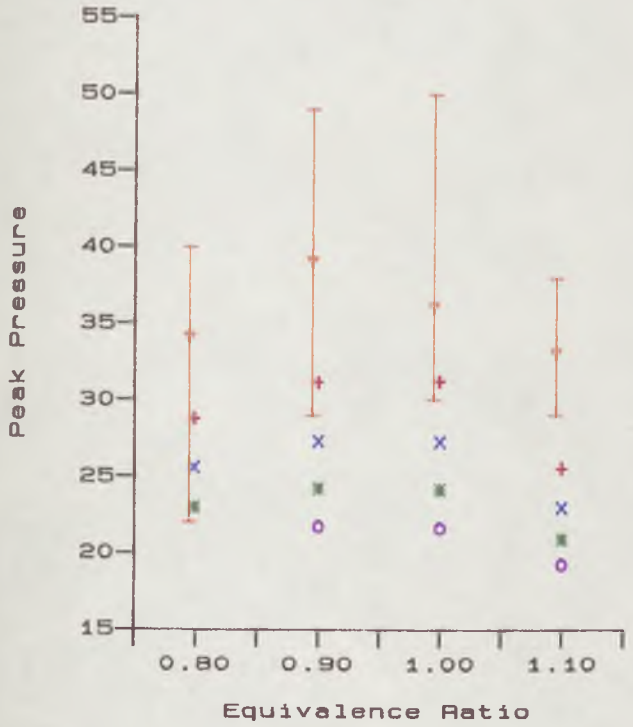
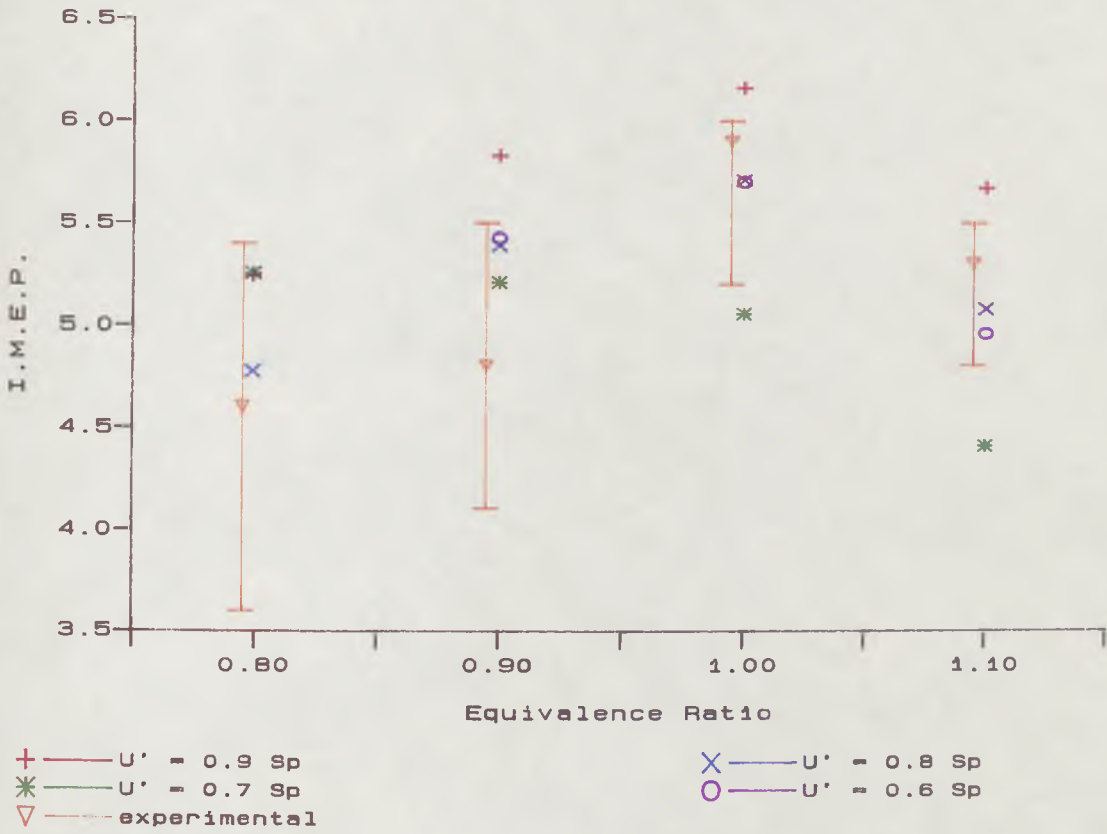
Fig.6.8 Effect of Varying Flame Speed Ratio



SINGLE CHAMBER (SIDE)
FUEL BP-4STAR
OPTIMUM SPARK ADVANCE

COMPRESSION RATIO = 8.0
ENGINE SPEED = 1400 rpm

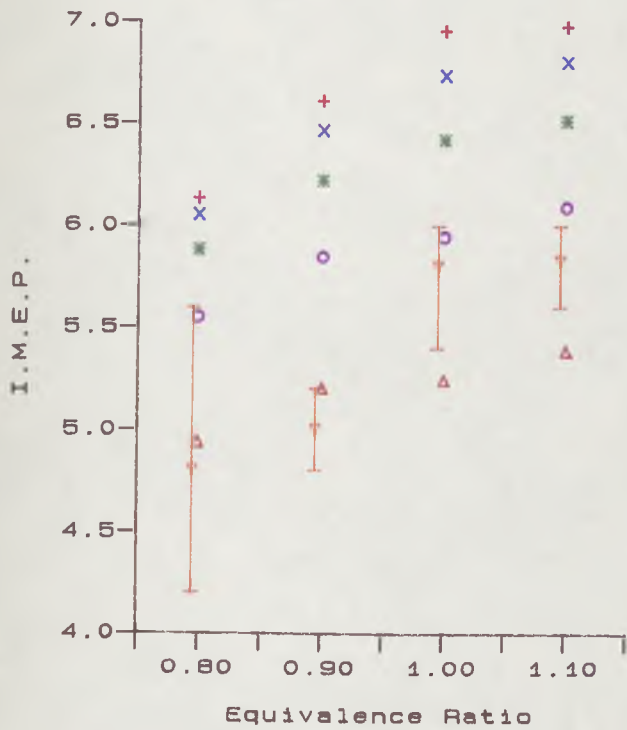
Fig.6.9 Comparison of Experimental
And Predicted Flame Radii



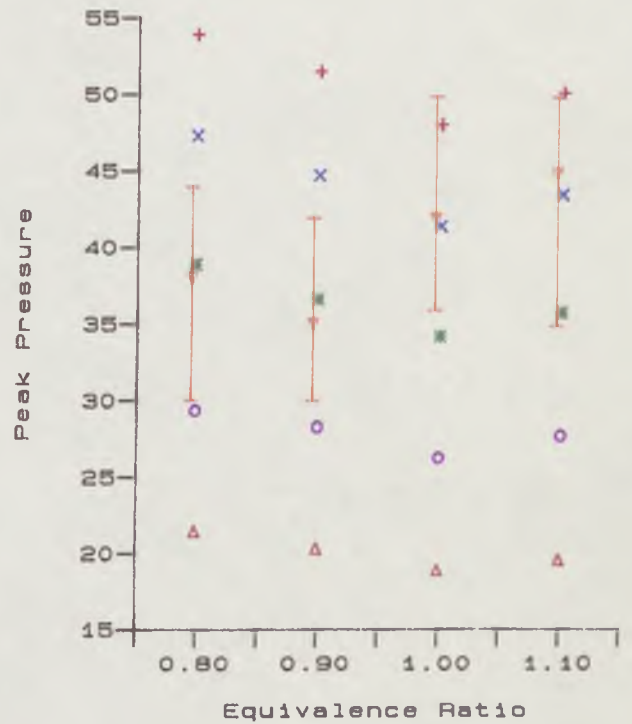
SIDE IGNITION
 OPTIMUM SPARK ADVANCE
 COMPRESSION RATIO = 8.0
 ENGINE SPEED = 1400

Fig. 6.10

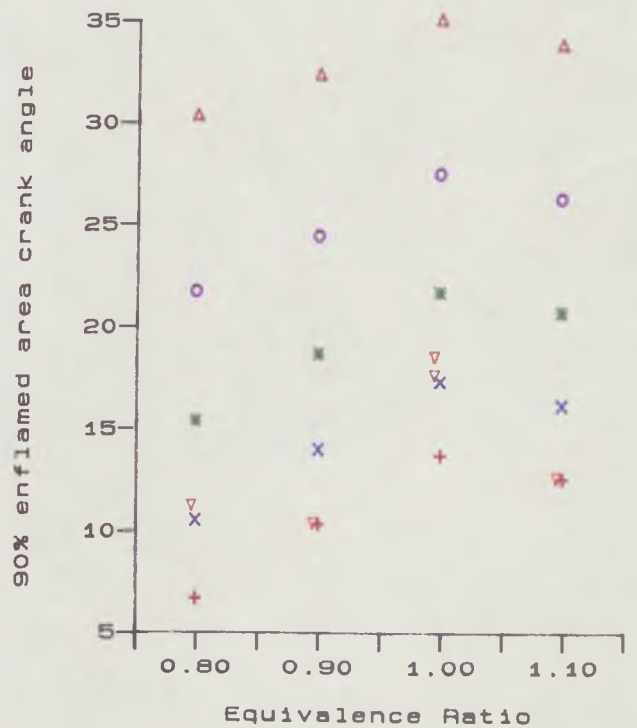
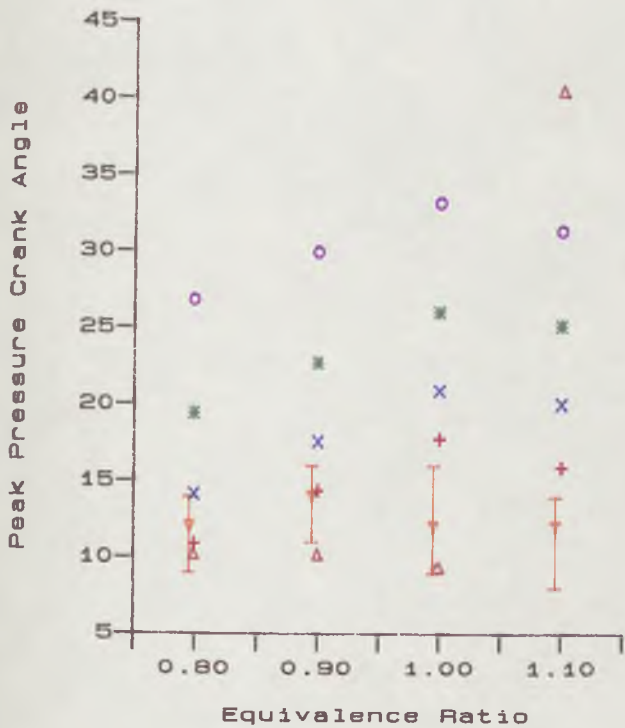
Effect of turbulence intensity at ignition on model predictions



+ — $U' = 0.9$ Sp
 * — $U' = 0.7$ Sp
 Δ — $U' = 0.5$ Sp



X — $U' = 0.8$ Sp
 O — $U' = 0.6$ Sp
 ▽ — experimental



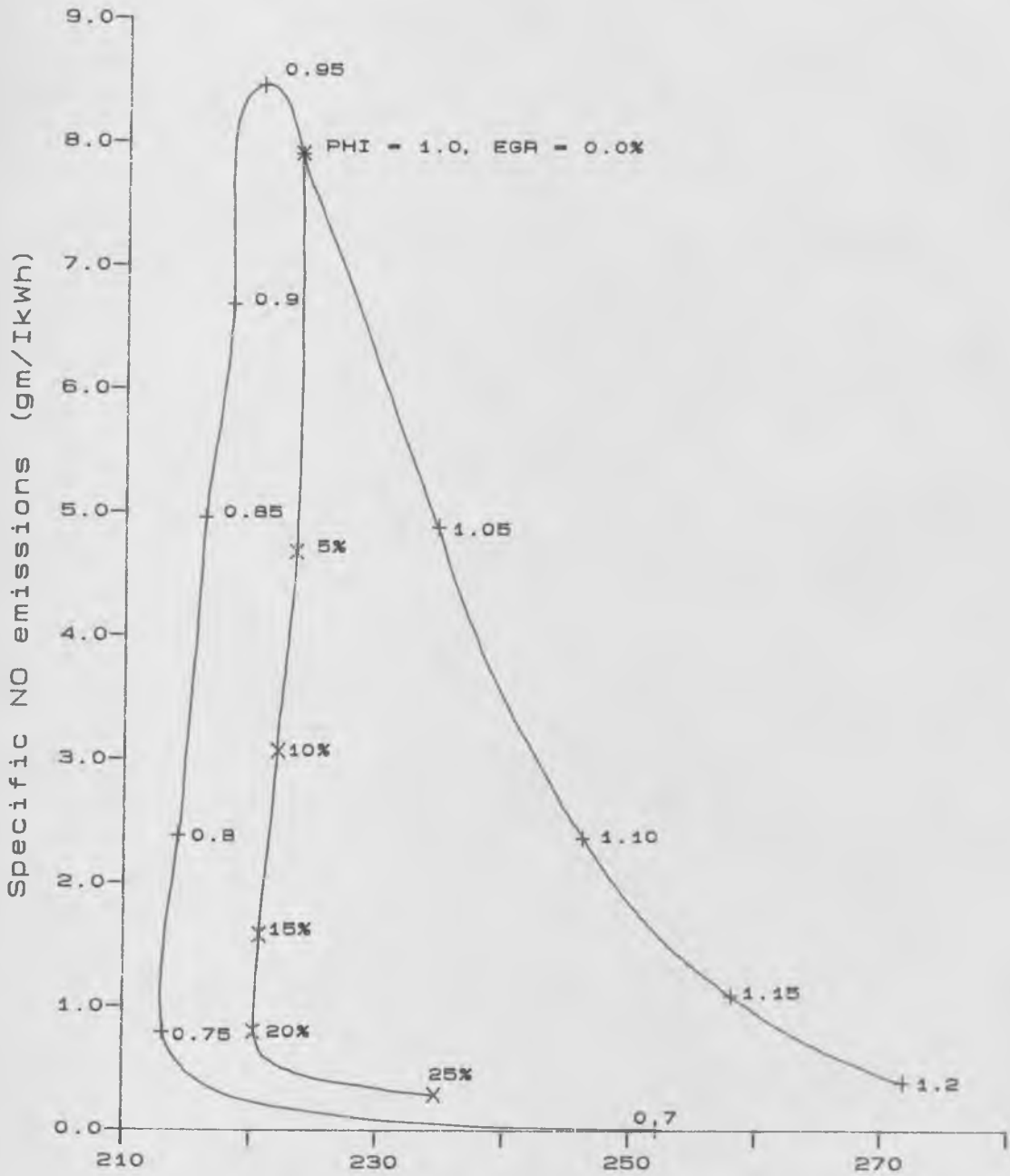
CENTRAL IGNITION
 OPTIMUM SPARK ADVANCE
 COMPRESSION RATIO = 8.0
 ENGINE SPEED = 1400

Fig. 6.11

Effect of turbulence intensity at ignition
 on model predictions

+ — Zero EGR

X — PHI = 1.0. varying EGR



Specific Fuel Consumption (gm/IkWh)

COMPRESSION RATIO = 10.5 SINGLE CHAMBER (CENTRAL)
MANIFOLD PRESSURE = 0.5 ENGINE SPEED = 1400 rpm

FIG.6.12

Effect of Dilution with Exhaust gas or air on NO emissions and fuel economy

CHAPTER 7

Divided Chamber Computer Model

CONTENTS

7.1	INTRODUCTION	157
7.2	COMPRESSION AND EXPANSION	158
7.3	COMBUSTION	160
	7.3.1 Instantaneous	160
	7.3.2 Burning Velocity Method	160
	7.3.2.1 Pre-Chamber Combustion	161
	7.3.2.2 Combustion in Both Chambers	162
	7.3.2.3 Main Chamber Combustion	162
7.4	EXHAUST PROCESS	163
7.5	INTAKE PROCESS	163
7.6	PERFORMANCE	163
7.7	RESULTS AND DISCUSSION	164
7.8	CONCLUSIONS	166

7.1. INTRODUCTION

The model for the divided chamber engine was developed from the single chamber model. Many aspects of the model were similar; however, the two chambers were allowed to contain charge of differing composition. This could be the result of different pressures and temperatures in the two chambers or (in the stratified charge case) different equivalence ratios. The two chambers were considered as thermodynamic sub-systems connected by an orifice, through which mass flow could occur to equalise pressure differences resultant from piston motion and combustion. When the model was used to consider an engine with stratified charge (i.e. with a richer mixture present in the pre-chamber), then the equivalence ratio in each chamber changed as the mass flow between chambers tended to reduce the degree of stratification.

Divided chamber models have been developed by other workers, who have used empirical laws to define the mass fraction burnt at a given time. Hires et al (1976) used cosine law expressions for mass burning rate in each chamber; they assumed that main chamber combustion started at a pre-defined crank angle after that in the pre-chamber. Wall et al (1978) used a cosine law expression for the burn rate in the pre-chamber and a Weibe function for that in the main chamber. Asanuma et al (1978) assumed the volume burn rate followed a linear relationship. With each of these models it was necessary to specify the combustion duration in each chamber and the crank angle at which main chamber combustion was initiated. In the single chamber model, when only one variable needed to be specified (combustion duration), the model could only realistically be used to give qualitative results when this variable was approximately constant. In the divided chamber case, since three variables need to be specified, such models were not considered useful. For this reason in the current work only burning velocity based methods were adopted.

The following assumptions were made in addition to those adopted previously in the single chamber model :-

- (1) The two chambers were considered as separate thermodynamic systems which were assumed to contain homogeneous mixtures, except during the combustion process.
- (2) Charge transfer from one chamber to the other was assumed to occur at constant enthalpy; the transferred mixture was assumed to mix instantaneously with the charge in the second chamber.
- (3) During combustion, burned and unburned zones were considered to exist in each of the two chambers; these zones being separated by a reaction region of negligible volume. Unburnt pockets of charge behind the flame front were allowed.

7.2. COMPRESSION AND EXPANSION

These two processes were treated in a manner similar to that used previously in the single chamber model. The thermodynamic properties in the main chamber were calculated from the change in cylinder volume due to piston motion and the isentropic assumption. However, in the revised version of the program, at the end of each crank angle increment a mass flow was allowed to occur from the higher pressure chamber to the lower. (i.e. from main to pre-chamber during compression). At the start of compression, both chambers were assumed to be at the same pressure.

The mass flowrate was calculated using classical expressions for flow through an orifice (Obert, 1968):-

for subsonic flow

$$\dot{m} = C_D A_o \frac{P_h RMW}{R T_h} \times \sqrt{\frac{\gamma R T_h}{RMW} \times \left[\frac{2}{\gamma-1} \left(\frac{P_l}{P_h} \right)^{\frac{2}{\gamma}} - \left(\frac{P_l}{P_h} \right)^{\frac{\gamma+1}{\gamma}} \right]^{\frac{1}{2}}} \quad (7.1)$$

for sonic flow

$$\dot{m} = C_D A_o \frac{P_h RMW}{R T_h} \times \sqrt{\frac{\gamma R T_h}{RMW} \times \left[\frac{2}{\gamma+1} \right]^{\frac{\gamma+1}{2(\gamma-1)}}} \quad (7.2)$$

The discharge coefficient C_D was assumed to be unity. In practice, for the orifice used in the experiments, a lower value would be more appropriate. In order to calculate the mass transferred during a crank angle increment, the time interval was further divided into 50 sub-increments, and at the end of each of these sub-increments the mass flowrate was re-calculated, on the basis of the revised pressure and temperature for each chamber.

For known mass flowrate \dot{m} , the mass transferred during each sub-increment was taken to be:-

$$m_t = \dot{m} \frac{\Delta\theta}{50} \cdot \frac{60}{360 RPM} \quad (7.3)$$

where $\Delta\theta$ is the crank angle increment in the compression or expansion stroke (5 degrees).

A reduction in pressure and temperature for the higher pressure chamber would result from the mass transfer. This process was assumed isentropic; heat transfer was not considered here, instead it was allowed to occur in each chamber after the fifty increments of mass transfer had taken place. For the expansion stroke the temperature after mass transfer had to be calculated iteratively, as the composition of the charge would change as it expanded.

The charge in the low pressure chamber would be subject to a corresponding increase in pressure, due to the mass transfer. If the transferred charge was burnt, or stratified, then its composition would differ from that already in the chamber, and therefore a mixing process needed to be considered. The mass transfer process was assumed to be isenthalpic. During the compression stroke, the temperature of the transferred charge would therefore remain constant. However, during expansion, the change in pressure during transfer could cause a change in composition of the charge (since it was in equilibrium); the temperature would therefore change. The new temperature was found by calculating the enthalpy at two different temperatures, and using linear interpolation-extrapolation to give a new estimate of the temperature where the enthalpy had remained constant; this process was repeated until the change in enthalpy was within a set error.

Once the temperature of the transferred charge was known, its volume was calculated from the mass and density. The volume of the charge already in the chamber could be calculated by subtraction, and its pressure and temperature calculated from the assumption of isentropy.

$$P_i = P_{i-1} \left[\frac{V_i}{V_{i-1}} \right]^\gamma \quad (7.4)$$

$$T_i = T_{i-1} \left[\frac{V_i}{V_{i-1}} \right]^{\gamma-1} \quad (7.5)$$

The two regions were then allowed to mix, using the same method as that adopted for mixing burnt regions in the rate-controlled combustion method of the single chamber program (Section 5.5.2). The mass transfer process was repeated until all 50 increments had occurred. For the stratified charge case, the actual equivalence ratio in each chamber (after mass transfer) had to be re-calculated. The orifice velocity was also calculated from the mass flowrate and the average density of the transferred charge during the transfer process. The next increment in the compression or expansion stroke could then be considered. In the stratified charge case, the extra fuel required in the pre-chamber was assumed to have been injected at the end of the compression stroke, and to have been (instantaneously) perfectly mixed with the charge already in the chamber.

Pollutant formation in each chamber during the expansion stroke was considered separately. At the end of each increment the average concentration of each pollutant was calculated, from the individual chamber concentrations.

7.3. COMBUSTION

7.3.1. Instantaneous

In this representation, combustion in each chamber was considered separately. Initially, the pre-chamber charge was assumed to burn instantaneously at TDC. The computational procedure used for this was exactly the same as that adopted in the instantaneous combustion single chamber model; the temperature of the products was calculated on the assumption of constant internal energy; the composition was deduced from thermochemical equilibrium considerations.

Following complete pre-chamber combustion, a mass flow was allowed to occur into the main chamber. This was treated in a fashion similar to that described in the compression and expansion strokes, except that the transferred charge was not allowed to mix with the unburnt charge. Instead it was assumed to remain as a separate region, until after the main chamber charge had burnt. The flow process was, again, considered in fifty increments; unlike the expansion stroke however, the process was considered to happen instantaneously. The mass transferred in each increment was chosen so that pressure equality would be achieved after the fifty increments had occurred.

Combustion in the main chamber was then assumed to be initiated. After completion of this burning, the pressure difference between the new products and the products transferred from the pre-chamber was considered to equalise; the two regions were then allowed to mix. As with previous mixing processes this was assumed to occur at constant internal energy; an iterative procedure was therefore necessary to find the mixture temperature and composition.

At this stage in the computation the main chamber would be at a much higher pressure than that of the pre-chamber; a reverse mass flow therefore had to be allowed. This was considered in a fashion similar to that adopted for the previous mass flow into the main chamber. However, each transferred increment of mass was allowed to mix immediately with the pre-chamber products. The initial 'kinetic' concentrations of pollutants were then set. As with the single chamber model, the initial concentration of NO was taken to be zero; the initial concentration of CO was taken to be the sum of the equilibrium concentrations of CO and CO₂ (i.e. all the carbon content of the fuel was assumed to be in the form of CO initially).

7.3.2. Burning Velocity Method

Described in Chapter 6, was a model which considered progressive combustion; at a rate determined on the basis of burning velocity. A number of alternative methods for defining the burning velocity were discussed in Chapter 6. To incorporate a computation of this type

into the divided chamber model proved considerably more complex. Hence, only one of the methods described in Chapter 6 was used (the wrinkled flame model of Damköhler, Section 6.3.2; incorporating the laminar burning equations of Metghalachi and Keck, Section 6.3.1).

The assumed ignition process in the pre-chamber was essentially the same as that adopted for single chamber combustion; a flame kernel of diameter equal to the Taylor microscale was considered to burn, instantaneously, at constant volume. This was then allowed to expand and compress the unburnt charge around it. During this period piston motion would also increase the pressure in the main chamber. A mass flow between chambers was allowed to occur; its direction dependent upon the process which gave the largest pressure rise, piston motion or combustion. The treatment of the mass flow process was identical to that in the compression routine, as only unburnt charge would be transferred. However, changes in volume for the two regions in the pre-chamber had to be considered. When modelling stratified operation, where the flow was into the pre-chamber, then allowance had to be made for dilution of the unburnt charge region within the pre-chamber (which would therefore then be at a lower equivalence ratio than the burnt charge region in the pre-chamber).

Abdel-Gayed et al (1986b) have shown that length scale in a combustion bomb is one tenth its diameter, and that turbulence generating this length scale was unaffected in the presence of a turbulence generating grid - suggesting that scale is principally a function of the size of the containing vessel. The length scale in the pre-chamber at ignition was therefore taken to be one tenth of the pre-chamber diameter and independent of the orifice diameter in the present work. The r.m.s. turbulent velocity at ignition was assumed to be proportional to the maximum orifice velocity. As no experimental data were available, the constant of proportionality was chosen by comparing model predictions with experimental results (at one test condition) and adjusting the constant until reasonable agreement was achieved in the pressure history.

7.3.2.1. Pre-Chamber Combustion

The rate of entrainment, and the rate of burning, were calculated in the manner adopted in the single chamber model. At the end of each increment (after the mass had burnt, expanded and mixed with the previous burnt charge) a mass transfer between chambers was allowed. As during the ignition phase, the direction of flow would be dependent on the relative magnitudes of pressure rise in each chamber; due to piston motion in the main chamber and combustion in the pre-chamber. Once the mass flow had been completed, heat transfer in each chamber was considered, followed by 'kinetic' calculation of pollutants concentrations

within the burnt charge.

Films of the combustion process in the Ruston engine, which had a spherical pre-chamber, showed that the flame growth was approximately spherical; however, the main chamber combustion started a considerable time before the flame reached the wall in the pre-chamber. In the model, although the overall flame growth was assumed spherical, main chamber combustion was therefore allowed to start when the flame radius in the pre-chamber reached 80% of the pre-chamber radius. This value was chosen as it appeared reasonable from observations of the films. It is possible, however, that it should vary with orifice diameter, engine speed, etc.

7.3.2.2. Combustion in Both Chambers

The initial length scale and r.m.s. turbulent velocity in the main chamber were calculated in a similar manner to that employed for the pre-chamber. The length scale at pre-chamber ignition was taken to be one tenth of the instantaneous chamber height; the r.m.s. velocity was calculated by assuming that the rapid distortion theory would apply to an eddy travelling through the orifice.

$$\text{i.e. } L_p u_p' = L_m u_m' \quad (7.6)$$

Once combustion in both chambers was occurring, mass flow through the orifice was assumed to consist of burnt charge only. The flow process was considered in a fashion similar to that during the expansion process; the change in volumes of the two unburnt regions, as the pressures in the two chambers attempted to equalise, were then considered. However, problems were encountered, because the quantity of unburnt charge behind the flame front was calculated from the mass entrained during each interval; mass flows between chambers altered the quantity of burnt charge in each chamber and could therefore cause errors in this calculation. To overcome this problem, any mass entering a chamber was assumed not to affect the calculation of mass burnt behind the flame (as given by the Blizzard and Keck expression, Eqn. 6.18). The process was considered to end when all the pre-chamber charge had burnt.

7.3.2.3. Main Chamber Combustion

Following completion of pre-chamber combustion, the main chamber combustion process was considered to proceed in a manner similar to that in the single chamber model. At the end of each combustion increment a mass flow was allowed to occur through the orifice. Initially this would be into the pre-chamber. Later, as combustion neared completion, the piston would be descending; hence the pressure drop due to piston motion could exceed any rise due to combustion; the flow direction would therefore then reverse. In either case the

mass flow process had to include expansion or compression of the unburnt zone.

Heat transfer was considered at the end of each increment, and the pollutant concentrations computed for each chamber.

7.4. EXHAUST PROCESS

The exhaust blowdown process was considered in a manner similar to that for the single chamber model; the only difference being the allowance for a mass flow from the pre-chamber to the main chamber after each of the blowdown increments. This mass flow was considered in a fashion identical to that for the reverse mass flow in the instantaneous combustion routine; it was assumed instantaneous, and each transferred mass increment was considered to mix immediately with the main chamber charge. During the exhaust stroke, heat transfer was considered, again in a manner similar to that adopted in the single chamber model. The pressure during the exhaust process would be essentially constant, there would hence be no flow between chambers if no heat transfer occurred. However, heat loss from the pre-chamber would cause a reduction in density of the charge present; therefore a mass flow into this chamber had to be allowed for.

7.5. INTAKE PROCESS

During the intake process, if there were no heat transfer, there would be no mass flow between chambers - as the main chamber pressure would remain essentially constant. The process would therefore be identical to that in the single chamber model. Heat transfer effects might, however, cause a mass flow to occur between chambers. At the end of the intake stroke, the main chamber would contain a mixture of fresh charge and residual products, while the bulk of the pre-chamber charge would comprise residual products. This would be diluted by fresh charge from the main chamber during the compression stroke.

7.6. PERFORMANCE

The essential difference between this routine in the divided and single chamber programs was in the calculation of pollutant emissions. In the divided chamber program the emissions in each individual chamber were calculated, together with the overall emissions. Work done and I.M.E.P. were calculated from pressure volume data in the main chamber only, while the fuel consumption included any extra injected into the pre-chamber at the end of compression. The maximum flow velocity through the orifice was also calculated.

As with the single chamber model the complete computational cycle was repeated until repeatable values, for composition and temperature of the charge at intake, were obtained in consecutive cycles.

7.7. RESULTS AND DISCUSSION

Al-Mamar conducted many computations with the instantaneous combustion routine for both single and divided chamber operation. For this reason they are not repeated here. The divided chamber model, using the burning velocity approach, is considerably more complex than the single chamber model. Although experimental work has been done on divided chamber engines using laser doppler anemometry (Asanuma and Obokata, 1979), the velocity measurements were for mean flows only. Lack of experimental data for turbulence intensity and scale made it difficult to test the model properly, because of uncertainties in the values assumed. A number of computations were performed, to model engine performance at volume ratios of 13% and 25%, with an orifice diameter of 5mm. These calculations involved altering the constant of proportionality used to find the initial pre-chamber turbulence intensity, given the maximum orifice velocity; a constant of 0.15 was chosen initially, as this was of the correct order of magnitude. With this value the model could be used to predict performance at all the operating conditions used in experiments by Al-Mamar, with the exception of his use of his smallest pre-chamber in combination with his largest orifice diameter (7%, 9mm). For this latter condition, combustion was not completed prior to exhaust valve opening.

The model was used to predict the optimum ignition advance (for maximum power) for each of the geometrical configurations used by Al-Mamar. These optimum ignition timings are plotted in Fig. 7.1, together with the experimental optimum found by Al-Mamar. The constant of proportionality, used to determine the turbulent intensity at ignition, was chosen from comparison of model predictions and experimental results with a 5mm orifice; agreement between predicted and experimental optimum timing is reasonable with this orifice size. However, with the larger orifice sizes the agreement was found to be less favourable, although the computed trends with increasing volume ratio and orifice size accord with the experimental results. This suggests that the assumption of a direct proportionality between turbulence intensity and peak orifice velocity during compression may not be valid. The discrepancy could also be due to errors in values of laminar burning velocity used in the calculation procedure. The method used to determine turbulent burning velocity was that of Damköhler (Method (i) Section 6.3.2). In this expression, as the turbulence intensity increases, errors in the laminar burning velocity become less significant.

Shown in Fig. 7.2 are the pressure diagrams for the 13% and 25% volume ratios (with 5mm orifice diameter), as predicted by the model, together with corresponding typical experimental data. In both cases the peak pressure predicted by the model is higher and occurs earlier than in the experimental cycle. The combustion rate predicted by the model is clearly too fast; however, the model shows qualitative agreement in the pressure trace. The

pressure peak in the pre-chamber (before main chamber combustion has started), as observed in experiments, is shown in the model predictions. However the modelled peaks are less pronounced than the experimental ones. If the modelled combustion rate were slowed down, so that this peak occurred at the same time as the experimental peak, then it would be even less pronounced. The modelled flow rate through the orifice must therefore be greater than the true flow rate as the pressure differential between chambers is too small. The orifice flow equations did not consider a discharge coefficient; this is clearly necessary in order to model the higher pre-chamber pressure found during the early stages of combustion.

In order to check the influence of the constant of proportionality used to determine the turbulence intensity, the model was modified so that the constant (K_i) was reduced from 0.15 to 0.10 and 0.08. The resulting pressure traces are shown in Fig. 7.3. Lower turbulence intensity results in lower peak pressure; this occurs later in the cycle. It would be possible to get agreement in the main chamber pressure trace by suitable adjustment of this constant. The pre-chamber peak is, however, much smaller than the experimental value. As previously mentioned, this could be due to the exclusion of the discharge coefficient from the flow velocity calculations. This, alone, may not account for the discrepancy in peak pre-chamber pressure. If the constant were chosen so that the theoretical and experimental peak main chamber pressures agreed, the pre-chamber combustion might be too slow. The assumed relation between main and pre-chamber turbulence levels (the rapid distortion theory) may not be valid for flow through an orifice. Without turbulence intensity measurements from a divided chamber engine it is difficult to speculate which, if any, of the above possible errors is responsible for the discrepancy between modelled and experimental pressures.

Shown in Fig. 7.4 are the flame radius and flame speed, calculated and experimental, for a 25% volume ratio (with the constant $K_i = 0.15$). Predicted flame growth in the pre-chamber starts much more quickly than in the filmed cycle, and the flame speed is considerably higher. Reducing the value of the constant used to determine turbulence intensity could produce better agreement in the flame speeds. However, this would not account for the much faster flame initiation. Modelling of the development process of the flame in the early stages is clearly less well understood than for a developed flame. In the main chamber, the predicted time for start of main chamber burning agrees well with the experimental observations. In this case the assumption used to determine the time when main chamber combustion should be initiated (i.e. when the pre-chamber flame radius reached 80% of the pre-chamber radius) was obviously valid. Initial flame growth is similar; the model, however, overpredicts the flame radius in the later stages. It also overpredicts the flame speed, although the trend is the same; with the peak flame speed occurring when the

flame radius is approximately 3cm.

In the 25% volume ratio condition described above, the experimental and predicted optimum ignition timing agreed within one degree crank angle. With the 13% volume ratio, the model predicted an optimum timing of 12 degrees, while experiments suggested 15 degrees. The flame propagation rates for this condition, using the relevant optimum timing, are presented in Fig. 7.5. In this case the theoretical and experimental flame growth rates in the pre-chamber are similar. Although the spark advance for the experimental test was 15 degrees, there was little observable flame growth until 12 degrees BTDC. Flame development in the main chamber follows the same trends, but quantitative agreement is poor. The predicted start of main chamber combustion is 4 degrees later than the experimental results showed. Considerably more investigation is required to determine the factors which govern the timing of main chamber combustion initiation. The peak flame speed, at this condition, occurs when the flame reaches approximately 1.5cm radius; this is shown by both experimental results and model predictions.

The predicted flow velocity through the orifice, for the two geometrical configurations used above, is shown in Fig.7.6. During compression the charge flows into the pre-chamber; its velocity would increase to a maximum at approximately 30 degrees BTDC. After ignition, the pressure rise in the pre-chamber, due to combustion, would cause a reversal of flow direction. Flow continues in this direction until soon after initiation of main chamber combustion, when the main chamber pressure rise becomes predominant. Finally, towards the end of combustion, the effect of the descending piston would cause a third flow reversal. For most of the cycle the flow velocity for the smaller (13%) volume ratio is approximately half that predicted for the larger (25%) chamber. However, the predicted peak velocity during pre-chamber combustion was of the same order of magnitude for both geometries. It is likely that the orifice is highly choked during this process.

The model was not used to explore the effects of charge stratification. The problems described above need to be resolved, before attempting to model the more complex stratified charge combustion process.

7.8. CONCLUSIONS

The burning velocity approach to combustion modelling has been applied to a divided chamber engine. This is considerably more complex than the single chamber model and results, at this stage, are only preliminary; a great deal more investigation is required to validate assumptions made in the model. The following points require more detailed investigation:-

- (1) A coefficient of discharge is required for the orifice flow velocity calculations. The pressure in each chamber, predicted by the model, did not show the large differential (during pre-chamber combustion) observed experimentally.
- (2) The model is not very accurate in the very early stages of combustion; observations showed that the flame took a few degrees crank angle to get established. This may be longer than for a single chamber engine due to the higher turbulence levels present.
- (3) The assumption that the turbulence intensity at ignition is proportional to peak orifice velocity, does not appear to be valid over the wide range of orifice velocities used. The relation between main and pre-chamber turbulence intensities is also not well understood. A better understanding of the effect of the orifice flow velocity on turbulence is clearly needed. Experimental measurements, using LDA or hot wire anemometry, of velocities in the engine would be very helpful in achieving this.
- (4) Combustion in the main chamber is initiated before the pre-chamber flame reaches the wall. This is clearly due to unburnt charge, which is moving towards the orifice, entraining the flame front, and moving it preferentially in that direction. To allow main chamber combustion to start when the pre-chamber flame reaches a given radius was a useful initial starting point, to get the model working. It is, however, not a good method if the model is required to predict behaviour for varying pre-chamber shapes. A more detailed investigation is required into the mechanism of this process in order to define the time the flame reaches the main chamber on a more fundamental basis.

The divided chamber model offers a good way of investigating the effect of turbulence on combustion, as the range of turbulence intensities available is very much greater than can be found in a single chamber engine.

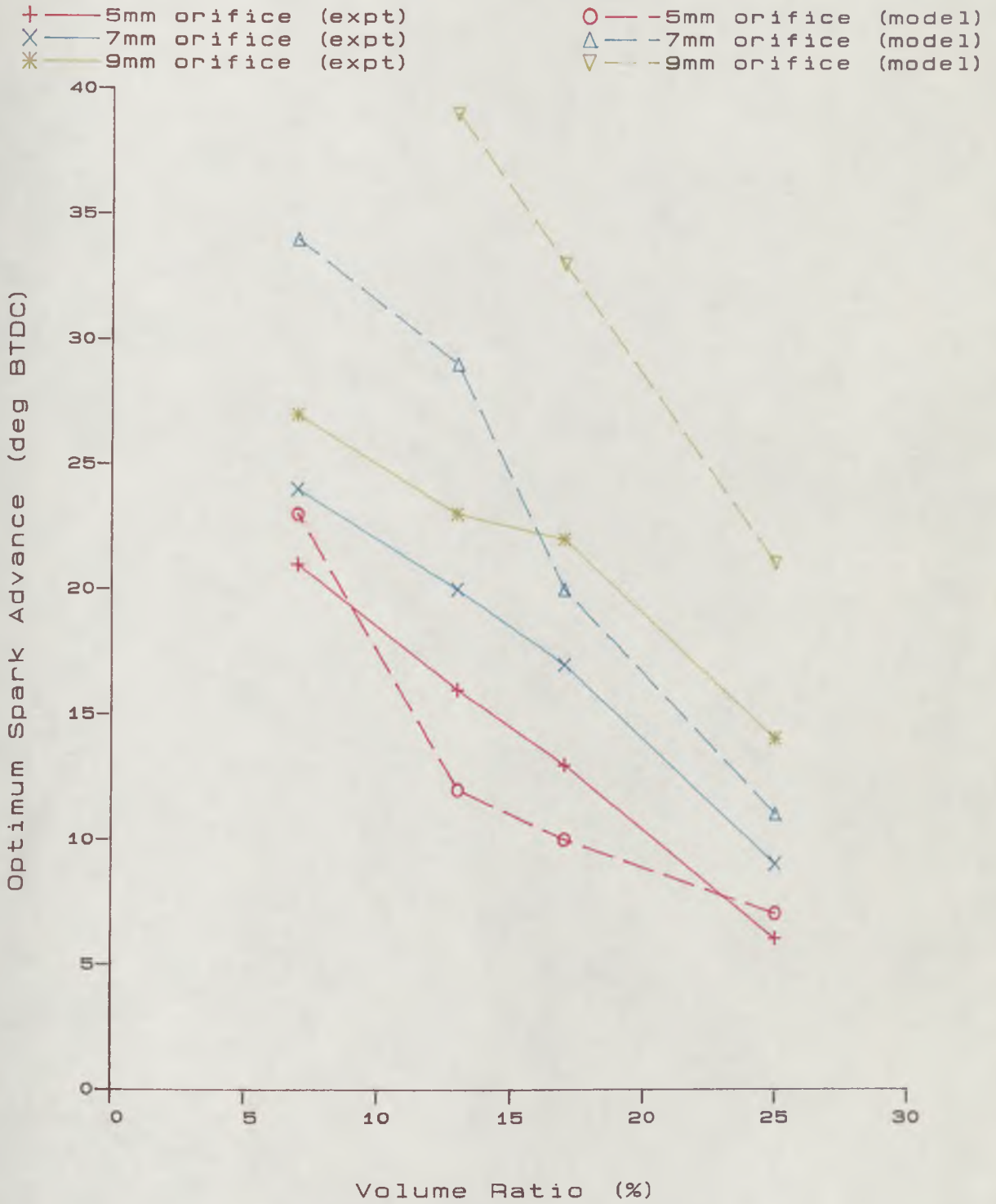
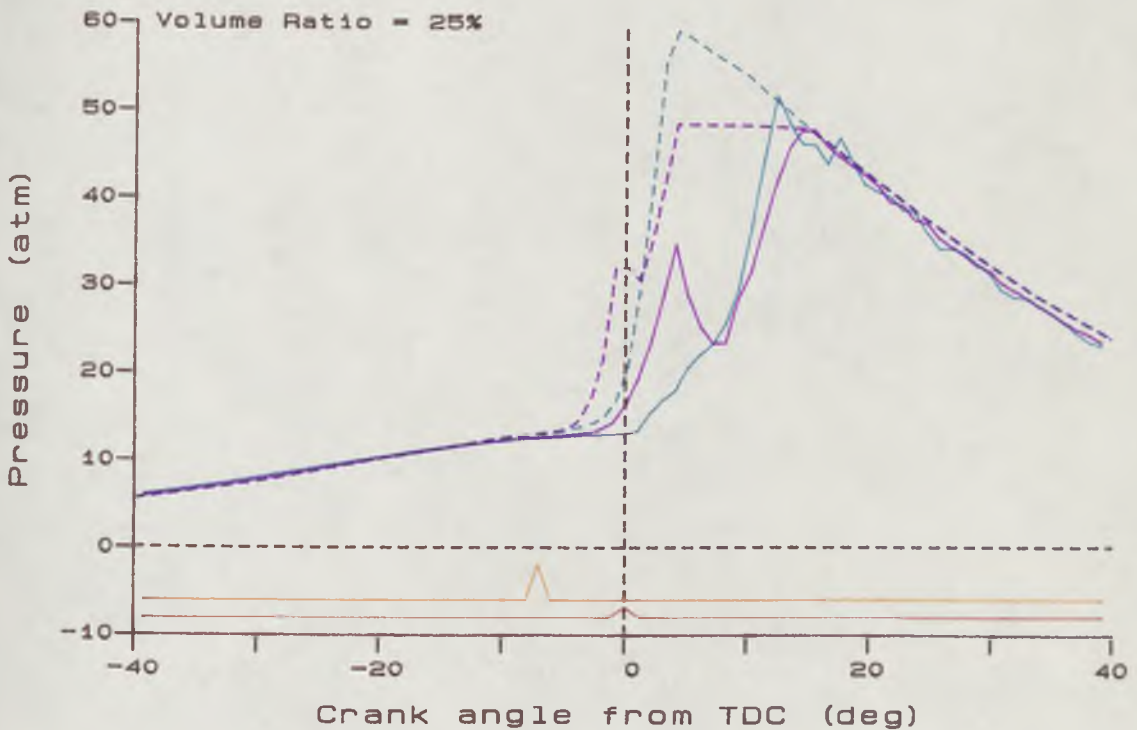
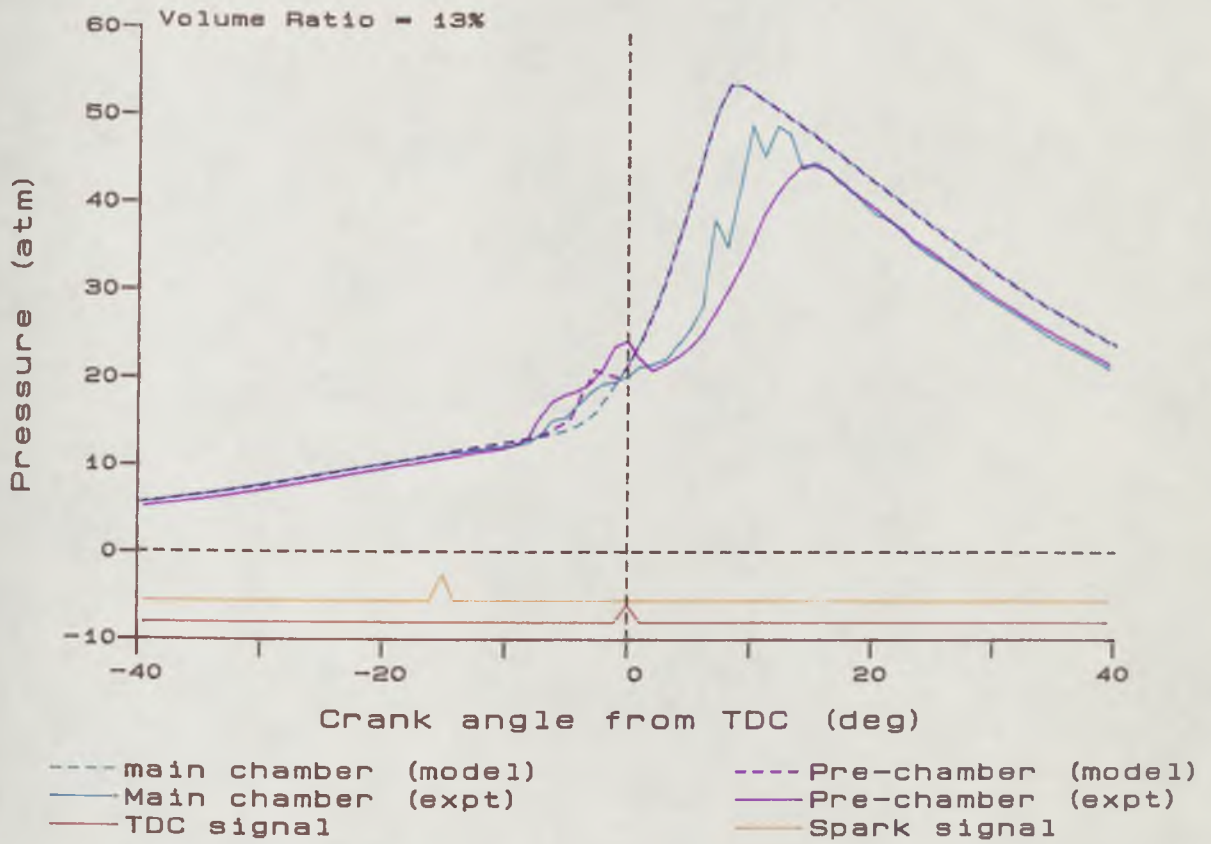


Fig.7.1

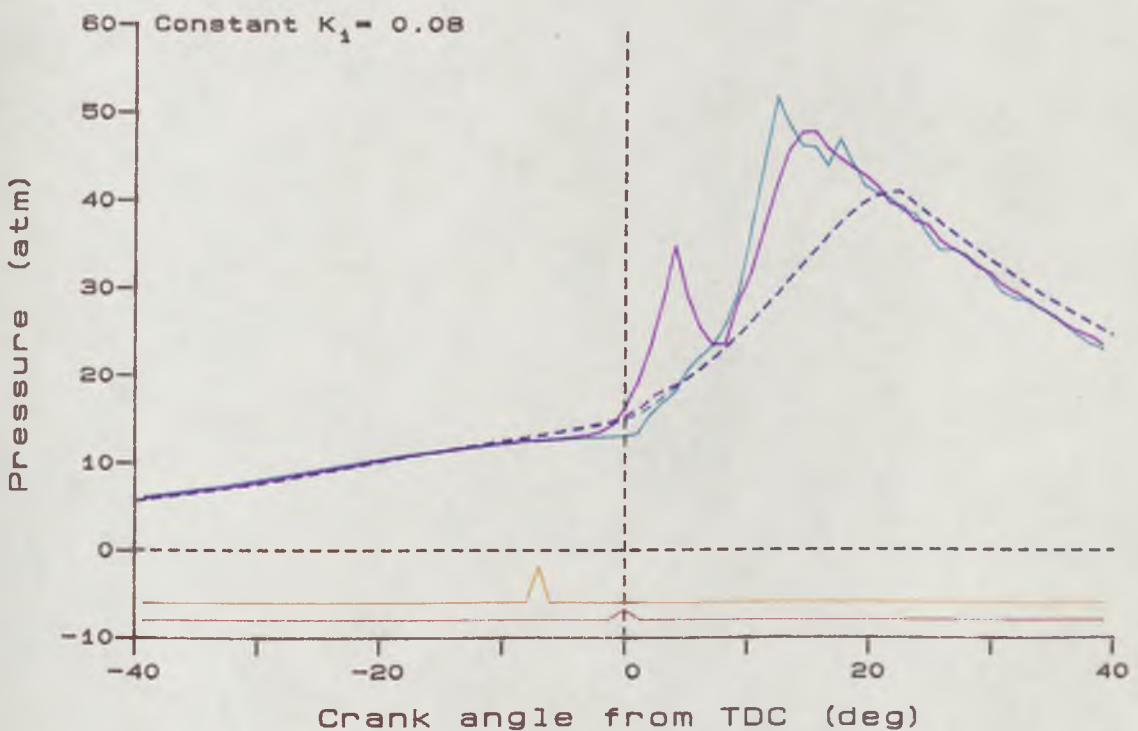
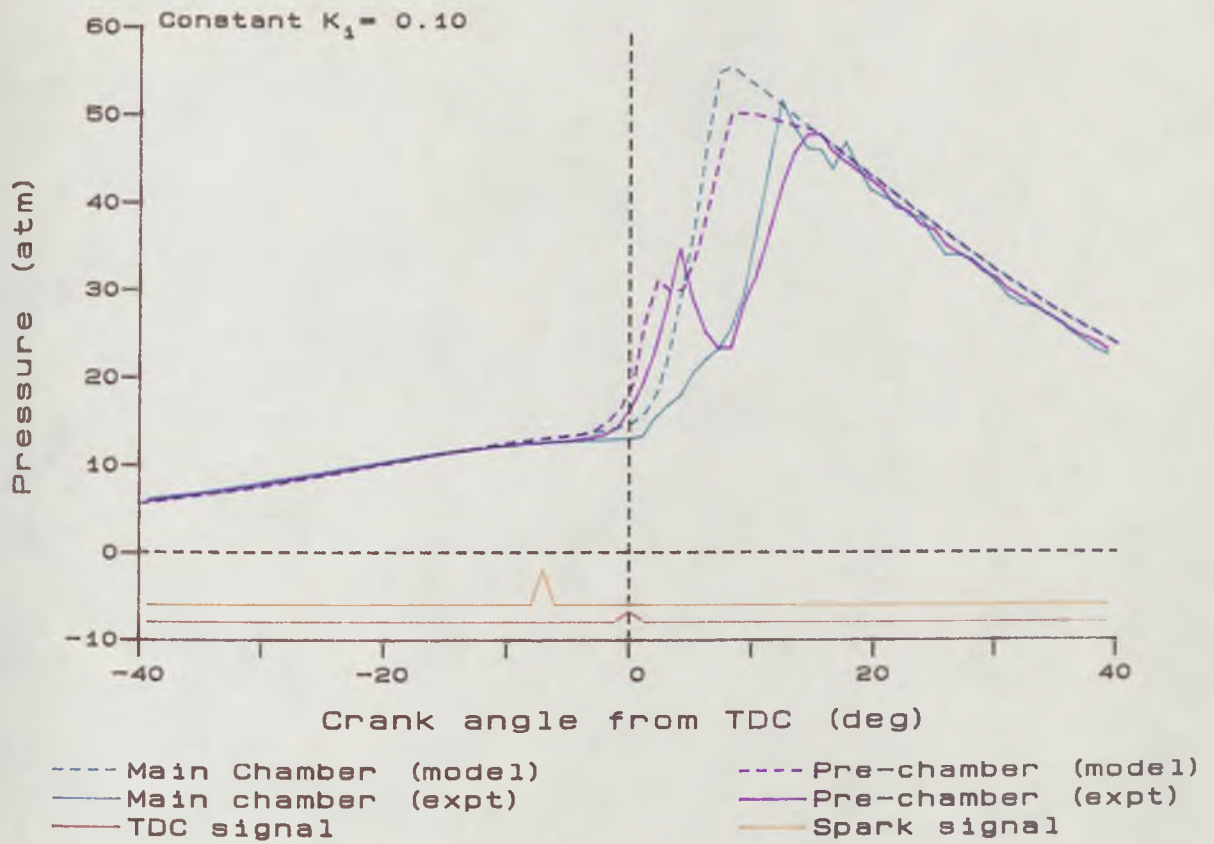
Comparison of experimental and predicted optimum ignition timing



COMPRESSION RATIO = 8.0
 EQUIVALENCE RATIO = 1.0
 ENGINE SPEED = 1400 rpm

OPTIMUM SPARK ADVANCE
 FUEL BP-4STAR
 ORIFICE DIAMETER = 5 mm

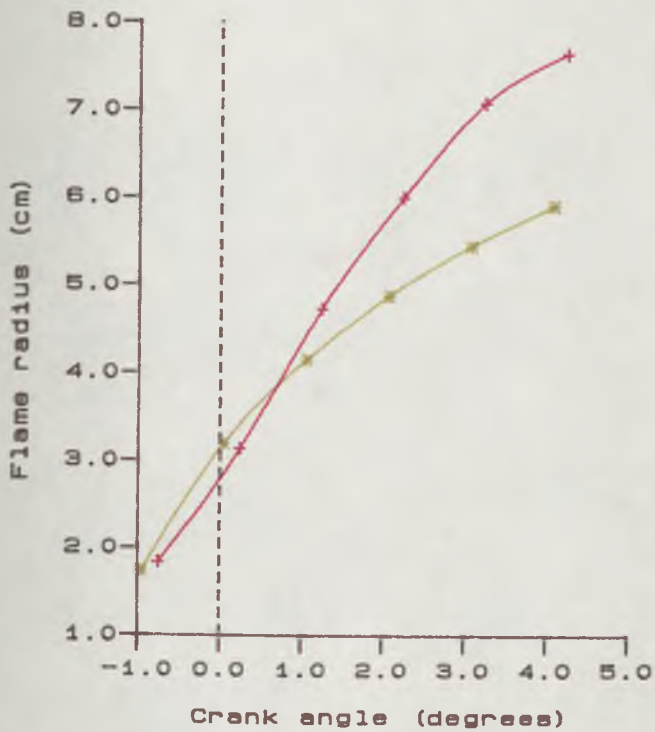
Fig.7.2 Comparison of pressure history



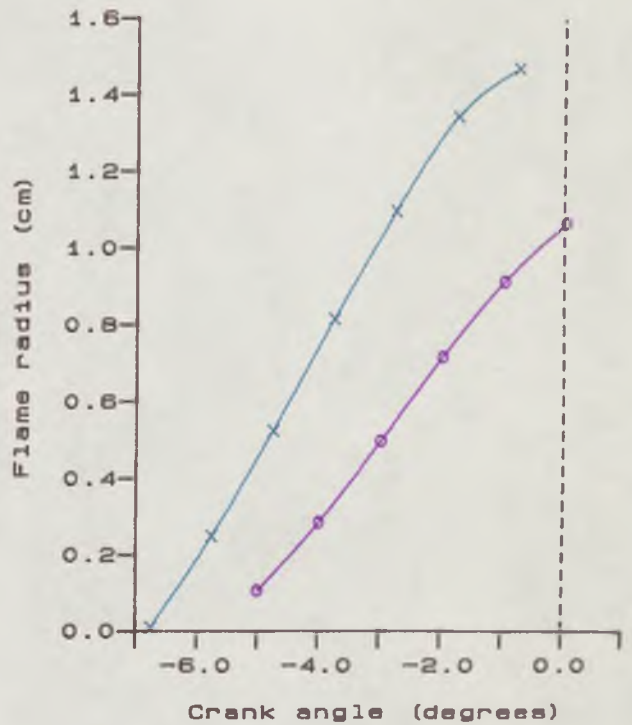
COMPRESSION RATIO = 8.0
 EQUIVALENCE RATIO = 1.0
 ENGINE SPEED = 1400 rpm
 ORIFICE DIAMETER = 5 mm

OPTIMUM SPARK ADVANCE
 FUEL BP-4STAR
 VOLUME RATIO = 25%

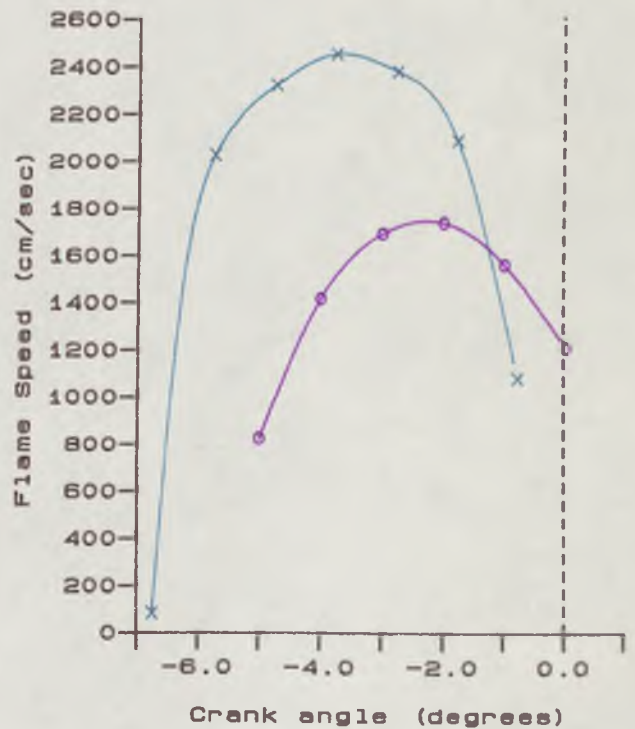
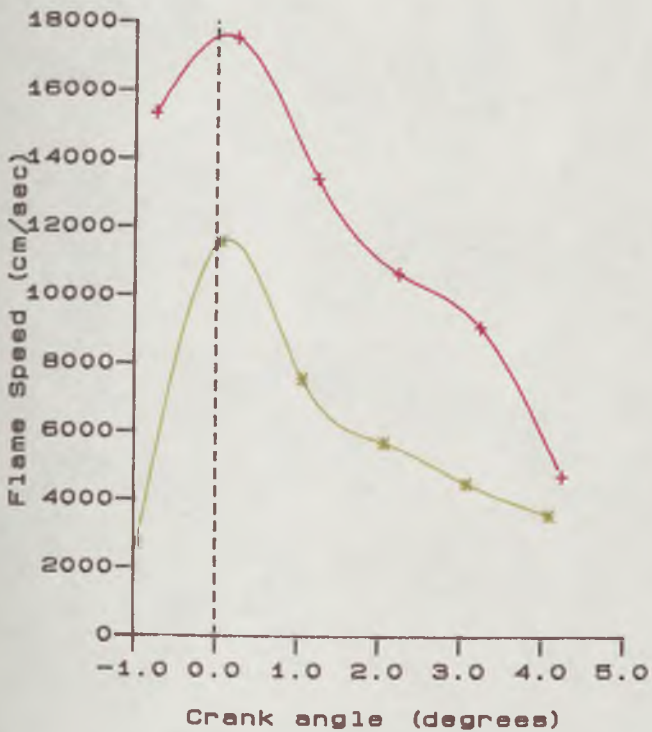
Fig. 7.3 Effect of turbulence intensity



+ Main chamber (model)
 x Pre-chamber (model)



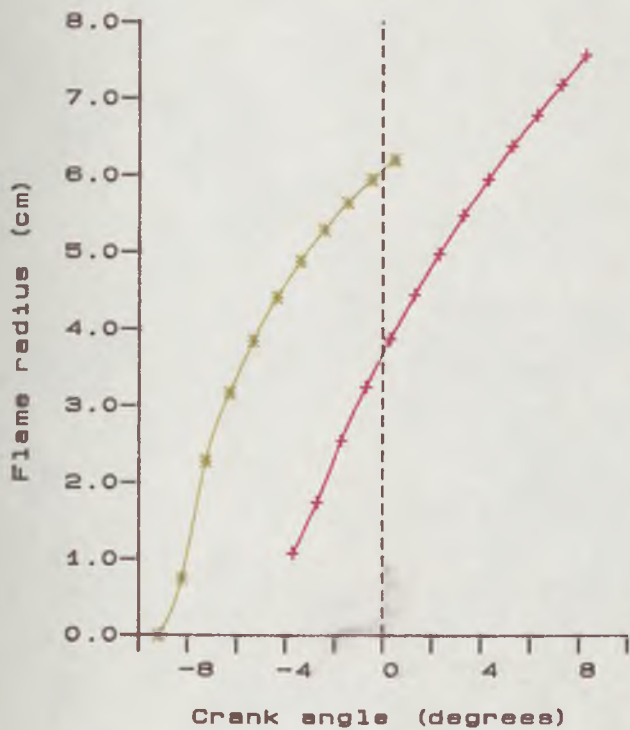
* Main chamber (expt)
 o Pre-chamber (expt)



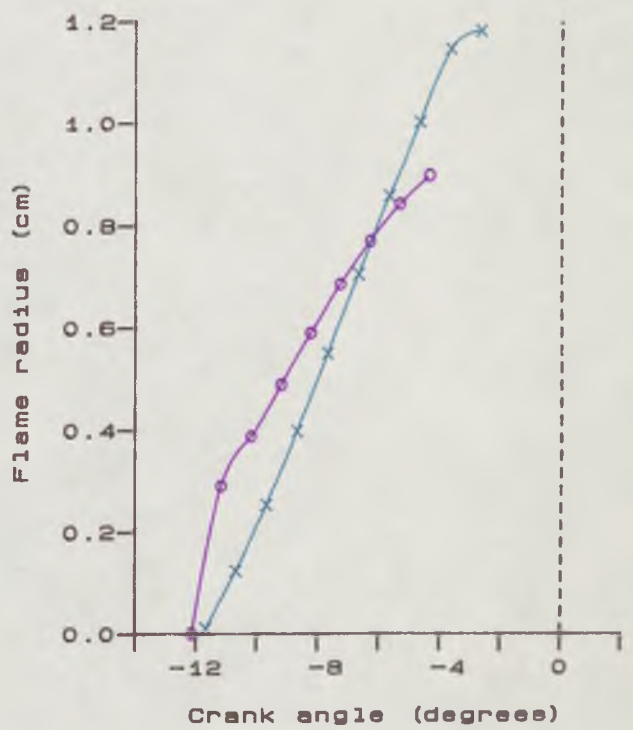
COMPRESSION RATIO = 8.0
 EQUIVALENCE RATIO = 1.0
 ENGINE SPEED = 1400 rpm

OPTIMUM SPARK ADVANCE
 VOLUME RATIO = 25%
 ORIFICE DIAMETER = 5 mm

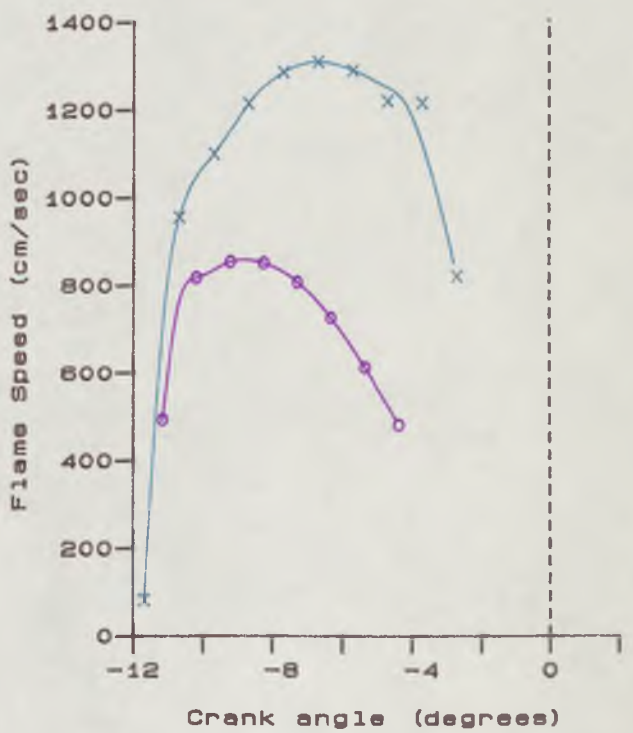
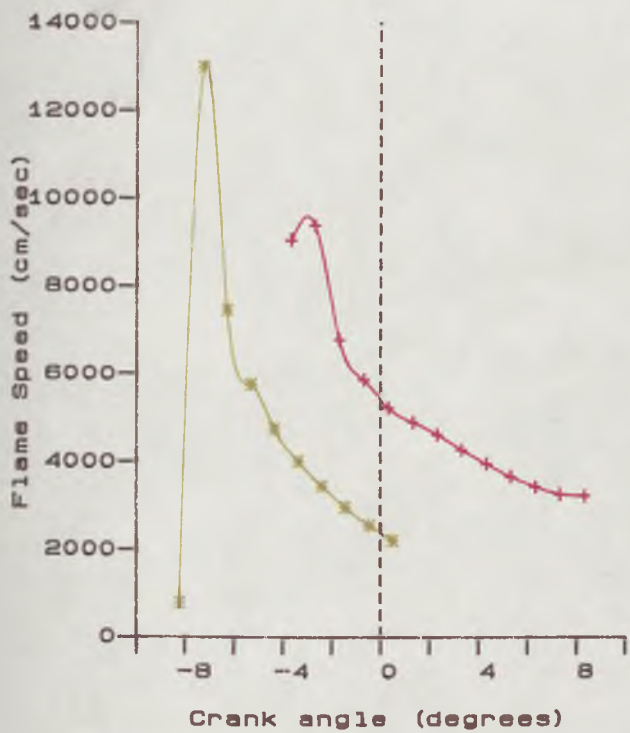
Fig. 7.4
 Comparison of flame propagation rates



+ Main chamber (model)
 X Pre-chamber (model)



* Main chamber (expt)
 o Pre-chamber (expt)



COMPRESSION RATIO = 8.0
 EQUIVALENCE RATIO = 1.0
 ENGINE SPEED = 1400 rpm

OPTIMUM SPARK ADVANCE
 VOLUME RATIO = 13%
 ORIFICE DIAMETER = 5 mm

Fig.7.5
 Comparison of flame propagation rates

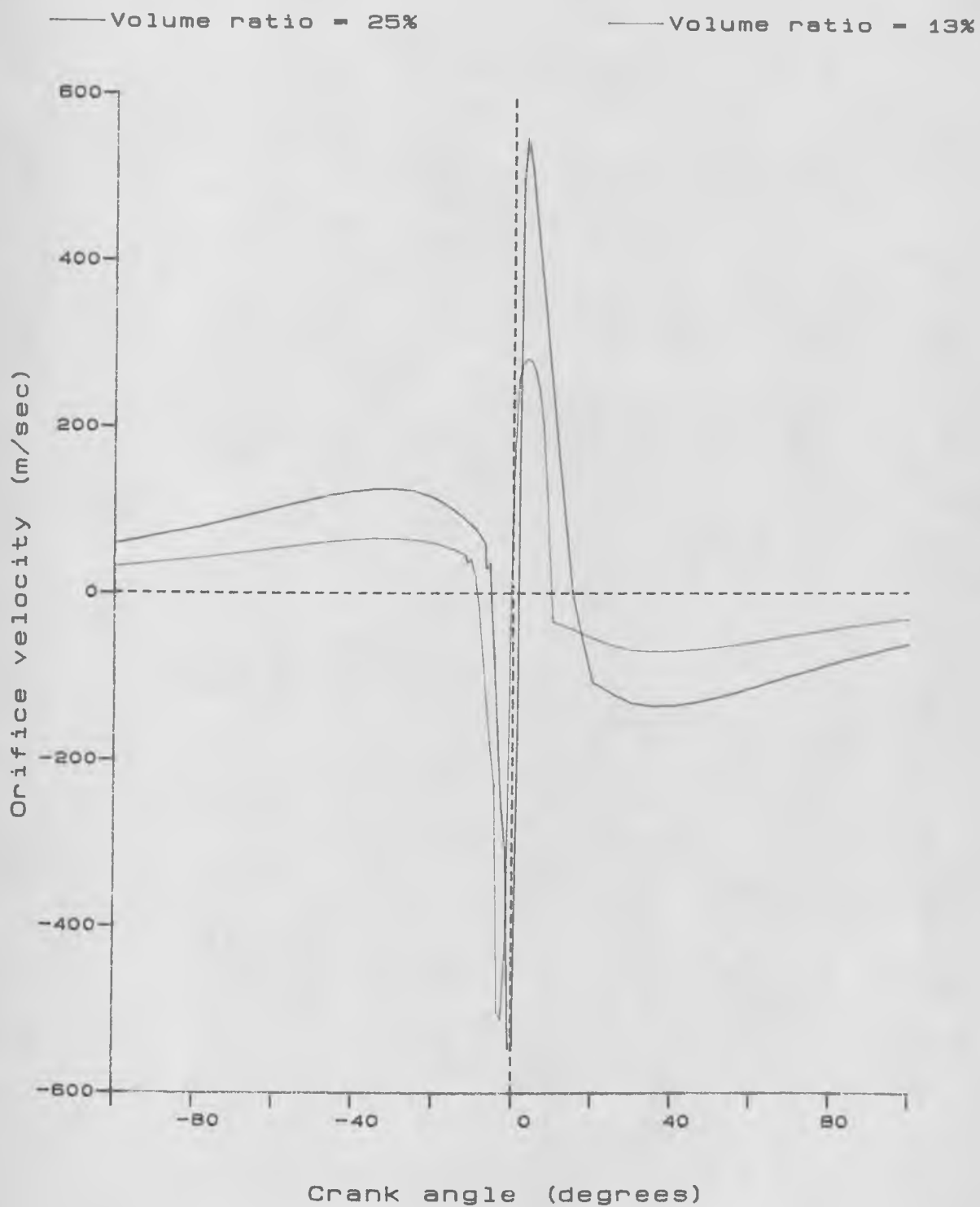


Fig. 7.6

Flow velocity through the orifice during a cycle

(+ve direction is main to pre-chamber)

CHAPTER 8

Further Experimental Data Analysis

CONTENTS

8.1	INTRODUCTION	176
8.2	CALCULATION PROCEDURE	176
8.3	RESULTS	177
8.4	CONCLUDING REMARKS	179

8.1. INTRODUCTION

In Chapter 6 a computer model for a single chamber engine was discussed. Predictions of pressure and flame speed from the model were compared with experimental data from an engine. Described in this chapter is an attempt made to modify the computer model. These modifications were incorporated to allow it to use experimentally measured cylinder pressure, together with film derived flame area data, in order to compute the mass fraction burnt during the combustion process. The mass fraction entrained was calculated, together with the mass fraction burnt behind the flame front. Beretta et al (1983) conducted a similar study; however, they used an overhead valve engine with a transparent piston. Consequently their field of view was only 43% of the cylinder bore area. The work described here used data from the Yamaha engine; this allowed the entire cylinder bore area to be viewed. Errors in calculation of entrained volume are therefore due to flame curvature alone, and not due to extrapolation of flame position.

8.2. CALCULATION PROCEDURE

In the calculations described here, the following assumptions were made:

- (1) Spatially uniform cylinder pressure.
- (2) Negligible reacting charge mass and crevice volume trapped mass, such that the total mass comprised only burnt and unburnt charge.
- (3) That the composition of the unburnt charge was that at inlet valve closure, while that of the burnt charge was that at equilibrium at the appropriate temperature and pressure.
- (4) Ideal gas behaviour within both unburnt and burnt regions.
- (5) Spherical flame growth, centred on the spark position.

In Chapter 4 experimental film derived flame area data were used to calculate the effective radius of an equivalent spherical flame. The enflamed volume could therefore be calculated, on the same basis as in the model (Appendix C).

The procedure used to calculate the mass fraction burnt was conducted in an iterative manner, similar to that used in the model (Chapter 6). Each time increment was considered to be that between frames on the film in question. The pressure rise during each increment, due to piston motion, was calculated by (initially) assuming isentropy, and then allowing heat transfer to occur. Constants in the heat transfer equations were chosen so that the experimental, and modelled pressure, prior to ignition were in agreement.

The combustion process was then considered in a similar fashion to that adopted in the model described previously. An estimate of the mass fraction burnt was found using a

cosine law expression (Chapter 5). This mass was allowed to burn instantaneously at constant volume, expand, and then mix with any previously burnt charge. The pressure at the end of this process was then compared with the smoothed experimental pressure. If it did not agree, then the process was repeated for two more mass fractions, one above and one below the initial value. A quadratic equation was fitted to the resulting pressures; this was solved for the mass fraction which, when burnt, would give the required experimental pressure. The entire process was repeated until the calculated and experimental pressures agreed within set accuracy (0.05%). From the pressure and temperature of each region at this stage, it was possible to calculate the mass fraction entrained behind the flame front (from its volume and the density). The mass unburnt behind the flame front could then be calculated by subtraction of the mass burnt from the total mass entrained. The computer program used for this is described in Hynes (1986e).

8.3. RESULTS

The output from the computer program described above, for stoichiometric and rich ($\phi = 1.1$) mixtures are shown in Fig. 8.1. In both cases the mass fraction burnt, at any given instant, was less than the mass fraction entrained; there was a considerable quantity of unburnt mass behind the flame front. With the rich mixture, at the end of combustion not all the fuel was burnt. This is due to there being insufficient oxygen present.

In the early stages of combustion, all the mass entrained by the charge was predicted to be completely burnt. This lends some support to the commonly held view that initial flame propagation is laminar. As the flame grew and became influenced by turbulence, the computed mass fraction burnt behind the flame front reduced. In the stoichiometric case, the fraction of the mass behind the flame which was burnt was approximately 75% for most of the combustion process. With the richer mixture this percentage fell to a lower value; this was probably due to oxygen deficiency.

The same trends were noted for leaner mixtures, (Fig. 8.2); however, the computed total mass burnt (after completion of the combustion process), was considerably less than the total mass present in the chamber. During the later stages of the combustion process, by when all the mass in the cylinder would be entrained, the piston would be descending rapidly; reducing the temperature in the chamber. It is possible that this reduction in temperature could quench reaction; this would be particularly likely with leaner mixtures, where reaction would still be taking place even late in the expansion stroke (for the leanest mixture shown in Fig. 8.2, combustion was noted to be still proceeding as much as 80 degrees ATDC). Although this would account for a lower total mass fraction burnt at the end of combustion, it is unlikely that this provides a complete explanation of the observed

phenomena. Calculations suggested that only 67% of the charge was ultimately burned in the case of the leanest mixture; the suggestion that (at one stage) as little as 3% of the entrained mass is actually burnt also seems unreasonable.

In the early stages of combustion, a considerable increase in the mass fraction entrained by the flame occurs, with little apparent increase in the calculated mass fraction burnt. When the flame is small, the pressure rise produced by burning is considerably less than that produced by piston motion; this effect is more prominent with the earlier spark timing associated with leaner mixtures. The calculated mass fraction burnt in these early stages may therefore be very inaccurate, since small errors in pressure measurement could be of the same order of magnitude as the pressure change produced by combustion. In order to accurately calculate the mass fraction burnt in these early stages, it would be necessary to use a different experimental method, such as the measurement of light emission from the CH radical. This technique has been used successfully in the 'pre-pressure' period by Abdel-Gayed et al (1986a). To use the technique in an engine would, however, be considerably more difficult, since the changes of pressure and temperature would have an effect on the light emission levels.

Shown in Fig.8.3 are two graphs for the lower engine speed of 800 rpm. The trends noted were similar to those observed at the higher engine speed. However, for the stoichiometric condition, the percentage of entrained mass burnt fell to a lower value (56%); since only one cycle was analysed, given the cyclic variation previously noted, one cannot be sure that the result is representative. The turbulence levels in the chamber would probably have been lower at the lower engine speed; one would therefore expect that, whilst the flame propagation speed would be lower at the slower speed, the proportion of entrained charge burnt ought to be higher. This was not the case; the differing pressure and temperature at each speed may also have had some influence on the burning rate.

Finally, shown in Fig.8.4 are the results from Beretta et al[†]. Data from the work reported here is also shown for comparison; the graphs show volume fraction burnt against flame radius (since Beretta presented his results in this fashion). Although both sets of results showed similar trends, the difference between the entrained and burnt volumes was larger in Beretta's results. The results presented in chapter 4 suggested that the Yamaha engine had relatively low turbulence. However, Beretta's engine was an overhead valve engine; it is likely that this would have had relatively high turbulence levels, and therefore a higher quantity of unburnt mass entrained (*vis à vis* the Yamaha).

[†] This graph is his Fig.12a, the different symbols for volume fraction burnt represent results from different cycles.

8.4. CONCLUDING REMARKS

An attempt has been made to calculate the mass fraction entrained and burnt during the combustion process. For a range of equivalence ratios, and for two engine speeds, the mass fraction burnt has been shown to be less than that entrained behind the flame front. This indicated that a considerable quantity of unburnt charge was present behind the flame as it propagated (up to 30% for a stoichiometric mixture). It has been reasoned that the calculation procedure might be inaccurate in the early stages of combustion, particularly with lean mixtures, where the pressure rise due to combustion was too small to be measured with confidence. An alternative method, using CH emissions, has been suggested as a means of determining the true mass burning rate during the early stages of the combustion process. However, calibration of the light emission associated with the CH radical might prove difficult - due to the varying temperature and pressure in an engine cylinder.

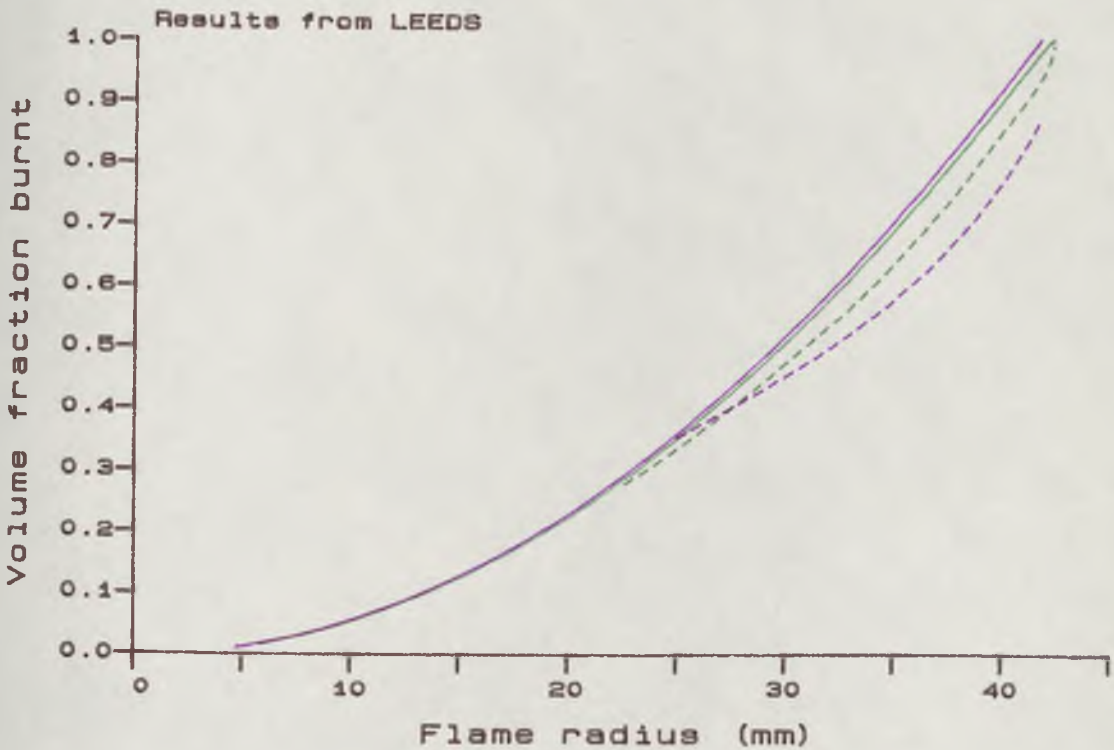
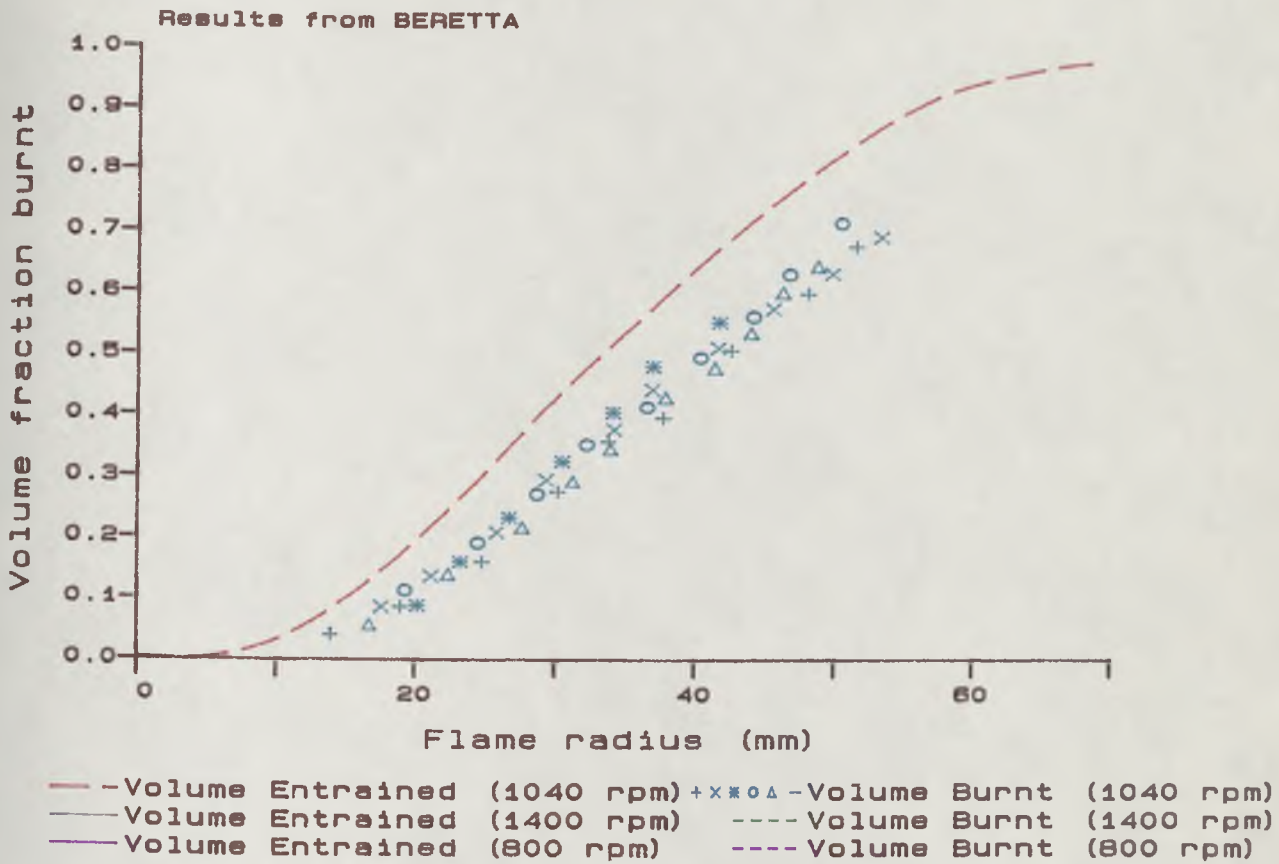


Fig. 8.4

The volume fraction burnt behind the flame front during combustion

CHAPTER 9

Summary and Conclusions

The separate experimental and theoretical results of the present work have been discussed in detail in Chapters 4 to 8. In this chapter these separate discussions are drawn together, and suggestions are made for further investigation of the phenomena encountered.

As discussed in the Introduction of this thesis, in order to improve fuel economy and meet emission legislation it is necessary to operate spark ignition engines with leaner mixtures and higher compression ratios. To achieve these requirements, and avoid knock, the turbulence level in the engine cylinder must be increased (although there may be a limit on how far it should be increased). Computer models for the turbulent combustion process are necessary, in order to reduce the high development cost of new spark ignition engines. These models must be able to correctly predict the burning rate in the chamber; they must also predict the flame position, since a small change in chamber shape can affect flame growth and mass burning rate.

The following conclusions can be drawn from the work reported here:

- (1) It has proved possible to achieve higher rates of burning in a homogeneous charge spark ignition engine when fitted with a dual chamber cylinder head than when equipped with a disc shaped single chamber.
- (2) The combustion rate has been shown to increase with increasing flow velocity through the interconnecting orifice (and hence with increased turbulence).
- (3) The divided chamber engine would seem to provide a useful means of generating controlled degrees of turbulence within a spark ignition engine. Such a combustion system has been shown to be useful for studying the effect of turbulence on burning rate.
- (4) The use of empirical laws, to allow for the progressive nature of combustion in thermodynamic cycle based computer models, has been shown to be ineffective. Uncertainty in the length of the combustion duration period, which one needs to specify when using empirical burning laws, restricts the usefulness of the technique.
- (5) The turbulent flame cannot be considered to be a thin reaction zone separating burnt and unburnt regions. Attempts to model it in this way (Chapter 5) failed; when the correct mass burning rate (pressure history) was achieved, the predicted flame propagation rate proved considerably faster than shown in experimental observations.
- (6) A considerable quantity of unburnt charge exists in pockets behind the flame front in a turbulent flame. This effect can be modelled by assuming that unburnt charge, once entrained, burns at an exponential rate. Agreement between predicted and experimental results was shown to be reasonable.

- (7) When a flame is small, it is not influenced by the full spectrum of turbulence. As it grows it is affected to a greater extent. To model this effect by a simple exponential law has been shown to be inaccurate.

Both the engines used in the experimental work suffered from a number of disadvantages. The calculated flame speeds and power output measured using the side valve Ruston engine, used in some of the earlier tests, will always be subject to an element of doubt - due to the effect of the valve clearance volume. Al-Mamar attempted to cut this space off from the main chamber when the piston was near TDC; however, unburnt reactants would be pushed into this space as it was uncovered soon after TDC, this would give rise to an increase in the observed flame speeds. The reactants trapped in the valve space would also burn, and contribute to the power stroke late in the combustion process. This problem could become more significant at higher compression ratios, as the valve chamber volume would constitute a greater proportion of the overall clearance volume.

In an attempt to overcome the valve chamber problem, the Ruston engine was replaced by the two-stroke Yamaha engine. This used ports in the cylinder bore instead of valves; a true disc shaped chamber (as assumed in the model) was therefore possible. Unfortunately, since the exhaust port only became covered (closed) as late as 91° BTDC, the effective piston movement (engine size) was much smaller than in the case of the Ruston engine. Also the cylinder bore was slightly larger than that of the Ruston engine; as a result the Yamaha had a particularly wide, flat combustion chamber at TDC. When high compression ratios were used, the very large surface area-volume ratio of the cylinder was thought to incur extremely large heat losses; hence the expected improvement in performance was not realised. Problems were also encountered with the divided chamber cylinder head fitted to this engine, as the small clearance height in the main chamber restricted the maximum orifice size that could be used. The small overall clearance volume at TDC also led to very small pre-chambers; these in turn required very high camera speeds for proper study of the initial flame growth in the pre-chamber. For future work, it would be helpful to use a larger two-stroke engine; this would permit the use of larger pre-chambers, orifice sizes and clearance heights. An alternative strategy might be to supercharge the engine, in order to restore the cylinder pressure at port closure to that at an equivalent crank angle in a four stroke engine.

Future modelling work should incorporate the recent theories on developing turbulent flames suggested by Bradley and his co-workers at Leeds. This developing phase is very important, since it encompasses much of the overall combustion time in a spark ignition engine. Computer modelling of the combustion process, for both single and dual chamber geometries, has been hindered by the lack of quantitative data for the turbulence intensity

and scale. Measurement of this data, in the engine concerned, would be most helpful for further development of the models. This could be obtained by either Laser Doppler Anemometry (LDA) or Hot Wire Anemometry (HWA); the laser technique would be preferable as it is more accurate. The present pre-chamber design (with through optical access) would require considerably less laser power for LDA than a more conventional engine, as a forward scattering technique could be employed. However, for study of the main chamber a back scattering technique would be necessary; this would require a high laser power due to the poor signal to noise ratios associated with back scatter. This problem might be circumvented by the use of cross-head mounted transparent piston and associated mirror system. This type of arrangement has been used by a number of workers for overhead valve engines; in a two-stroke engine it would allow through optical access, thus permitting forward scattering LDA and schlieren photography to be employed.

To overcome the oil problem encountered when schlieren photography was attempted, the engine would need to be re-designed to prevent oil from mixing with the cylinder charge. This might involve the use of graphite piston rings and an oil filled crank case to lubricate the bearings. With such an arrangement the intake charge would have to be blown directly into the transfer ports; rather than being drawn into the crank case for pre-compression, as in the case of a conventional two-stroke engine. As discussed previously, with such a technique it might be possible to supercharge the mixture to restore the cylinder pressure at port closure to that one would expect in a naturally aspirated four stroke engine at the same crank angle. This would allow the use of a larger clearance volume, larger pre-chambers and orifice sizes.

In calculating the mass fraction burnt in Chapter 8, problems were encountered when considering the early stages of combustion; these were due to the early mass burnt not giving an appreciable pressure rise. The measurement of CH light emission might prove a useful technique for calculation of the mass burning rate during the early stages, although calibration of the emissions could be very difficult as pressure and temperature are not constant in an engine.

In both computer models, and in the calculation of mass burning rate, a number of assumptions were made about heat transfer rates. To validate these assumptions it would be necessary to measure cylinder wall temperature, and exhaust gas temperature, in the engine being modelled. Exhaust gas sampling would also be helpful in verification of the exhaust gas composition computed by the programs.

Finally, consideration should be given to extension of the divided chamber study to include charge stratification. As discussed in Chapter 2, this type of system offers even better prospects for lean burning than does the homogeneous charge dual chamber system.

References

Abdel-Gayed R.G., Bradley D. (1980)

'*Turbulence length scales and the turbulent transport number for Isotropic turbulence*', Journal of Fluids Engineering, Vol. 102, p389.

Abdel-Gayed R.G., Bradley D. (1981)

'*A two eddy theory of pre-mixed flame propagation*', Philosophical Transactions of the Royal Society of London, A301, pp 1-25.

Abdel-Gayed R.G., Al-Khishali K.J., Bradley D. (1984a)

'*Turbulent burning velocities and flame straining in explosions*', Proceedings of the Royal Society of London, Vol. 391, pp 393-414

Abdel-Gayed R.G., Bradley D., Hamid M.N., Lawes M. (1984b)

'*Lewis number effects on turbulent burning velocity*', Twentieth Symposium (International) on Combustion, The Combustion Institute.

Abdel-Gayed R.G., Bradley D. (1985)

'*Criteria for turbulent propagation limits of premixed flames*', To Appear in Combustion and Flame.

Abdel-Gayed R.G., Bradley D., Lawes M., Lung F.K-K. (1986a)

'*Premixed turbulent burning during the early stages of an explosion*', To be presented at the 21st International Symposium on Combustion, Munich 1986.

Abdel-Gayed R.G., Bradley D., Forster H., Lawes M. (1986b)

In Preparation.

Abdel-Gayed R.G., Bradley D., Lawes M. (1986c)

In Preparation.

Adachi T., Kato S., Tsujimura H. (1982)

'*Numerical analysis of scavenging flow in two-cycle internal combustion engine*', Proceedings of the Winter Annual meeting of the A.S.M.E., Phoenix, Arizona.

Adams T.G. (1979)

'*Torch ignition for combustion control of lean mixtures*' SAE 790440

Akindele O.O., Bradley D., Mak P.W., McMahan M. (1982)

'*Spark ignition of turbulent gases*', Combustion and Flame, Vol. 47, pp 129-155

- Al-Mamar F.N.A.A. (1983)
'Combustion in a dual chamber spark ignition engine.', Ph.D. Thesis, Department of Mechanical Engineering, Leeds University.
- Al-Mamar F.N.A.A., Desoky A.R.A.A, Sheppard C.G.W. (1983)
'Combustion in a divided chamber spark ignition engine.' paper C46/83, Conference on Combustion in Engineering, I.Mech.E., Oxford, 11-14 April
- Al-Mamar F.N.A.A., Hynes J., Sheppard C.G.W. (1985)
'Combustion rate in a dual chamber S.I. engine', Combustion Science and Technology, Vol. 45, Nos. 1+2, pp 85-100.
- Alkidas A.C. (1982)
'Thermal loading of the cylinder head of a spark ignition engine', Heat Transfer Engineering, Vol. 3, pp 66-75
- Anderson R.W., Asik J.R. (1983)
'Ignitability experiments in a fast burn, lean burn engine', SAE 830477
- Andrews G.E., Bradley, D. (1972)
'Determination of burning velocities: a critical review', Combustion and Flame, Vol. 18, pp 133-153.
- Andrews G.E., Bradley D., Lwakabamba S.B. (1975)
'Turbulence and Turbulent flame propagation - a critical appraisal', Combustion and Flame, Vol. 24, pp 285-304.
- Annand W.J.D. (1963)
'Heat transfer in the cylinders of reciprocating internal combustion engines', Proceedings of the I.Mech.E, Vol. 177, pp 973-990.
- Annand W.J.D. (1971)
'Instantaneous heat transfer rates to the cylinder head surface of a small compression-ignition engine', Proceedings of the I.Mech.E, Vol. 185, pp 976-987.
- Annand W.J.D., Pinfold D. (1980)
'Heat transfer in the cylinder of a motored reciprocating engine', SAE 800457
- A.P.I. American Petroleum Institute Research Project 44 (1983)
'Selected values of properties of hydrocarbons and related compounds', Vol. 4, Thermodynamics Research centre, Texas A&M University.

Arici O., Tabaczynski R.J., Arpacı V.S. (1983)

'A model for lean misfire limit in spark ignition engines', *Combustion science and Technology*, Vol. 30, pp 31-45

Asanuma T., Gajendra Babu M.K., Yagi S. (1978)

'Simulation of thermodynamic cycle of three valve stratified charge engine' SAE 780319

Asanuma T., Obokata T. (1979)

'Gas velocity measurements of a motored and firing engine by laser anemometry', SAE 790096

Babkin V.S., V'yun A.V., Kozachenko L.S. (1967)

'Determination of burning velocity from the pressure record in a constant volume bomb', *Fizika Goreniya i vzryva*, Vol. 3, no. 3, pp 362-370.

Ballal D.R., Lefebvre A.H. (1975)

'The structure and propagation of turbulent flames', *Proceedings of the Royal society of London*, A344, pp 217-234.

Baudequin F., Rochelle P. (1980)

'Some scavenging models for two-stroke engines', *Proceedings of the I.Mech.E.*, Vol. 194, pp 203-210

Belaire R.C., Davis G.C., Kent J.C., Tabaczynski R.J. (1983)

'Combustion chamber effects on burn rates in a high swirl spark ignition engine', SAE 830335

Benson R.S., Whitehouse N.D. (1979)

'The internal combustion engine', Pergamon Press, Oxford.

Beretta G.P., Rashidi M., Keck J.C. (1983)

'Turbulent flame propagation and combustion in spark ignition engines', *Combustion and Flame*, Vol. 52, pp 217-245

Bishop I.N., Simko A. (1968)

'A new concept of stratified charge combustion- the Ford Combustion Process (FCP)', SAE 680041

Blackmore D.R., Thomas A. (1979)

'The scope for improving the fuel economy of the gasoline engine', *Conference on*

"The passenger car power plant of the future", I.Mech.E, Paper C206/79.

Blizard N.C., Keck J.C. (1974)

'Experimental and theoretical investigation of turbulent burning model for internal combustion engines', SAE 740191

Borgnakke C. (1984)

'Flame propagation and heat transfer effects in spark ignition engines', from "Fuel economy in road vehicles powered by spark ignition engines", (Editors - Hillard J.C., Springer G.S.), Plenum Press, New York.

Borgnakke C., Arpaci V.S., Tabaczynski R.J. (1980)

'A model for the instantaneous heat transfer and turbulence in a spark ignition engine' SAE 800287

Boston P.M., Bradley D., Lung F.K-K., Vince I.M., Weinberg F.J.

'Flame initiation in lean, quiescent and turbulent mixtures with various igniters', Twentieth Symposium (International) on combustion, The Combustion Institute, Pittsburg.

Bouchard C.L., Taylor C.F., Taylor E.S. (1937)

'Variables affecting flame speed in the Otto-cycle engine', SAE Journal, Vol. 41, pp 514-519

Brandstetter W.R., Decker G. (1975)

'Fundamental studies on the Volkswagon stratified combustion process' Combustion & Flame, Vol.25, No. 1, pp 15-23

Brandstetter W. (1976)

'Experimental results from Volkswagon's pre-chamber stratified charge engines' Conference on Stratified Charge Engines, I.Mech.E., paper C249/76

Brandstetter W. (1980)

'The Volkswagon lean burn PC concept' SAE 800456

Bullock K.J., Corkhill W.J., Wigley G. (1980)

'Flow and combustion measurements within a dual chamber stratified charge engine', Conference on Stratified Charge Automotive Engines, I.Mech.E., Paper C402/80

Campbell A.S. (1979)

'Thermodynamic analysis of combustion engines', John Wiley and sons (publishers).

- Carter D., Hemstead P.J. (1982)
'Commissioning of a two stroke motorcycle engine for photographic investigation of the combustion process' Final year project report, Department of Mechanical Engineering, University of Leeds
- Chaibongsai S., Kadota T., Henein N.A. (1980)
'The burning velocity in a CFR engine with different turbulent flow generated by intake valves', SAE 800860
- Chomiak J., Jarosinski J. (1982)
'Flame quenching by turbulence', Combustion and Flame, Vol. 48, pp 241-249
- Cole J.B., Swords M.D. (1980)
'An investigation of the ignition process in a lean burn engine using conditionally sampled laser doppler anemometry', SAE 800043
- Corkhill W.J., Bullock K.J., Wigley G. (1980)
'Flow and combustion measurements within a dual chamber stratified charge engine', Conference on Stratified Charge Automobile Engines, Paper C402/80, I.Mech.E.
- Damköhler G. (1940)
'The effect of turbulence on the flame velocity in gas mixtures', Z. Elektrochemie Angewandte Phys. Chem. Vol. 46. (English translation NACA TM-1112).
- Date T., Yagi S., Ishizuya A., Fujii I. (1974)
'Research and development of the Honda CVCC engine', SAE 740605
- Davis G.C., Borgnakke C. (1982)
'The effect of in cylinder flow processes (swirl, squish and turbulence intensity) on engine efficiency - model predictions', SAE 820045
- Davis G.C., Krieger R.B., Tabaczynski R.J. (1974)
'Analysis of the flow and combustion processes of a three-valve stratified charge engine with a small prechamber', SAE 741170
- Davis G.C., Tabaczynski R.J., Belaire R.C. (1984)
'The effect of intake valve lift on turbulence intensity and burn rate in S.I. engines-model versus experiment.', SAE 840030

Desoky A.R.A.A. (1981)

'An experimental and theoretical study of the combustion process in a divided chamber spark ignition engine', Ph.D Thesis, Department of Mechanical Engineering, Leeds University

Dimick D.L., Genslak S.L., Greib R.E., Malik M.J. (1979)

'Emissions and economy potential of prechamber stratified charge engines', SAE 790436

Douaud A., De Soete G., Henault C. (1983)

'Experimental analysis of the initiation and development of part load combustions in spark ignition engines', SAE 830338

Durbin E.J., Tsai K.C. (1983)

'Extending the lean limit operation of an SI engine with a multiple electrode spark plug', SAE 830476

Edson M.H. (1961)

'The influence of compression ratio and dissociation of the ideal Otto cycle efficiency', SAE 380C.

Edwards C.F., Oppenheim A.K., Dale J.D. (1983)

'A comparative study of plasma ignition systems', SAE 830479

Edwards D.K., Denny V.E., Mills A.F. (1973)

'Transfer processes' Holt, Rinehart and Winston (publishers).

Gallant R.W. (1968)

'Physical properties of hydrocarbons', Vol. 1, pp 139-148, Gulf Publishing Co., Texas, ISBN 0-87201-689-7

Gaydon A.G., Wolfhard H.G. (1970)

'Flames: their structure, radiation, and temperature', Chapman and Hall (publishers), London.

Groff E.G., Matekunas F.A. (1980)

'The nature of turbulent flame propagation in a homogeneous spark-ignited engine' SAE 800133

Gruden D. (1975)

'Combustion and exhaust emission of an engine using the Porsche-stratified-charge-chamber-system', SAE 750888

Gruden D., Markovac U., Lorcher H. (1976)

'*Development of the Porsche SKS engine*' Conference on Stratified Charge Engines, I.Mech.E., paper C243/76

Gulder O.L. (1982)

'*Laminar burning velocities of Methanol, Ethanol and Iso-octane/air mixtures*', Nineteenth symposium (International) on combustion, The combustion Institute.

Gussak L.A. (1983)

'*The role of chemical reactivity and turbulence intensity in pre-chamber-torch organisation of combustion of a stationary flow of a fuel-air mixture*', SAE 830592

Gussak L.A., Karpov V.P., Tikhnov Y.V. (1979)

'*The application of lag process in pre-chamber engines*', SAE 790692

Gussak L.A., Turkish M.C. (1976)

'*Lag-process of combustion and its application in automobile gasoline engines*' Conference on Stratified Charge Engines, I.Mech.E., paper C257/76

Hamamoto Y., Wakisaka T., Ohigashi S. (1976)

'*Limits of flame propagation in spark ignition engines - behaviour of flames and exhaust emissions*', Sixteenth International Automotive Technical Congress FISITA.

Hamamoto Y., Wakisaka T., Ohnishi M. (1982)

'*Cycle to cycle fluctuations of lean mixture combustion in spark ignition engines*', Bulletin of the JSME, No. 25, pp 61-67

Hamid M.N. (1986)

'*Fundamental turbulent combustion problems related to gasoline engines*', Ph.D. Thesis, Department of Mechanical Engineering, Leeds University.

Haslett R.A., Monaghan M.L., McFadden J.J. (1976)

'*Stratified charge engines*', SAE 760755

Hassan H. (1971)

'*Unsteady heat transfer in a motored I.C. engine cylinder*', Proceedings of the I.Mech.E, Vol. 185, pp 1139-1148.

Heywood J.B. (1976)

'*Pollutant formation and control in spark-ignition engines*', Progress in Energy and Combustion Science, Vol. 1, pp 135-164

- Heywood J.B. (1984)
'Combustion chamber design for optimum spark-ignition engine performance', International Journal of Vehicle Design, Vol. 5, pp 336-357
- Hinze J.O. (1959)
'Turbulence - An introduction to its mechanism and theory', McGraw-Hill (publishers).
- Hires S.D., Ekchian A., Heywood J.B., Tabaczynski R.J., Wall J.C. (1976)
'Performance and NOx emissions modeling of a jet ignition pre-chamber stratified charge engine', SAE 760161
- Hires S.D., Tabaczynski R.J., Novak J.M. (1978)
'The prediction of ignition delay and combustion intervals for a homogeneous charge spark ignition engine', SAE 780232
- Hirschfelder J.O., Curtiss C.F., Bird R.B. (1964)
'Molecular theory of gases and liquids' John Wiley and sons (publishers).
- Hugelman R.D., Ong S-H. (1982)
'Recent developments in swirl induced turbulent mixing for 4-stroke cycle engines', SAE 820157
- Hui K.S.J., Kwa G.S. (1975)
'Transport properties of combustion products', Final Year Project Report, Mechanical Engineering Department, University of Leeds.
- Hull W., Sorenson S.C. (1978)
'Research on a dual chamber stratified charge engine' SAE 780488
- Hynes J. (1986a)
'A computer model for simulation of the combustion process in a single chamber spark ignition engine', Report No. T43, Department of Mechanical Engineering, University of Leeds.
- Hynes J. (1986b)
'A computer model for simulation of the combustion process in a divided chamber spark ignition engine', Report No. T44, Department of Mechanical Engineering, University of Leeds.

- Hynes J. (1986c)
'Digitisation of Area's and graphs using a bitpad', Report No. T45, Department of Mechanical Engineering, University of Leeds.
- Hynes J. (1986d)
'Spark ignition engine data acquisition and processing', Report No. T46, Department of Mechanical Engineering, University of Leeds.
- Hynes J. (1986e)
'A computer program to calculate the mass fraction burnt during combustion in a single chamber spark ignition engine', Report No. T47, Department of Mechanical Engineering, University of Leeds.
- JANAF (1971)
'Thermochemical tables', 2nd edition, NSRDS-MBS 37, June 1971
- Karlovitz B., Denniston D.W., Wells F.E. (1951)
'Investigation of turbulent flames', Journal of Chemical Physics, Vol. 19, pp 541-547.
- Kataoka K., Hirako Y., Takahata Y. (1984)
'Combustion process of torch-ignited nonhomogeneous mixtures (an experiment with a constant volume bomb)', Bulletin of the JSME, Vol. 27, No 224-12, pp 227-234
- Keck J.C. (1983)
'Turbulent flame structure and speed in spark ignition engines', Nineteenth Symposium (International) on Combustion, The Combustion Institute, Pittsburg, pp 1451-1466
- Kennard E.H. (1938)
'Kinetic theory of gases' McGraw Hill (publishers).
- Kerimov N.A., Mektiev R.I. (1978)
'Engines with stratified charge', SAE 780342
- Konishi M., Nakamura N., Oono E., Baika T., Sanda S. (1979)
'Effects of a pre-chamber on NOx formation process in the S.I. engine' SAE 790389
- Krieger R.B., Davis G.C. (1976)
'The influence of stratification on jet-ignition engine emissions and fuel consumption' Conference on Stratified Charge Engines, I.Mech.E., paper C254/76
- Lancaster D.R. (1976)
'Effect of engine variables on turbulence in SI engines', SAE 760159

- Lancaster D.R., Krieger R.B., Sorenson S.C., Hull W.L. (1976)
'Effect of turbulence on SI engine combustion', SAE 760160
- Lawes M. (1986)
'Effects of engine turbulence on burning rates', Ph.D. Thesis, Department of Mechanical Engineering, Leeds University.
- Lee W., Schaefer H.J. (1983)
'Analysis of local pressures, surface temperatures and engine damages under knock conditions', SAE 830508
- Liou T.M., Hall M., Santavicca D.A., Bracco F.V. (1984)
'Laser doppler velocimetry measurements in valved and ported engines', SAE 840375
- Liou T.M., Santavicca D.A. (1983)
'Cycle resolved turbulence measurements in a ported engine with and without swirl', SAE 830419
- Lucas G.G., James E.H. (1973)
'A computer simulation of a spark ignition engine', SAE 730053
- Maly R., Saggau B. Wagner E., Ziegler G. (1983a)
'Prospects of ignition enhancement', SAE 830478
- Mason E.A., Monchick L. (1962)
'Transport properties of polar gas mixtures' Journal of Chemical Physics, Vol. 36, pp 2746-2757
- Mathur H.B., Gajendra Babu M.K., Subba Reddi K. (1983)
'A thermodynamic simulation model for a methanol fueled spark ignition engine', SAE 830333
- May M.G. (1979)
'The high compression lean burn spark ignited 4-stroke engine', I.Mech.E., C97/79
- McCuiston F.D., Lavoie G.A., Kaufmann C.W. (1977)
'Validation of a turbulent flame propagation model for a spark ignition engine', SAE 770045
- Metghalachi M., Keck J.C. (1982)
'Burning velocities of air and methanol, isooctane, and indolene at high pressure and temperature', Combustion and Flame, Vol. 48, pp 191-210.

- Milane R.E., Tabaczynski R.J., Arpaci V.S. (1983)
'A stochastic model of turbulent mixing for the prediction of burn rate in a spark ignition engine', Combustion Science and Technology, Vol. 32, pp 211-235
- Mitchell E., Alperstein M. (1973)
'Texaco controlled-combustion system-multifuel, efficient, clean and practical', Combustion Science and Technology, Vol. 8, pp 39-49
- Nakagawa Y., Nakai M., Hamai K. (1982)
'A study of the relationships between cycle to cycle variations of combustion and heat release delay in a spark ignition engine', Bulletin of the JSME, No. 25, pp 54-60
- Nakamura N., Kobayashi T., Manaoka M., Takagi N. (1983)
'A new platinum tipped spark plug extends the lean misfire limit and useful life', SAE 830480
- Namazian M., Hansen S., Lyford-Pike E., Sanchez-Barsse J., Heywood J., Rife J. (1980)
'Schlieren visualization of the flow and density fields in the cylinder of a spark-ignition engine', SAE 800044
- Newhall H.K., El-Messiri I.A. (1970a)
'A combustion chamber concept for control of engine exhaust air pollutant emissions', Combustion & Flame, Vol. 14, pp 155-158
- Newhall H.K., El-Messiri I.A. (1970b)
'A combustion chamber designed for minimum engine exhaust emissions', SAE 700491
- Norris-Jones S.R., Russell J.T. (1982)
'"FM" - A high efficiency system for the future light duty engine?', SAE 820760
- Obert E.F. (1968)
'The Internal Combustion Engine', International Textbook company, Scranton, Pennsylvania.
- Oppenheim A.K., Cheng R.K., Teichman K., Smith O.I., Sawyer R.F., Hom K., Stewart H.E. (1976)
'A cinematographic study of combustion in an enclosure fitted with a reciprocating piston' Conference on Stratified Charge Engines, I.Mech.E., paper C256/76

- Overington M.T., Haslett R.A. (1976)
'A new stratified charge engine based on the Ricardo Comet design', Conference on Stratified Charge Engines, I.Mech.E., paper C253/76
- Panicker K. (1982)
'Combustion study in single chamber engine' MSc project report no.14.6.55 Department of Mechanical Engineering, University of Leeds.
- Petrovic S. (1982)
'Cycle by cycle variations of flame propagation in a spark ignition engine', SAE 820091
- Pischinger F.F., Klockner, K.J. (1974)
'Single cylinder study of stratified charge process with pre-chamber injection' SAE 741162
- Pischinger F., Kreykenbohm B., Adams W. (1976)
'Experimental and theoretical investigations on a stratified charge engine with pre-chamber injection' Conference on Stratified Charge Engines, I.Mech.E., paper C240/76
- Povinelli L.A., Fuhs A.E. (1962)
'The spectral theory of turbulent flame propagation', Eighth symposium (international) on combustion, pp 554-566, Williams and Wilkins (publishers).
- Prothero A. (1969)
'Computing with thermochemical data', Combustion and Flame, Vol. 13, pp 399-408.
- Purins E.A. (1974)
'Pre-chamber stratified charge engine combustion studies' SAE 741159
- Quader A.A. (1974)
'Lean combustion and the misfire limit in spark ignition engines', SAE 741055
- Quader A.A. (1976)
'What limits lean operation in spark ignition engines - flame initiation or propagation', SAE 760760
- Rask R.B. (1979)
'Laser doppler anemometer measurements in an internal combustion engine', SAE 790094
- Ricardo H.R. (1922)
'Recent work on the internal combustion engine', SAE transactions, Vol. 17.

Ricardo H.R., Hempson J.G.G. (1968)

'The high speed internal combustion engine', fifth edition, Blackie.

Ryan T.W., Lestz S.S. (1980)

'The laminar burning velocity of isooctane, n-heptane, methanol, methane and propane at elevated temperatures and pressures in the presence of a diluent', SAE 800103

Sakai Y., Kunii K., Sasaki M., Kakuta N., Aihara H. (1976)

'Combustion characteristics of a torch ignited engine - analytical measurements of gas temperature and mixture formation', Conference on Stratified Charge Engines, I.Mech.E., paper C247/76

Shiozaki T. Suzuki T., Shimoda M. (1980)

'Observation of combustion process in D.I. Diesel engine via high speed direct and Schlieren photography', SAE 800025

Sinnamon J.F., Cole D.E. (1979)

'The influence of overall equivalence ratio and degree of stratification on the fuel consumption and emissions of a prechamber, stratified-charge-engine', SAE 790438

Smith J.R. (1982a)

'Turbulent flame structure in a homogeneous-charge engine', SAE 820043

Smith J.R. (1982b)

'The influence of turbulence on flame structure in an engine', Sandia National Laboratories Report, SAND82-8722. Presented at ASME Annual Winter Meeting.

Sorenson S.C., Pan S.S. (1979)

'A one-dimensional combustion model for a dual chamber stratified charge spark ignition engine', SAE 790355

Sutton D.L. (1983)

'Combustion chamber design for improved performance and economy with high compression lean burn operation', SAE 830336

Swords M.D., Kalghatgi G.T., Watts A.J. (1982)

'An experimental study of ignition and flame development in a spark ignition engine', SAE 821220

Svehla R.A. (1962)

'*Estimated viscosities and thermal conductivities of gases at high temperatures*', NASA technical report R-132.

Tabaczynski R.J. (1976)

'*Turbulence and turbulent combustion in spark-ignition engines*', Progress in Energy and Combustion Science., Vol. 2, pp 143-165

Tabaczynski R.J., Klomp E.D. (1974)

'*Calculated NO emissions of an unthrottled SI stratified charge I.C. engine*', SAE 741171.

Tabaczynski R.J., Heywood J.B., Keck J.C. (1972)

'*Time-resolved measurements of hydrocarbon mass flowrate in the exhaust of a spark-ignition engine*', SAE 720112

Tabaczynski R.J., Ferguson C.R., Radhakrishnan K. (1977)

'*A turbulent entrainment model for spark ignition engine combustion*', SAE 770647

Tabaczynski R.J., Trinker F.H., Shannon B.A.S. (1980)

'*Further refinement and validation of a turbulent flame propagation model for spark-ignition engines*', Combustion and Flame, Vol. 39, pp 111-121.

T.R.C. Thermodynamics Research Centre Data Project (1983)

'*Selected values of chemical compounds*', Vol. 2, Thermodynamics Research centre, Texas A&M University.

Turkish M.C. (1974)

'*3-valve stratified charge engines : Evolvment, analysis and progression*', SAE 741163

Turkish M.C. (1975)

'*Prechamber and valve gear design for 3-valve stratified charge engines*', SAE 751004

Van Tiggelen A., Deckers J. (1956)

'*Chain branching and flame propagation*', Sixth Symposium (International) on combustion, The Combustion Institute, pp 61-66.

Varde K.S., Lubin M.J. (1974)

'*The roll of connecting nozzle and the flame initiation point in the performance of a dual chamber stratified charge engine*', SAE 741161

- Varde K.S. (1976)
'Sensitivity of fuel economy characteristics in a dual chamber stratified charge engine'
Conference on Stratified Charge Engines, I.Mech.E., paper C241/76
- Vickland C.W., Strange F.M. Bell R.A. Starkman E.S. (1962)
'A consideration of the high temperature of internal combustion engines', SAE transactions,
Vol. 70, p785.
- Wall J.C., Heywood J.B. (1978)
'The influence of operating variables and prechamber size on combustion in a prechamber stratified-charge engine', SAE 780966
- Wall J.C., Heywood J.B., Woods W.A. (1978)
'Parametric studies of performance and NOx emissions of the three valve stratified charge engine using cycle simulation', SAE 780320
- Wafsa M., Fuller D.E., Daneshyar H. (1974)
'The effects of charge stratification on nitric oxide emission from spark ignition engines',
SAE 741175
- Watson J.T.R. (1972)
'Viscosity of gases in metric units', National Engineering Laboratory, Edinburgh,
H.M. Stationary Office.
- Weaving J.H. (1982) *'A fundamental investigation of the combustion process in a stratified charge engine of the pre-chamber type'*
Report no. ETR 3271, B.L. Technology Ltd.
- Weaving J.H., Corkhill W.J. (1976)
'British Leyland experimental stratified charge engine' Conference on Stratified Charge
Engines, I.Mech.E., paper C246/76
- Westenberg A.A. (1971)
'Kinetics of NO and CO in lean pre-mixed hydrocarbon-air flames', Combustion Science
and Technology, Vol. 4, pp 59-64.
- Wimmer D.B., Lee R.C. (1973)
'Evaluation of the performance and emissions of a CFR engine equipped with a prechamber', SAE 730474

- Witze P.O. (1975)
'Hot-wire turbulence measurements in a motored internal combustion engine',
Second Symposium (European) on Combustion, pp 812-819
- Witze P.O. (1980a)
'A critical comparison of hot-wire anemometry and laser Doppler velocimetry for I.C. engine applications', SAE 800132
- Witze P.O. (1980b)
'Influence of air motion variation on the performance of a direct injection stratified charge engine', Conference on Stratified Charge Automotive Engines, Paper C394/80, I.Mech.E.
- Witze P.O., Martin J.K., Borgnakke C. (1983)
'Measurements and predictions of the pre-combustion fluid motion and combustion rate in a spark ignition engine', SAE 831697
- Witze P.O., Martin J.K., Borgnakke C. (1984a)
'Conditionally sampled velocity and turbulence measurements in a spark ignition engine',
Combustion Science and Technology, Vol. 36, pp 301-317
- Witze P.O., Martin J.K., Borgnakke C. (1984b)
'Fluid motion during flame propagation in a spark ignition engine', SAE 840377
- Wong K.W., Hoult D.P. (1979)
'Rapid distortion theory applied to Turbulent combustion', SAE 790357
- Woschni G. (1967)
'A universally applicable equation for the instantaneous heat transfer coefficient in the internal combustion engine', SAE 670931
- Wyczalek F.A., Harned J.L., Maksymiuk S., Blevins J.R. (1975a)
'EFI pre-chamber torch ignition of lean mixtures' SAE 750351
- Wyczalek F.A., Frank D.L., Neuman J.G. (1975b)
'Plasma jet ignition of lean mixtures' SAE 750349
- Yagi S., Fujii I., Nishikawa M., Shirai H. (1979)
'A new combustion system in the three-valve stratified charge engine', SAE 790439
- Yagi S., Fujii I., Nishikawa M., Shirai H. (1980)
'A newly developed 1.5L CVCC engine for some 1980 models', SAE 800321

Yoshida M., Harigaya Y., Sato K. (1982)

'Variation of heat flux through a combustion chamber wall of pre-chamber type diesel engine', Bulletin of the JSME, No. 25, pp 426-436

APPENDIX A

Engine and Fuel Details

A.1. Engine Details

	Yamaha	Ruston	
Type	2-stroke 7 port	4-stroke side valve	
Bore	85.0	76.2	mm
Stroke	70.0	82.5	mm
con-rod length/ crank shaft throw	3.674	4.134	
Displacement volume	397.0	376.5	cc
Effective volume ¹	213.25	376.5	cc
Inlet valve opens	124	25	BTDC
Inlet valve closes	124	138	BTDC
Exhaust valve opens	91	138	ATDC
Exhaust valve closes	91	15	ATDC
Valve chamber volume	nil	25.5	cc
Cylinder volume at TDC ²	30.46	53.75	cc

¹ Volume used for calculation of compression ratio and I.M.E.P. (measured from exhaust valve closure in the Yamaha)

² For an 8:1 compression ratio

A.2. Fuel Details

The fuel used for the experimental tests was a reference four star fuel supplied by B.P. Details for Iso-octane are also shown for comparison.

Property	BP-4STAR	Iso-octane
Density @25°C (g/cc)	0.7199	0.6878
Density @15.5°C (g/cc)	0.7286	0.6956
% Hydrogen	13.34	15.79
Octane rating (RON)	97.8	100
Stoichiometric air/fuel ratio	14.506	15.065
Molecular weight	≅ 80 ~ 100	114.5
Approx. empirical formula	$C_{6.5}H_{12}$	C_8H_{18}

APPENDIX B

Calculation of Mixture Properties

This appendix describes the method of calculation for gas properties used in the cycle modelling program.

B.1. Properties of individual species

Entropy and enthalpy data can be related to specific heat capacity at constant pressure (Prothero, 1969). The specific heat was calculated using sixth order polynomials given by Prothero. This polynomial was not available for the fuels; for methanol one was fitted to data from Svehla (1962), and for iso-octane the data was from the American Petroleum Institute (A.P.I., 1983). The enthalpy of each species at a given temperature is related to the enthalpy at a base temperature (298.15K) by:-

$$H(T)_i = H(T_b)_i + \int_{T_b}^T C_{p_i} dT \quad \text{cal/gmole} \quad (\text{B.1})$$

This can easily be integrated using the polynomial for C_p in terms of T . The entropy is given by:-

$$\int dS = \int \frac{C_p}{T} dT + \int \left[\frac{V}{T} \right]_p dp \quad (\text{B.2})$$

Assuming ideal gas behaviour this becomes:-

$$S(T)_i = S(T_b)_i + \int_{T_b}^T C_{p_i} d(\ln T) - R \ln \left[\frac{P}{P_0} \right] \quad \text{cal/gmole} \quad (\text{B.3})$$

where $S(T_b)_i$ is the entropy of the species at a base temperature (293K), and atmospheric pressure (P_0).

The integral can be reduced to:-

$$\int_{T_b/1000}^{T/1000} \left[\frac{a_0}{S} + a_1 + a_2 S + \dots + a_6 S^5 \right] \quad (\text{B.4})$$

where $S=T/1000$

Integrating gives:-

$$S(T)_i = S(T_b)_i + \left[a_0 \ln(S) + a_1 S + \frac{a_2 S^2}{2} \dots + \frac{a_6 S^6}{6} \right] - R \ln \left[\frac{P}{P_0} \right] \quad (\text{B.5})$$

Values for the enthalpy of formation and entropy at a base temperature are from JANAF (1971), except for iso-octane (from A.P.I., 1983) and methanol (from T.R.C., 1983).

Experiments to find the viscosity of CO₂, H₂, O₂, and N₂ were conducted by Watson (1972). He fitted polynomials to this data, of the form:-

$$\mu = \frac{10\sqrt{T}}{[a_0 + a_1 S + \dots + a_5 S^5]} \text{ micropoise} \tag{B.6}$$

where $S = 100/T$

These have been extended to sixth order for consistency. For species where there is no experimental data available it is necessary to calculate the viscosity by theoretical means. Hirschfelder et al (1964) show:-

$$\mu = 26.693 \times \sqrt{\frac{MWT}{\sigma^2 \Omega^{(2,2)*}(T^*)}} \tag{B.7}$$

where T^* is the reduced temperature: $T^* = \frac{T}{\epsilon/\kappa}$

$\Omega^{(2,2)*}$ is the reduced collision integral and is tabulated against the reduced temperature by Hirschfelder et al.

Hui and Kwa (1975) fitted polynomials of varying degrees to this data. They found the best fit was obtained by considering the data in three sections, ($T^* \leq 2$, $2 < T^* \leq 10$, $T^* > 10$) and fitting sixth order polynomials to each section; the polynomials are constrained to be equal at the separation points. The collision diameter (σ) and the potential parameter (ϵ/κ) are tabulated in many references. (Edwards et al, 1973; Svehla, 1969; Mason et al, 1962; Kennard, 1938; Westenberg, 1957). For steam these values were highly inconsistent. Data for the viscosity of steam in the range 200-1000°C is given by Arnold (1970), Horvath (1975) and Nagashima (1970). The theory using constants from Svehla gave the best fit to this data; Svehla's data was therefore chosen to calculate the viscosity at higher temperatures. The experimental data for steam is for a wide range of pressures; it shows the assumption of no pressure effect on viscosity to be justifiable.

For iso-octane there are no tabulated values of collision diameter and potential parameter. However, it is possible to estimate these from critical properties of the fuel. (Svehla 1962):-

$$\frac{\epsilon}{\kappa} \approx 0.75 \times T_c \tag{B.8}$$

$$\frac{2}{3} \pi N \sigma^3 \approx 2.0V_b - 5 \tag{B.9}$$

where T_c is the critical temperature (271.1°C for iso-octane), N is Avogadro's number and V_b

is the molar volume at the boiling point. The values given by these formulae give good agreement with the limited experimental data available (Gallant, 1968). As already mentioned, the fuel is only present in small quantities and so small errors in its viscosity have negligible effect on the overall mixture viscosity.

The thermal conductivity can be calculated from the viscosity (Svehla, 1962) by:-

$$\kappa_i = \mu_i \frac{R}{M} \left[\frac{15}{4} + 1.32 \times \left(\frac{C_{p_i}}{R} - \frac{5}{2} \right) \right] \quad (\text{B.10})$$

B.2. Properties of mixtures

The specific heat and enthalpy of a mixture of gases can simply be calculated by:-

$$\left[C_p \text{ or } H \right]_{\text{mix}} = \sum MF_i \left[C_p \text{ or } H \right]_i \quad (\text{B.11})$$

where MF_i is the mole fraction of each species.

For entropy the procedure is similar, however the term which takes account of the pressure change need only be calculated once as the sum of partial pressures for each individual species is equal to the total pressure. The entropy of the mixture is therefore given by:-

$$S_{\text{mix}} = \sum MF_i S_i - R \ln(P) \quad (\text{B.12})$$

where S_i is the entropy of each individual species at constant pressure (1 atmosphere).

Wilke (1950) gives an expression for the viscosity of a mixture of gases:-

$$\mu_{\text{mix}} = \sum_{\text{all species } i} \left[\frac{\mu_i}{1 + \frac{C}{MF_i} \times \sum_{\substack{\text{all species} \\ j \neq i}} MF_j \phi_{ij}} \right] \quad (\text{B.13})$$

where the constant C is equal to 1.0, and:-

$$\phi_{ij} = \frac{\left[1 + \left(\frac{\mu_i}{\mu_j} \right)^{1/2} \times \left(\frac{MW_j}{MW_i} \right)^{1/4} \right]^2}{2\sqrt{2} \left[1 + \frac{MW_i}{MW_j} \right]^{1/2}} \quad (\text{B.14})$$

For thermal conductivity the form of the equation is the same apart from the constant C being 1.065.

APPENDIX C

Calculation of Enflamed Volumes

For a cylinder of bore B and instantaneous height h , the total cylinder volume is given by:

$$V_t = \frac{\pi B^2}{4} \cdot h \tag{C.1}$$

The volume occupied by the burnt charge was calculated by assuming flame growth to be spherical; when small the volume of the flame would be equal to that of a sphere, as it grew its volume would be restricted by the cylinder walls (see Fig. C.1). The calculation procedure adopted was therefore different each time the flame made contact with one of the cylinder walls. The volume of the unburnt charge could be found by subtraction of the burnt charge volume from the total cylinder volume.

C.1. Central Ignition - Single Chamber

(1) $r \leq x$ and $r < h-x$ and $r < B/2$

$$V_e = \frac{4}{3} \pi r^3 \tag{C.2}$$

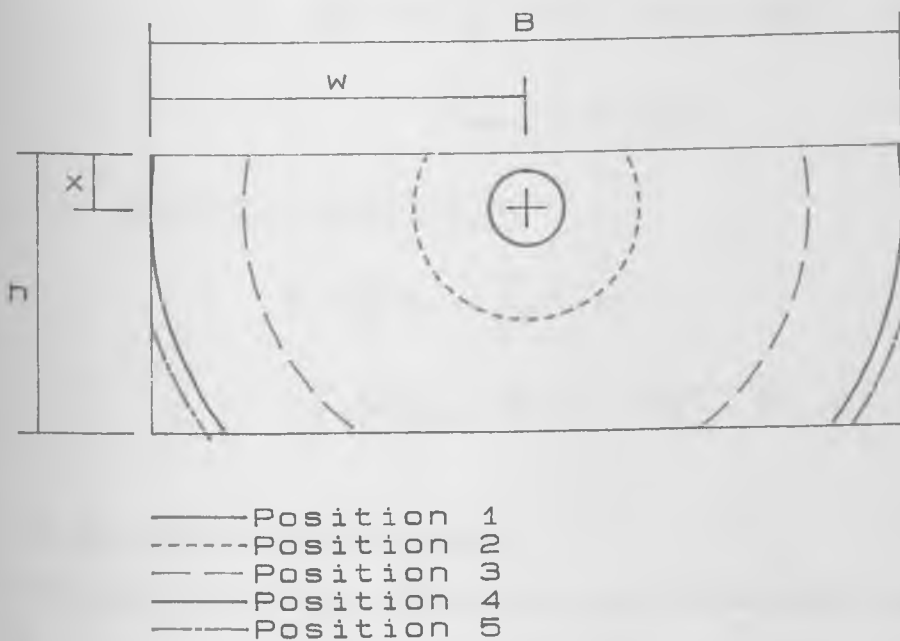


Fig.C.1 Cross section of cylinder showing volume occupied by flame at different radii (central ignition)

(2) $r > x$ and $r < h-x$ and $r < B/2$

$$V_e = \int_{-x}^r \pi(r^2 - y^2) dy$$

$$= \pi \left[\frac{2}{3} r^3 + r^2 x - \frac{x^3}{3} \right] \quad (\text{C.3})$$

(3) $r > x$ and $r > h-x$ and $r < B/2$

$$V_e = \int_{-x}^{h-x} \pi(r^2 - y^2) dy$$

$$= \pi(r^2 h - \frac{h^3}{3} + h^2 x - hx^2) \quad (\text{C.4})$$

(4) $r > h-x$ and $r \geq B/2$ and $r \leq \sqrt{(B/2)^2 + x^2}$

$$V_e = \int_{-x}^{-Z} \pi(r^2 - y^2) dy + 2Z \frac{\pi B^2}{4} + \int_Z^{h-x} \pi(r^2 - y^2) dy$$

$$= \pi \left[r^2 x - \frac{x^3}{3} - r^2 Z + \frac{Z^3}{3} + 2Z \frac{B^2}{4} + r^2(h-x) - \frac{(h-x)^3}{3} - r^2 Z + \frac{Z^3}{3} \right] \quad (\text{C.5})$$

$$\text{where } Z = \sqrt{r^2 - (B/2)^2}$$

(5) $\sqrt{(B/2)^2 + x^2} \leq r \leq \sqrt{(B/2)^2 + (h-x)^2}$

$$V_e = \frac{\pi B^2}{4}(Z+x) + \int_Z^{h-x} \pi(r^2 - y^2) dy$$

$$= \pi \left[\frac{B^2}{4}(Z+x) + \frac{2}{3} r^2(h-x) - \frac{(h-x)^3}{3} - r^2 Z + \frac{Z^3}{3} \right] \quad (\text{C.6})$$

C.2. Side Ignition and Main chamber

This section includes the case of flame growth in the divided chamber engine (when $w = 0$).

(a) $r \leq x$ and $r \leq w$

$$V_b = \frac{4}{3} \pi r^3 \quad (\text{C.7})$$

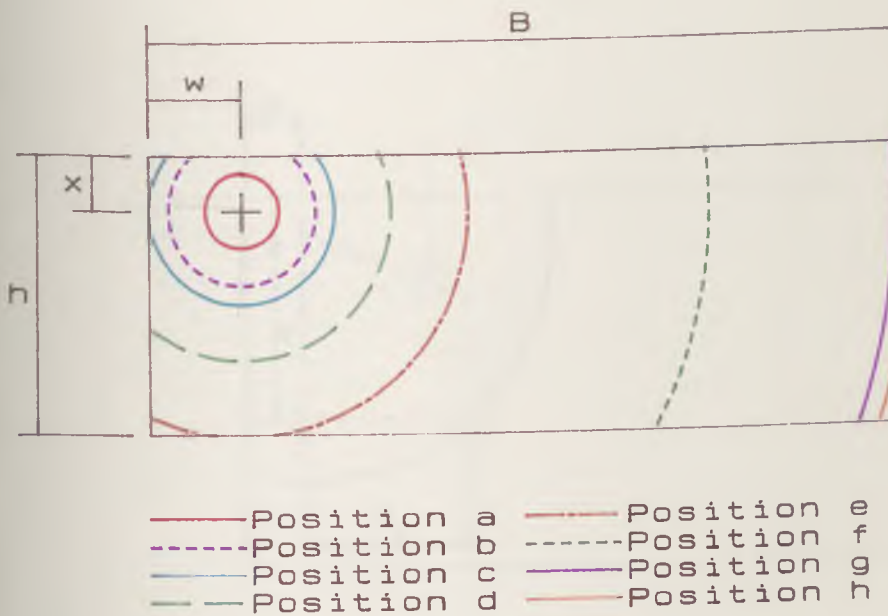


Fig.C.2 Cross section of cylinder showing volume occupied by flame at different radii (side ignition)

(b) $x < r \leq w$

$$V_e = \int_{-r}^x \pi r^2 y \, dy \tag{C.8}$$

For larger flame sizes, the volume becomes a complex shape. Consider a plane perpendicular to the cylinder axis, distance y from the flame centre (Fig.C.3). Its radius in this plane (R_y) is given by:

$$R_y = \sqrt{r^2 - y^2} \tag{C.9}$$

The projected area of the flame in this plane (Fig.C.4) is given by:

$$AREA(R_y) = R_y^2(\pi - \alpha) + \left[\frac{B}{2} \right]^2 - \left[\frac{B}{2} \right]^2 \sin(\beta)\cos(\beta) + R_y^2 \sin(\alpha)\cos(\alpha) \tag{C.10}$$

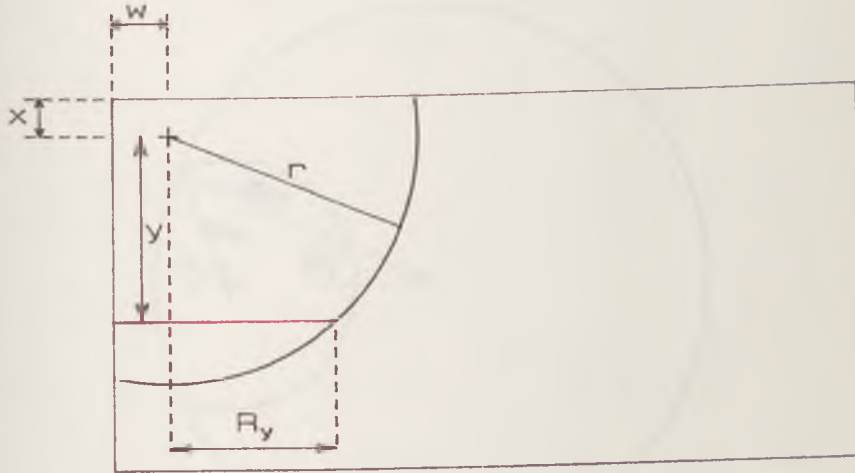


Fig.C.3

The angles β and α are:

$$\cos(\beta) = \frac{\left[\frac{B}{2}\right]^2 + \left[\frac{B}{2}-w\right]^2 - R_y^2}{2 \cdot \frac{B}{2} \cdot \left[\frac{B}{2}-w\right]} \tag{C.11}$$

$$\cos(\pi - \alpha) = \frac{\left[\frac{B}{2}-w\right]^2 + R_y^2 - \left[\frac{B}{2}\right]^2}{2R_y \left[\frac{B}{2}-w\right]}$$

Equation (C.10) only applies to planes where the flame has made partial contact with the wall. If the flame has made complete contact with the wall in a particular plane, then the area in that plane will be given by:

$$AREA(R_y) = \frac{\pi B^2}{4} \tag{C.12}$$

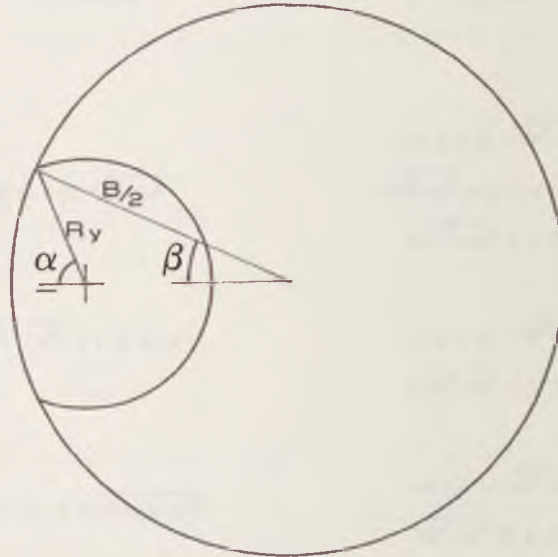


Fig.C.4

If the flame has not reached the cylinder wall in a particular plane its area in that plane will be:

$$AREA(R_y) = \pi R_y^2 \tag{C.13}$$

For each of the flame positions (c)-(h) shown in Fig.C.2, the equation which represents the flame area ($AREA(R_y)$) in a plane at a distance y from the flame centre is shown in table C.1.

The volume entrained behind this spherical flame is therefore given by:

$$V_e = \int AREA(R_y) dy \tag{C.14}$$

This integral is difficult to evaluate. The volume was therefore calculated using Simpsons rule. The projected area was calculated in 1000 axial planes; the distance (d) between each plane is given by:

$$r/1000 \text{ for } r \leq x$$

$$(r+x)/1000 \text{ for } x < r \leq h-x$$

TABLE C.1

Position	Condition	Region	Equation (for AREA(R_y))
(c)	$x < r \leq \sqrt{x^2 + w^2}$	$-x \leq y \leq -\sqrt{r^2 - w^2}$ $-\sqrt{r^2 - w^2} < y < +\sqrt{r^2 - w^2}$ $+\sqrt{r^2 - w^2} \leq y \leq r$	(C.13) (C.10) (C.13)
(d)	$\sqrt{x^2 + w^2} < r \leq h - x$	$-x \leq y \leq +\sqrt{r^2 - w^2}$ $+\sqrt{r^2 - w^2} < y \leq r$	(C.10) (C.13)
(e)	$h - x < r \leq \sqrt{w^2 + (h - x)^2}$	$-x \leq y < \sqrt{r^2 - w^2}$ $\sqrt{r^2 - w^2} \leq y \leq r$	(C.10) (C.13)
(f)	$\sqrt{w^2 + (h - x)^2} < r \leq B - w$	$-x \leq y \leq h - x$	(C.10)
(g)	$h - x < r \leq \sqrt{(B - w)^2 + x^2}$	$-x \leq y \leq -\sqrt{r^2 - (B - w)^2}$ $-\sqrt{r^2 - (B - w)^2} < y < +\sqrt{r^2 - (B - w)^2}$ $+\sqrt{r^2 - (B - w)^2} \leq y \leq h - x$	(C.10) (C.12) (C.10)
(h)	$\sqrt{(B - w)^2 + x^2} < r \leq \sqrt{(B - w)^2 + (h - x)^2}$	$-x \leq y \leq +\sqrt{r^2 - (B - w)^2}$ $\sqrt{r^2 - (B - w)^2} < y < h - x$	(C.12) (C.10)

and $(h-x)/1000$ for $r > h-x$.

The projected area of the flame in each plane is then calculated using the relevant equation from table C.1, given the radius R_y in the projected plane:-

$$R_y = \sqrt{r^2 - (y - x)^2} \tag{C.15}$$

The total enflamed volume is therefore given by:-

$$V_e = \frac{d}{3} \times \left[AREA(R_0) + 4 \sum_{y=1}^{500} AREA(R_{2y-1}) + 2 \sum_{y=1}^{499} AREA(R_{2y}) + AREA(R_{1000}) \right] \quad (C.16)$$

C.3. Spherical Pre-chamber

For a spherical pre-chamber of radius R_p , the total volume is given by:

$$V_t = \frac{4}{3} \pi R_p^3 \quad (C.17)$$

and the enflamed volume is given by:

$$V_e = \frac{4}{3} \pi r^3 \quad (C.18)$$

C.4. Cylindrical Pre-chamber

For a pre-chamber of radius R_p and aspect ratio 1, the height of the chamber is $2R_p$. The total chamber volume is therefore $2\pi R_p^3$. If r is less than R_p then the flame has not reached the walls, its volume is given by equation (C.18).

If $r > R_p$ and $r \leq \sqrt{R_p^2 + R_p^2}$ then:

$$V_e = 2\sqrt{r^2 - R_p^2} \times \frac{\pi B^2}{4} + 2\pi \int_{\sqrt{r^2 - R_p^2}}^{R_p} (r^2 - y^2) dy \quad (C.19)$$

APPENDIX D

Calculation of Wall Surface Areas

In order to calculate the heat transfer rates from the charge to the cylinder walls during combustion it is necessary to know the surface area of the walls in contact with the unburnt and burnt regions. As with the enflamed volume calculations (Appendix C), this surface area was dependent upon with which of the cylinder walls the flame had come into contact. In the heat transfer calculations the piston crown, cylinder walls and cylinder head were treated as separate regions; each region was assumed to be at a uniform temperature. Once the surface area in contact with the burnt charge was known, the area in contact with the unburnt charge could be found by subtraction from the total surface area.

D.1. Central Ignition - Single Chamber

The total cylinder wall surface area A_w , is given by $2\pi Bh$, and the cylinder head and piston crown surface areas (A_{h_t} and A_{p_t} , respectively) are both equal to $\pi B^2/4$.

(1) $r \leq x$

Only unburnt charge is in contact with the cylinder walls

$$A_{p_b} = A_{h_b} = A_{w_b} = 0 \quad (D.1)$$

(2) $r \geq x$ and $r < h-x$ and $r < B/2$

The burnt charge is in contact with cylinder head only

$$A_{h_b} = \pi(r^2 - x^2) \quad (D.2)$$

(3) $r \geq x$ and $r \geq h-x$ and $r \leq B/2$

The burnt charge is in contact with the cylinder head (equation (D.2)) and the piston crown:

$$A_{p_b} = \pi(r^2 - (h-x)^2) \quad (D.3)$$

(4) $r \geq x$ and $r \geq h-x$ and $r > B/2$

The burnt charge is in contact with the cylinder head (D.2), piston crown (D.3) and cylinder walls:

$$A_{w_b} = 2\pi B \sqrt{r^2 - \frac{B^2}{4}} \quad (D.4)$$

(5) $r > \sqrt{B^2 + x^2}$

The cylinder head is now in contact with burnt charge only.

$$A_{h_b} = A_{h_t}, \quad \text{and} \quad A_{w_b} = \pi B \left[x + \sqrt{r^2 - \frac{B^2}{4}} \right] \quad (D.5)$$

(6) $r > \sqrt{B^2 + (h-x)^2}$

All the cylinder walls are now in contact with burnt charge.

$$A_{h_b} = A_{h_r}, \quad A_{p_b} = A_{p_r}, \quad A_{w_b} = A_{w_r} \quad (D.6)$$

D.2. Side Ignition

This section includes the main chamber during divided chamber operation (with $w = 0$). The cylinder head and piston crown were treated in a similar manner to the central ignition condition. When the flame has reached the cylinder walls, the wall surface area in contact with the burnt charge is an ellipse; this is due to the curvature of the walls.

(a) $r \leq x$

Only unburnt charge is in contact with the cylinder walls (equation D.1)

(b) $x < r \leq w$

The burnt charge is in contact with cylinder head only

$$A_{h_b} = \pi(r^2 - x^2) \quad (D.7)$$

(c) $x < r \leq \sqrt{w^2 + x^2}$

The burnt charge is in contact with the cylinder walls and the cylinder head. Shown in Fig. C.4 is a cross section of the flame in the plane of the spark. The cylinder wall surface in contact with the burnt charge will be an ellipse, of height (in the axial direction) $\sqrt{r^2 - w^2}$, and length (around the circumference) equal to $B/2 \times \beta$. The surface area of the wall in contact with the burnt charge is therefore:

$$\pi \sqrt{r^2 - w^2} \times \frac{B \beta}{2} \quad (D.8)$$

where β is described by equation C.11

(d) $\sqrt{w^2 + x^2} < r \leq h-x$

The area in contact with the cylinder head can be defined in the same manner as in appendix C (equation C.10):

$$\text{i.e. } AREA(R_y) = R_y^2(\pi - \alpha) + \left[\frac{B}{2} \right]^2 - \left[\frac{B}{2} \right]^2 \sin(\beta)\cos(\beta) + R_y^2 \sin(\alpha)\cos(\alpha) \quad (D.9)$$

where the radius R_y , is equal to $\sqrt{r^2 - x^2}$, and α and β are described by equation C.11. The area in contact with the cylinder walls is an ellipse, which is partially cut off by the head.

$$\text{i.e. } A_{w_b} = 2b \int_{-x}^{\sqrt{r^2-w^2}} \sqrt{1 - \frac{y^2}{a^2}} dy$$

$$\text{where: } a = \sqrt{r^2-w^2}$$

$$b = \frac{B}{2} \cdot \beta = \frac{B}{2} \cos^{-1} \left[\frac{\left[\frac{B}{2} \right]^2 + \left[\frac{B-w}{2} \right]^2 - r^2}{2 \frac{B}{2} \left[\frac{B-w}{2} \right]} \right] \tag{D.10}$$

(e) $h-x < r \leq \sqrt{w^2 + (h-x)^2}$

The burnt charge is in contact with the cylinder head (D.9), piston crown and cylinder walls. The surface area in contact with the piston crown is a circle of radius $\sqrt{r^2-(h-x)^2}$. The surface area of the cylinder walls in contact with the burnt charge is:

$$A_{w_b} = 2b \int_{-x}^{h-x} \sqrt{1 - \frac{y^2}{a^2}} dy \tag{D.11}$$

where a and b are given by equation (D.10)

(f) $\sqrt{w^2 + (h-x)^2} < r \leq B-w$

The surface area of the cylinder head and piston crown in contact with burnt charge can be described by equation (D.9), while the area of the cylinder walls can be described by (D.11).

(g) $B-w < r \leq \sqrt{x^2 + (B-w)^2}$

At this stage, the surface area in contact with the cylinder walls is:

$$A_{w_b} = \int_{-x}^{-\sqrt{r^2-(B-w)^2}} \sqrt{1 - \frac{y^2}{a^2}} dy + \frac{\pi B^2}{4} \cdot 2\sqrt{r^2-(B-w)^2} + \int_{\sqrt{r^2-(B-w)^2}}^{(h-x)} \sqrt{1 - \frac{y^2}{a^2}} dy \tag{D.12}$$

(h) $\sqrt{x^2 + (B-w)^2} < r \leq \sqrt{(h-x)^2 + (B-w)^2}$

The cylinder head is now in contact with burnt charge only.

$$A_{h_b} = A_{h_i} \tag{D.13}$$

and

$$A_{w_b} = \frac{\pi B^2}{4} \cdot \left[x + \sqrt{r^2-(B-w)^2} \right] + \int_{\sqrt{r^2-(B-w)^2}}^{(h-x)} \sqrt{1 - \frac{y^2}{a^2}} dy \tag{D.14}$$

$$(i) \quad r \geq \sqrt{(h-x)^2 + (B-w)^2}$$

All the cylinder walls are now in contact with burnt charge.

$$A_{h_b} = A_{h_t}, \quad A_{p_b} = A_{p_t}, \quad A_{w_b} = A_{w_t} \quad (D.15)$$

D.3. Spherical Pre-chamber

The pre-chamber walls were assumed to be at uniform temperature. In a spherical pre-chamber, with central ignition and spherical flame growth, the burnt charge does not make contact with the cylinder walls until the flame radius is equal to the pre-chamber radius.

$$\begin{aligned} \text{i.e. } r < R_p \quad A_{p_b} &= 0 \\ r \geq R_p \quad A_{p_b} &= A_{p_t} \end{aligned} \quad (D.16)$$

D.4. Cylindrical Pre-chamber

In a cylindrical pre-chamber, of aspect ratio 1, the burnt charge makes contact with the cylinder walls when the flame radius (r) is equal to the pre-chamber radius (R_p).

$$\begin{aligned} r < R_p \quad A_{p_b} &= 0 \\ R_p \leq r < \sqrt{R_p^2 + R_p^2} \quad A_{p_b} &= 2 \pi (r^2 - R_p^2) + 4 \pi R_p (r^2 - R_p^2) \\ r \geq \sqrt{R_p^2 + R_p^2} \quad A_{p_b} &= A_{p_t} \end{aligned} \quad (D.17)$$